Imperial College London

Experimental and computational study of two-phase slug flow

Min Lu

Department of Chemical Engineering
Imperial College London

Supervised by Professor Geoffrey F. Hewitt
Co-supervised by Professor Omar K. Matar

A thesis submitted for the degree of

Doctor of Philosophy

June 2015

To my loving parents:

I would like to dedicate this thesis to my parents for their continuous love and support.

谢谢我最爱的父亲和母亲！

Declaration

This thesis is a description of the work carried out in the Department of Chemical Engineering, Imperial College London, under the supervision of Emeritus Professor Geoffrey F. Hewitt and Professor Omar K. Matar. Except where acknowledged, the material is the original work of the author and no part of it has been submitted for a degree.

Abstract

This thesis presents a computational and experimental investigation of horizontal gas-liquid two-phase slug flow. The overall aim of the present project was to carry out analytical and computational studies to model the processes of slug initiation, growth and collapse in horizontal pipes. The literature of two-phase flow, with a focus on slug flow, is reviewed. A "Benchmark exercise" of predicting the horizontal two-phase slug flow on the WASP (Water, Air, Sand and Petroleum) facility was set up for CFD simulations with the aim of investigating the capability of CFD codes in the prediction of slug flow characteristics in large scale pipe (78 mm ID, 37 m long). Six CFD codes (TRIOMPH, LedaFlow, STAR-CD, TransAT, FLUENT and CFX) were participated in this exercise. The complex nature of the slug flow mechanism and the relatively large-scale of the associated modelling domain contribute to the challenges of this CFD exercise; this is particularly challenging for three-dimensional simulations. It has proven difficult to carry out direct comparisons between the performances of the various codes; this is due to the difference in the assumptions and approximations made in each case. Successive slugging was captured by most of the CFD codes, apart from CFX in which the flow was remaining stratified. In terms of flow characteristics, comparison against the measurements was mainly focused on the distribution of slug frequency at various locations. Satisfactory agreement was obtained by the 1D code TRIOMPH, whereas the rest of the codes were failed to reproduce the observed trend of slug frequency distribution.

The ability of the TRIOMPH code in the prediction of horizontal slug flow is limited in a restrain region, where the two-fluid equations employed in the code has to be well-posed, therefore a validation case study was examined. For a well-posed system, a unique solution can be obtained, whereas for an ill-posed system, the solution would become mesh dependent. However, the lack of unique solution of the ill-posed case can be altered by applying unsteady inlet condition prescribed in terms of a train of slugs, which can be generated by an alternative code namely slug-tracking code.

CFD prediction of horizontal slug flow in a channel with rectangular cross-section (100 mm x 30 mm x 8000 mm) was systematically studied using STAR-CCM+. The experimental data was provided by Forschungszentrum Rossendorf (FZD) from Germany. Mesh sensitivity and parametric study were conducted to determine the settings that optimise accuracy and stability. The polyhedral mesh was found to give a fast and better convergence of the numerical solutions. A sufficient small grid size is important in order to resolve the velocity gradient throughout the two fluids. The onset of interfacial instability, wave growth, and slug generation processes were captured in the simulation. However, the predicted slug initiation site was shifted further downstream than the actual site observed in the experiment, leading to the discrepancy in the prediction of the flow characteristics.

Experimental studies on slug initiation and their subsequent development were carried out on the LOWPRSS (Low Pressure) facility at Imperial College London. The motion of the slug is followed using high-speed imaging and conductivity probes for air-oil and air-water systems, respectively. The slug frequency results demonstrate that rapid initiation events occur near the inlet region, and the slug frequency exhibits a maximum at intermediate axial distances before eventually reaching an approximately constant value at sufficiently large distances downstream of the inlet. Particular attention was given to the slug initiation mechanism observed using the LOWPRESS facility. Together with a set of air-water slug flow data obtained on the WASP facility, the influence of inlet geometry was examined. It was shown that the inlet geometry significantly influences slug initiation; however, the effect of inlet geometry on the slug development reduces along the pipe length. Beyond a certain distance, slug frequency approaches a constant value invariant with inlet geometry.

Acknowledgements

First of all, my sincere appreciation goes to Professor Geoffrey F. Hewitt who gives me the opportunity of pursuing this PhD degree and brilliantly supervised my work. His wisdom, devotion, and achievement for multiphase flow is unrivaled, and his enthusiasm in work is incredibly contagious, I feel deeply honored to be his doctoral student.

I would also express my gratitude to Professor Omar K. Matar, his continuous guidance since my undergraduate study and throughout my research work, with particularly appreciation for his effort in reading this thesis.

I would like to thank Dr. Colin Hale, Dr. Zhizhao Che and Dr. Ivan Zadrazil who has been generously share their knowledge in multiphase flow, and I thoroughly enjoyed working with them. Their dedication to research has always inspired me, without their support, some of the work in this thesis would not have been possible.

I would also like to thank Professor Raad Issa, Dr. Fabio Di Salvo, Dr. Simon Lo, Dr. Antonino Tomasello, for their kindly support on my computational modelling work.

Thanks to Tony Meredith, Richard Wallington and Bob Brace for their advices and efforts in manufacturing the instruments for LOWPRESS and WASP experiments.

To my colleagues and friends in ACXE405: Yujie Zhao, Jessy Zeng, Fu Liu, Stefanie Glassford, Jerzy Pental, Richard Mathie, James Freeman, Ajay Gupta, Vincent Poulichet, Rhys Morgan, Francesco Garcia, it was great time to spend with you, and thanks for the great working atmosphere.

Finally, my deeply thanks to my parents Mr. Jiaqi Lu and Mrs. Weiying Yan, thanks for your unceasing support and understanding throughout my study in Imperial College. To my dearest husband Hui Ru, thanks for standing by me through the tough times and giving me the love I needed, these five years have been the most memorable time of my life.

Table of Contents

LIST OF FIGURES AND TABLES

List of Figures

List of Tables

NOMENCLATURE

Roman symbols:

$\widetilde{A}$ dimensionless wetted area (-)

A_{Lf} cross-sectional area of the liquid film in front of the slug (m^2)

$\widetilde{D}_L$ dimensionless hydraulic liquid diameter (-)

$\widetilde{h}_L$ dimensionless height (-)

$\dot{m}$ mass velocity (kg/s)

$\widetilde{S}$ dimensionless wetted perimeter (-)

$\dot{V}_G$ net gas volumetric flow rate per unit area (m/s)

$\dot{V}_L$ net liquid volumetric flow rate per unit area (m/s)

B_o distribution parameter of Zuber and Findlay (1965)

C wave propagation velocity(m/s)

C_R real part of the wave velocity (m/s)

Ca_{Mix} the capillary number (Ooi, 2002)

C_0 distribution parameter for bubble velocity (Nicklin et al., 1962)

f friction factor

f_{wG} friction factor between the gas and the pipe wall (-)

f_{wL} friction factor between the liquid and the pipe wall (-)

f_i friction factor between the liquid and the gas (-)

F dimensionless liquid frequency (-)

Fr Froude number (-)

Fr_c critical Froude number - Bendiksen (1984)

Fr_G gas Froude number in Taitel and Dukler (1977) model

Fr_s Froude number evaluated using the liquid velocity within the liquid slug (-)

Fr_{T-D} Taitel and Dukler parameter

f_s friction factor in the slug body (-)

f_{Mix} two-phase friction factor (-)

h height (m)

$\overline{h}_G$ mean height of the gas phaseis

H rectangular channel height (m)

h_{Lf} liquid film height immediately in front of the slug (m)

k wave number

K_{K-R} Kordyban and Ranov (1970) transition coefficient - Eqn. 2.170

$K_{S(T-D)}$ Taitel and Dukler parameter

K_{S-I} stratified to intermittent transition coefficient

Ku Kutateladze number

l length (m)

l_f film length (m)

l_s slug length (m)

l_u slug unit length (m)

$\dot{M}_L$ liquid mass flow rate (kg.m/s)

$\dot{M}_L$ liquid pick up mass flow rate (kg.m/s)

N_{μ} ratio of viscous and gravitational force (Gokcal et al., 2009)

p pressure (N/m^2)

Re Reynolds number (-)

Re_s Reynolds number in the slug body (-)

S wetted perimeter (m)

s_{T-D} sheltering coefficient

t time (s)

T temperature (K)

T_{T-D} Taitel and Dukler parameter - Eqn. 2.48 (Taitel and Dukler, 1976)

U superficial velocity (m/s)

u_b velocity of dispersed bubbles in liquid slug (m/s)

u_d drift velocity (m/s)

$\overline{u}_{GStr}$ average gas velocity in the stratified layer (m/s)

$\overline{u}_{LStr}$ average liquid velocity in the stratified layer (m/s)

$\overline{u}_a$ average of the velocities of the two phases (m/s)

$u_{Lbubble}$ average velocity of liquid droplets in elongated bubble (Bendiksen and Espedal, 1992)

u_{Lf} liquid velocity in the film region immediately in front of the slug (m/s)

u_{Ls} liquid velocity within the slug body (m/s)

u_{M0} limiting velocity (m/s) (Andreussi and Bendiksen, 1989)

u_{Mf} limiting velocity (m/s) (Andreussi and Bendiksen, 1989)

U_{mix} mixture velocity (m/s)

U_T translational velocity of the slug (m/s)

V_{T} net loss rate of small bubbles at the slug tail (-) (Andreussi & Bendiksen, 1984)

V_{F} the net entrainment rate at the slug front (-) (Andreussi & Bendiksen, 1984)

V_{PR} bubble production rate (-) (Andreussi & Bendiksen, 1984)

V_{PB} small bubble shedding rate to elongated bubble (-) (Andreussi & Bendiksen, 1984)

V_W wave crest velocity

We Weber number

X_{L-M} Lockhart and Martinelli parameter (-)

Greek symbols:

ε holdup (-)

ε_G volume fraction of gas (-)

ε_{Ghog} volume fraction of gas in homogeneous void fraction model (-)

ε_{Gsep} volume fraction of gas in separated void fraction model (-)

η wave profile (-)

$\varepsilon_{Lbubble}$ volumetric fraction of liquid droplets in elongated bubble (Bendiksen and Espedal, 1992)

ε_{LEmod} modified stratified equilibrium liquid holdup (-) (Hill and Wood, 1994)

$\varepsilon_{\mathrm{Ls}}$ liquid holdup in the slug body (-)

$\varepsilon_{\mathrm{Gs}}$ gas holdup in the slug body (-)

ε_{Lfilm} average liquid holdup in an aerated film (Bendiksen et al., 1996)

α input liquid fraction (-)

λ_B Fluid property correction factor – Eqn. 2.3 (Baker, 1954)

μ dynamic viscosity (Ns/ m^2)

μ_{LB} reference dynamic viscosity (Baker, 1954)

ν_s slug frequency (slugs/s)

θ pipe inclination degree

ρ density (kg/m^3)

ρ_{LB} reference liquid density (Baker, 1954)

σ surface tension (N/m)

σ_B reference surface tension (Baker, 1954)

τ shear stress (N/m2)

τ_s fluid-wall shear stress in the slug body (N/ m^2)

υ_G relative gas velocity (m/s)

υ_L relative liquid velocity (m/s)

ψ_B fluid property correction factor – Eqn. 2.4 (Baker, 1954)

Subscripts:

SL superficial liquid

G gas

Gf gas properties within the film region

Gs gas properties within the slug body

Gu Gas properties within the slug unit

L liquid

Lf liquid properties within the film region

Ls liquid properties within the slug body

Mix mixture

s Properties evaluated for the slug body

u Properties evaluated for the entire slug unit

Chapter 1

Introduction

1.1 Summary

This chapter begins with a general introduction to multiphase flow and a discussion of its industrial significance. Two-phase gas-liquid flow is then introduced, stressing its importance, the conditions at which it is likely to occur, and the physical forms it takes (namely the "flow patterns"). Slug flow is then discussed, emphasizing its central position in gas-liquid systems. Having presented the causes of slug flow, the consequences of slug flow are then discussed. Based on this discussion, the main aims and objectives of the work studied in this thesis are stated. Finally, a brief summary of each chapter is presented together with details of how they contribute to the work as a whole.

1.2 Introduction to multiphase flow

Multiphase flow is the simultaneous flow through a pipe or a channel of two or more phases. These phases can be any combinations of gas, miscible liquid, immiscible liquid or solids. Multiphase flow occurs in oil and natural gas reservoirs, and in many cases of hydrocarbon production such as in oil wells, in pipelines from wellheads to separators, from process equipment to the exporting terminals. Multiphase transportation in pipelines becomes more critical since oil and gas companies are increasingly operating in harsher and more remote environments. Thus the design of pipelines has to be carefully carried out to withstand extreme conditions of pressure, flow surges, so that they can be operated safely in adverse situations. Therefore, it is important to investigate the behaviour of multiphase flow within pipelines to ensure a safe design of the transportation process.

Multiphase flows can be classified in terms of various characteristic phase distributions known as "flow patterns" or "flow regimes". The regions of existence of these regimes

depend on the flow rate of the two phases, the fluid properties and the configuration of the pipeline system. The classification of the phase distributions is introduced in the next section.

1.3 Gas-liquid flow patterns

The present work is principally concerned with gas-liquid two-phase flows. Several forms of interfacial distributions, known as "flow regimes" or "flow patterns" can be observed in gas-liquid flow. The classifications can be done in various ways; horizontal gas-liquid flow is traditionally classified into six flow patterns as illustrated in Figure 1.1 and described as follows.

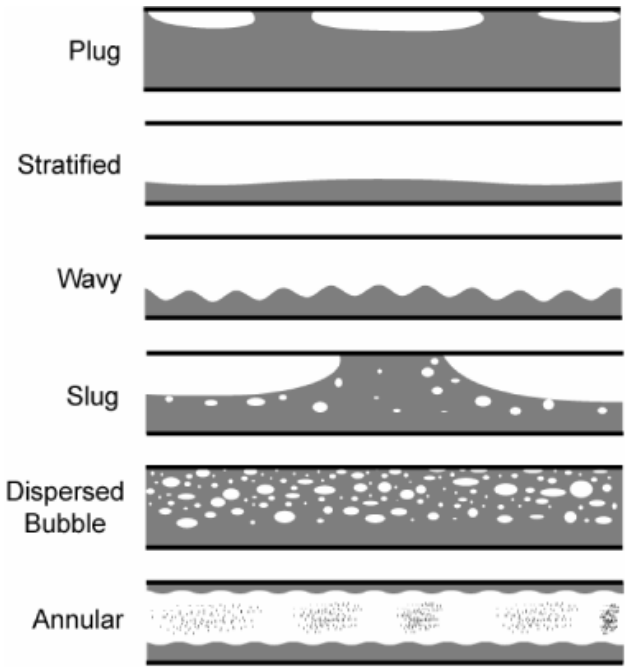

Figure 1.1: Flow regimes in horizontal multiphase flows.

- **Separated flows** (continuous gas and liquid phase)

  a) Stratified flow: The liquid flows along the bottom of the pipe and the gas flow above. The gas-liquid interface is smooth.

  b) Stratified wavy flow: An increase in gas velocity causes the formation of waves on the stratified interface.

- **Intermittent flows** (discontinuous gas or liquid phase)

a) Plug flow: Liquid flowing in the bottom of the pipe, whereas elongated bullet-shaped gas and plugs of liquid alternate along the upper part of the pipe

b) Slug flow: When the growing waves bridges the top of pipe, liquid slugs form and fill the entire pipe section, alternating with dispersed flow. When the gas velocity is increased, aeration takes place at the slug front. The liquid slugs move at a velocity greater than the average liquid velocity.

- **Dispersed flows** (continuous liquid phase, gas phase discontinuous)

a) Dispersed bubble flow: Dispersed bubbles flow along top of the pipe in a continuous flow of liquid. The bubbles move along the pipe at approximately the same velocity as the liquid.

b) Annular flow: The liquid is distributed as an annulus around the pipe periphery. The gas flowing in the centre of the pipe, with some liquid entrained as small droplets.

1.4 Introduction to slug flow

Slug flow is a common flow regime in multiphase flow and the most common one in hydrocarbon transportation. As mentioned above, this flow regime is characterised by the passage of liquid-continuous zones (slugs) along the channel, separated by large gas bubble zones. In the slugs, the liquid phase is continuous but the slug may contain a dispersion of smaller bubbles; these bubbles are entrained at the slug front and are discharged continuously at the slug tail. In the large gas bubble regions, liquid discharged from the slug tail may flow as a stratified layer along the bottom of the gas bubble region before joining the next slug front.

Slug flow is a highly complex flow which is inherently unsteady. Even though the liquid and gas flow rate remain steady, the component mass flow rates, phase velocities and pressure, at any pipeline cross section, exhibit large variation with respect to time. As a result, processes such as heat and mass transfer are unsteady. Moreover, the intermittent nature of slug flow causes vibrations and a high pressure drop along the pipe. This increases the chance of

damaging the pipe supports and bend, and of erosion-corrosion of the pipe if the flow contains sand. Further downstream, slug flow may cause problems for the control of separation equipment, which requires large pre-separation stage vessels called "slug catchers" to safely collect the slugs.

Horizontal slug flow can be classified into three different groups:

- Hydrodynamic slugs: These are caused by instability of waves on the gas-liquid interface in stratified flow; the wave grows on the interface to a height sufficient to bridge the pipe. Initially, the hydrodynamic slugs are relatively short; however, the slugs can coalesce to form long slugs. Hydrodynamic slugging is difficult to prevent since it occurs over a wide range of flow conditions.
- Terrain-induced slugs: These are caused by accumulation and periodic purging of liquid in dips along the pipeline. Liquid tends to accumulate at the lowest points of the flow line until the pressure upstream of this accumulation becomes sufficient to push the liquid onwards through the rest of the pipe. An extreme case of terrain induced slugging occurs when a slightly downwards inclined flow line is connected to a vertical riser which connects the flow line to the platform-mounted separator. The large flow surges associated with severe slugs can cause serious operational problems for topside equipment such as separators and compressors.
- Operationally-induced slugs: These are caused by operational transients. For instance, at the start up, the accumulated liquid exits the pipeline as slugs. Pigging of a pipeline causes most of the liquid inventory to be pushed from the lines as a liquid slug ahead of the pig. Such operational slugs can also occur if the flow is stratified and the gas flow rate is increased, a slug or train of slugs may be formed near the entrance which grows by picking up the previously existing thicker liquid layer ahead of the slug.

The predominance of the slug flow regime and its possible adverse implications necessitate accurate predictions of slug flow characteristics; various codes have therefore been developed to model slug flow.

1.5 Project objectives

The overall aim of the present project was to carry out analytical and computational studies to model the processes of slug initiation, growth and collapse in horizontal pipes. Specific objectives associated with this overall aim are:

- To carry out a validation exercise involving the prediction of a benchmark case of slug initiation and evolution using various computational fluid dynamics (CFD) codes.

- To use the validation CFD tool to study slug flow evolution and characteristics in channels of rectangular cross-sections.

- To employ a "slug-capturing" method embedded within a one-dimensional code, TRIOMPH, to study the effect of inlet conditions on slug flow characteristics.

- To collect data on two-phase slug flow characteristics in horizontal pipes and to analyse previously unpublished data, gathered under complementary conditions, on the Imperial College WASP facility with a view to assessing the influence of inlet geometry on slug evolution.

1.6 Summary of subsequent chapters

In what follows, a literature review is presented in Chapter 2. In this chapter, the various models of flow pattern maps for two-phase horizontal flow are considered first together with the primary design parameters, pressure gradient and void fraction, thus establishing the conditions for the presence of slug flow. Next, the literature on slug flow is covered; this is divided into three main parts: slug initiation, slug growth and fully-developed slug flow.

In Chapter 3, CFD results are presented from a benchmark study of slug flow experiments conducted using the Imperial College WASP facility by Ujang (2003). Six different CFD codes have been used in this validation study, including TRIOMPH, FLUENT, STARCD, LedaFlow, TransAT, CFX, STAR-CCM+. Experimental data, such as time traces of liquid

hold-ups and slug frequency at various probe locations, are provided as reference for comparisons against the simulations.

Chapter 4 describes the numerical evolution of slug flow characteristics based on a one-dimensional "slug-capturing model" which forms the basis of the TRIOMPH code. Slug frequency predictions with both steady and unsteady inlet conditions are presented. A slug tracking code (developed by Ujang, 2003) was employed to obtain a train of slugs which then be fed into the TRIOMPH code, results are illustrated.

Chapter 5 presents a three-dimensional numerical study of slug flow evolution in a rectangular channel, using the commercial CFD code STAR-CCM+. The experimental data was provided by Forschungszentrum Dresden-Rossendorf (FZD). The test section is 8m long acrylic glass with a rectangular cross-section of 100 mm×30 mm (height×width). The slug evolution mechanisms are captured by the numerical simulation and qualitatively good agreement with the experimental data is demonstrated.

Chapter 6 describes the experimental apparatus and procedures used in the experiments that were performed on the LOWPRESS rig, with special attention given to instrumentation such as the high-speed video photography and conductivity probes. Design details of the alternative inlet arrangements used on the LOWPRESS rig are also provided.

Chapter 7 describes a series of horizontal air-oil and air-water slug flow experiments performed on the LOWPRESS rig. The mechanism of slug initiation with different types of inlet arrangements and the subsequent development of slugs is discussed. A brief description of the WASP facility and previously unpublished data on horizontal slug flow are provided; the key parameters such as slug frequency and holdup are analysed and compared with TRIOMPH predictions.

Chapter 8 summarises the contribution of each chapter in reaching the overall objective. The main conclusions of each section are stated and areas for further work are recommended.

Chapter 2

Literature review

2.1 Summary

This chapter considers the prediction of gas-liquid flow behaviour in general terms, with particular emphasis on the literature associated with the slug flow. First, the work on flow patterns is reviewed in Section 2.2; this is relevant to delineate the conditions over which slug flow occurs. Section 2.3 deals with slug flow modelling: the mechanisms of slug flow evolution are introduced in Section 2.3.1 and the interfacial instabilities from which slugs arise in Section 2.3.2. Section 2.3.3 introduces the models which have been reported in the literature for steady-state, fully-developed flow, including the so-called "unit cell" model. These models need supplementary closures; hence, closure relationships for slug flow are reviewed in Section 2.3.4. The intermediate stage between slug initiation and steady-state slug flow are reviewed in Section 2.3.5.

2.2 Flow pattern maps

In order to establish the conditions at which each flow regime occurs, large amounts of data on multiphase flow patterns have been collected from previous studies and these data have been mapped using a wide variety of empirical and semi-empirical models. Typically, empirical flow pattern maps are constructed by plotting experimental data using dimensionless groups, superficial phase velocities, mass fluxes, qualities or momentum fluxes as coordinate axes. In these maps, various two-phase flow regimes are presented in the form of regions divided by transition lines.

The flow pattern maps available in literature were first developed for the petrochemical industry (Baker, 1954) for flow of oil and gas in large diameter pipes, this is shown in Figure 2.1. Baker took into account the effects of fluid physical properties by using fluid property correlation factors λ_B and ψ_B, which are used to enable the predominantly atmospheric air-water data to be applied to other systems. These factors are given by:

$$\lambda_B = \left[\left(\frac{\rho_G}{\rho_{GB}} \right) \left(\frac{\rho_L}{\rho_{LB}} \right) \right]^{1/2} \qquad [2.1]$$

$$\psi_B = \frac{\sigma_B}{\sigma} \left[\left(\frac{\mu_L}{\mu_{LB}} \right) \left(\frac{\rho_{LB}}{\rho_L} \right)^2 \right]^{1/3} \qquad [2.2]$$

where ρ_L, ρ_G are the liquid and gas density, σ is the surface tension, μ_L is the dynamic viscosity of the liquid. The reference values are σ_B = 0.073 N/m, μ_{LB} = 1.0 × 10 Ns/ m^2, ρ_{LB} = 997.9 kg/ m^3 and ρ_{GB} =1.201kg /m^3 so that both λ_B and ψ_B are equal to 1 for an air-water system at atmospheric pressure. Baker (1954) divided his map into the stratified, wavy, slug, plug, annular, dispersed and bubble (or froth) flow regions and produced transition lines on a plot of $\dot{m}_G / \lambda_B$ versus $\dot{m}_L \lambda_B \lambda_B / \dot{m}_G$. In the plot the gas mass velocity $\dot{m}_G$ is given by:

$$\dot{m}_G = \rho_G U_{SG} \qquad [2.3]$$

the liquid mass velocity $\dot{m}_L$ is given by:

$$\dot{m}_L = \rho_L U_{SL} \qquad [2.4]$$

where U_{SL} and U_{SG} are respectively the superficial liquid and superficial gas velocities.

Later studies showed that the Baker map was incapable of representing the effects of various parameters which could be expected as it did not take into consideration pipe diameter effects. This had led to the development of alternative transition maps. Scott (1964) modified the Baker map by illustrating the transitions between regimes as regions rather than lines to show levels of uncertainty, as shown in Figure 2.1; Scott (1964) also excluded the transition line between annular and dispersed flow previously due to Baker (1954). Furthermore, in the following years, the limitations of Baker map were further highlighted when it was also shown to be incapable of handling a wide range of system parameters: as the ordinates were not dimensionless, the map could not be applied universally. The map also does not account for a number of interacting forces in two-phase flow such as gravity and surface tension.

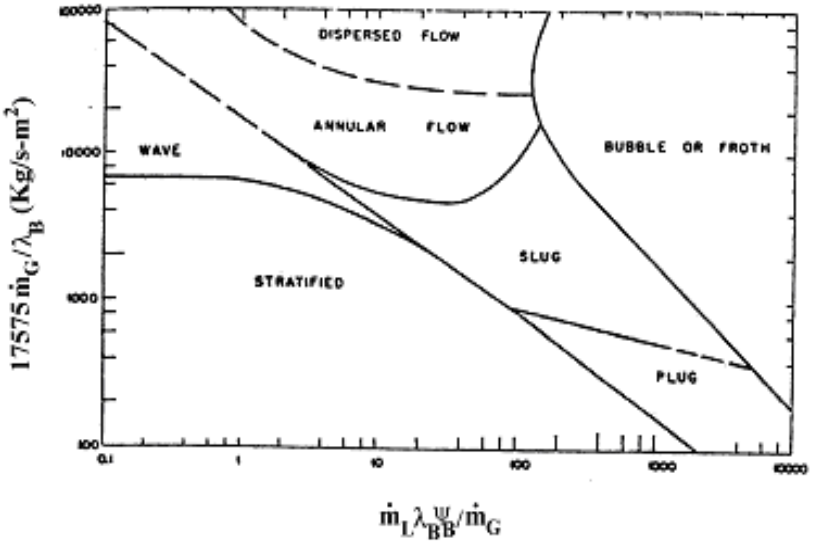

Figure 2.1: Flow pattern map of Baker (1954), modified by Scott (1964).

Beggs & Brill (1973) tried to simplify their maps by considering only three regimes: 'separated' (stratified, wavy and annular), 'intermittent' (plug and slug) and 'dispersed' (bubbly flow). However, their map was based on a system of fixed properties and failed to account for density, viscosity and interfacial tension variation. Moreover, the transition lines

are 'best-fit' and are only applicable to systems similar to those on which they were obtained. Mandhane (1974) used 5935 flow pattern observations from the University of Calgary Multiphase Pipe Flow Data Bank to generate a basic flow pattern map of superficial gas velocity versus superficial liquid velocity, as shown in Figure 2.2. The map was based on air-water flow data and was divided into five regimes: stratified wavy, elongated bubble, slug, dispersed and annular. Despite its limitation in being a purely correlational approach, it was constructed using a comparatively large database (approximately 6000 observation points) and provided a better prediction over a wider range of conditions than the Beggs & Brill (1973) map.

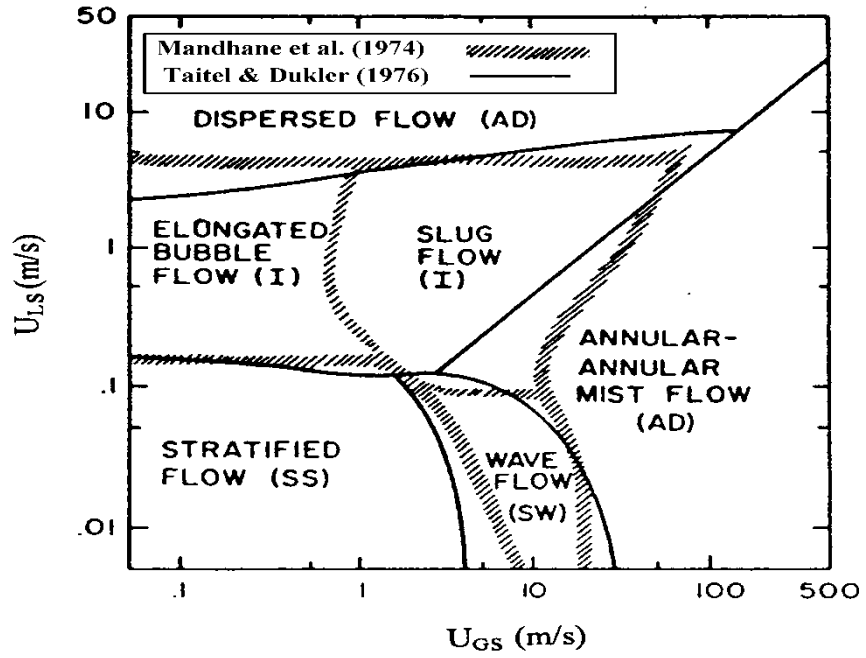

Figure 2.2: Flow pattern maps of Mandhane (1974) and Taitel & Dukler (1976).

It is not possible to represent all the appropriate transitions in terms of a single set of parameters; for instance, there is a need to predict flow patterns at higher system pressures and for larger diameter pipes than those covered by existing data bases. Thus, there is a requirement for more generalized methods. In response to this requirement, Taitel & Dukler (1976) developed a semi-theoretical description of flow regime transitions. This approach starts with a solution (for stratified flow) of one-dimensional steady state separated flow models. They ignored the effects of acceleration and hydraulic gradient in the liquid phase and

combined the two momentum equations by eliminating the pressure gradient. Assuming that the liquid layer is of constant height, with a smooth gas-liquid interface, and that the interfacial shear term is equal to the gas-wall shear term, they then derived a non-dimensional form of this combined momentum balance given by:

$$X_{L-M}{}^2(\tilde{u}_L\tilde{D}_L)^{-n}\tilde{u}_L^2\frac{\tilde{S}_L}{\tilde{A}_L}-(\tilde{u}_G\tilde{D}_G)^{-m}\left(\frac{\tilde{S}_L}{\tilde{A}_L}+\frac{\tilde{S}_G}{\tilde{A}_G}+\frac{\tilde{S}_I}{\tilde{A}_G}\right)-4Y_{L-M}=0 \quad [2.5]$$

where:

$$\tilde{A}_L=A_L/D^2=0.25\left\{\pi-\cos^{-1}\left[2\tilde{h}_L-1\right]+\left[2\tilde{h}_L-1\right]\sqrt{\left(1-\left[2\tilde{h}_L-1\right]^2\right)}\right\} \quad [2.6]$$

$$\tilde{A}_G=A_G/D^2=0.25\left\{\cos^{-1}\left[2\tilde{h}_L-1\right]-\left[2\tilde{h}_L-1\right]\sqrt{\left(1-\left[2\tilde{h}_L-1\right]^2\right)}\right\} \quad [2.7]$$

$$\tilde{S}_L=S_L/D=\left[\pi-\cos^{-1}\left(2\tilde{h}_L-1\right)\right] \quad [2.8]$$

$$\tilde{S}_G=S_G/D=\pi-\tilde{S}_L \quad [2.9]$$

$$\tilde{S}_I=S_I/D=d\tilde{A}_L/d\tilde{h}_L=\sqrt{\left(1-\left[2\tilde{h}_L-1\right]^2\right)} \quad [2.10]$$

$$\tilde{u}_L=u_L/U_{SL}=\tilde{A}/\tilde{A}_L=\pi/(4\tilde{A}_L) \quad [2.11]$$

$$\tilde{u}_G=u_G/U_{SG}=\tilde{A}/\tilde{A}_G=\pi/(4\tilde{A}_G) \quad [2.12]$$

$$\tilde{h}_L=h_L/D \quad [2.13]$$

$$\tilde{D}_L=4\tilde{A}_L/\tilde{S}_L \quad [2.14]$$

$$\tilde{D}_G=4\tilde{A}_G/\left(\tilde{S}_G+\tilde{S}_I\right) \quad [2.15]$$

where h_L is the liquid height, A *is* the cross-sectional area, S is wetted periphery, u is the actual phase velocity. The subscripts G, L and, I refer to gas phase, liquid phase and interface respectively. D_L, D_G are the the equivalent diameters for the gas and liquid phases. n and m are respectively the coefficients used in the liquid and gas phase Blasius friction factor expressions. For a laminar liquid flow, n = 1, and laminar gas flow, m = 1, while for a turbulent liquid flow, n = 0.2, and turbulent gas flow, m = 0.2. $X_{L\text{-}M}$ is the Lockhart-Martinelli (1949) parameter which represents the ratio of the pressure gradients for the two phases, and $Y_{L\text{-}M}$ is an inclination parameter:

$$X_{L-M} = \left[\frac{\left(dp/dx \right)_{SL}}{\left(dp/dx \right)_{SG}} \right]^{1/2} \qquad [2.16]$$

$$Y_{L-M} = \frac{(\rho_L - \rho_G) g \sin \beta}{\left| \left(dp/dx \right)_{SG} \right|} \qquad [2.17]$$

$$\left(\frac{dp}{dx} \right)_{SL} = \frac{4 f_L}{D} \frac{\rho_L U_{SL}^2}{2} \qquad [2.18]$$

$$\left(\frac{dp}{dx} \right)_{SG} = \frac{4 f_G}{D} \frac{\rho_G U_{SG}^2}{2} \qquad [2.19]$$

$$\mathrm{Re}_L = \frac{\rho_L U_{SL} D}{\mu_L} \qquad [2.20]$$

$$\mathrm{Re}_G = \frac{\rho_G U_{SG} D}{\mu_G} \qquad [2.21]$$

where f_L, f_G and are the liquid-wall, gas-wall friction factors respectively, Re_L, Re_G are the Reynolds number for the liquid and gas phase, U_{SL}, U_{SG} are the superficial velocities for the liquid and gas phase.

Taitel & Dukler (1976) then developed semi-empirical models for the transitions in terms of h_L/D for specified values of $X_{L\text{-}M}$ and $Y_{L\text{-}M,}$ and these transitions could then be also expressed in terms of three groups of dimensionless quantities:

$$Fr_{T-D} = U_{SG}\left[\frac{\rho_G}{gD(\rho_L - \rho_G)\cos\beta}\right]^{1/2} \quad [2.22]$$

$$T_{T-D} = \left[\frac{\left(dp/dx\right)_{LS}}{(\rho_L - \rho_G)g\cos\beta}\right]^{1/2} \quad [2.23]$$

$$K_{S(T-D)} = U_{SG}\left[\frac{\rho_G}{gD(\rho_L - \rho_G)\cos\beta}\right]^{1/2}\left[\frac{\rho_L U_{SL} D}{\mu_L}\right]^{1/2} = Fr_{T-D}\left(\mathrm{Re}_L\right)^{1/2} \quad [2.24]$$

For transition from stratified to intermittent or annular flow:

$$Fr_{T-D}^2\left[\frac{1}{\left(1-\tilde{h}_L\right)^2}\frac{\tilde{u}_G^2 d\tilde{A}_L/d\tilde{h}_L}{\tilde{A}_G}\right] \geq 1 \quad [2.25]$$

For transition from stratified smooth to stratified wavy flow:

$$K_{S(T-D)} \geq \left[\frac{2}{\tilde{u}_G\sqrt{\tilde{u}_L}\sqrt{\tilde{S}_{T-D}}}\right] \quad [2.26]$$

where S_{T-D} is a sheltering coefficient and S_{T-D} = 0.01.

For transition from intermittent to dispersed bubble flow:

$$T_{T-D}^2 \geq \left[\frac{8\tilde{A}_G}{\tilde{S}_I\tilde{u}_L^2\left(\tilde{u}_L\tilde{D}_L\right)^{-n}}\right] \quad [2.27]$$

and for transition from intermittent to annular flow:

$$\tilde{h}_L < 0.5 \qquad [2.28]$$

In Figure 2.3, these transition lines are shown as a function of h_L/D for a general system.

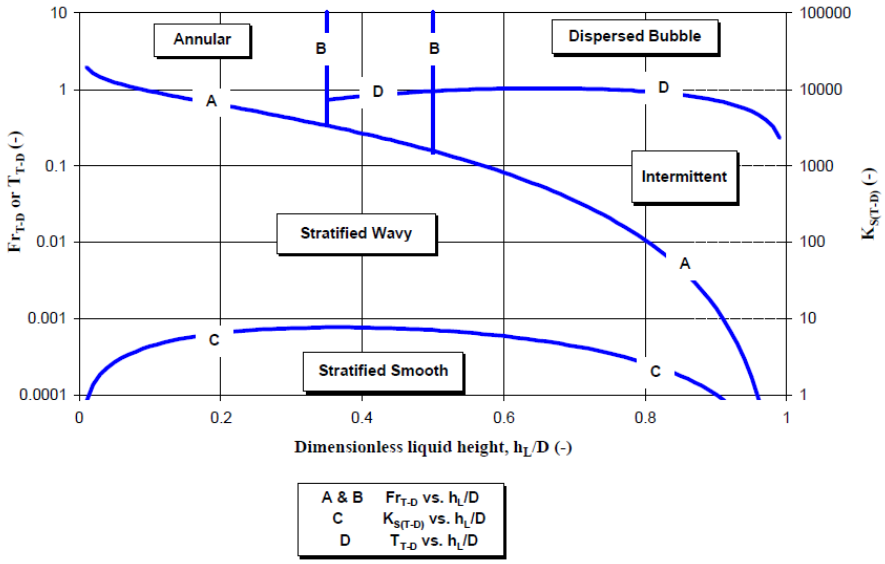

Figure 2.3: The Taitel & Dukler (1976) flow pattern map in dimensionless form.

Together with a holdup plot, such as the one shown in Figure 2.1, flow patterns can be readily determined for specified gas and liquid feed rates of known pipe diameter and inclination. However, the effect of pipe roughness and interfacial shear are not properly accounted for and the transition criterion for intermittent to annular flow is rather arbitrary. Figure 2.2 shows a comparison of the Taitel and Dukler (1976) and Mandhane (1974) maps for horizontal air water flows. There is good agreement for this case [which is not surprising since the Mandhane results were used to calibrate the Taitel and Dukler (1976) representation] but it should be recalled that the Taitel and Dukler (1976) map can, in principle, be used for any arbitrary set of physical properties.

Weisman *et al*. (1979) set out to provide a method to account for differences in fluid properties as well as various pipe diameters. They aimed to carry out the study in such a way that changing one fluid property would not significantly affect other fluid properties. The

pipe diameters used in the study were 0.012, 0.025 and 0.051m and a wide range of fluid velocities was examined. In their map, they included the stratified smooth, stratified wavy, intermittent, annular and dispersed regimes. The intermittent region combined slug and plug flow as well as the dispersed region. Consequently, the transitions proposed were those for stratified smooth to stratified wavy flow, separated to intermittent flow, the transition to dispersed flow and the onset of annular flow. When these transition lines are compared to those proposed by Mandhane (1974) and Taitel & Dukler (1976) the most notable feature is the annular-intermittent boundary, which exhibits an opposite trend to their predictions. Weisman *et al.* (1979) proposed a number of dimensionless correlations for the flow regime transitions; the transition boundary for stratified smooth to stratified wavy flow is given by:

$$\left[\frac{\sigma}{(\rho_L-\rho_G)gD^2}\right]^{0.20}\left[\frac{\rho_G U_{SG} D}{\mu_G}\right]^{0.45} = 8\left(\frac{U_{SG}}{U_{SL}}\right)^{0.16} \qquad [2.29]$$

the separated-intermittent transition is given by:

$$(\mathrm{Fr}_G)^{1/2} = 0.25\left(\frac{U_{SG}}{U_{SL}}\right)^{1.1} \qquad [2.30]$$

the transition to dispersed flow is given by:

$$\left[\frac{(dp/dx)_{SL}}{(\rho_L-\rho_G)g}\right]^{0.5}\left[\frac{\sigma}{(\rho_L-\rho_G)gD^2}\right]^{-0.25} = 9.7 \qquad [2.31]$$

and the transition to annular flow is given by:

$$1.9\left(\frac{U_{SG}}{U_{SL}}\right)^{1/8} = Ku_G{}^{0.2}\mathrm{Fr}_G{}^{0.18} \qquad [2.32]$$

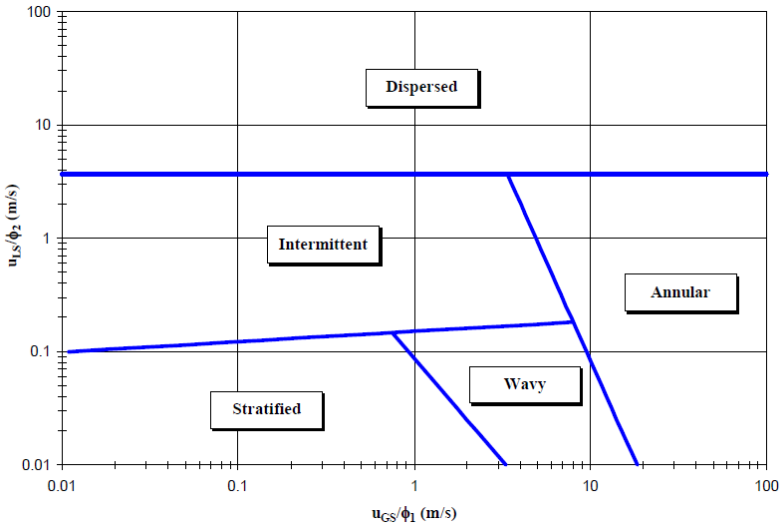

Figure 2.4: The flow pattern map of Weisman et al. (1979).

Based on the Taitel & Dukler (1976) transition criteria, Barnea (1987) proposed a comprehensive model that can predict the steady-state transition boundaries for the whole range of pipe inclinations. The flow pattern map is slightly different from that proposed by Taitel & Dukler (1976) . Figure 2.5 shows the Barnea map calculated for air-water flow at 1 bar pressure in the WASP facility.

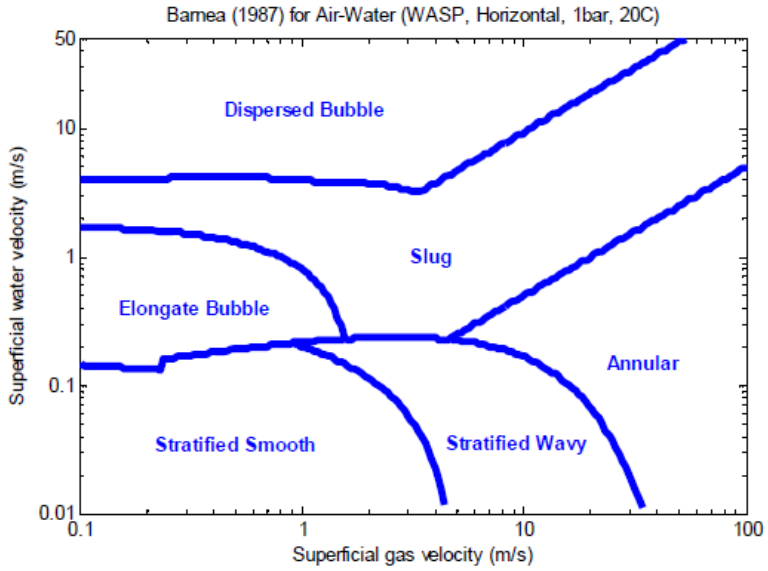

Figure 2.5: The flow pattern map of Barnea (1987) applied to WASP air-water system with test section on horizontal configuration.

Zhang et al. (2003a) develops a unified model for gas-liquid flow to predict flow pattern transition at the pipe inclination from -90° to 90°. All the flow patterns they discussed are grouped into three categories, bubble and dispersed flow, elongated bubble, slug and churn flows, and stratified and annular flow. A series of experimental measurements have been employed to compare with the model prediction and found the model provided a good prediction for horizontal and upward inclined flow. For a steep downward flow discrepancies are at the region of unstable stratified and annular flow.

Xu *et al*. (2007) presented the results of an extensive study of flow regime transitions for air/non-Newtonian shear-thinning fluid systems using 10m long, 20-60 mm diameter tubes inclined at various angles; for shallow inclinations, their measurements were in good agreement with the Barnea (1987) flow pattern maps.

2.3 Slug flow modelling

Due to the wide occurrence of slug flow in industry, a vast amount of work has been dedicated to the understanding and prediction of the stratified-intermittent transition in horizontal and near horizontal pipes. The following sections include the experimental observations of slug generation from stratified flows, the Kelvin-Helmholtz instability theory which is commonly used to account for the wave growth, and other existing theories for wave generation. Then the discussion continues to the fully-developed, steady-state slug flow models, in particular the "Unit Cell" models and the proposed empirical correlations for them. The supplementary relationships (slug translational velocity, dispersed bubbles velocity, slug length, slug frequency and slug body holdup) associated with the slug flow properties will then be discussed. Finally, the models account for the developing slug flow will be reviewed.

2.3.1 Evolution of slug flow

Initially, at the inlet, the flow in a pipe is stratified with a liquid layer flowing at the bottom and gas above it; the liquid layer experience shear forces due to the wall and starts to decelerate. As the liquid velocity decreases, waves begin to form on the gas-liquid interface with a distribution of wavelengths and growth rates. The amplitude of certain waves increases eventually leading to bridging of the pipe and the formation of a blockage known as a 'slug

precursor'. This blocks the flow of gas and causes the pressure upstream of the slug precursor to build up, accelerating the latter downstream. The fast-moving slug precursor picks up the slow-moving liquid ahead of it and sheds it behind it, leading to the formation of the liquid film region which is terminated by the next precursor. The slug precursor grows in volume to form a 'slug'. The slug has a larger kinetic energy than the liquid film ahead of it, leading to the creation of a region of relatively high turbulence activity at the slug front, which forms a mixing vortex and results in the entrainment of gas. Some of the gas bubbles will be dispersed at the top of the slug due to buoyancy, some of the entrained bubbles are released back into gas phase at the tail of the slug, and some will also be released along with the liquid into the film region behind the tail. Ultimately, the slug approaches a steady, fully-developed state in which the shedding and pickup rates are equal, as shown in Figure 2.6.

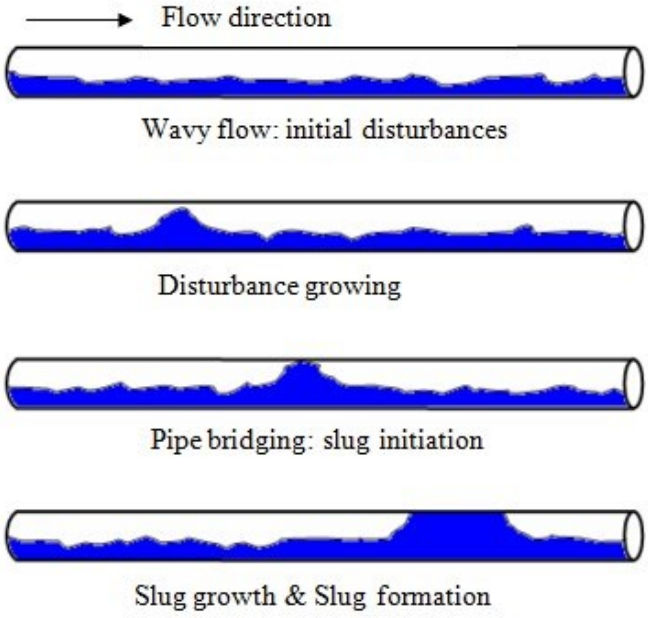

Figure 2.6: Transition of slug flow from stratified flow.

2.3.2 Wave Growth Analysis – Slug Flow Initiation

The manner by which slugs are formed is of considerable importance for predicting the conditions for slug initiation as well as the frequency of slugging. Several visual observations have provided some understanding of the physical mechanisms that lead to the onset of slugging (Andritsos *et al*., 1989; Fan *et al*., 1993). The first disturbances to appear on the interface are usually very small sinusoidal waves, which suddenly give rise to a large-

amplitude wave that bridges the pipe and forms a slug. Sometimes a few large-amplitude waves coalesce with one another resulting in a longer wave before a slug is formed. Kordyban (1985), Davies (1992), Hale (2000) and Ujang *et al*. (2006), amongst others, presented images of the development of large-amplitude waves into slugs. The images show the development of small-amplitude waves on the crest of the large wave, just before the wave bridges the pipe. Those researchers have considered slug initiation to occur when a wave becomes large enough to bridge the pipe cross-section. Most attempts at modelling this phenomenon have used some form of stability analysis to examine the conditions necessary for wave growth.

2.3.2.1 Kelvin-Helmholtz Instability Criterion

When the waves occur at the gas-liquid interface, the gas phase velocity varies throughout the wave with a maximum at the peak and a minimum at the trough. There exists also a pressure variation within the gas over the wave profile with a maximum at the trough and a minimum at the crest which causes an aerodynamic lift in the wave presenting a destabilising effect. The pressure variation includes a component that is 180° out of phase with the wave and one that is in phase with the wave slope. When the destabilising effects from the pressure variations of the gas phase and of liquid inertia overcome the surface tension and gravity stabilising effects, the waves increase in amplitude rapidly, this is so called the Kelvin-Helmholtz (K-H) instability.

Ishii (1982) discussed the applicability of a criterion based on the Kelvin-Helmholtz (K-H) instability for the prediction of wave formation depending on the stability of the two-phase fluid interface. Considering the flow of a gas phase over a liquid phase in a horizontal channel, where the phases flow at velocities u_L and u_G with densities ρ_L and ρ_G for the respective phases, an analysis of the interface was performed to derive the propagation velocity, C, for the surface waves and it follows that:

$$C = \frac{\rho_L u_L + \rho_G u_G}{\rho_L + \rho_G} \pm \left[C_\infty^2 - \rho_L \rho_G \left(\frac{u_L - u_G}{\rho_L + \rho_G} \right)^2 \right]^{0.5} \qquad [2.33]$$

where

$$C_{\infty}^{2} = \frac{g}{k}\frac{\rho_L - \rho_G}{\rho_L + \rho_G} + \frac{\sigma k}{\rho_L + \rho_G} \qquad [2.34]$$

k is the wave number and σ is the surface tension. The instability criterion is then:

$$\frac{g}{k}\frac{\rho_L - \rho_G}{\rho_L + \rho_G} + \frac{\sigma k}{\rho_L + \rho_G} < \rho_L \rho_G \left(\frac{u_G - u_L}{\rho_L + \rho_G}\right)^2 \qquad [2.35]$$

The three forces governing the stability of waves on the interface include gravity, surface tension, and relative motion. Bernoulli's principle accounts for the effect of pressure on the relative motion of the wave. If $\rho_L > \rho_G$, the gravity factor tends to stabilise the system. The surface tension force always acts towards stabilising the system while the relative motion between the two phases always destabilises the system. If the viscosity difference between the two fluids is very large (e.g. for air-water flows, which are widely studied in the literature), this analysis has been found to fail (McCready, 1989).

2.3.2.2 Studies of Slug Flow Initiation and Mechanisms

In general, the initiation of slug flow is modelled by either the classical K-H long-wave (i.e. waves with small wave number, k) instability, or from other wave generation theories. The prominent slug initiation mechanism studied in literature can be grouped into four categories, as discussed below.

Group I

The first of these groups analysed the K-H instability as the underlying principle for the wave formation using wave motion theories. The K-H instability was first used as a rationale in the description of slug flow initiation by Kordyban & Ranov (1970). The transition to slug flow was described as a K-H instability of stratified flow where the gradual formation and growth of waves and ripples give rise to slugs within the channel. By making the assumptions that surface tension effects are negligible, $\rho_L \geq \rho_G$, allowing for the contribution of the liquid

velocity and using an experimental relationship $k\eta = 0.9$ between the wave amplitude η (displacement of the interface from the equilibrium level) and wave number *k*, the simplified the instability criterion is given by:

$$\left(\bar{u}_{GStr} - \bar{u}_{LStr}\right) > K_{S-I}\sqrt{\frac{g\bar{h}_G\rho_L}{\rho_G}} \qquad [2.36]$$

$K_{S\text{-}I}$ is the stratified to intermittent transition coefficient:

$$K_{S-I} \equiv K_{K-R} = \left[\frac{1}{k\bar{h}_G[\coth(k\bar{h}_G - 0.9) + 0.45\coth^2(k\bar{h}_G - 0.9)]}\right]^{1/2} \qquad [2.37]$$

where $\bar{u}_{GStr}$ is the average gas velocity in the stratified layer, $\bar{u}_{LStr}$ is the average liquid velocity in the stratified layer, $\bar{h}_G$ is the mean height of the gas phase.

The finite amplitude wave formed is influenced by the proximity of the top wall of the horizontal channel, and hence the amplitude of the wave is dependent on the diameter of the channel. The increase in amplitude of the waves is as a result of the gas flowing over the liquid phase and as this is increased, the waves grow. That being said, there is a minimum gas velocity for this to occur as the stabilizing forces due to the gravity have to be overcome before the waves begin to develop. The results of Kordyban & Ranov (1970) study showed a unique relationship between gas velocity and liquid level, although the variation of wave length has no significant effect. Good agreement was found between their theory and the Baker flow regime map for a strictly horizontal configuration.

Kordyban (1977) proposed that wave instability occurs at approximately:

$$\frac{1.35V_C^2}{gh_C}\frac{\rho_G}{\rho_L - \rho_G} = 1 \qquad [2.38]$$

where V_C is the velocity of the wave crest, and h_C is the distance from the wave crest to the top of the channel.

Mishima & Ishii (1980) delved further into the finite amplitude analysis by Kordyban & Ranov (1970). With the assumption that $\rho_L \geq \rho_G$, the surface tension effects were neglected, $k\eta = 1$ the condition for instability was given by:

$$\bar{u}_{GStr} > K_{S-I}\sqrt{\frac{g\bar{h}_G\rho_L}{\rho_G}} \qquad [2.39]$$

$$K_{S-I} \equiv K_{M-I} = \frac{1}{\sqrt{k\bar{h}_G\left[1+0.5\coth(k\bar{h}_G-1)\right]\coth(k\bar{h}_G-1)}} \qquad [2.40]$$

By using the concept of the fastest growing ("most dangerous") wave, they further proposed that $k\bar{h}_G$ =2.26, and so $K_{S-I} \equiv K_{M-I}$ = 0.487. This was in good agreement with the experimental data of Wallis & Dobson (1973), indicating that the classical inviscid Kelvin-Helmholtz value of $K_{S-I} \equiv K_{IK-H}$ was too high by a factor of approximately two. The assumption of $k\eta = 1$ corresponded to a wave height to length ratio of 0.204, in contrast to the generally accepted value of 0.142 as was found by Michell (1893).

This group of studies shows a strong influence of wavelength on slug formation although this differed from experimental observations where wavelength did not indicate a specific trend with respect to slug formation.

Group II

The second group of studies couple Bernoulli effect with the K-H instability in their analysis of the slug initiation mechanisms although they ignore the wave motion aspect and only consider low and high liquid level within the conduit.

Like Kordyban & Ranov (1970), Wallis & Dobson (1973) contested the K-H instability criterion as the explanation for the initiation of slugs. When they applied the one-dimensional Bernoulli equation, they found the pressure amplitude at transition to slug flow to be a factor of two lower. They carried out experiments to determine an approach for predicting the onset of slugging in horizontal rectangular ducts with 25.4 and 305mm heights of varying lengths

and uniform water depths. The two phases in use were water and air at atmospheric pressure in co-current and counter-current configurations. For each setup the slope of the channel was adjusted slightly from the horizontal so that the void fraction (also liquid height) remained constant throughout the run to reduce uncertainties in results. They proposed that $j^* = 0.5\varepsilon_G^{3/2}$ could describe the transition to slug flow, where j^* is the dimensionless gas velocity. Hence they deduced that all their results could be correlated by the following expression:

$$U_{SG}\left[\frac{\rho_G}{gH(\rho_L-\rho_G)}\right]^{1/2} = 0.5\varepsilon_G^{3/2} \qquad [2.41]$$

where H is the height of the channel and ε_G is the void fraction. The prediction described by Eqn. (2.83) was found not to be entirely corroborated by experimental results. This was as a result of the phenomena they described as 'premature slugging' caused by large disturbances induced into the system via using a paddle or tilting the channel rapidly to develop slugs. Hence, triggering conditions in the system that agitates the water phase instead of the air at high enough air flux would lead to premature slugging.

Wallis & Dobson (1973) described slugging as the result of the rapid development of a large wave which rides over the underlying liquid and can eventually fill the channel to form a slug. They modelled a flooding wave that illustrates the transition to slug flow by applying an inverse of Benjamin (1968) bubble theory:

$$U_{SG} = 0.5\left[\frac{gh_G(\rho_L-\rho_G)}{\rho_G}\right]^{1/2} \qquad [2.42]$$

which describes the gas velocity required to maintain a stationary liquid wave over a liquid layer. However, Taitel & Dukler (1976) contested this method of modelling slug flow as they did not see a theoretical basis for applying this to describing the transition to slug flow. Taitel & Dukler (1976) described the slug formation mechanism as an "entrance phenomenon" as they deduced the entire slug phenomenon occurs near the entrance of the channel. They recorded visual observations of the slug formation cycle. Starting from the instant at which a

wave bridged the pipe, the process was divided into two steps, each designated a time. The first time, t_1, was the time required to sweep away the liquid in front of the wave and for the level to drop to its lowest value. The second time, t_2, was the time required to rebuild the film to its equilibrium level. It was observed that t_1 was very short compared to the cycle time and almost immediately after the level rebuilt to its equilibrium value, a solitary wave formed upstream and moved across the surface. The frequency of such solitary waves was an order of magnitude larger than the slug frequency so that effective closure took place immediately after the equilibrium level was reestablished. If a wave bridged the pipe before the level had rebuilt to the equilibrium level, the slug would not persist. Taitel and Dukler (1976) then proposed a mechanistic model to predict slug frequency as the inverse of t_2.

Kordyban (1977) aimed to present experimental data to support the work of Wallis & Dobson (1973) and Taitel & Dukler (1976). He found evidence of the well-known phenomenon that the slugs travel at a higher velocity than the wave which serves as a slug precursor, as well as proof that there is minimum pressure downstream of the wave crest. Good agreement was found between Wallis & Dobson's relationship and experimental data, as well as extending the case to that where large waves are present. The Taitel & Dukler (1976) method was found to be a good approximation for the transition from stratified-wavy to slug flow.

Kordyban (1985) revisited the development of a slug and its relationship with the K-H Instability to explain some discrepancies by using a photographic method. Slugs were generated artificially rather than naturally in this experimental study. The instability criterion was proposed to be:

$$(\rho_L - \rho_G)g = K\rho_G V \frac{V_G h_G}{(h_G - \eta)^2} \qquad [2.43]$$

where K is a constant. Kordyban (1985) hypothesised that this would show the instability of the wave crest before the entire wave becomes unstable as V and η have the highest values. He proposed a modification to the slug formation mechanism. The faster moving gas over the smooth liquid layer causes the initiation of waves at the interface. Although the growth of the wave is relatively slow, the waves grow to block the passage of the air leading to a larger pressure drop, approaching the Kelvin-Helmholtz instability. This is the basis of the

suggestion of slug initiation not being the direct result of K-H instability but rather a mechanism that occurs prior to K-H instability. He noticed the presence of tiny wavelets on the crest on the wave which were caused by a local instability from a high pressure difference and low wave slope (see Figure 2.7). The K-H instability describes the instability of the entire wave, and this occurs after the observation of the wavelets at the crest of the wave. He also mentioned that not all the unstable waves' transition to slugs as they returned to points of stability.

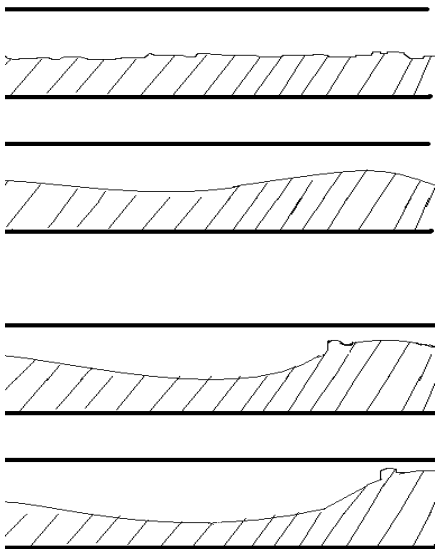

Figure 2.7: Slug initiation mechanism suggested by Kordyban (1985).

Davies (1992) and Hale (2000) used a flow visualisation method to study slug flow regime characteristics in a horizontal configuration. After analysing the Taitel & Dukler (1976) method for predicting slug formation and frequency, they observed that although the model was generally representative, a number of assumptions and suggestions made by Taitel & Dukler did not hold:

- The liquid level behind the slug changes gradually along the pipe and is dependent on the slug tail shedding rate leading to an overestimation by the model of the liquid level rebuild time and underestimation of the slug frequency.

- At constant liquid superficial velocity and increasing gas flow rate, it was found that slugs form on the rebuilding liquid level which has not reached its equilibrium level and that these slugs become fully-developed and reach the end of the test section.

This contradicts the assumption made by Taitel & Dukler that any slugs formed before the equilibrium level is re-established will not result in a fully-developed slug. Hence, their model underestimates the slug frequency.

Mathematically, the Taitel & Dukler (1976) model was also shown to exclude a significant "Bernoulli" term which determines the formation of unstable waves on the gas-liquid interface as a result of pressure differences. Hence, they suggested a modified mechanism of slug formation in horizontal channels which can be seen in Figure 2.8.

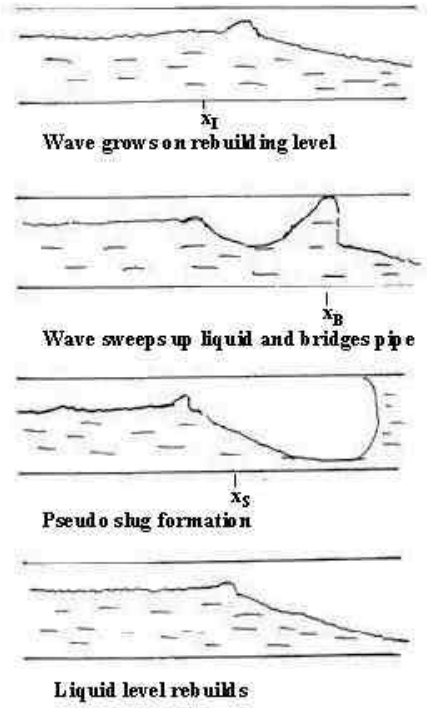

Figure 2.8: Proposed slug mechanism by Davies (1992) and Hale (2000).

They suggested a point downstream, x_I where there is an initial disturbance on the gas-liquid interface representing the appearance of unstable waves. This is where the waves begin to grow and eventually lead to a pipe blockage at a position x_B which is downstream of x_I. The gas accelerates the liquid packet down the channel forming the slug. As the slug travels through the channel, the liquid level varies from the equilibrium level with a slope where the resulting liquid level depends on the amount of liquid that is shed from the tail of the

developed slug. Downstream of x_I, the liquid level begins to rebuild to the equilibrium level as a result of the hydrostatic forces from the liquid slope. Meanwhile, at x_I, unstable waves continue to form and move onto the rebuilding surface. These waves travel over the rebuilding surface and grow until they reach the neutral stability point, x_s at which the liquid height is below the level necessary for waves to grow, and those waves begin to dissipate and eventually completely disappear. Therefore, waves will only grow on the interface between the initiation point, x_I and the neutral stability point, x_s. If the decrease in the liquid height is greater than the gain in amplitude of the waves, the waves may increase in size but no bridging events will occur. Whereas, if a wave grows in amplitude more quickly than the decrease in height of the interface, a bridging event will occur providing there is a sufficient distance for the wave to continue to grow. Davies (1992) suggests that slugs may have a feedback effect on slug formation frequency, which depends on the length of the pipe, gas-liquid flow condition, and the slug pressure drop.

This category of studies agree better with experimental data as the wavelength or wave shape may not necessarily be significant in determining the transition to slug flow but rather the focus should be on the proximity of the top wall of the channel relative to the liquid level, and on the gas velocity.

Group III

The third group of slug initiation theories analyses the transition to slug flow by considering kinetic energy transfer. Gardner (1979) developed a criterion to predict the onset of slugging through determining the wave height.

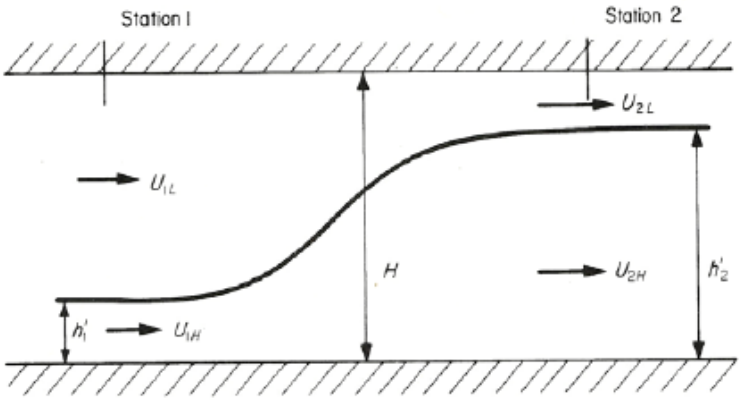

Figure 2.9: Definition sketch of system with wave stationary (after Gardner (1979).

Gardner did not agree with the Taitel & Dukler (1976) analysis which suggested that the wave velocity was zero (i.e. the large waves were stationary), since they are actually observed to be in motion. Also the velocities predicted by Taitel & Dukler (1976) were twice those obtained by Wallis & Dobson (1973) who found good agreement with experimental data. Gardner analysed the initiation of slug flow through energy transfer from the gas to the liquid phase. He used conservation of energy and momentum principles to derive the lossless wave system where he assumed that the velocity profile is uniform with depth at stations 1 and 2. The onset of slugging was described to occur at the point of maximum energy transfer. Hence, he proposed two equations, which when solved simultaneously give the wave height at which the onset of slugging occurs:

$$\left(h_2 - h_1\right) = \frac{h_2(1-h_2)^2 - \dfrac{h_2^3}{P^2}}{(3h_2 - 1)(1-h_2) + 3\left(\dfrac{h_2}{P}\right)^2} \qquad [2.44]$$

and

$$\left(1 - h_2\right) = \left(1 - h_2\right) + \left(h_2 - h_1\right) \qquad [2.45]$$

where the subscripts 1 and 2 represent stations 1 and 2 in Figure 2.9 above.

He found satisfactory upper bound agreement between his model and experimental data although Taitel & Dukler (1976) and Wallis & Dobson (1973) models were found to predict higher wave heights as they had assumed that the liquid velocity is the same at both low and

high liquid levels. The advantage of this analysis is that the need to predict wave heights is not necessary for predicting the transition to slug flow.

By accounting for the contribution of the liquid kinetic energy to growth of waves on the interface, Minato *et al*. (1986) were able to develop a model to predict the transition to slug flow. They suggested that this liquid kinetic energy added a lifting force to that of the gas phase accelerating over the wave crest. They concluded that wave growth occurs when the lift force is positive. For air-water flow, they found good agreement with the Taitel & Dukler (1976) model; although, difficulties arise in making comparisons with other theories as reliable interfacial shear values are required.

Group IV

The fourth group of studies view slug flow initiation through linear stability analysis where inertia and friction effects are taken into account. This is also known as the Viscous K-H instability which generally gives better predictions for the onset of slug flow. However, it must be noted that the analysis fails when the viscosity difference between the two phases is very large.

Lin & Hanratty (1986) aimed to explore the onset of slugging with respect to the application of the K-H instability theory. They pointed out that the inviscid K-H criterion did not account for the liquid phase inertia components and they aimed to include these terms. They also chose to include the shear stresses at the gas-liquid interface as well as the pressure component out of phase with the wave height. In their analysis, they found the instability occurs at lower velocities than those predicted by the inviscid Kelvin Helmholtz analysis. In order to develop their theory, the authors derived continuity and momentum equations for stratified flows upon which they introduced a small amplitude long wavelength disturbance and arrived to the following equation for neutral stability:

$$\frac{U_{SL}^2}{gH\sin\theta}\frac{1}{(1-\varepsilon_G)^3}\left(\frac{C_R}{\overline{u}_a}-1\right)+\frac{U_{SG}^2}{gH\sin\theta}\frac{\rho_G}{\rho_L}\frac{1}{\varepsilon_G{}^3}-\left(\frac{\rho_L-\rho_G}{\rho_L}\right)=0 \qquad [2.46]$$

where $\bar{u}_a$ is the average of the velocities of the two phases, C_R is real part of the wave velocity.

The first term in Eqn. (2.46) represents the liquid inertia destabilising effect, while the second represents the destabilising effect of the gas phase pressure variations; the stabilising effect of gravity is accounted for in the third term. Hence for a fully-developed horizontal flow, they derived a condition for neutral stability:

$$\left(\frac{U_{SG}}{U_{SL}}\right)^{1.75}\sqrt{\frac{\rho_G}{\rho_L-\rho_G}}=K\varepsilon_G{}^{3/2} \qquad [2.47]$$

$$\frac{1}{K^2}=1+\left(\frac{\varepsilon_G}{1-\varepsilon_G}\right)^{0.714}\left(\frac{C_R}{u_a}-1\right)^2\left[1+(1+\phi)\left(\frac{1-\varepsilon_G}{\varepsilon_G}\right)\right]^{1.14}\left(\frac{\rho_G}{\rho_L}\right)^{0.143}\left(\frac{f_i}{f_s}\right)^{1.17}\left(\frac{\upsilon_G}{\upsilon_L}\right)^{0.286} \qquad [2.48]$$

where ϕ is the ratio of the wall interfacial shear stresses, f_i is the interfacial friction factor and f_s is the interfacial friction factor assuming a hydraulically smooth interface. They compared their viscous K-H instability criterion with the inviscid K-H inviscid theory for fully-developed air-water flow, and found that the inviscid K-H instability over predicted the critical superficial liquid velocity relative to theirs. Furthermore, they found good agreement with the revised K-H instability criterion developed by Taitel & Dukler (1976), which accounts for inertia in air-water flow although the Taitel & Dukler relation did not hold for liquid with viscosity different to that of water.

Barnea & Taitel (1993) analysed the stability of separated flow (stratified and annular flow). They investigated two approaches to stability analyses, which included the interfacial stability and the structural stability where they studied the steady state solutions for each stability case. For the interfacial stability, both the linear Inviscid Kelvin-Helmholtz (IKH), which determines the stability neglecting the interfacial shear stresses, and the Viscous Kelvin-Helmholtz (VKH) instability, which includes the shear stress terms, criterions were brought into play. The interfacial instability illustrates the stability of the gas-liquid interface whilst the structural stability illustrates whether the steady state solution is stable with respect to the average film thickness even though the interface is unstable.

The predictions made by the neutral stability conditions for the VKH and the IKH indicate that the VKH shows the formation of large-amplitude waves on the interface while the IKH relates to the uncontrolled growth of unstable interfacial waves which transition to slugs or annular flow (although this depends on the liquid holdup).

The results of the linear stability studies suggest a reduction in the predicted gas velocity at the point of instability although the assumption of small amplitude wave instability does not hold as the slugs do not form on smooth gas-liquid interfaces.

2.3.3 Steady State Slug Flow Models

The most distinctive feature of slug flow is its intermittent nature; therefore attempting to model it by a standard time-average procedure would not be wholly representative of the phenomena. The phenomenological model of slug flow must use concepts from the dispersed and stratified flow models; however, it must also account for the exchange of fluid between each region.

Wallis (1973) first introduced the concept of modelling the slug as an "equivalent unit cell" for predicting the pressure gradient dependent on contributions from the liquid slug, the ends of the long bubble and the slug body. Hubbard & Dukler (1975) further developed this model for horizontal flow. For slug flow to appear steady, the "equivalent unit cell" is a control volume enveloping a liquid slug and a long gas bubble, which is a moving reference frame. Hence, balance equations (mass and momentum) which are conserved across the interface between the liquid and gas components, can be developed.

2.3.3.1 Taitel & Barnea (1990) "Unit-Cell" model

Figure 2.10 shows a basic 'Unit-Cell' model, which follows the approach of Taitel & Barnea (1990). Here, l_s is the length of a slug region and l_f is the length of a film region. The liquid slug region could contain gas in the form of bubbles. The liquid holdup of this region is denoted by ε_{Ls}, u_{Ls} is the average liquid velocity in the slug, and u_{Gs} is the average axial velocity of the dispersed bubbles. In the case of horizontal flow, these velocities, although not

necessarily the same, are assumed to be equal. The gas bubble remains at the top of the pipe, u_{Lf} is the velocity of the liquid in the film region, and u_{Gf} is the gas velocity, the gas and liquid velocities are not axially homogeneous in the film region due to the varying film thickness, h_{Lfe}, along the pipe.

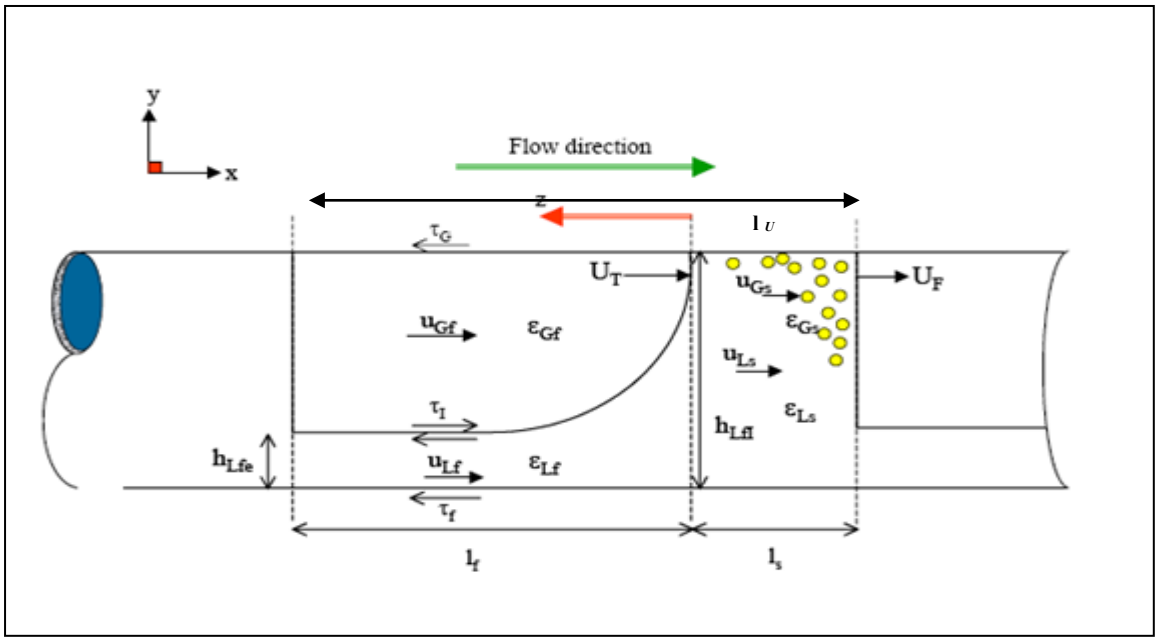

Figure 2.10: A schematic illustration of the unit-cell model.

Steady-state mass and momentum balances can be derived as the system moves with the translational velocity, U_T, of the elongated bubble; in this frame of reference, the slug unit is stationary.

2.3.3.2 Mass Balances

Considering the volume of liquid present in a slug unit, a mass balance of the liquid in the slug unit can be determined:

$$\dot{M}_L = \frac{1}{t_U}\left(A\varepsilon_{LS}\rho_L l_S + \int_0^{l_f} \rho_L A\varepsilon_{LF} dx \right) - \dot{M}_{LP} \qquad [2.49]$$

where $\dot{M}_{\mathrm{L}}$ is the mass flowrate of the liquid fed into the pipe, t_{U} is the time for the passage of a slug unit, ε_{LF} is the liquid holdup in the film region and $\dot{M}_{LP}$ is the mass flowrate of liquid "pick-up" at the front of the slug. The term in parenthesis represents the mass of the liquid in the slug unit. During the propagation of the slug unit along the pipe, a quantity of liquid, $\dot{M}_{LP}\, t_U$, moves upstream relative to the gas-liquid interface and is captured by the following slug in a time span of t_U :

$$t_U = l_U / U_T \qquad [2.50]$$

This rate of liquid picked up is given by the expression:

$$\dot{M}_{LP} = (U_T - u_{Ls})\rho_L A\varepsilon_{LS} = (U_T - u_{Lf})\rho_L A\varepsilon_{Lf} \qquad [2.51]$$

Combining the Eqn.2.49, Eqn.2.50 and 2.51 gives

$$U_{SL} = u_{Ls}\varepsilon_{LS} + U_T(1-\varepsilon_{LS})\frac{l_F}{l_U} - \frac{U_T}{l_U}\int_0^{l_f}(1-\varepsilon_{Lf})dx \qquad [2.52]$$

A similar derivation can be carried out to obtain the superficial gas velocity.

2.3.3.3 Momentum balance

The momentum balances enable the hydrodynamics of the liquid film in the elongated bubble region to be modeled. To simplify calculations, one-dimensional channel flow theory (Taitel and Barnea, 1990) is used. This further enables the pressure drop over a full slug unit to be calculated. Solutions for the film velocity and the film holdup, as a function of position from the rear of the liquid slug may be obtained by considering gas and liquid momentum balances over the film region, relative to the tail velocity:

$$\rho_l \upsilon_L \frac{\partial \upsilon_L}{\partial z} = -\frac{\partial P}{\partial z} + \frac{\tau_L S_L}{A_L} - \frac{\tau_I S_I}{A_L} + \rho_l g \sin\beta - \rho_l g \cos\beta \frac{\partial h_{Lf}}{\partial z} \quad [2.53]$$

$$\rho_G \upsilon_G \frac{\partial \upsilon_G}{\partial z} = -\frac{\partial P}{\partial z} + \frac{\tau_G S_G}{A_G} + \frac{\tau_I S_I}{A_G} + \rho_G g \sin\beta - \rho_G g \cos\beta \frac{\partial h_{Lf}}{\partial z} \quad [2.54]$$

where the relative velocities are defined by $\upsilon_L = U_T - u_{Lf}$ and $\upsilon_G = U_T - u_{Gf}$, and the shear stresses are given by:

$$\tau_F = f_f \left(\rho_L |u_{Lf}| u_{Lf} / 2 \right) \quad [2.55]$$

$$\tau_G = f_G \left(\rho_G |u_{Gf}| u_{Gf} / 2 \right) \quad [2.56]$$

$$\tau_I = f_I \left[\rho_G |u_{Gf} - u_{Lf}| \left(u_{Gf} - u_{Lf} \right) / 2 \right] \quad [2.57]$$

Here, f_f f_G and f_I are the friction factors between the liquid and the wall, the gas and the wall, and for the gas-liquid interface, respectively; correlations for these friction factors are discussed below.

The following overall momentum balance may be obtained by eliminating the pressure gradient terms from Eqn. 2.53 and Eqn. 2.54:

$$\rho_l \upsilon_L \frac{\partial \upsilon_L}{\partial z} - \rho_G \upsilon_G \frac{\partial \upsilon_G}{\partial z} = \frac{\tau_L S_L}{A_L} - \frac{\tau_G S_G}{A_G} - \tau_I S_I \left(\frac{1}{A_L} + \frac{1}{A_G} \right) + (\rho_L - \rho_G) g \sin\beta - (\rho_L - \rho_G) g \cos\beta \frac{\partial h_{Lf}}{\partial z} \quad [2.58]$$

From the material balance, the relative velocities are given by:

$$\upsilon_L \equiv \left(U_T - u_{Lf} \right) = \left(U_T - u_{Ls} \right) \varepsilon_{LS} / \varepsilon_{LF} \quad [2.59]$$

$$\upsilon_G \equiv \left(U_T - u_{Gf} \right) = \left(U_T - u_{Gs} \right) \varepsilon_{Gs} / \varepsilon_{Gf} \quad [2.60]$$

by substituting these expressions into Eqn. 2.58, a differential equation for h_{Lf} is obtained:

$$\frac{\partial h_{Lf}}{\partial z} = \frac{\dfrac{\tau_L S_L}{A_L} - \dfrac{\tau_G S_G}{A_G} - \tau_I S_I \left(\dfrac{1}{A_L} + \dfrac{1}{A_G} \right) + (\rho_L - \rho_G) g \sin\beta}{(\rho_L - \rho_G) g \cos\beta - \rho_L \upsilon_L \dfrac{(U_T - u_{Lf})\varepsilon_{Ls}}{\varepsilon_{Lf}^2} \dfrac{d\varepsilon_{Lf}}{dh_{Lf}} - \rho_G \upsilon_G \dfrac{(U_T - u_{Gs})(1-\varepsilon_{Ls})}{(1-\varepsilon_{Lf})^2} \dfrac{d\varepsilon_{Lf}}{dh_{Lf}}} \quad [2.61]$$

where for the case of a stratified film:

$$\frac{d\varepsilon_{Lf}}{dh_{Lf}} = \frac{4}{\pi D} \sqrt{1 - \left(2\frac{h_{Lf}}{D} - 1 \right)^2} \quad [2.62]$$

The liquid height of the film, h_{Lf}, may thus be obtained by numerical solution of Eqn. 2.61. Using the mass balance in Eqn.2.51, the corresponding film velocity, u_{Lf}, may also be determined. To obtain the liquid film length, the film holdup and the film velocity values just before pick-up, the integration should be performed until the mass balance is satisfied.

The starting holdup used in the integration of Eqn. 2.61 depends on the assumptions made about the liquid content at the tail of the slug. If the gas being shed from the slug is assumed to separate rapidly then the liquid holdup just upstream of the tail can be approximated by the slug body holdup.

A full solution of the model requires closures for the slug tail velocity and the amount of gas pick up at the front of the slug. The presence of the gas phase in the slug body results in a complex distribution of the gas, where there exists a region in the slug body in which the flow is non-homogeneously mixed. Correlations are also required for the friction factors. If a smooth pipe is assumed, a Blasius-type expression may be used for the gas-wall and the liquid-wall friction factors:

$$f_k = C_k \, \mathrm{Re}_k^n \quad [2.63]$$

where the Reynolds number of phase *k* (Re_k) is given by:

$$\mathrm{Re}_k = \frac{\rho_k D_k u_k}{\mu_k} \qquad [2.64]$$

where D_k is the hydraulic diameter of phase k, $D_L = \frac{4A_f}{S_f}$ for the liquid film and $D_G = \frac{4A_G}{(S_G + S_i)}$ for the gas bubble (Taitel & Dukler 1976), A_f, A_G are the cross-sectional areas of the liquid film and gas, respectively, and S_f, S_G, and S_i are the wetted perimeters of the film, gas, and interface, respectively. For laminar flow, $C_k = 16$ and $n = -1$, while for turbulent flow $C_k = 0.046$ and $n = -0.2$.

To estimate the interfacial friction factor, f_i, a smooth friction factor may be used for low liquid and gas velocities. However, this is inadequate in situations wherein the interface is wavy, exhibiting complex dynamics. In the literature, crude approximations and simple correlations are used, one example of which is provided by the correlation of Kowalski (1987):

$$f_i = 7.5 \times 10^{-5} (1 - \varepsilon_{Gf})^{-0.25} \mathrm{Re}_G^{-0.3} \mathrm{Re}_L^{0.8.3} \qquad [2.65]$$

An alternative is provided by the correlation of Andritsos & Hanratty (1989):

$$\frac{f_i}{f_g} = 1 \qquad \left(U_{SG} \le U_{SG}^*\right) \qquad [2.66]$$

$$\frac{f_i}{f_g} = 1 + 15\left(\frac{U_{SG}}{U_{SG}^*} - 1\right)\sqrt{\frac{h_L}{D}} \qquad \left(U_{SG} > U_{SG}^*\right) \qquad [2.67]$$

where U_{SG}^* is the gas velocity at which large amplitude waves appear, given by

$$U_{\mathrm{SG}}^* = 5\sqrt{\frac{\rho_{\mathrm{G,atm}}}{\rho_{\mathrm{G}}}} \qquad [2.68]$$

where, $\rho_{G,atm}$ is the gas density at atmospheric pressure. Reviews of further interfacial friction factor correlations may be found in Srichai (1994) and Khor (1998).

Since the slug is not uniform along its length, the local axial pressure drop is not constant. This means an average pressure drop over the slug unit must be used instead. It can be calculated by performing a force balance over the entire slug unit. It is determined from the 'Unit Cell' model that the momentum fluxes in and out of the slug unit are equivalent and therefore cancel out. Hence, the total pressure drop across the slug unit is:

$$\Delta P_u = l_u \rho_u g \sin\beta + \frac{\tau_S \pi D}{A} l_S + \int_0^{l_F} \frac{\tau_F S_F + \tau_G S_G}{A} dz \qquad [2.69]$$

where ρ_u is the average density of a slug unit defined as:

$$\rho_u = \varepsilon_{Gu}\rho_G + (1-\varepsilon_{Gu})\rho_L \qquad [2.70]$$

ε_{Gu} is the average void fraction obtained using:

$$\varepsilon_{Gu} = (-U_{SL} + u_{Ls}\varepsilon_{Ls} + U_T\varepsilon_{Gs})/U_T \qquad [2.71]$$

and τ_S is the fluid–wall shear stress in the slug body, expressed as:

$$\tau_S = f_S(\rho_S |u_{Ls}| u_{Ls}/2) \qquad [2.72]$$

here, the slug friction factor, f_s, is found using the standard friction factor correlations (Eqn. 2.63) in terms of the slug Reynolds number, Re_S:

$$\mathrm{Re}_S = \frac{\rho_s u_{Ls} D}{\mu_s} \qquad [2.73]$$

where ρ_s is the homogeneous mixture density and μ_s is the homogeneous mixture viscosity. These are defined as:

$$\rho_s = \rho_L \varepsilon_{Ls} + \rho_G \varepsilon_{Gs} \qquad [2.74]$$

$$\mu_s = \mu_L \varepsilon_{Ls} + \mu_G \varepsilon_{Gs} \qquad [2.75]$$

The first term on the right-hand side of Eqn. 2.69 is the gravitational contribution to the pressure drop and the second and third terms are respectively the frictional components in the slug and film zones.

Thus, the pressure gradient across the slug unit is given by a similar manner:

$$\frac{\Delta P_u}{l_u} = \rho_u g \sin\beta + \frac{\tau_S \pi D}{A}\frac{l_S}{l_u} + \frac{1}{l_u}\int_0^{l_F} \frac{\tau_L S_L + \tau_G S_G}{A} dz \qquad [2.76]$$

2.3.4 Slug flow supplementary relationships

From the description of the models discussed above it is apparent that a solution of the steady-state mass and momentum balances cannot be obtained when only the values of the system parameters (dispersed bubble translational velocity, u_{Gs} , the elongated bubble translational velocity, U_T , the slug body liquid holdup, ε_{Gs} , the liquid slug length, l_s and the slug frequency, v_s) are specified. In order to progress and close these models, we need to use supplementary information.

2.3.4.1 The translational velocity of the slug

Dukler and Hubbard (1975) proposed that the translational velocity of the slug, U_T , tends to be greater than the mixture velocity , which is due to the shedding process that occurs at the slug tail. These authors first introduced U_{T} in terms of the so-called "*C*-ratio":

$$C = \frac{U_T}{U_{mix}} - 1 \qquad [2.77]$$

Dukler and Hubbard (1975) assumed a universal velocity profile in the slug body and developed an expression for the *C*-ratio:

$$C = 0.021\ln(\mathrm{Re}) + 0.022 \qquad [2.78]$$

However, recent researches have shown that in developing flows, the slug velocity may differ greatly from the equilibrium values predicted by the Dukler and Hubbard (1975). Benjamin (1968) considered the drift velocity of a bubble in horizontal flow, generally regarded as equivalent to the velocity of penetration of a bubble when liquid is drained from a horizontal pipe. In this study, a horizontal pipe was initially filled with liquid and opened at one end, so the bubble front propagates towards the closed end. By applying inviscid theory on this draining pipe model, the drift velocity is given by:

$$u_{\mathrm{d}} = 0.542(gD)^{\frac{1}{2}} \qquad [2.79]$$

Bendiksen (1984) observed that at high superficial velocities in horizontal slug flow, the nose of the Benjamin bubble does not remain at the top of the pipe but starts to move closer to the axial centerline of the pipe. Based on his observation, Bendiksen (1984) proposed that there was a critical Froude number at which the drift velocity suddenly changed:

$$u_d \approx 0.54(gD)^{1/2}, \quad \text{For } Fr_C < 2 \qquad [2.80]$$

$$u_d = 0, \quad \text{For } Fr_{\mathrm{C}} \geq 3.5 \qquad [2.81]$$

Here, the Froude number is: $Fr_C = u_{Ls} / \sqrt{gD}$.

Manolis (1995) conducted a "Push-out" experiment at Imperial College WASP facility to study the translational velocity of a slug tail, for the case of an un-aerated liquid slug. Based on his measurements, Manolis (1995) correlated these data and obtained a slug tail velocity expression in the same form as that of Bendiksen (1984) :

$$u_d \approx 0.48(gD)^{1/2} \quad \text{For } Fr_C < 2.86 \qquad [2.82]$$

$$u_d = 0 \quad \text{For } Fr_C \geq 2.86 \qquad [2.83]$$

In order to investigate the effects of slug body aeration on the translational velocity of the slug, Hale (2000) designed an experiment called the "Gassy push-out" in Imperial College LPR and WASP test facilities. His experiment was similar to that of Manolis (1995) except that he used an aerated liquid mixture instead of a single-phase liquid. The results of his measurements indicate an increase in the C-ratio with increasing slug body aeration (Figure 2.11, Figure 2.12 and Figure 2.13). Hale (2000) proposed that this was attributed to three factors: i) the distribution parameter which was affected by the velocity profile in the slug body, ii) the drift component of the elongated bubble velocity, and iii) the de-aeration of the liquid film.

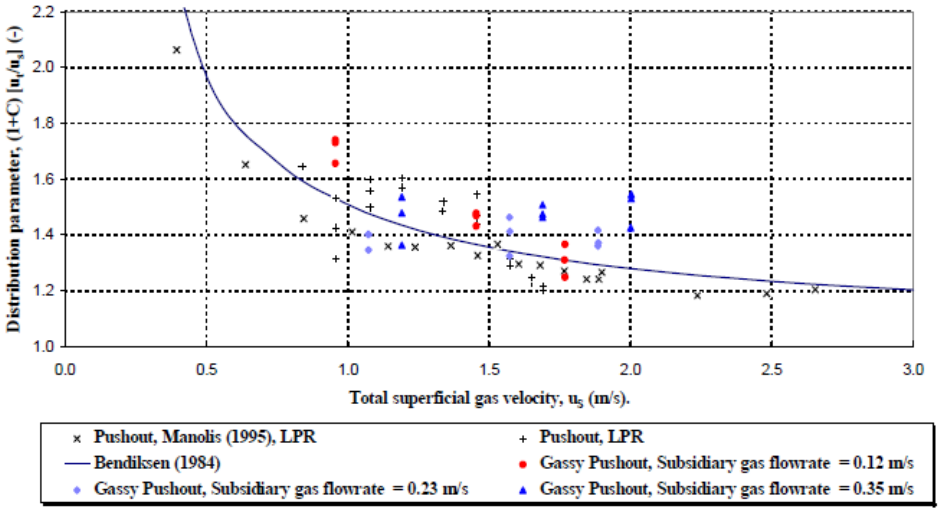

Figure 2.11: C+1 as a function of mixture velocity - Low Pressure Rig (Hale, 2000).

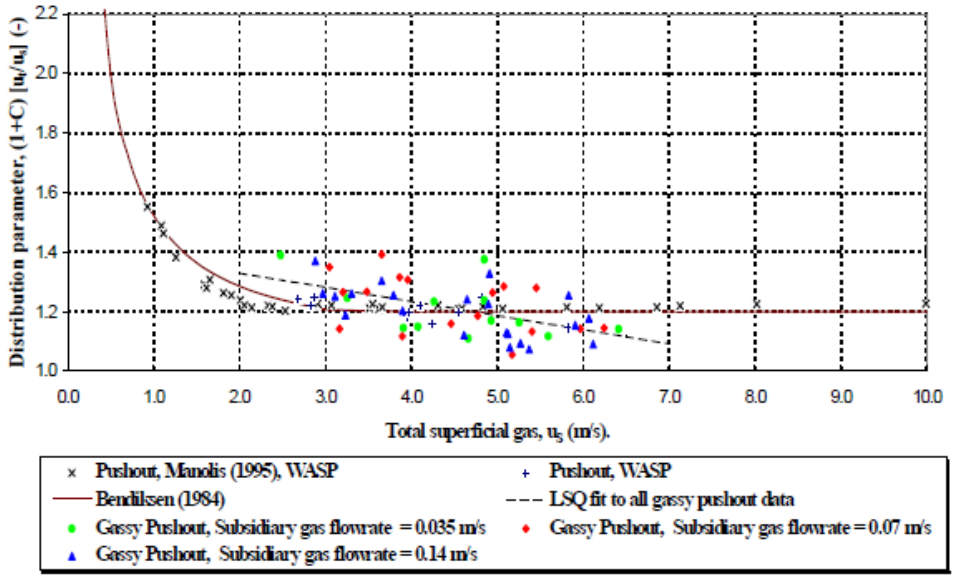

Figure 2.12: C+1 as a function of mixture velocity – WASP (Hale, 2000).

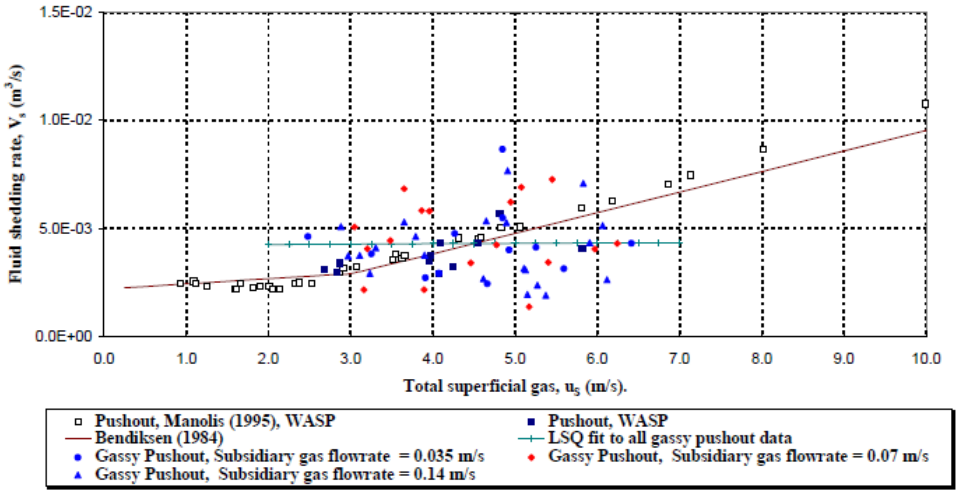

Figure 2.13: Fluid shedding rate from the tail of a slug for the experiments performed on the WASP rig (Hale, 2000).

2.3.4.2 The velocity of dispersed bubbles in the liquid slug

The velocity of dispersed bubbles in the flowing liquid can be expressed as:

$$u_b = B_0 U_{mix} + u_d \qquad [2.84]$$

where B_0 is the distribution parameter proposed by Zuber and Findlay (1965). u_d is the drift velocity in stagnant liquid and U_{Mix} is the mixture velocity. For horizontal pipe flow, Taitel and Barnea (1990) generally assumed B_0 to be equal to unity. The drift velocity, $u_{d,}$ is often neglected for non-slip flow.

2.3.4.3 Slug length

The slug lengths, unlike many other characteristics properties of slugs, tend to be widely dispersed around an average value. The methods that exist for the prediction of slug length fall into two categories: correlations and analytical methods. Barnea and Brauner (1985) simulated the mixing process between the film and the slug by a wall jet entering a large reservoir. They suggested that, since the average total mixture velocity (U_{mix}) at any cross section is the same, the maximum velocity decreases asymptotically towards a value of 1.2 U_{mix} with increasing distance from the front of the slug. They also suggested that since the tail velocity is related to the local maximum ahead of it, the tail behind a short slug (where the velocity profile is not fully-developed) moves faster than a tail behind a slug with a fully-developed velocity profile. This causes the tails of shorter slugs to overtake their fronts and allows the slugs to dissipate into waves. When considering vertical flow, Barnea and Brauner (1985) found that the minimum stable length that a slug could have without dissipating in its motion downstream is 16D, whilst for horizontal flow the length was found to be 32D.

Using the assumption that the liquid is well-mixed at the front of the slug with a uniform velocity profile and that, from this point, a boundary-layer develops at the pipe wall until a fully-developed profile is achieved, Dukler *et al*. (1985) found that the minimum stable slug length is approximately 20D. This is in reasonable agreement with the aforementioned value obtained by Barnea and Brauner (1985). The technique used, however, implies that the tails of short slugs would move slower than tails of long slugs since the velocity profile does not become fully-developed in short slugs. This, though is contrary to the observations of Fagundes Netto *et al*. (1998) and others who found that tail velocity varies with slug length in a non-uniform manner.

The models described so far provide reasonable estimates in pipes of small diameters, however, they greatly under-predict typical slug lengths in large diameter pipes of 0.4-0.5m. For example, in many oil pipelines, slugs are typically 300 to 350D long, as observed by Scott *et al*. (1986). In the absence of any theory to predict such lengths satisfactorily, they suggest that the slug length should be given by the following empirical equation:

$$\ln\left(l_S/0.3048\right) = -25.414 + 28.4948\left[\ln\left(D/0.0254\right)\right]^{0.1} \qquad [2.85]$$

Based on similar data taken at Prudhoe Bay, Gordon and Fairhurst (1987) suggest that for pipes of 304.8 mm, 406.4 mm and 508 mm internal diameter:

$$\ln\left(l_S\right) = -3.871 + 5.441\left(\ln D + 3.673\right)^{0.5} + 0.059\ln\left(U_{mix}\right) \qquad [2.86]$$

and following the addition of data from 588 mm internal diameter pipes this became:

$$\ln\left(l_S\right) = -3.287 + 4.589\left(\ln D + 3.673\right)^{0.5} \qquad [2.87]$$

Based on data collected from a selection of 3 mile long pipes with diameters between 101.6 mm and 406.4 mm in the Prudhoe Bay oil field, Brill *et al.* (1981) found a right skewed distribution of slug lengths and consequently suggested that it can be represented by a log-normal distribution.

Performing experiments on a 430m long 8-inch diameter test-line, Fairhurst (1988) notes that the Prudhoe Bay tests were all close to the stratified-slug transition where the potential for slug growth led to slug lengths an order of magnitude larger than those typically encountered in hydrodynamic slug flow. He also notes that slug length distributions are not necessarily log-normal in shape. Dhulesia et al. (1993) suggest that an inverse Gaussian distribution is more representative of experimental measurement. However, statistically log-normal and Inverse Gaussian distributions are hard to distinguish without a very large data set.

2.3.4.4 Slug Frequency

A critical issue in developing the slug flow models is the prediction of slug frequency and the distribution of slug lengths. More accurate predictions of the slug frequency would lead to improved prediction of the pressure drop; the latter is strongly frequency-dependent. The frequency model would also provide a basis for developing simplified correlations, which, nevertheless, retain the important physics.

Not many phenomenological models have been developed to predict slug frequency, as most researchers have preferred to report data as a function of gas and liquid flowrate or present simplistic correlations which have limited applicability outside the conditions for which they were first developed.

Gregory & Scott (1969) determined slug frequency from visual observations and pressure pulse recordings, from experiments on carbon dioxide/water two-phase flows in horizontal 0.75 inch diameter pipe. Based on their measurements, these authors came up with the following expression for the slug frequency:

$$v_S = 0.0226\left[\frac{U_{LS}}{gD}\left(\frac{19.75}{U_{mix}} + U_{mix}\right)\right]^{1.2} \qquad [2.88]$$

Using data recorded from a 6" internal diameter pipe, this was later re-arranged by Greskovich & Shrier (1971) to give:

$$v_S = 0.0226\left[\frac{U_{LS}}{U_{mix}}\left(\frac{2.02}{D} + Fr_S\right)\right]^{1.2} \qquad [2.89]$$

However, data collected from a 6" internal diameter line suggest that the diameter effects are over-predicted by these equations. Therefore, to overcome this deficiency Greskovich & Shrier (1971) recommended that their graphical correlation is used instead for cases involving large diameters.

The γ-ray absorption method was employed by Heywood & Richardson (1979) for air-water flow in a 42mm diameter pipe, they estimated the average slug frequency through holdup probability density functions (PDF) and power spectral densities (PSD). A single, approximately Gaussian, peak was obtained for most holdup traces and the average slug frequency was taken to be that corresponding to the maximum power value. Heywood & Richardson (1979) proposed that the slug frequency may be obtained by using the following correlation:

$$v_S = 0.0434\left[\frac{U_{LS}}{U_{mix}}\left(\frac{2.02}{D} + Fr_S\right)\right]^{1.02} \qquad [2.90]$$

In order to validate this correlation, Heywood & Richardson (1979) visually estimated the frequency at which slugs passed along the test-section, resulting in the following expression:

$$v_S = 0.0364\left[\frac{U_{LS}}{U_{mix}}\left(\frac{2.02}{D} + Fr_S\right)\right]^{1.08} \qquad [2.91]$$

Manolis et al. (1995) used the WASP facility at Imperial College London to collect data for air-water at various system pressures. The slug frequency was estimated by counting the number of slugs passing through a fixed point over a period of time. They used the approach adopted by Gregory & Scott (1969) and proposed that the slug frequency for air-water system is given by:

$$v_S = 0.037 Fr_{Man}^{1.8} \qquad [2.92]$$

where Fr_{Man} is the modified Froude number, given by:

$$Fr_{Man} = \frac{U_{SL}}{gD}\left(\frac{U_{mix,\min}^2 + U_{mix}^2}{U_{mix}}\right) \qquad [2.93]$$

where $U_{mix,\min}$ is the mixture velocity at minimum frequency which occurred at U_{SL} between 3 to 5 m/s for U_{SG} between 0.5 to 1.0 m/s and at several pressures.

Adopting a slightly different approach and using air-water data collected from a 30cm internal diameter horizontal pipe, Jepson & Taylor (1988) suggested that, for large bore pipelines, the slug frequency is well correlated by:

$$\frac{v_S D}{U_{SL}} = 4.76 \times 10^{-3} U_{mix} + 0.035 \qquad [2.94]$$

Based on a larger database of slug flow characteristics from two sources: low-pressure test rigs and field production flow lines, Hill and Wood (1990) suggested that low-frequency slugs with low equilibrium stratified liquid holdups in large diameter pipes may be better correlated by:

$$\frac{v_S D}{U_{SL}} = \frac{0.275 \times 10^{(2.68\varepsilon_{LE})}}{3600} \qquad [2.95]$$

where the equilibrium stratified liquid holdup ε_{LS} is calculated using the Taitel and Dukler (1976) method. For a more general correlation, they recommend:

$$\frac{v_S D}{u_{GE} - u_{LE}} = \frac{2.74}{3600} \frac{\varepsilon_{LE}}{(1 - \varepsilon_{LE})} \qquad [2.96]$$

where u_{GE} and u_{LE} represent the *in situ* gas and liquid velocities, respectively, and are calculated within the method used to obtain the equilibrium stratified liquid holdup.

Hill and Wood (1994) pointed out that by taking the equilibrium stratified level as the basis for correlating slug frequency, it is without doubt implied that the equilibrium level is immediately re-established following the generation of a slug. Therefore, to allow for the extra time required for the film depth to rebuild to the equilibrium level so that further slugs may be initiated, they proposed the following double-bounded exponential correlation, which they claimed provides a better fit to field data:

$$\left(\frac{v_S D}{U_{mix}}\right)_{\text{mod}} = \frac{1}{3600}\left[-24.729 + 0.00766\exp\left(9.912\varepsilon_{LE\,\text{mod}}\right) + 24.721\exp\left(0.20524\varepsilon_{LE\,\text{mod}}\right)\right] \quad [2.97]$$

where

$$\left(\frac{v_S D}{U_{mix}}\right)_{\text{mod}} = \frac{v_S D}{U_{mix}}\left(1 - 0.05U_{SG}\right)D^{0.3} \quad [2.98]$$

$$\varepsilon_{LE\,\text{mod}} = \varepsilon_{LE}\left(1 - \frac{0.068}{U_{SL}}\right) \quad [2.99]$$

Tronconi (1990) believed that the slug frequency in horizontal two-phase intermittent flow could be predicted accurately by assuming that the slug frequency is one half of the frequency of the unstable waves precursors of slugs, as determined according to published analyses of finite amplitude waves in conduits. Tronconi (1990) adopted the theoretical analysis of wave instability of Kordyban and Ranov (1970) and that of Mishima and Ishii (1980) to derive a formula for the slug frequency:

$$v_s = 0.61 - \frac{\rho_G u_G}{\rho_L (D - h_L)} \quad [2.100]$$

Where h_L is the equilibrium liquid depth for stratified flow, and u_G is the actual gas velocity. Prediction of the slug frequency is thus reduced to the problem of determining the configuration of the inlet stratified flow. This was accomplished by the methodology provided by Taitel and Dukler (1976) that showed that the equilibrium liquid thickness is uniquely a function of the Lockhart-Martinelli parameter $X_{L\text{-}M}$ provided that the ratio between the interfacial friction factor and the wall gas factor $_{is}$ equal to 1. The Blasius correlations were proposed for the calculations of the gas and liquid friction factors.

Zabaras (2000) compared various correlations and mechanistic models for predicting the slug frequency in horizontal and inclined pipes against the data. He found that the performance of existing methods is not sufficiently accurate for inclined slug flow. He modified the Gregory and Scott (1969) correlation, taking into account the effect of inclination angle, θ:

$$v_S = 0.0226\left(\frac{U_{SL}}{gD}\right)^{1.2}\left[\frac{212.6}{U_{Mix}} + U_{Mix}\right]^{1.2}\left[0.836 + 2.75\sin^{0.25}\theta\right] \quad [2.101]$$

Al-Safran (2008) experimentally investigated the effect of the slug-initiation mechanism and flow development on slug frequency in gas/liquid horizontal flow and developed a correlation for the slug frequency as a function of pipe diameter, actual liquid velocity and ratio of slip to mixture velocities. The slip and actual liquid velocities can be calculated from the stratified liquid height, assuming stratified flow at the entrance of the pipeline. The slug-frequency correlation was expressed as:

$$Ln(v_s) = 0.8 + 1.53Ln(U_{SL}) + 0.27(\frac{U_{SL}}{U_{mix}}) - 34.1(D) \quad [2.102]$$

Gokcal *et al.* (2009) performed experiments with oil viscosities between 0.181 and 0.589 Pa.s in a horizontal pipe. The experimental results revealed that viscosity is a significant parameter which affects the slug frequency significantly. The slug frequency was found to increase with increasing liquid viscosity. On the basis of a dimensionless analysis approach, a slug frequency closure model for high-viscosity oil in horizontal pipes was given as:

$$v_s = 2.816\frac{U_{SL}}{D}N_{\mu}^{0.612} \quad [2.103]$$

in which N_{μ} denotes the ratio of viscous and gravitational forces.

$$N_{\mu} = \mu_L / (D^{3/2}\sqrt{\rho_L(\rho_L - \rho_G)g}) \quad [2.104]$$

Although this model is a better alternative than the rest of the above correlations for high-viscosity oils, the comparison against published data indicated that this model is not valid for water or kerosene fluids, which have very low viscosity.

Schulkes (2011) reviewed a wide range of published experimental data and a number of Statoil in-house data sets, and then derived a slug frequency correlation valid for all available

data. The starting point of this analysis is an assumption that the slug frequency is a function of 8 parameters:

$$v_s = F(U_{SL}, U_{SG}, g, D, \mu_L, \rho_L, \rho_G, \theta) \quad [2.105]$$

where θ is the pipe inclination degree. There are 8 parameters and 3 independent dimensions (length, time and mass), hence 5 dimensionless groups; the gas viscosity was not included since it is relatively constant for different gases under different pressure conditions. Motivated by the fact that the slug front propagation velocity is known to be proportional to the mixture velocity (Bendiksen, 1984), Schulkes (2011) converted defined the following dimensionless slug frequency:

$$F = v_s D / U_{mix} \quad [2.106]$$

The dimensionless slug frequency F is a function of the 5 dimensionless groups defined as:

a) The input liquid fraction:

$$\alpha = U_{SL} / U_{mix} \quad [2.107]$$

b) The Froude number:

$$Fr = U_{SL} / \sqrt{Dg\cos\theta} \quad [2.108]$$

c) The Reynolds number:

$$\mathrm{Re}_L = \rho_L U_{SL} D / \mu_L \quad [2.109]$$

d) The pipe inclination: θ

e) The density ratio:

$$\rho = \rho_G / \rho_L \quad [2.110]$$

Therefore, the dimensionless slug frequency can be re-expressed as:

$$F = \Psi(a) \times \Phi(\mathrm{Re}_L) \times \Theta(\theta, Fr) \times \Pi(\rho) \quad [2.111]$$

A unified slug frequency correlation was established base on a large set of experimental data. The correlation performs well for horizontal flow with low and high-viscosity fluids, and for upward inclined flows with low viscosity fluids. However, the correlation was uncertain for inclined flow with high-viscosity fluids. The available experimental data does not indicate a significant pressure-dependence of the slug frequency. Therefore the final slug frequency correlation was written as:

$$F = \Psi(a) \times \Phi(\mathrm{Re}_L) \times \Theta(\theta, Fr) \quad [2.112]$$

which:

$$\Psi(a) = 0.016\alpha(2 + 3\alpha) \quad [2.113]$$

$$\Phi(\mathrm{Re}_L) = 12.1\mathrm{Re}_L^{-0.37} \quad for\ \mathrm{Re}_L < 4000 \quad [2.114]$$

$$\Phi(\mathrm{Re}_L) = 1 \quad for\ \mathrm{Re}_L \geq 4000 \quad [2.115]$$

$$\Theta(\theta, Fr) = 1 + \frac{2}{Fr}\mathrm{sgn}(\theta)\sqrt{|\theta|} \quad for|\theta| \leq 0.17 \quad [2.116]$$

$$\Theta(\theta, Fr) = \frac{1.8}{Fr} \times (0.6 + 2\theta - \theta^2) \quad for\,\theta > 0.17 \quad [2.117]$$

Though various empirical correlations have been developed based on the experimental data, the accuracy of the slug frequency measurement is of central importance. The experimental traces of the slug flow are always recorded either by pressure pulse recordings, conductivity probes and gamma densitometers. Researchers usually identify slugs by the peaks observed on recorded traces. These peaks seldom reach a value of unity; this may either be due to the entrainment of gas bubbles within the slug, or due to the inability of the instrumentation to measure the holdup precisely. However, in the wavy regime, the peaks produced by big

waves can be occasionally similar to slug traces thereby leading to ambiguity in distinguishing waves from slugs; this leads to higher slug frequency evaluation. Therefore it is important to distinguish between real slugs from large waves. The most straightforward method is to apply a threshold to the experimental traces and count all the peaks above this criterion.

Ujang (2003) used a velocity discrimination method to identify slugs from large waves. From holdup traces given by each conductivity probe (see Figure 2.14), she determined the translational velocity of each peak front (wave or slug). From knowledge of the distance between two probes and the time the peak front takes to travel between those probes (Δt_{slug} or Δt_{wave} in Figure 2.14), the front velocity could be evaluated. Following the Bendiksen (1984) finding that slugs travel more rapidly than simple waves, Ujang (2003) could identify real slugs thereby managing to obtain accurate slug frequency determination by only considering the holdup peak for which $U_T > U_{MIX}$.

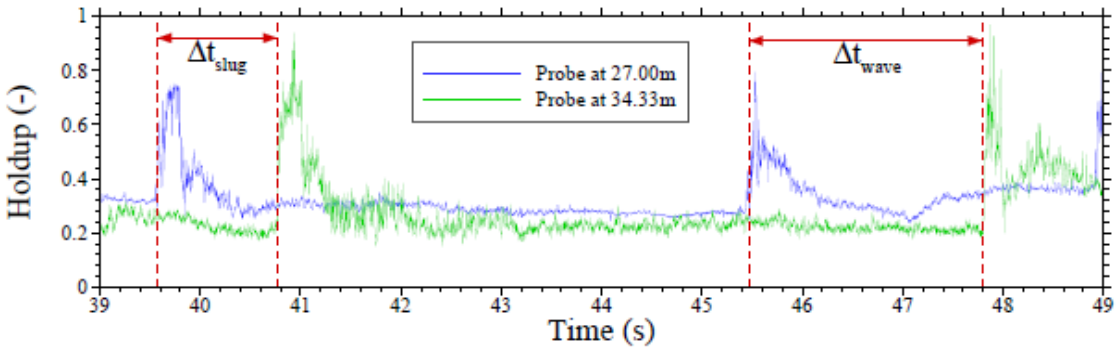

Figure 2.14: Experimental traces recorded from two conductivity probes.

2.3.4.5 Slug body holdup

The slug body holdup is the volume fraction of liquid in the slug body. A significant amount of research has been devoted to measuring and correlating the slug body holdup. However, none of the correlations give reliable predictions due to the complexity of slug flow, which is neither periodic in space nor in time.

Graphical correlations have been provided by several researchers. Greskovich & Shrier (1971) presented a graphical correlation for air-water mixtures in a 1.5 cm horizontal tube using mixture Froude number and the input quantity of liquid. They obtained holdup values between 0.5 and 1.0. Heywood & Richardson (1979) used the gamma ray absorption technique for air-water flow in a 42 mm diameter pipe and plotted ε_{Ls} against the superficial gas velocity with superficial liquid velocity as an additional parameter, producing results similar to the empirical correlation of Gregory *et al*. (1978).

Various empirical correlations have also been adopted to predict the slug body holdup. For instance, Gregory *et al*. (1978) investigated air-light-oil mixtures in pipes of 25.8 mm and 51.2 mm ID. After plotting liquid holdup ε_{Ls} against the mixture velocity, they proposed the liquid hold up to be equal to:

$$\varepsilon_{Ls} = \frac{1}{1 + (U_{\text{mix}} / 8.66)^{1.39}} \qquad [2.118]$$

Andreussi & Bendiksen (1984) collected data on the void fraction in liquid slugs of air-water two systems in horizontal and near-horizontal pipes. The apparatus includes an inclined pipe 17 m long, the slope of which can be varied continuously in the range of ±7%. They developed a semi-empirical correlation for the slug holdup by equating the net loss rate of small bubbles at the slug tail (V_{T}) to the net entrainment rate at the slug front (V_{F}). Also, assuming that the net entrainment rate is given by the difference between the bubble production rate, V_{PR}, and the rate at which small bubbles are returned to the elongated bubble from which they were formed, V_{RB}, the following relation was obtained:

$$V_{\text{T}} = V_{\text{F}} = V_{\text{PR}} - V_{\text{RB}} \qquad [2.119]$$

After processing each term and rearranging the resultant expression, this yields (Paglianti *et al.*, 1993):

$$\varepsilon_{Ls} = 1 - \frac{U_{mix} - u_{Mf}}{\left(U_{mix} + u_{M0}\right)^{n_{AB}}} \quad \text{for } U_{mix} > u_{Mf} \qquad [2.120]$$

and:

$$\varepsilon_{Ls} = 1 \qquad \text{for } U_{mix} \le u_{Mf} : \qquad [2.121]$$

where

$$u_{Mf} = 2.6\left(1 - 2\left(\frac{d}{D}\right)^2\right)\sqrt{\left(gD\frac{(\rho_L - \rho_G)}{\rho_L}\right)} \qquad [2.122]$$

with d_{AB} = 2.5cm, and:

$$u_{M0} = 2400\left(1 - \frac{\sin\beta}{3}\right)Bo^{-3/4}\sqrt{\left(gD\frac{(\rho_L - \rho_G)}{\rho_L}\right)} \qquad [2.123]$$

with the Bond number *Bo:*

$$Bo = \frac{(\rho_L - \rho_G)gD^2}{\sigma} \qquad [2.124]$$

and

$$n_{AB} = 1 - 3\frac{\rho_G}{\rho_L} \qquad [2.125]$$

Nydal & Andreussi (1991) carried out a detailed investigation of the liquid holdup in the slug body. This was based on air-water two-phase experiments carried out in horizontal and inclined pipes. A slug body holdup was measured using conductance probes. They examined the aeration of a body of injected water as it flows over a slow moving liquid layer. It was observed that increasing the pipe inclination led to an increase in slug body length.

Ooi (2002) analysed data from the two-phase fluid systems which operated with different fluids at different conditions. He proposed a correlation for slug holdup base on eight data sets and found good agreement with the data of Nydal *et al.* (1991). In particular, he found that the effect of surface tension on slug body holdup was particularly strong:

$$\varepsilon_{Ls} = 1 - 0474 Ca_{Mix}^{0.883} \mathrm{Re}_{Mix}^{0.203} \left(\frac{\rho_G}{\rho_L}\right)^{0.1} \left(\frac{\mu_G}{\mu_L}\right)^{0.302} \quad [2.126]$$

where $$Ca_{Mix} = \frac{U_{mix}\mu_L}{\sigma} \text{ and } \mathrm{Re}_{Mix} = \frac{\rho_L U_{mix} D}{\mu_L} \quad [2.127]$$

Based on the three phase air-oil-water slug flow experiments performed on the Imperial college WASP facility, Wong (2003) "best-fits" an expression to a large data set with the specific aim of ensuring that the effect of fluid viscosity was taken into account. The new slug body holdup correlation was given by:

$$\varepsilon_{Ls} = \frac{1}{1 + C(\frac{\mu_L U_{mix}}{\sigma_L})^m U_{mix}} \quad [2.128]$$

where C =0.1 and m =0.5. The dimensionless group $Ca_{Mix} = \frac{U_{mix}\mu_L}{\sigma}$, the capillary number, takes into account the viscosity and surface tension effects.

Barnea & Brauner (1985) proposed a mechanistic model for the slug body holdup. In their model, the gas in a fully-developed slug is assumed to appear only in the form of dispersed bubbles and consequently the gas holdup in the liquid slug is determined by a balance between breakage forces acting on the bubbles due to turbulence and coalescence forces resulting from the effect of gravity and surface tension. When turbulent forces dominate, the large bubbles break up and produce dispersed bubbles. When coalescence forces dominate, the small bubbles agglomerate to form elongated bubbles separated by further liquid slugs. Therefore, the maximum possible holdup in the slug occurs when turbulence is just sufficient to break up the elongated bubbles into smaller ones. This is the value of the dispersed bubble void fraction at the dispersed bubble-slug transition boundary:

$$\varepsilon_{\mathrm{GS}} = \frac{(U_{SG})_{BS}}{(U_{SG})_{BS} + (U_{SL})_{BS}} \quad [2.129]$$

where $(U_{SG})_{BS}$ and $(U_{SL})_{BS}$ are the superficial gas and liquid velocities at the transition boundary and $\varepsilon_{Ls} = 1 - \varepsilon_{Gs}$ respectively. Now, if it is assumed that the mixture velocity U_{mix} solely determines the turbulent level in the dispersed bubble flow at this boundary, then along a line of constant U_{mix}, as the superficial gas velocity U_{SG} increases, and the transition to slug flow occurs, the turbulence within any resultant slug remains equal to the value at the boundary. Consequently, along a line of constant U_{mix}, the gas holdup in any slug is fixed and equal to the holdup in the dispersed bubble flow at the boundary, as given by Eqn. 2.129. Therefore once the dispersed bubble-slug transition is known, the slug holdup can be easily estimated. Barnea & Brauner (1985) found the slug holdup estimation to be in reasonable agreement with both the correlation of Gregory *et al*. (1978) and with experimental data.

2.3.5 Developing slug flow

The intermediate stage between the initiation of short slugs and the state in which slugs are fully-developed is important in determining whether the short slugs can grow into fully-developed slugs or dissipate. Hence, several researchers (Ruder *et al*., 1989; Jepson, 1988; Lunde & Asheim, 1989; Bendiksen & Espedal, 1989; Woods & Hanratty, 1996) have attempted to provide a more widely applicable transition criterion for the formation of the fully-developed slug flow. Ruder *et al*. (1989) considered the equivalent slug unit in a frame of reference moving at the slug front velocity U_F. The slug front was defined as a hydraulic jump, and the following condition for an un-aerated slug to exit in a rectangular channel of height *H* was given:

$$\frac{\left(U_F - u_{Lf}\right)}{\left(gH\right)^{1/2}} > 1 \qquad [2.130]$$

where u_{Lf} is the liquid velocity in the film region immediately in front of the slug.

For circular pipes of diameter *D*, the term on the left-hand-side of this inequality is similar but the value on its right-hand-side varies is replaced by the dimensionless liquid height (h_{Lf} / D) at the front of the slug (see Table 2.1).

Table 2.1: Critical values for the existence of a slug (Ruder *et al.*, 1989)

h_{Lf} / D	$\frac{(U_F - u_{Lf})}{(gD)^{1/2}}$
0.100	0.9459
0.200	0.9200
0.300	0.9090
0.400	0.9459
0.500	0.9200
0.563 (Benjamin's (1968) analysis)	0.9350
0.600	0.9440
0.700	0.9937
0.800	1.0778
0.850	1.1444
0.890	1.2106

Furthermore, using the inviscid steady-state model of Benjamin (1968) for the slug tail and setting the volumetric flowrate for the slug tail equal to the pickup rate at the slug front, Ruder *et al*. (1989) obtained a set of critical conditions to ensure that a stable slug is formed. For the case of a rectangular channel, this condition is:

$$\frac{(U_F - u_{Lf})}{(gH)^{1/2}} \frac{h_{Lf}}{H} = 0.5 \qquad [2.131]$$

For a circular pipe, the condition is:

$$\frac{(U_F - u_{Lf})}{(gD)^{1/2}} \frac{4A_{Lf}}{\pi D^2} = 0.542 \qquad [2.132]$$

where A_{Lf} is the cross-sectional area of the liquid film in front of the slug.

The criterion obtained from the steady slug tail analysis predicts much lower critical values of h_{Lf}/D than the critical film height predicted by the linear stability condition of Lin and Hanratty (1986). Ruder *et al*. (1989) concluded that stable slug flow could be generated at lower liquid flow rates than predicted by linear theory due to disturbances at the inlet of the pipe or channel.

Jepson (1989) performed an unsteady slug tail analysis for the case of aerated slugs. A transient dam break model (Stoker, 1957) was used to approximate the slug tail. Jepson (1989) chose this alternative for the slug case because the film height at the rear of the slug was experimentally found to be as low as 0.2 of the pipe diameter; whereas the Benjamin (1968) model precludes the possibility of having a film thickness less than 0.563 of the pipe diameter. Consequently, Jepson (1989) suggested that the Benjamin (1968) analysis should only be used for the elongated bubble or plug flow, which occur at low gas velocities. Using the dam break analysis, a critical value of h_{Lf}/D = 0.38 was obtained for a pure liquid tail, and h_{Lf}/D = 0.15 for a fully aerated one. This was in good agreement with experimental data.

Bendiksen & Espedal (1992) calculated the slug tail velocity using the expressions proposed by Bendiksen (1984) for the translational velocity of the elongated bubble. The slug front velocity was then estimated by performing a mass balance across the front of the slug. For the case of no droplet entrainment within the gas phase, this gives:

$$U_F = u_{Gf}\frac{\varepsilon_{Gf} - \varepsilon_{Gs}\dfrac{u_{Gs}}{u_{Gf}}}{\varepsilon_{Gf} - \varepsilon_{Gs}} \qquad [2.133]$$

where u_{Gf} is the average gas velocity in the region above the film at the front of the slug and ε_{Gf} is the corresponding void fraction. For the case in which droplets are entrained within the gas, this gives:

$$U_F = \frac{u_{Ls}\varepsilon_{Ls} - \varepsilon_{Lf}\varepsilon_{Lfilm}u_{Lf} - \varepsilon_{Gf}\varepsilon_{Lbubble}u_{Lbubble}}{(1-\varepsilon_{Lf}\varepsilon_{Lfilm} - \varepsilon_{Gf}\varepsilon_{Lbubble}) - \varepsilon_{Gs}} \qquad [2.134]$$

where ε_{Lfilm} is the liquid fraction within the film at the front of the slug, $\varepsilon_{Lbubble}$ is the fraction of liquid in the form of droplets in the gas above the film at the front of the slug and $u_{Lbubble}$ is the average velocity of these droplets.

The prediction of the slug front velocity was found to be in good agreement with nitrogen-diesel oil data at 20 bar and 30 bar in a 0.19 m internal diameter, 38 m long horizontal test-section.

Woods & Hanratty (1996) extended the work of Ruder *et al*. (1989) to account for slip within the slug body. The liquid velocity within the slug body u_{Ls} is given by:

$$u_{Ls} = \frac{U_{SL} + U_{SG}}{[1 + (S-1)\varepsilon_{Gs}]} = \frac{U_{mix}}{[1 + (S-1)\varepsilon_{Gs}]} \qquad [2.135]$$

where the slip ratio within the slug body was given by

$$S = \frac{u_{Gs}}{u_{Ls}} \qquad [2.136]$$

The elongated bubble translational velocity U_{TB} was defined in the form proposed by Nicklin *et al*. (1962):

$$U_{TB} = C_o u_{Ls} + u_d = C_{O,S} U_{mix} + u_d \qquad [2.137]$$

where C_o is a weighted-velocity/liquid fraction distribution parameter, and u_d is the drift velocity. The distribution parameter for the case of slip within the slug body, $C_{o,s}$ is given by:

$$C_{o,s} = \frac{C_o}{[1 + (S-1)\varepsilon_{Gs}]} \qquad [2.138]$$

Equating the slug front pickup rate and the slug tail shedding rate, the critical film holdup for is given by:

$$\varepsilon_{Lf} = \frac{\left[\left(C_{o,s} - \frac{1}{1+(S-1)\varepsilon_{Gs}}\right)U_{mix} + u_d\right]\varepsilon_{Ls}}{C_o U_{mix} + u_d - u_{Lf}} \qquad [2.139]$$

To obtain the values of S, $C_{o,s}$ and u_d, Woods & Hanratty (1996) experimentally measured the film height, assumed the elongated bubble velocity is equal to the slug tail velocity, and calculated the liquid film velocity using the steady momentum balance defined by Andritsos & Hanratty (1987). The following values for these parameters were proposed:

$$\begin{aligned} &S = 1 \\ &C_{o,s} = 1.1 \qquad\qquad U_{mix} < 3m/s \\ &u_d = 0.542(gD)^{1/2} \end{aligned} \qquad [2.140]$$

$$\begin{aligned} &S = 1 \\ &C_{o,s} = 1.2 \qquad 3m/s < U_{mix} < 7m/s \\ &u_d = 0 \end{aligned} \qquad [2.141]$$

$$\begin{aligned} &S = 1.5 \\ &C_{o,s} = 1.2 \qquad\qquad U_{mix} > 7m/s \end{aligned} \qquad [2.142]$$

Alternatively, numerical simulations have been widely used to predict the initiation, growth and development of slugs. Since it is not feasible to have all the details of flow processes, the existing simulation models require closure relationships. Two of the common used methods for simulating the slug flows are: "slug-tracking" where the front and back of a slug is tracked using adaptations of the "unit-cell" model (Zhang *et al*., 1994; King, 1998; Manfield, 2000; Taitel & Barnea,1998; Ujang, 2004, Nydal *et al*., 2009); "slug-capturing" where slugs are captured from the growth of instabilities in stratified flows and their subsequent development into fully-developed slug flow. The slug-capturing approach is based on the numerical solution of the transient two-fluid model equations and the flow regime identification which in turn, is based on the local limiting liquid volumetric fraction for separated and dispersed flows (Issa & Bonizzi, 2003; Issa & Kempf, 2003; Fabien, 2007;

Ansari & Shokri, 2010). The details of the slug-tracking and slug-capturing methods are given in Chapter 4.

Chapter 3

Computational modeling of slug flow: A benchmark exercise

3.1 Summary

As discussed in Chapter 1, the slug flow regime is encountered in numerous industrial processes. Of particular significance is the case of pipeline flows in hydrocarbon recovery, the context of the work reported in this thesis. The occurrence of slugging leads to the fluctuation in the gas and liquid phase outlet flow rate as well as strong oscillations of pressure, which put a strain on the operability of equipment facilities such as slug catchers and separators. Although slug flow cannot be entirely eliminated, mitigating and control of its effects have become a high priority. The safety issues and economic costs of slug flow control facilities makes desirable the accurate prediction of flow behaviour within the pipeline. Computational Fluid Dynamics (CFD) is being increasingly used by industry to predict complex multiphase flow cases and it is important to establish whether this methodology gives a realistic prediction of the actual flow. A well-established methodology for evaluating models is the use of "benchmark exercises" in which candidate models are compared with experimental data. This chapter describes the results from such a benchmark exercise whose aim was to explore the capability of various computational methods in predicting the initiation and evolution of slugs in slug flow.

In what follows, an introduction to the exercise problem is giving in Section 3.2. In Section 3.3, the results of the calculations using different computational codes including TRIOMPH, FLUENT, STARCD, LedaFlow, TransAT, and CFX are presented. Section 3.4 gives an overview of the work described in this Chapter.

3.2 Introduction

To provide a benchmark against which a variety of computational methods could be tested, it was decided to use some very detailed data on air-water slug flow obtained by Ujang (2005) in the Imperial College WASP facility. The test-section used was horizontal and was 37meter long with an inner diameter of 78mm. The two phase flow is introduced as a stratified layer at the inlet. Water is introduced below a stratification plate at the bottom of the test-section and the air is introduced above it. Large waves and slugs are initiated at the interface between the water and air; the thickness of the liquid layer was monitored using 14 twin-wire conductivity probes at various locations along the channel. Each probe essentially measured the instantaneous local liquid height at the probe location. It is difficult to distinguish, on the basis of local holdup measurements alone, between large waves and slugs containing entrained gas. However; in the data set presented, care was taken to discriminate between large waves and slugs on the basis of measurements of the velocity the specific features; slugs travel at a velocity greater that the total superficial velocity whereas waves travel much slower (at a velocity around that of the stratified layer interface). Times of arrivals and departures of each wave and slug at two adjacent probes were identified, velocity of each slug candidate was measured using cross correlation of the outputs of successive probes. The superficial velocities of water and air for present study case are 0.611m/s and 4.64m/s respectively. Each conductivity probe record signals at 500Hz for 300 seconds, and they were located at 0.76m, 1.46m, 2.86m, 3.56m, 5.01m, 5.695m, 6.995m, 13.319m, 14.392m, 20.574m, 26.62m, 27.22m, 34.548m, 35.105m from the inlet. The physical properties for air and water at atmospheric conditions are given in Table 3.1

Table 3.1: Physical properties for air and water used in the WASPfacility.

	Air	Water
Density (kg/m^3)	1.18	997.1
Viscosity(Pa s)	0.0000183(20° C)	0.00098(20°C)
Surface tension(N/m)	--	0.037 (20°C)

The essential result from the measurements was a plot (Figure 3.1) of slug frequency versus distance from the injector. It can be seen that the slugs began to appear at around 2 m from the inlet and their frequency passes through a peak at around 5 m before reducing again and reaching a value nearly independent of distance after around 20 m.

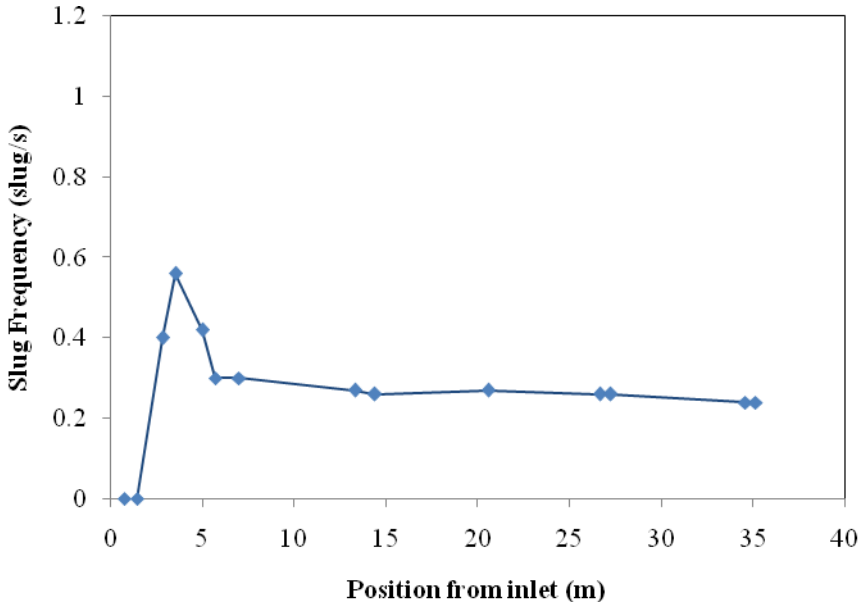

Figure 3.1: Slug frequency along the test-section.

Figure 3.2 to Figure 3.5 show the experimental time series at distance of 0.76m to 35.11m which explain the evolution of slug flow initiation and development.

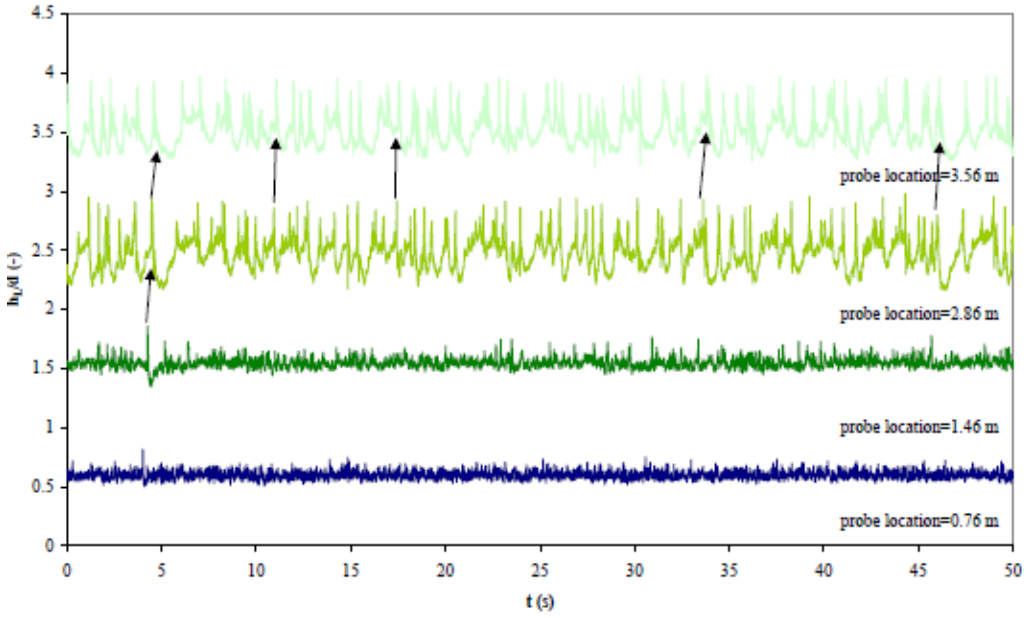

Figure 3.2: Development structure for U_{sL}= 0.611m/s and U_{sG}= 4.64m/s (Probe location from 0.76m to 3.56m).

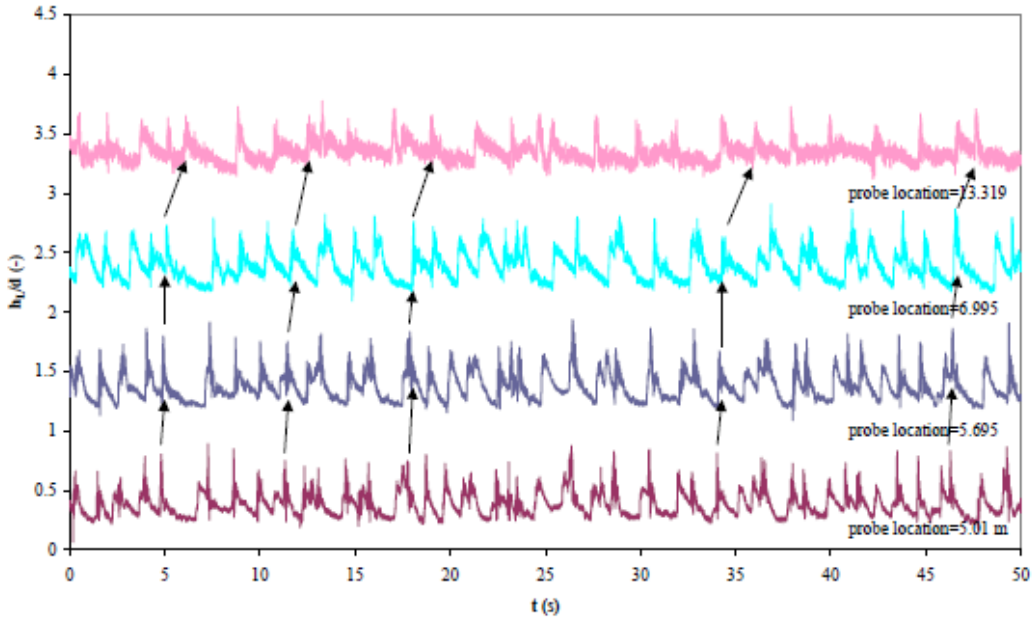

Figure 3.3: Development structure for U_{sL}= 0.611m/s and U_{sG}= 4.64m/s(Probe location from 5.01m to 13.319m).

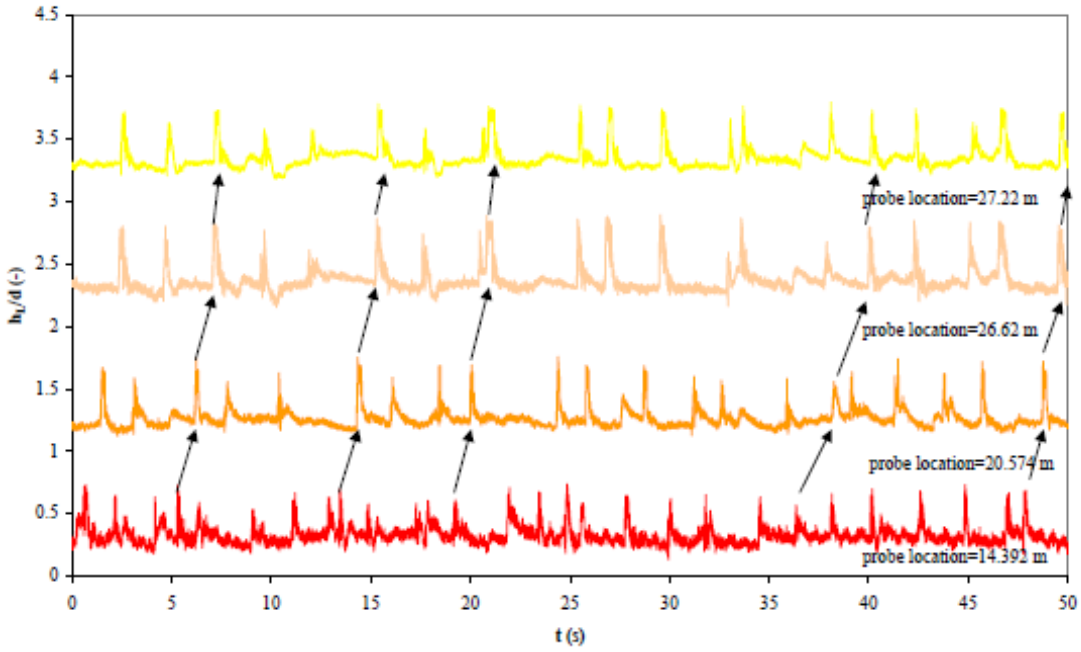

Figure 3.4: Development structure for U_{sL}= 0.611m/s and U_{sG}= 4.64m/s (Probe location from 14.392m to 27.22m).

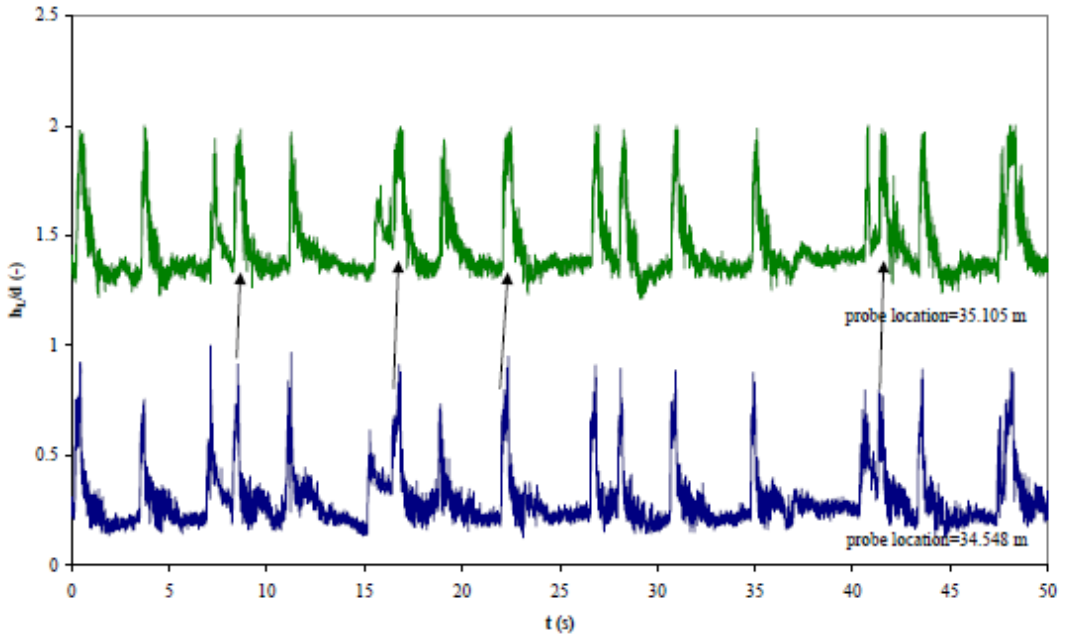

Figure 3.5: Development structure for U_{sL}= 0.611m/s and U_{sG}= 4.64m/s (Probe location from 34.548m to 25.105m).

Calculations of the benchmark case were performed by six independent groups. The main objectives were:

- To provide plots displaying the distribution of the slug frequency with position in the test section for given liquid and gas velocities.
- To provide the time series of the liquid holdup.

3.3 CFD prediction of slug flow

CFD (Computational Fluid Dynamics) is the computer-aided analysis of systems involving fluid flow, heat transfer, mass transfer or a chemical reaction. The concept of CFD is to solve the fundamental governing equations for momentum, heat or mass transport using appropriate numerical techniques under specific boundary conditions. These governing equations solved within each CFD calculation are the conservation equations for mass, momentum and energy. Combining the governing equations of a compressible Newtonian fluid flow gives a system of seven equations with seven unknowns (u, v, w, P, ρ, T, i). Table 3.2 summarizes the full set of governing equations used by a CFD solver.

Table 3.2: Governing Equations for Fluid Flow.

Property	Equation
Mass	$\frac{\partial \rho}{\partial t} + div(\rho U) = 0$
x-component momentum	$\frac{\partial(\rho u)}{\partial t} + div(\rho u U) = -\frac{\partial p}{\partial x} + div(\mu\ grad\ u) + S_{Mx}$
y-component momentum	$\frac{\partial(\rho v)}{\partial t} + div(\rho v U) = -\frac{\partial p}{\partial y} + div(\mu\ grad\ v) + S_{My}$
z-component momentum	$\frac{\partial(\rho w)}{\partial t} + div(\rho w U) = -\frac{\partial p}{\partial z} + div(\mu\ grad\ w) + S_{Mz}$
Internal Energy	$\frac{\partial(\rho i)}{\partial t} + div(\rho i U) = -p\,div U + div(\lambda\ grad\ T) + \Phi + S_i$
Equations of state	$p = p(\rho, T)$ and $i = i(\rho, T)$

The solution of these differential equations is complicated due to the fact that they are nonlinear and coupled. Therefore to obtain approximate solutions, a discretisation method is used that approximates the differential equations by a system of algebraic equations, which can then be solved on a computer. There are three discretisation methods available: i) finite difference, ii) finite volume and iii) finite element methods. The finite volume technique is the most established and thoroughly validated general purpose CFD technique and is central

to most commercial codes. The numerical grid defines the discrete locations, at which the variables are to be calculated; it essentially divides the computational domain into a finite number of sub domains. Discretisation yields a large system of nonlinear algebraic equations; hence an iteration scheme is used to solve them by setting appropriate convergence criteria. Another complicating factor is that the flows are often turbulent; turbulent flows cannot be solved fundamentally for practical cases (including the case studied here) and it is necessary to invoke a turbulence model. This point is discussed further below.

3.3.1 TRIOMPH

The TRIOMPH(TRansient Implicit One-dimensional Multi-PHase) code was original created by Issa & Abrishami(1986) at Imperial College. The code is based on the "slug-capturing" technique, where slugging is automatically captured as a natural outcome of flow instabilities giving rise to perturbation growth in stratified flows leading to the formation of slugs. The equations solved are one-dimensional in nature. Thus, at any given location along the pipe one velocity is assigned for the each phase, The benchmark exercise of using TRIOMPH was carried out by Montini & Issa (2009).

3.3.1.1 TRIOMPH model for slug flow evolution

The slug capturing technique implemented in the TRIOMPH code uses an Eulerian approach to solve the one-dimensional two-fluid model. The same set of equations are retained regardless of the local flow pattern (slug or stratified) that generates in the pipe. The method adopted to discretise the conservation equations is a finite volume method for which an upwind first order scheme is applied for the spatial discretisation and a fully implicit method in time. A detail description of the TRIOMPH code is given in chapter 4.

3.3.1.2 Geometry, mesh and boundary conditions

In the simulation, 1250 nodes were used to represent the test section (though grid refinement tests were also conducted with 2500 and 5000 nodes). With a time step of around 0.1 ms, the total integration time was around 300 seconds.

The code solves for one of the phase volumetric fractions α_G, the two phase velocities (u_L and u_G), and the gas-liquid interfacial pressure p. The liquid phase is regarded as incompressible; the compressibility effects in the gas phase are accounted for using the law of perfect gas. An equation for pressure is derived from the overall continuity (Issa &Abrishami,1986), in order to enforce the global mass conservation. The boundary conditions imposed in the calculations of the code are as follows:

- At the inlet: the liquid hold-up, the liquid and gas superficial velocities are fixed.
- At the outlet: the absolute pressure is fixed.
- The initial condition: assumes a uniform stratified flow field, where hold-ups, gas and liquid velocities, and the pressure are uniform throughout the pipe.

The calculation adopted a criterion when the liquid volume fraction exceeds a certain threshold value (α_L>0.98) the cell is considered "slugged"- i.e. liquid filled (Montini,2011). The slug frequency is defined as the number of slugs passing through a specific point per unit time. Two simulation cases were carried out with different liquid fraction α_L specified at the inlet. One was set to be 0.5 which is same as the value specified in experiment; another one was set to be 0.72 which was given by the equilibrium state of a stratified flow.

3.3.1.3 Results

The prediction of slug frequencies at various locations along the test-section is plotted in Figure 3.6. It reveals that the flow developed towards its final state was predicted to be dependent on the assumptions made about the inlet condition, for example, the inlet liquid hold-up in this case. In simulation case 1, when α_L = 0.5, no slug was predicted for the first 7 meters whereas slugs were observed at 2.86m in experiment. The reason may be the initiation process whereby the initial slug characteristics were damped out which led to an under-prediction of slugs within the developing region. Comparing with experimental data, the initiation and development process of slug flow were better captured when the stratified flow was set to be equilibrium. The result indicated that a more precise specification of inlet conditions was desirable. A detailed discussion of the influence of inlet hold-up is given in Chapter 7.

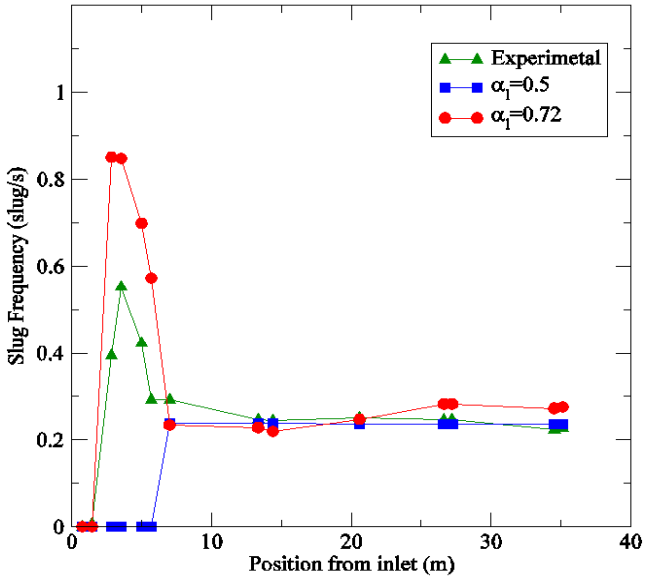

Figure 3.6: Slug frequency along the test-section. The green line represents the experimental data, the blue line and red line represent the TRIOMPH predictions with different hold-up values at inlet.

It was concluded that, though the 1D model was unable to predict multidimensional effects, the important effects in slug flow were represented well by a slug capturing methodology as embodied in TRIOMPH. Though the calculations indicated a sensitivity of the initial development to the precise inlet conditions, it was found that the slug flow finally asymptotes to one which was the same, independent of inlet conditions.

3.3.2 FLUENT

FLUENT is commercial CFD software package that is used in a wide range of applications, including multiphase flow. The prediction of benchmark case of using CFD code FLUENT was carried out by Thompson et al. (2010) of Cranfield University**.**

3.3.2.1 CFD model for slug flow evolution

There are three main models to resolve a gas/liquid two-phase flow in Fluent: The Volume Of Fluid (VOF) model, the mixture model and the Eulerian model. For stratified/slug flow, it's advisable to use VOF model as it is fastest and simplest (ANSYS-Fluent Inc, 2008) and it has proven record in tracking interfaces.

The VOF formulation relies on the fact that two or more phases are not interpenetrating. The model considers the momentum equation and turbulence transport only for the mixture; therefore it solves a single set of momentum equations and tracks the volume fraction of each fluid throughout the domain. All variables and properties such as velocity, density, viscosity and turbulence of the mixture are averaged via volume fractions of individual phases. It's clear that at high velocity, density, or viscosity ratio, the jump in the material properties across the interface is smoothed. This diffusive nature can leads to the loss of the sharpness of the interface, hence causing error in the estimation of the surface tension and shear stress across the interface. The transport of the turbulence can be also affected and diffused in the vicinity of the interface. One solution is to use of a high resolution grid at the interface which helps to limit the effect; however, it is computationally expensive, especially for a 3D simulation. In order to overcome his limitation, FLUENT uses a modified version of the High Resolution Interface Capturing (HRIC) scheme; this is a composite NVD (normalised variable diagram) scheme that consists of a non-linear blend of upwind and downwind differencing (Muzaferija et al., 1998).The donor-acceptor approach is used near the interface (FLUENT, 2006). The scheme identifies one cell as a donor of an amount of fluid from one phase and another (neighbour) cell as the acceptor of that same amount of fluid, and is used to prevent numerical diffusion near the interface.

In principle, both laminar and turbulent flows can be represented in terms of the Navier-Stokes equations. However, turbulent flows at realistic Reynolds numbers span a large range of turbulent length and time scales, and would generally involve length scales much smaller than the smallest finite volume mesh, which can be practically used in a numerical analysis. Therefore, semi-empirical turbulence models have been developed to account for the effect of the turbulence. In this Benchmark case, the classical Reynolds averaged Navier-Stokes (RANS) model was employed together with the VOF model. This statistical turbulence model seeks to solve a modified set of transport equations by introducing averaged and fluctuating components. For example, a velocity U may be divided into an average component $\overline{U}$, and a time varying component u.

$$U = \overline{U} + u \qquad [3.1]$$

The average velocity is then given by:

$$\overline{U} = \frac{1}{\Delta t}\int_{t}^{t+\Delta t} U dt \qquad [3.2]$$

Substituting the averaged quantities into the original momentum equation gives additional terms, the so-called Reynolds stresses $\rho\overline{u_i' u_j'}$. In order to solve for the Reynolds stresses, two classes of turbulence models have been used, namely eddy viscosity models and Reynolds stress models. The eddy viscosity turbulence models assume that the Reynolds stresses can be related to the mean velocity gradients and an eddy (turbulent) viscosity by the Boussinesq hypothesis; in particular the *k*-*ε* and *k*-*ω* two-equation models are most commonly used to calculate local turbulent viscosities. The *k*-*ε* model was employed in the FLUENT simulation of slug flow for this benchmark case.

3.3.2.2 Geometry, mesh and boundary conditions

To predict the slug flow evolution in a horizontal pipe, the first attempt of the 3D simulation was performed in a pipe of length 12m, only half of the pipe cross-section was modeled by assuming symmetry over the Y axial direction. To work on the mesh sensitivity analysis, coarse and fine grids were tested. Figure 3.7 shows the cross sectional view of each mesh, the image is mirrored in order to represent the whole cross-section.

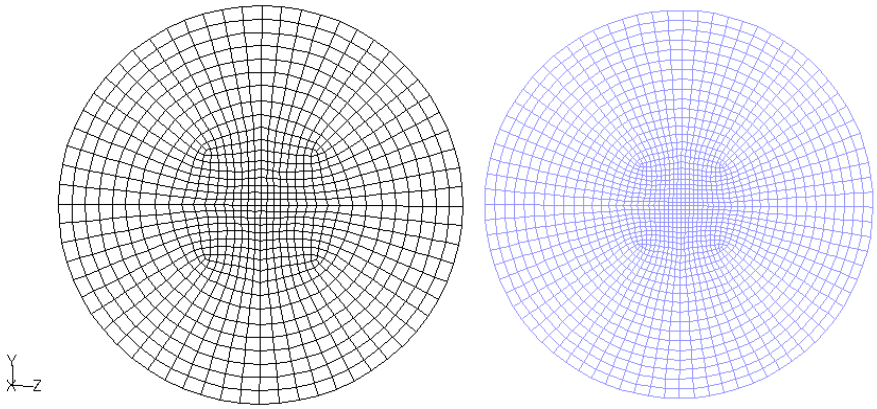

Figure 3.7: Cross sectional view of coarse grid (left) and fine grid (right) used in FLUENT simulations of Cslug flow.

It was noted even with multiple processors, the time taken for the simulations was substantial, i.e. around 18 days. As summarised in Table 3.2, for the case with fine mesh, the calculation time for the 12m pipe simulation was 18 days by using 8 processors to simulate 20s real time. And for the case with coarse mesh, the calculation time was 18 days by using 4 processors to simulate 23s real time.

Table 3.3: The number of CPU and simulation time used in FLUENT simulations.

	No. of Processors	CPU time	Simulation time
Fine Grid 1 008 000 nodes	8	≈ 18 days	≈ 40 s
Coarse Grid 322 560 nodes	4	≈ 18 days	≈ 23 s

3.3.2.3 Results

Slugs were captured in both cases. Figure 3.8 shows the contours of volume fraction plotted from the post processing of the result, slug can be seen in this snapshot.

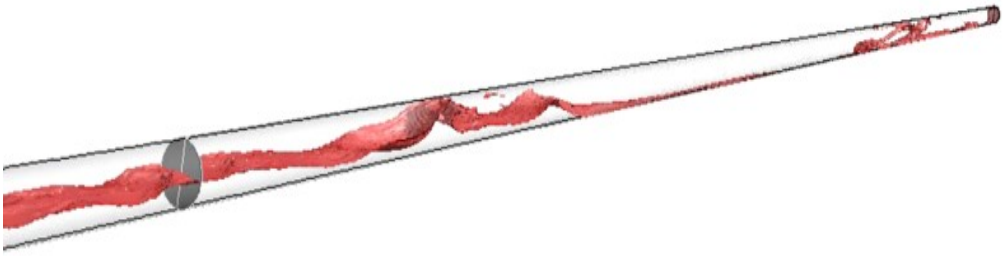

Figure 3.8: Contours of liquid volume fraction using FLUENT 3D simulation.

Points were monitored at various probe locations along the pipe, in order to investigate the slug initiation and developing process. Time traces of liquid hold-up were plotted at the monitoring points of 2.86m and 3.56m, e.g. Figure 3.9 shows the times traces recorded at 3.56m. It's difficult to directly compare two graphs as the starting time is different; however the duration of the simulation results presented is the same which is 25 seconds. Slug frequencies were evaluated based on a liquid hold-up threshold of 0.7 in both cases; the value of the threshold was chosen to account for the presence of gas inside the slug body due to numerical diffusion. Results are given in Table 3.3. Discrepancies between the coarse grid and fine grid simulation results are 5% and 11% for the results obtained at 2.86m and 3.56m respectively, indicating a rather good mesh independency. Mean error between prediction and experiments are 15% and 4% for fine grid and coarse grid simulation, respectively. Note that the interpretation of slug frequency provided by the code operator was based solely on the liquid hold-up threshold, the threshold is changed to 0.8, and the discrepancy with experiment is increased to 27% and 15 %.

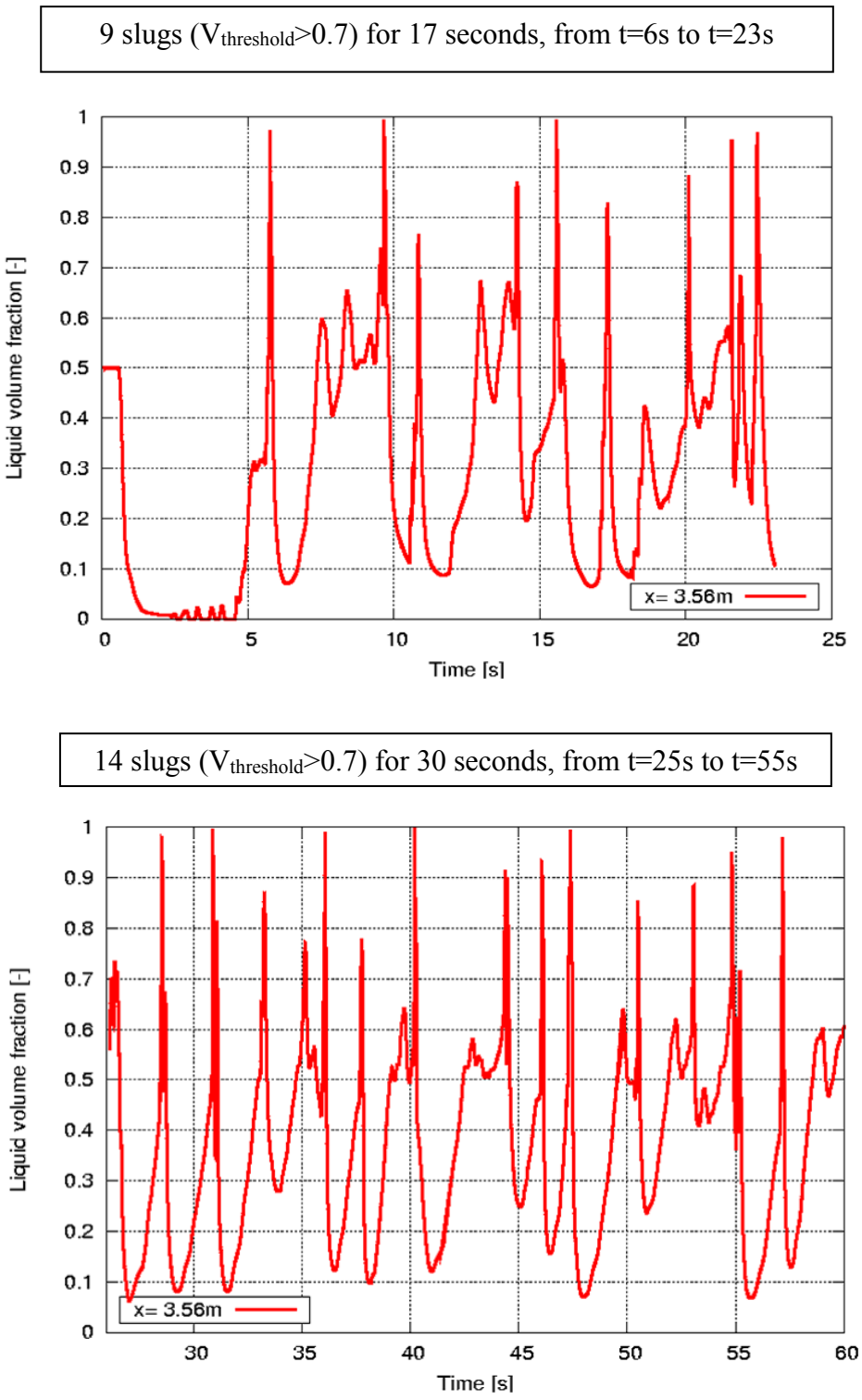

Figure 3.9: Calculated liquid hold-up time traces at 3.56m from the inlet, with coarse mesh (above) and fine mesh (below).

Table 3.4: Predictions of slug frequencies at two locations (hold-up threshold=0.7).

Location (m)	Frequency (slugs/s)		
	Exp.	Sim. Fine Grid	Sim. Coarse grid
2.86	≈ 0.4	≈ 0.43	≈0.41
3.56	≈ 0.55	≈ 0.47	≈0.53

Work was proceeding on extending the length of the computational domain to 37m long and using full pipe simulation. The grid size of the full pipe simulation is 1989120 cells. The results have revealed that full pipe and longer pipe length simulation has improved the prediction accuracy. For example, at the monitoring location of 5.01m and during the 25 seconds, see Figure 3.10:

- 3 slugs were observed from 12m symmetric half pipe simulation, the discrepancy between prediction and experiment is 70%.
- 10 slugs were observed from 37m full pipe simulation, the discrepancy between prediction and experiment is 5.0%.

The 70% error with half pipe simulation indicates a poor agreement with experiments. The error maybe attributed to the length of the simulating domain, a sufficient distance maybe required for slug flow to develop. In contrast to half pipe simulation results, the error associated with full pipe simulation reduced to 5%, and the good agreement with experiments reveals the pipe length is an important parameter in the prediction of slug flow.

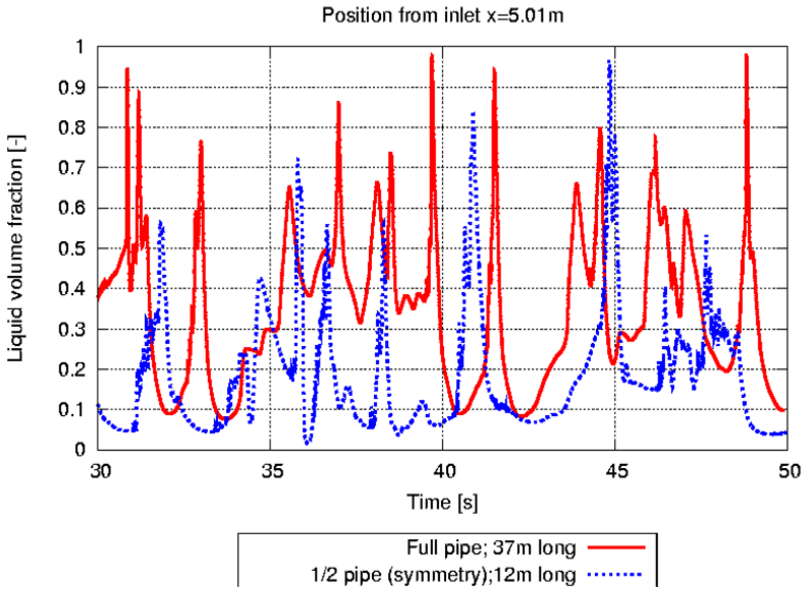

Figure 3.10: Calculated liquid hold-up time traces at 5.01m from the inlet, using full pipe and half pipe simulations.

Moreover, the effect of the outlet boundary was investigated in the full pipe simulation, including the open outlet and pressure controlled outlet. Figure 3.11 show the plot of slug frequency at various probe locations with different outlet boundary conditions. In both cases, the peak in the slug frequency was predicted and agreed well with measurements. However in further downstream, the simulations failed to predict the asymptotic trend of the frequency, the reason can be partly attributed to the insufficient simulation time. Among two cases, a better agreement is obtained with pressure controlled outlet.

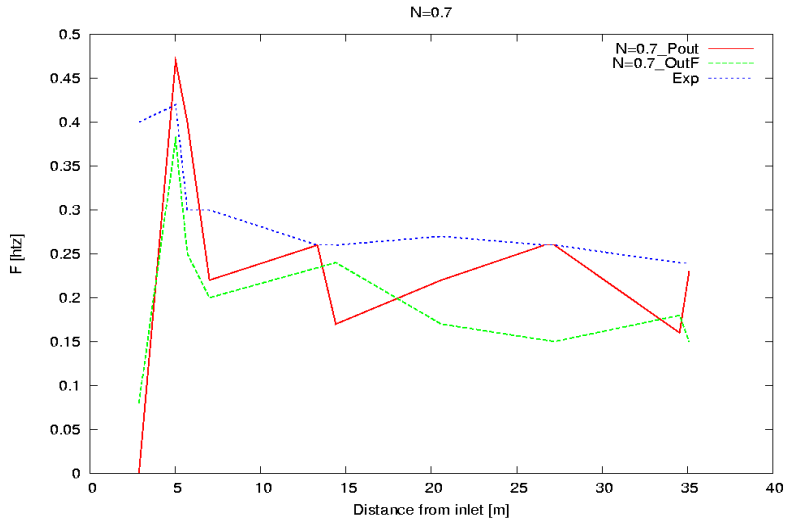

Figure 3.11: FLUENT predictions of slug frequecy along the test-section with different outlet boundaries.

To conclude, the simulation of slug flow evolution using FLUENT with the VOF model has shown its ability to qualitatively predict the initiation and development of slugs. Because slug flow is intrinsically complex, the 3D simulation of such flow is inevitably computationally expensive. Although a half pipe simulations with 12m is a compromise to the simulation time, they failed to predict the slug frequency downstream as most of the slugs initiated upstream collapsed while they propagating towards the exit. In contrast, a more accurate prediction of slug frequency was obtained using full pipe simulation. The discrepancies between the experiments and simulations reveal the importance of the pipe length in the accuracy of slug flow predictions. The pressure outlet boundary was proved to be more robust than then open outlet. Furthermore, longer simulation time is also advisable to achieve a better slug statistics.

3.3.3 STAR-CD

STAR-CD is commercial CFD software which was developed by the CD adapco Group. The code uses the finite volume method to solve the two-fluid model. The calculation of the slug flow benchmark exercise was carried out by Tomasello & Lo (2009) of CD-adapco.

3.3.3.1 CFD model for slug flow evolution

The STAR-CD calculations of slug flow benchmark exercise had been done using a VOF method and High Resolution Interface Capture (HRIC) scheme for volume fraction. The k-ω based SST turbulence model was selected with interface damping.The SST k-ω turbulence model is a two-equation eddy-viscosity model developed by Menter (1994) to effectively blends k-ω model in the near-wall region with the k-ε model in the far field. The advantage of the mode is it accounts for the transport of the turbulent shear stress and gives highly accurate predictions of the onset and the amount of flow separation.

3.3.3.2 Geometry, mesh and boundary conditions

The half pipe geometry with full pipe length was simulated, assuming symmetry over the central plane of the pipe. Figure 3.12 show the mesh of the domain which containing

384 cells in the cross plane, and each cell is 2.5 cm in length giving 568512 cells for the whole domain.

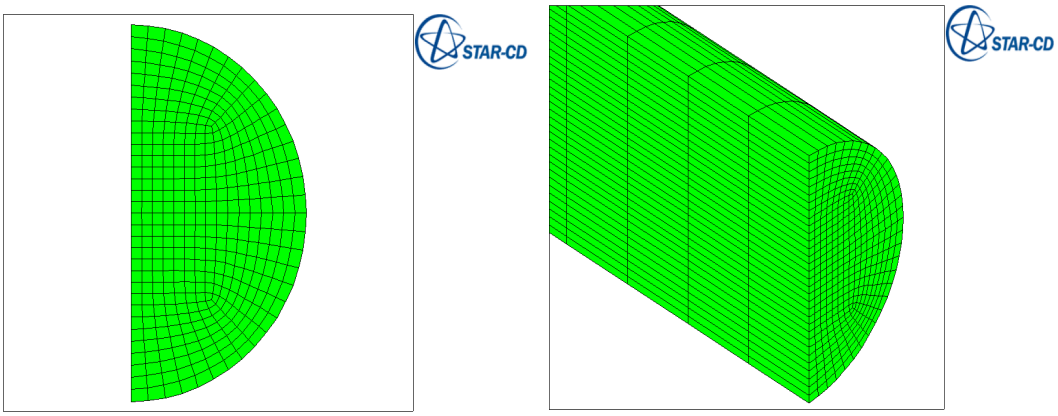

Figure 3.12: Mesh of the domain in STAR-CD prediction of Benchmark case.

A uniform mass flow inlet boundary was applied for the injection of both gas and liquid phases, whereas the pressure outlet boundary was applied. Non-slip boundary conditions at the wall were also applied. The gas was treated as compressible and liquid as incompressible. An initial disturbance was applied in the flow domain. With a time step of 8e-4 s and with 20 processors, it took 10 days to simulate 100s of real time.

3.3.3.3 Results

During the simulation, monitoring points were set around the same locations as in the experimental facility. At each location, three point A, B and C with B being the monitoring point at the experimental location, A is located 0.5m before B and C is located 0.5m after B; this was repeated for each experimental location. The liquid volume fraction integrated across each monitoring section was recorded. A slug candidate was detected when the integrated volume fraction at point A reached a value above a chosen threshold. The value of the threshold was chosen to account for the presence of gas inside the slug body due to numerical diffusion. Point C checks when the integrated liquid volume fraction goes above the threshold. The time difference between point A and C divided by the distance between point A and C gives the translational velocity, which is expect to be roughly 1.2 times the

liquid velocity. The method applied to evaluate slug frequency is similar to the experiments in that slugs were discriminated from large waves by means of their translational velocity; hence it's more accurate than only looking at the liquid fraction. Meanwhile point B is monitoring the liquid volume fraction and provides the two instants when the liquid volume fraction goes above and below the threshold respectively (i.e. the moments when the front and the tail of the slug transit at point B). This time interval multiplied by the slug translational velocity gives the slug body length. The velocity discrimination method was coded in a subroutine and executed by STAR-CD during the simulation. The calculated slug body lengths were recorded in an output file and then an average was calculated for each location. Figure 3.13 and Figure 3.14 show the comparison of slug flow development structure between the experimental data and predictions using STAR-CD.

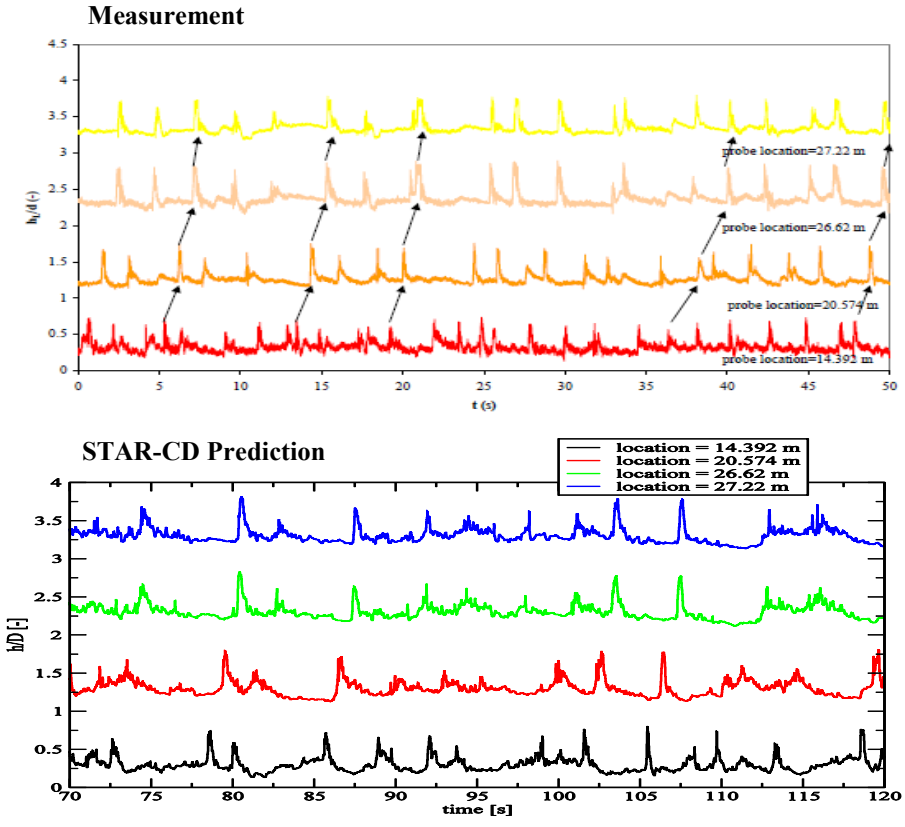

Figure 3.13: Comparison of slug flow development structure between the experiment and prediction, (Probe location from 14.992m to 27.22m).

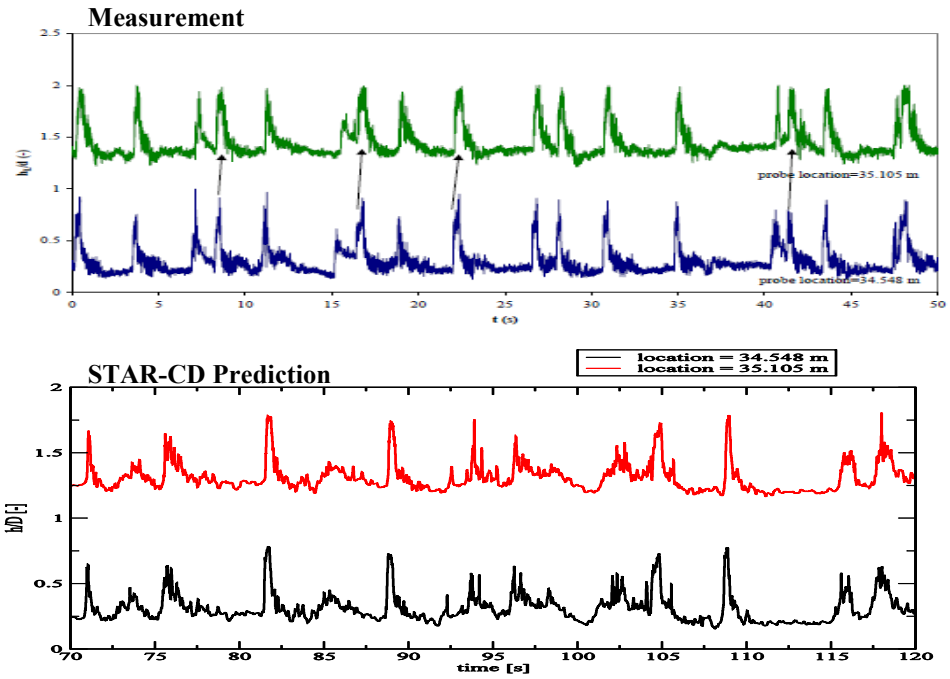

Figure 3.14: Comparison of slug flow development structure between the experiment and prediction, (Probe location from 34.548m to 25.105m).

The continuous development of slug length over the pipe was captured in the simulations and this trend is in qualitative agreement with the measurements of Ujang (2005). As shown in Figure 3.15, the predicted slug length remains zero in the first 5 meters, which means no slug was captured within that distance, whereas slugs appeared closer to the inlet in the experiments. The prediction under-estimates the average slug length at different locations.

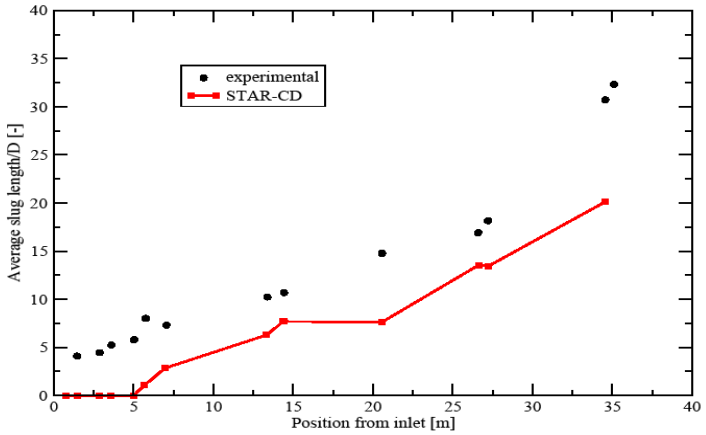

Figure 3.15: Comparision of slug length development over the pipe length between the simulation results(red line) and measurement data (black dots).

Regarding to the prediction of slug frequency, the code operator has concluded that the prediction of slug frequency especially the peak close to the inlet region was particularly challenging. The calculation was very sensitive to the inlet geometry and boundary condition; the discrepancy can be attributed to the some experimental features (inlet region with the plate, fluctuations in the pump feed etc.) were not modeled precisely in the simulation.

To conclude, the prediction of slug flow benchmark case using STAR-CD with VOF model has shown its ability to predict slug flow. Disturbances were introduced at the inlet which enhanced formation of slugs. A velocity discrimination method was coded in the simulation and enables an accurate evaluation of slugs. Continuous development of slug length was captured in the simulation, and this trend agreed with observation from the experiments. The prediction of the slug frequency variation with pipe length failed to match experimental data and further investigation is needed to improve the modeling of the inlet region.

3.3.4 LedaFlow

LedaFlow is a multiphase flow prediction tool, developed by collaboration of SINTEF, ConocoPhillips and Total (Laux et al., 2007, 2008a, 2008b), and is further commercialized as an integrated tool for oil & gas engineers by Kongsberg. The prediction of benchmark case was carried out by Ashrafian A. (2012) of SINTEF.

3.3.4.1 CFD model for slug flow evolution

LedaFlow is made up of four different mathematical models: a steady-state point model, a transient 1D model, a profile model and the Q3D (quasi-3D) model. The Q3D module can be used as stand-alone tool or in combination with the 1D model. This model is based on a multi-fluid multi-field formulation with construction and tracking of the large-scale interfaces (LSIs). An important feature of Quasi 3D (Q3D) is by slicing the pipe in one direction, as demonstrated in Figure 3.16, the flow can be resolved as 2-dimensional but the code still be able to describe the complete flow in a pipe (Ashrafian, 2012). This approach can significantly reduce the computation time, offering a good compromise of accuracy and speed.

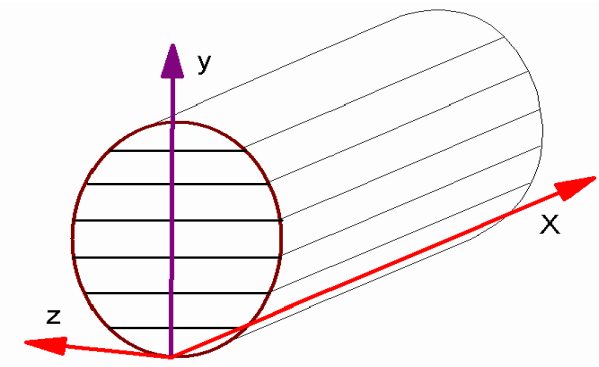

Figure 3.16: Quasi 3D grid cells, showing one axial (xdirection) and 7 vertical cells.

The full 3D model equations are averaged over the transversal distance *z* to create slice averaged model equations. The 3D structures become homogenized and the flow is represented by slice averaged fields. In this process the wall fluxes, such as shear stresses, turbulence production at side walls, become source terms. The numerical solution is performed on a staggered Cartesian mesh, where the discrete mass, pressure and momentum equations are solved by an extended phase coupled SIMPLE method (Patankar,1980). The implicit solver uses first order time discretisation and up to third order in space (Laux et al. 2007).

3.3.4.2 Geometry, mesh and boundary conditions

A pipe length of 30m was simulated. The domain contained 10x2440 cells which uniformly distributed across pipe diameter and in the axial direction, respectively. The grid aspect ratio was 1.5. Gas was treated as compressible and liquid is treated as incompressible. No perturbations were imposed at the inlet so that fluid phases were entering the pipe fully stratified. The details of inlet arrangement for air and water streams were not included in the simulations. The inlet superficial velocities of air and water were specified as given from the experiments. Initially, the pipe was filled with stratified air and water, with 50% of liquid fraction and zero velocity. Computations were carried out in parallel on 4CPUs using MPI. It took 2.3 days to run 52.5s of real flow time.

3.3.4.3 Results

Figure 3.17 shows snapshots of predicted slug evolution, the pipe diameter is magnified 5 times for clarity of the flow details. The red represents liquid and blue represents gas. Initially flow is stratified and the interface is flat and smooth, then the first wave is developed and blocks the pipe cross section, forming a slug. The slug propagates along the pipe and grows in size. However this very large slug is not periodic, suggesting the initial large slug is generated out of the initial condition of the flow inside the pipe. After the initial slug has exited, the pipe was almost drained from the water. The liquid level built up until it reached a critical level at which the interfacial instabilities are created. These instabilities are captured by the model and as the simulation proceeds further, they form waves. When one of the waves grows large enough to block the pipe, a new slug is formed. In contrast to the initial slug, this slug is much shorter, as can been seen from the snapshots.

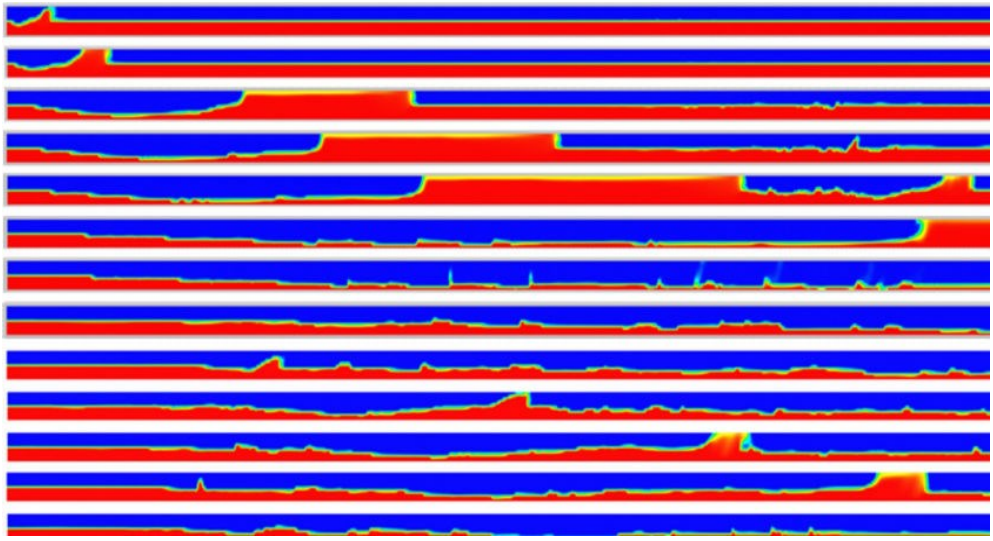

Figure 3.17: Snapshots of Q3D results showing the time evolution of slugs in a 30 m long horizontal pipe.

Figure 3.18 shows the prediction of the liquid hold-up time traces at different probe locations along the horizontal pipe. At 7.5m, the interface remains stratified wavy apart from the initial slug captured at the beginning of the simulation. In contrast, successive slugs were observed in experiment at the same location. Further downstream, the interface appeared much wavier with large wave structures at 11.25m, some waves were developed large enough to form slugs at 15m, and the slugs formed propagate between 15m and 30m.

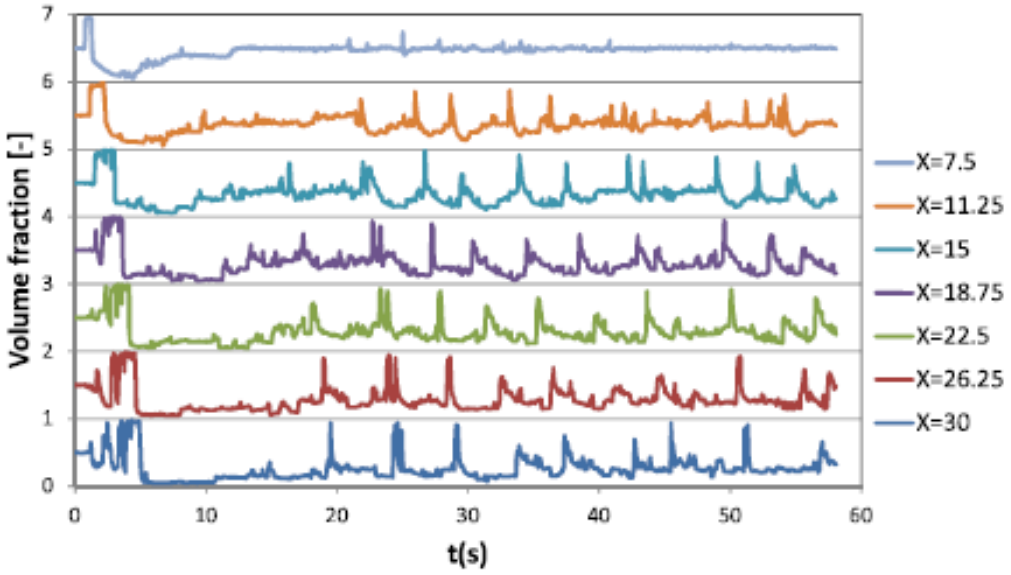

Figure 3.18: Liquid hold-up time trace for slug flow at different locations along the pipe.

The slug frequency is evaluated from hold-up time traces based on 60% or 80% liquid volume fractions as a defined threshold. The prediction of slug frequency as a function of distance from the inlet is plotted in Figure 3.19 and compared with the experimental data. In the experiments, a peak of slug frequency within the first 5m of the pipe is observed, however the peak of slug frequency is shifted further downstream in the simulation. The code operator suggested the inlet condition in the experiments has strong effect on the slug initiation, and it is difficult to predict by the model with the current inlet and initial conditions. However, a better agreement is obtained for the slug frequency further downstream.

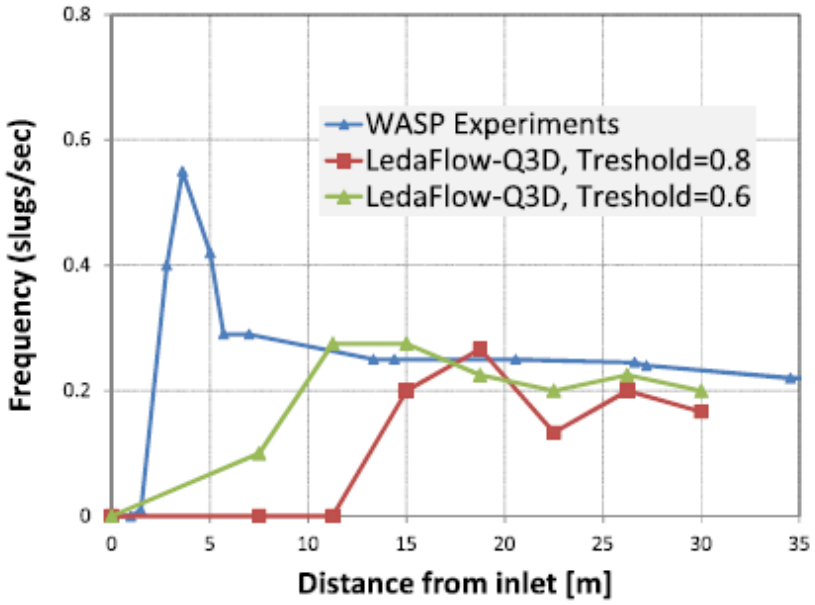

Figure 3.19: Slug frequency distributionsat various locaitons. Blue line represents the measurement data; green and red line represent predicted slug frequencies, based on different thresholds.

It may be concluded that LedaFlow Q3D is able to predict slugs from unperturbed inlet conditions. The mechanism of slug initiation and development is qualitatively well reproduced. However, apart from the initial slug which is considered to be unphysical, formation of successive slugs has shifted further downstream in the simulation comparing to the experiments. The reason is partly attributed to the simplification of the inlet section applied in the model. The actual geometry of the inlet section, including the air and water feed streams and a horizontal plate, are expected to trigger instabilities and waves. Secondly, the grid used in the simulation is too coarse to resolve capillary waves which could impact the onset of instabilities. As discussed above, slug frequency close to the inlet region is difficult to reproduce with the current setting of the model. However, the slug frequencies predicted in the developed region have shown a reason a good agreement with the experiments.

3.3.5 TransAT

The commercial CFD code TransAT was developed at ASCOMP in Zurich. The prediction of slug flow benchmark case was by Lakehal at al. (2011) of ASCOMP GmbH Switzerland.

3.3.5.1 CFD model for slug flow evolution

The Large Eddy & Interface Simulation (LEIS) is implemented in TransAT code and applied to the prediction of WASP slug flow benchmark case. The concept of LEIS approach is to combine the strength of Interface Tracking Method (ITM) with large scale, time-dependent simulation to better capture turbulence anisotropy and transient motion (Lakehal, 2009, 2010). It could be used in conjunction with large eddy simulation (LES) or very large eddy simulation (VLES).

The turbulence model V-LES (Very Large Eddy Simulation) model implemented in TransAT is based on the use of k-ε model as a sub-filter model. The filter width is made proportional to a characteristics length-scale, which should be larger than grid size, but smaller than the macro length-scale of the flow. Increasing the filter width beyond the largest length scales will lead to predictions similar to the output of RANS models, whereas in the limit of a small filter-width (approaching the grid size) the model predictions should tend towards those of LES. Hence V-LES works as a natural link between LES and RANS. If the filter width is smaller than the length scale of turbulence provided by the RANS model, then larger turbulent flow structures will be able to develop during the simulation.

The interface tracking techniques includes Level Set and VOF approaches. The Level Set method was employed in the TransAT simulation to track free surface flows, combined with the V-LES approach to cope with turbulence. Sub scale modeling of turbulence was achieved with the k-ε model with filter width set equal to 0.1D (Labois & Lakehal, 2011). The solver is pressure based, corrected for compressible flows. 3rd order Quick scheme was employed for convection. Mass conservation is enforced using global and local mass-conserving schemes.

3.3.5.2 Geometry, mesh and boundary conditions

TransAT uses the Immersed Surfaces Technique (IST) to map complex system components into a simple rectangular Cartesian grid. The idea of IST is to represent solid walls by a Level Set function which representing the exact distance to the surface: zero at the surface, positive in the fluid and negative in the solid (Labois et al., 2010). Near wall regions are handled

differently by Block-based Mesh Refinement (BMR), a sort of geometrical multi-grid approach in which refined grid blocks or manifolds are placed. The connectivity between blocks can be achieved in parallel up to 8-to-1 cell mapping. The combination IST/BMR saves up to 70% grid cells in 3D.

To simulate the slug flow case, an IST technique was used to mesh the pipe. Figure 3.20 shows the modeled pipe is immersed in a Cartesian grid. The geometry of the pipe front is very similar to the actual design; where air is injected from the top inlet and water is injected from the bottom inlet. The rectangular block in the middle of the inlet represents the phase separating plate.

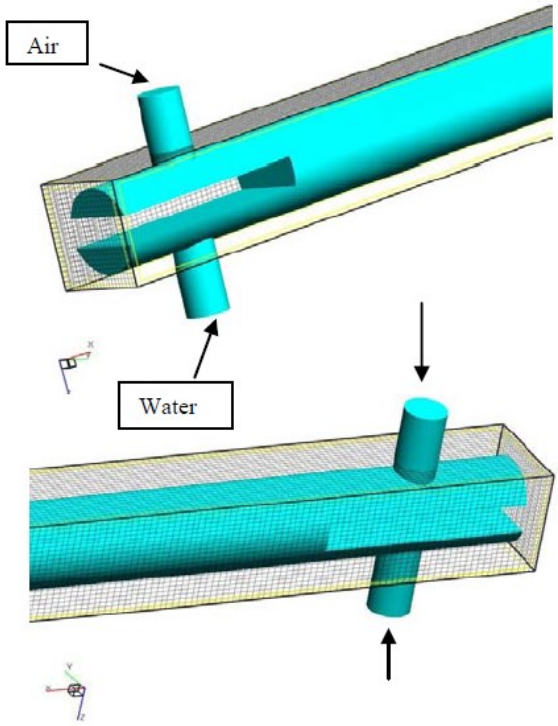

Figure 3.20: Computational IST grid. The modeled is immersed in a Cartesian grid, air & water inlet are shown.

The inflow boundary conditions were set with fixed superficial phase velocities and the liquid fraction, which were specified in the experiment. Initial flow disturbances based on the wall shear Reynolds number were applied to the entire flow domain to sustain turbulence.

3.3.5.3 Results

Initially, 2D simulation was performed in a pipe of length 17m. Plots of series of liquid hold-up time traces at various probe location measured in Ujang experiment are given in Figure 3.2 and Figure 3.3 in Section 3.1. To compare with the measurements, Figure 3.21 and Figure 3.22 give the liquid hold-up time traces captured in the 2D simulation. Slugs or large-wave structures are captured from 3m and further downstream. Various locations exhibit liquid hold-up of about 0.8-0.9, although the signal is qualitatively similar to the measured one in terms of slug or large-wave structures intermittency, it is unclear whether slugs were indeed captured. It was also noticed that large surface perturbations were captured upstream close to the inlet at 0.76m and 1.46m, but the flow regime was observed as stratified wave at those locations in the experiment.

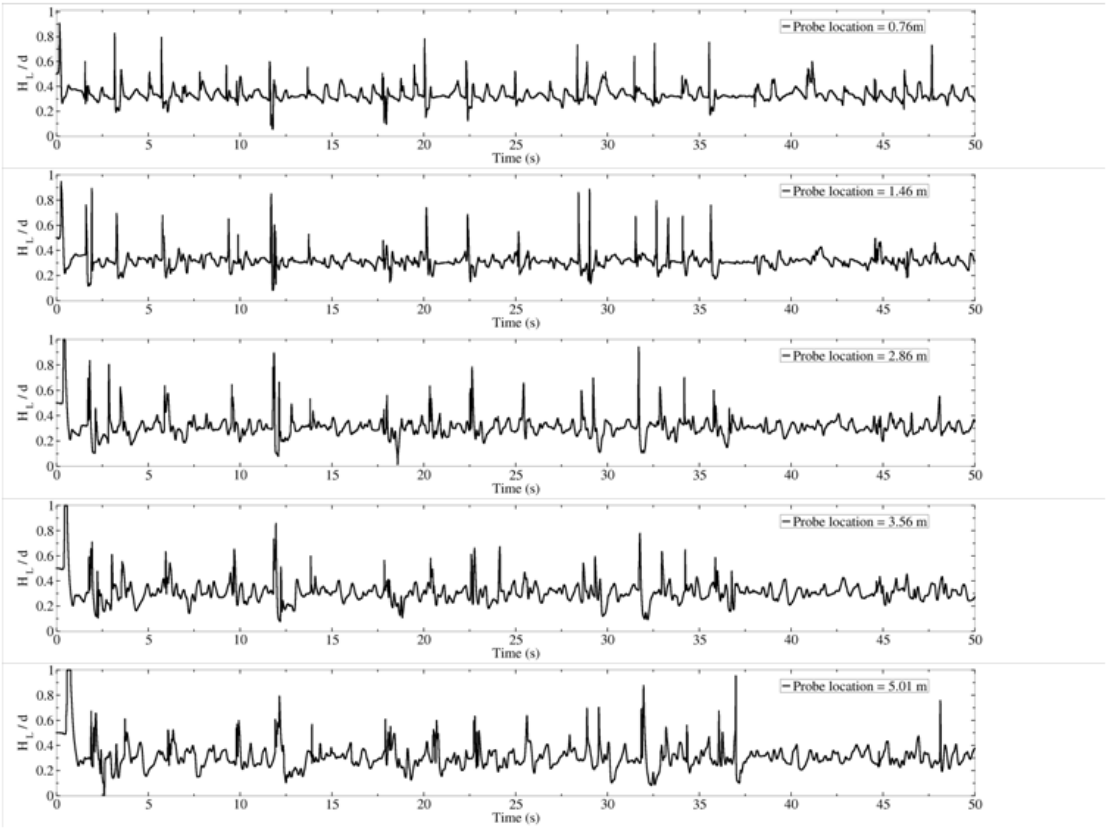

Figure 3.21: 2D TransAT calculation of liquid hold-up development for U_{sL}= 0.611m/s and U_{sG}= 4.64m/s (Probe location from 0.76m to 3.56m).

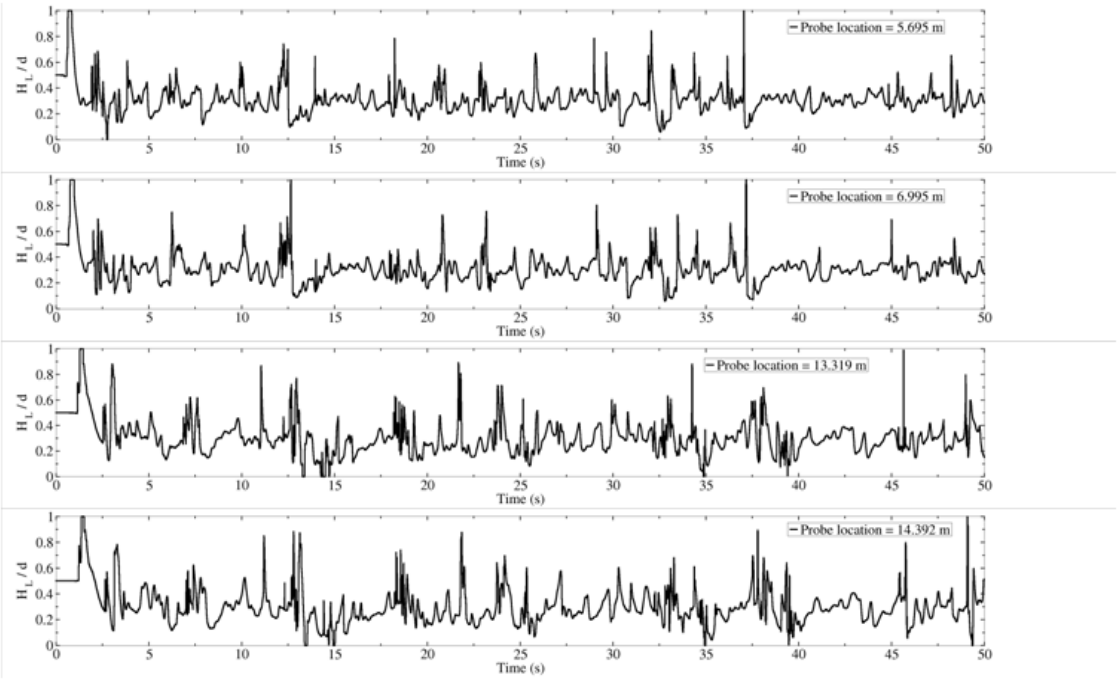

Figure 3.22: 2D TransAT calculation of liquid hold-up development for U_{sL}= 0.611m/s and U_{sG}= 4.64m/s (Probe location from 5.695m to 14.392m).

3D simulations were then performed on the length of 8m and 17m to address the effect of pipe length on the result. Initially the 3D simulations were performed in a shorter domain of 8m, consisting of 715.000 cells, then in a longer one of 16m, consisting of 1.200.000 cells. The simulation time for the 8m pipe simulation was 10 days on a low bandwidth Dell PC (2 nodes x 4 core) for 20s real time, and 53 hours on a high bandwidth 18 nodes IBM multi-core computer.

Figure 3.23 and Figure 3.24 show the 3D predictions of liquid hold-up time traces at various probe locations between 1.46m to 6.995m, from the short pipe (L=8m) case. Slugs or large-wave structures were initially captured at 7m from the inlet, however in reality slugs were observed much closer to the inlet.

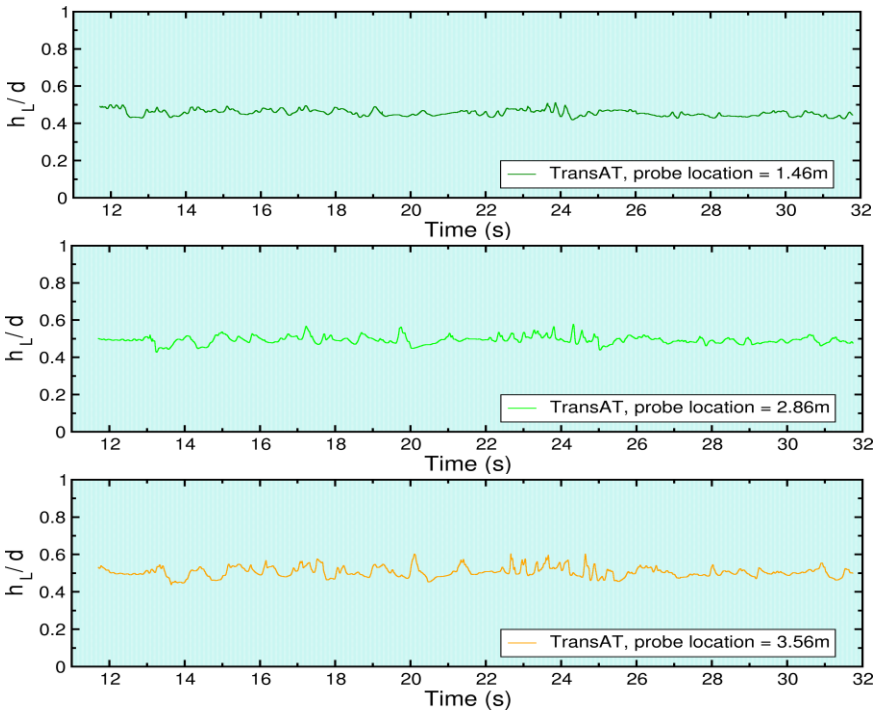

Figure 3.23: 3D TransAT calculation of liquid hold-up development for U_{sL}= 0.611m/s and U_{sG}= 4.64m/s (Probe location from1.46m to 3.56m).

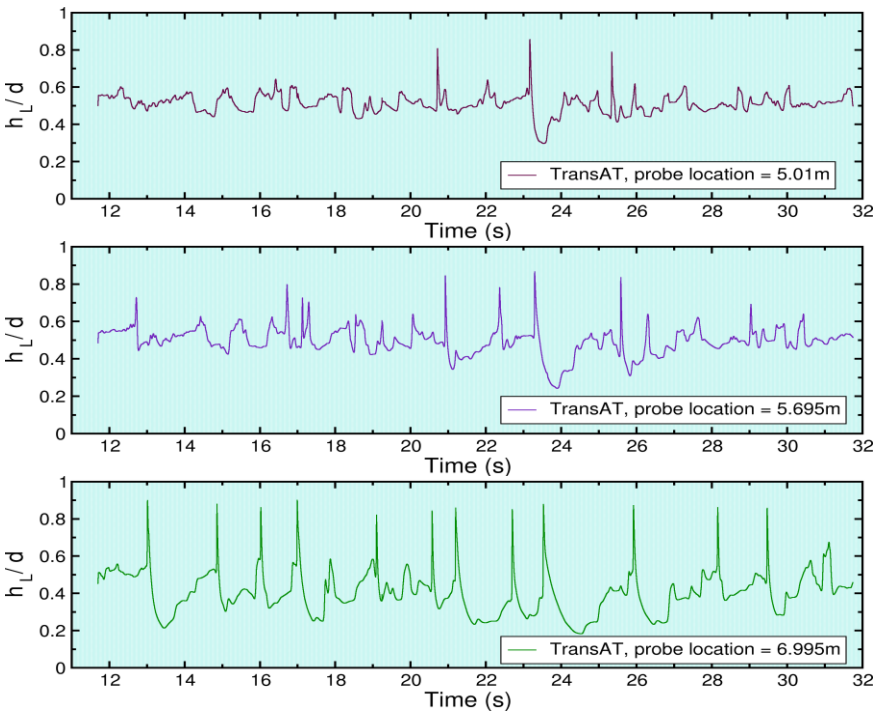

Figure 3.24: 3D TransAT calculation of liquid hold-up development for U_{sL}= 0.611m/s and U_{sG}= 4.64m/s (Probe location from5.01m to 6.995m).

For the simulation case with a 16m long pipe, different types of slugs were predicted. As illustrated in Figure 3.25 a, a large slug is formed upstream close to the inlet (<5m) and fills entirely of the pipe, the average slug length is around order of 2-4 of the pipe diameter. The second type of slug does not show 100% water filling the pipe as illustrated in Figure 3.26. It can be observed from the flow animation that liquid slug is travelling faster than the mean flow, which indicates it as slug. Gas bubbles are caught inside the slug, which explains that the measured liquid hold-up is less than unity. Those slugs are shorter than the first type and formed beyond the first 5 meters.

Figure 3.25: The formation of initial slug, liquid hold-up equal to unity.

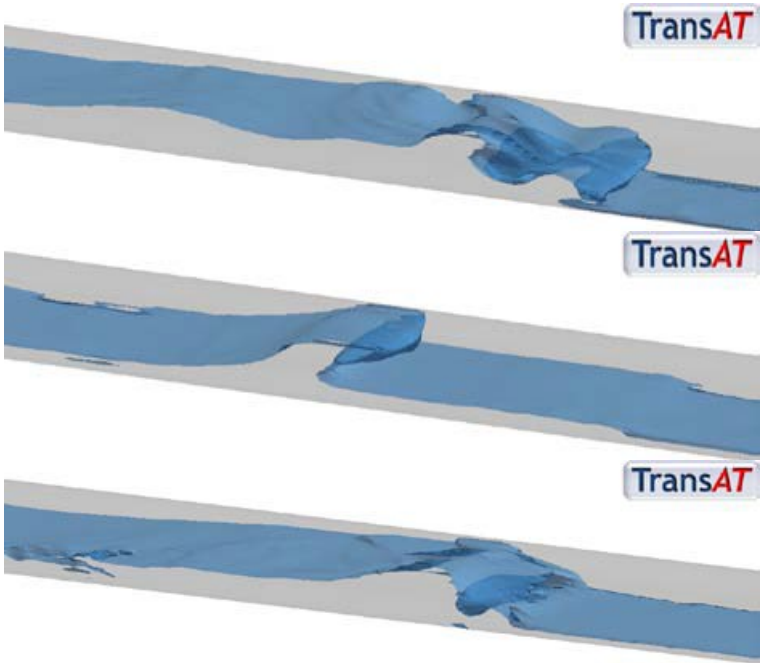

Figure 3.26: The formation of slugs with hold-up less than unity.

The 3D predictions of slug/large wave frequency are illustrated in Figure 3.27, it can be seen from the graph, a better match with the measurements are obtained with the longer pipe

simulation than the shorter pipe simulation. The peak in frequency is predicted around 3.5m in the longer pipe simulation, which is similar to the value delivered in the experiments. In contrast, the peak is shifted downstream with the shorter pipe, revealing the slug initiation process was under predicted. Among three graphs, there is a difference in terms of interpretation of slug frequency; each graph evaluates slug frequency based on different liquid hold-up threshold value: 0.8, 0.85 or 0.9. Apparently, the threshold of 0.85 agrees best with measurement. Furthermore, both simulations failed to reproduce the slug frequency development downstream towards the pipe exit. The frequency falls to zero at some locations whereas the frequency asymptotes to a constant value in experiment. Labois (2010) suggested that the simulation time was not sufficient to acquire all the slugs with frequency lower than 0.3 slug/s, therefore a longer simulation time is needed to improve the validations.

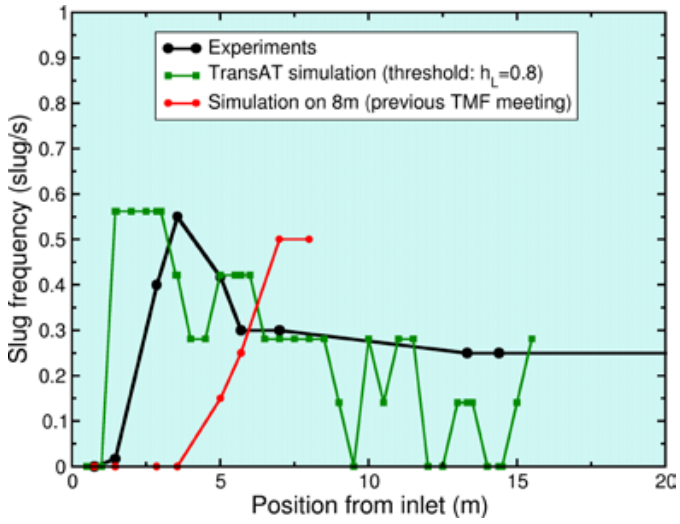

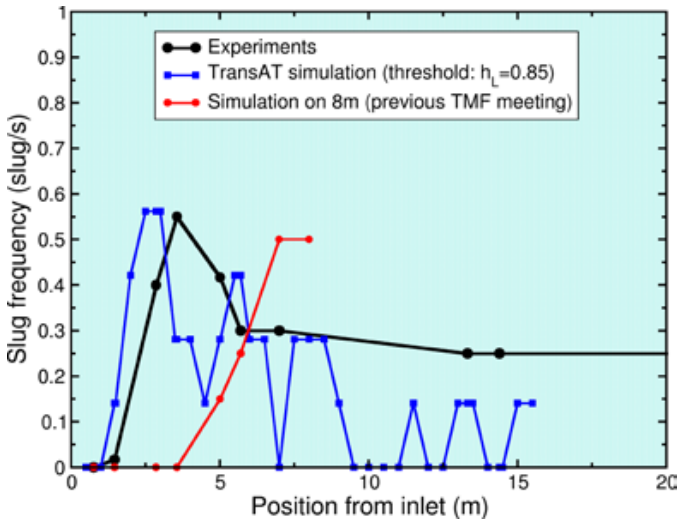

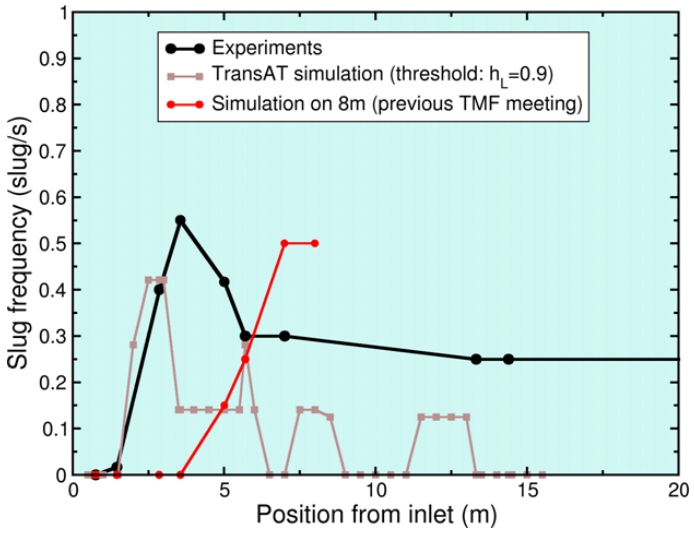

Figure 3.27: Comparison of experiment and predictions of slug frequency for 2 pipe lengths; L= 8m and 16m. hold-up threshold = 0.8/0.85/0.9.

As already mentioned in the previous sections, some of the CFD groups have used body fitted mesh and simplified inlet geometry, it was of interest to test the model with the TransAT code. This simulation was performed by Min Lu, the present author. The details of the inlet geometry were not included, and the modeling domain was the 16m long test-section, as shown in Figure 3.28. Water and air were introduced co-currently at the inlet and liquid fraction was specified as 0.5 throughout the domain. The inlet boundary condition was velocity and liquid fraction specified and outlet boundary condition was pressure controlled. Initially, a liquid fraction of 0.5 was assumed throughout the domain. A body-fitted mesh was built rather than Immersed Surfaces Technique (IST) hence a more precise refinement of the mesh near the wall region could be achieved. The multi-block grid strategy was used to cover the domain with adjacent sub-domains. The block is distributed between 32 processors for MPI parallel execution. The V-LES model was used for the turbulence and level set method for front tracking. Adaptive time stepping was enabled and controlled by the stability criteria; the interface was set to move between 0.6 to 1 cells during one time step. The domain contain about 5 million cells, on 32 CPUs, it took 1300hours (~53 days) to get 10s. Figure 3.29 shows the appearance of small instabilities at the air water interface at 0.35s.

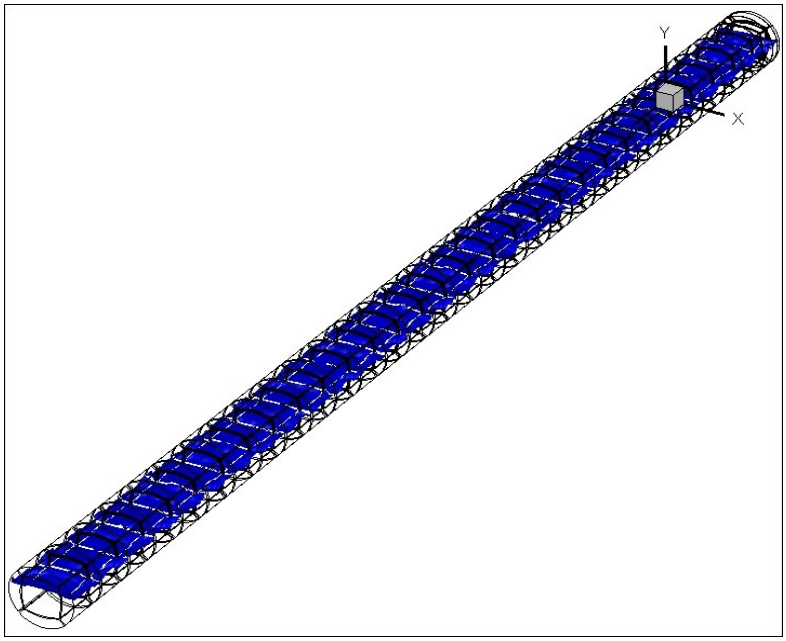

Figure 3.28: Perspective view of the simulated domain.

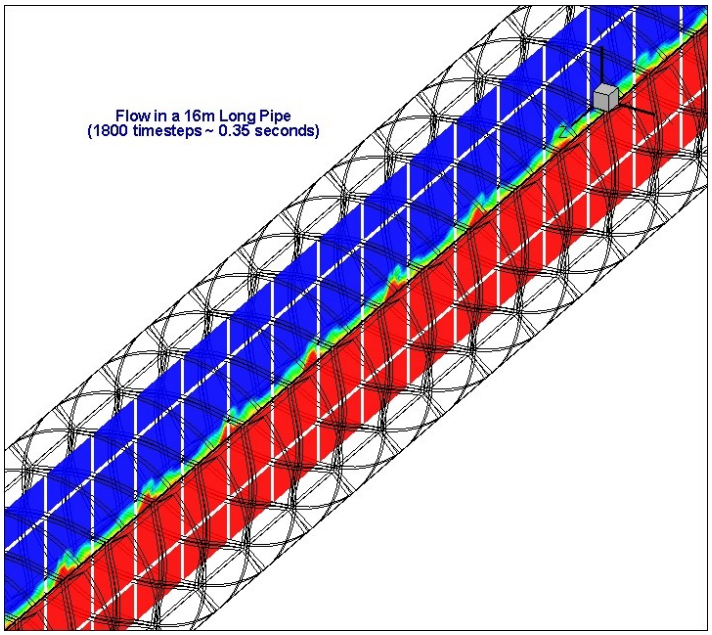

Figure 3.29: Prediction of small disturbances at the gas-liquid interface (zoomed views), t=0.35s.

An initial slug was captured around 4s at 5.01m. However, it was noticed when the second slug begin to occur at around 10s, the total volume flux passing through the pipe cross section began to oscillate largely as can be seen in Figure 3.30. Since the inflow flux is constant and flow is solving incompressible, the volume flux through every cross section of the pipe should remain constant to the level of convergence due to continuity condition. Therefore the

oscillation indicates the pressure equation was not converged, hence the prediction results was not reliable. The pressure solver employed in the simulation was the Algebraic Multi-grid (AMG) solvers which is most robust solver available in the code, therefore the simulation could not precede further due to the convergence problem. Suggested by the code developer, the Cartesian grid and embedded interface is simpler to converge for the pressure solver though it has disadvantage of not having precise mesh refinement near the wall as body fitted mesh does.

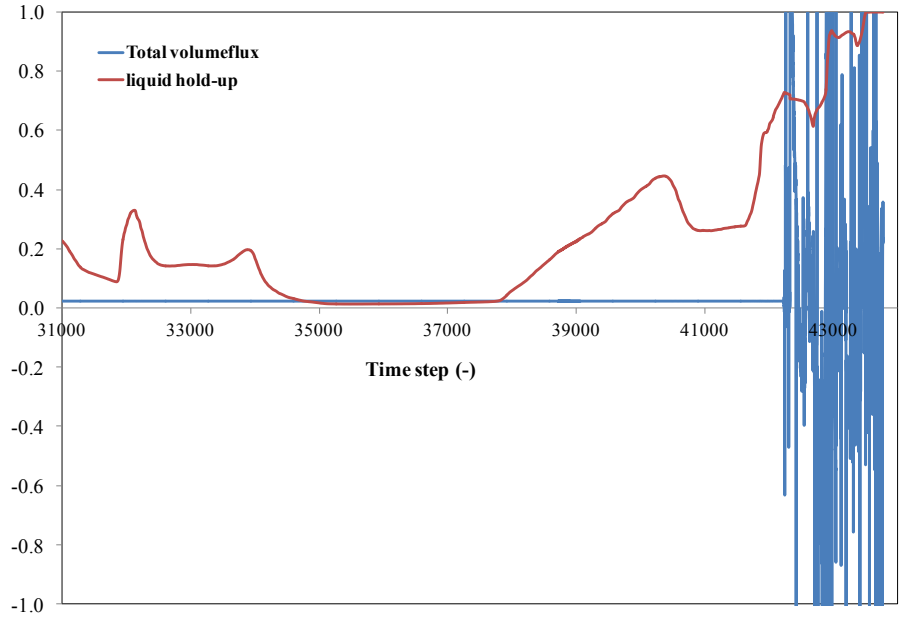

Figure 3.30: Oscilation of total volumeflux when liquid hold-up approaching to unity.

To conclude, the evolution of slug flow has been examined using TransAT simulations. The grid of domain was built with combination of Immersed Surfaces Technique (IST) / Block-based Mesh Refinement (BMR) meshing technique. The model has combined Level-Set approach for interface tracking and VLES for turbulence modeling, this combination of the model is also referred to as LEIS (Large Eddy & Interface Simulation) approach. The 3D flow simulation has shown the ability of LEIS model in the prediction of onset of slug formation. However, a longer simulation time is needed to provide a better slug statistics in order to quantitatively compare with measurements. However, the interpretation of slug frequency should be more precise than use of a liquid hold-up threshold only. With simplified domain, the disturbance introduced by the inlet geometry cannot be modeled; hence a more dense mesh is required to capture the surface instabilities. The body fitted mesh generates a

much larger number of cells than the one with the IST/BMR mesh, as a result, a much longer simulation time was required. The pressure solver was found difficult to converge for the body fitted grid, revealing the simulation is sensitive to the mesh type.

3.3.6 CFX

CFX was developed at the UKAEA Harwell Laboratory and was acquired and further developed by ANSYS. The prediction of slug flow benchmark case using CFX was carried out by Min Lu, the present author. The version of the code used in the present study was CFX-12.

3.3.6.1 CFD model for slug flow evolution

The multiphase formulations available in CFX code are: Lagrangian particle tracking, homogeneous multi-phase model, and Eulerian-Eulerian multi-phase formulation (mixture model).As discussed in Section 3.3.2, the homogenous VOF model is the most economical approach if the gas and liquid phase in slug flow are assumed to be fully segregated. However, experimental observations show that on the front of a slug, gas is entrained into the liquid phase. The homogeneous model which assumes phases share the same velocity field and not interpenetrating to each other, this usually leads to different behavior of the multiphase mixture in the region of higher gas entrainment. To cope with this deficiency, the work presented in this section used inhomogeneous multi-fluid Euler-Euler approach to simulate slug flow which is recommended by Frank (2003). The Eulerian modeling framework is based on mass-weighted averaged mass and momentum transport equations for all phases, therefore the modeling gas and liquid can be segregated or mixed at a macroscopic level. The “homogeneous” setting has been adopted for turbulence together with the SST model.

Different to the explicit slug tracking method, the “Standard free surface” model implemented in CFX is based on the interface capturing method. The model applies a controlled down-winding scheme to the volume fraction equations in order to avoid smearing of the interface between the two phases due to numerical diffusion of the solution algorithm

(Zwart et al.,2005).The computation is performed on a fixed grid that extends beyond the free surface; hence the shape of the free surface is determined by computing the phase content at each near-interface cell. In the simulation, the interface is defined as a region where the volume fractions of both fluids are equal to 0.5.

It is difficult to resolve the spatial structure of the interface into the micro-scale with the CFD model, due to the geometrical scale of the pipe. Therefore a slug flow simulation cannot cover onset and evolution of Kelvin-Helmholtz instabilities at the interface. The interface drag law applied to the location of the free surface must consider the influence of these free surface instabilities on the macro-scale flow properties (Vallee, 2005). The total drag force D is expressed in terms of the dimensionless drag coefficient C_D:

$$D = \frac{1}{2} \times \rho_{\alpha\beta} \times (U_\alpha - U_\beta)^2 \times A \times C_D \qquad [3.3]$$

where ρ is the fluid density, (U_α - U_β) is the relative speed and A is the projected area of the body inflow direction, α describes the liquid phase and β the gaseous phase.

3.3.6.2 Geometry, mesh and boundary conditions

The calculation of transient slug flow requires very high numerical efforts due to the intricate nature of the flow; an eight meters long pipe was modeled in order to save the computation time. The geometry and grid was created using ANSYS ICEM, the mesh consisted of 910,000 hexahedral cells. For the circular geometry, it's advisable to construct the O-grid mesh, which arranges grid lines into an O shape, hence improve efficiency of node clustering near walls. Figure 3.31 shows the cross-sectional view of the mesh. Elements refinement has been provided near the walls and at the expected region of interface between fluids.

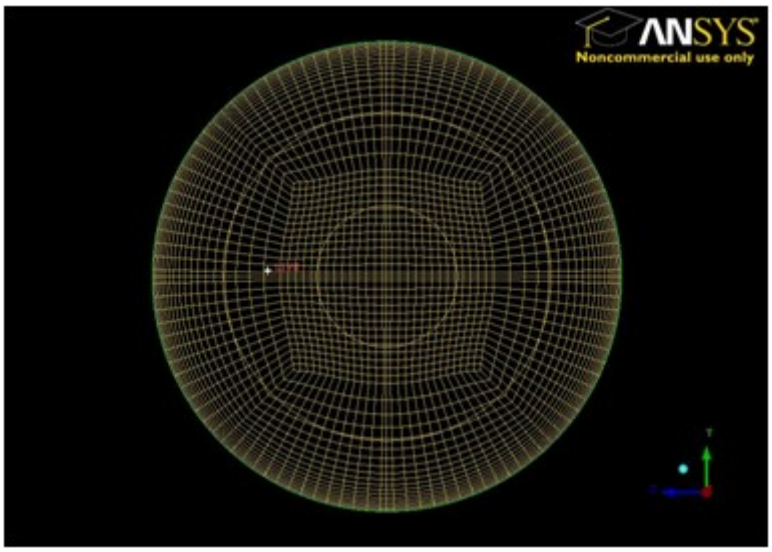

Figure 3.31: The cross sectional view of the mesh used in the CFX simulation of slug flow evolution.

At the inlet, air and water superficial velocities are set to constant values as specified in experiments. The turbulent kinetic energy and dissipation rate at the inlet were set to the default values. The outlet boundary condition was set to be pressure controlled. The inner wall of the pipe was assumed as hydraulically smooth with a non-slip boundary condition applied to both gaseous and liquid phases. The initial volume fraction is shown in XY plane of the domain, assuming stratified flow over the entire model length, with 50% of liquid fraction, see Figure 3.32.

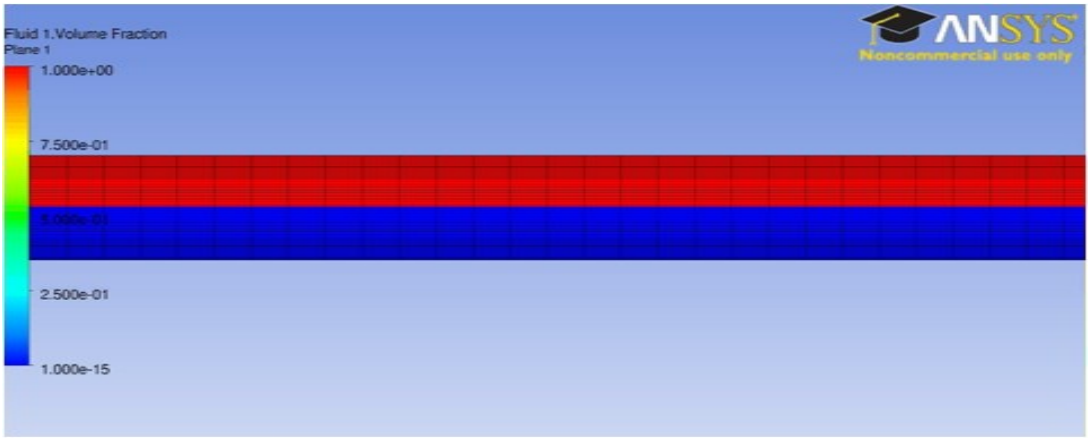

Figure 3.32: Initially condition of the simulation, pipe is filled with 50% of liquid and 50% of gas.

3.3.6.3 Results

Transient simulation was carried out on Dell PC with 2 processors; the time step was 0.0001s, with 10^{-5} convergence criteria. It took 40 days to simulate 15s of real time.

After 5 seconds since simulation had started, the gas and liquid flow remain stratified, with small amplitude waves observed at the interface. The development of the velocity profile along the pipe is illustrated in Figure 3.33, the zoomed pictures shows a series of velocity contours in the axial direction of the pipe, each image represents the velocity distribution at the corresponding cross-section. The averaged transversal phase velocity profiles is illustrated in Figure 3.34, the blue line represent the water velocity profile in the vertical direction, it increases towards the interface due to the interfacial drag from the fast moving gas velocity. The red line represent the air velocity profile, between interface and up wall, it show an upwardly inclined parabolic shape. The maximum velocity towards the pipe wall and the minimum velocity near the interface demonstrate an upward motion from the interface to the up wall. The gas flow is not parallel and it can be attributed to the contrast of roughness between the smooth wall and the wavy interface (Liné et al.,1991).

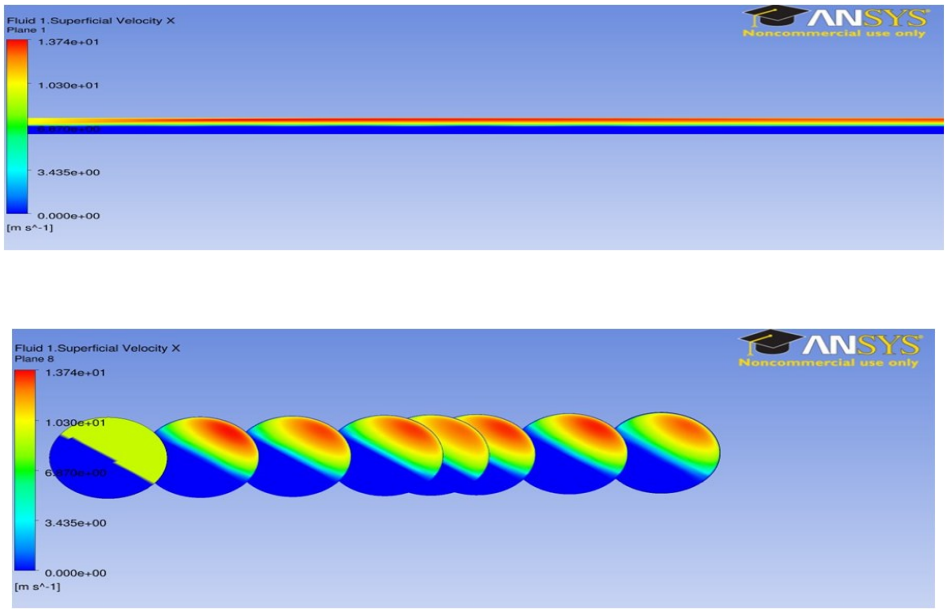

Figure 3.33: Contours of gas and liquid velocity in axial direction (first graph) and cross sectional planes (second graph).

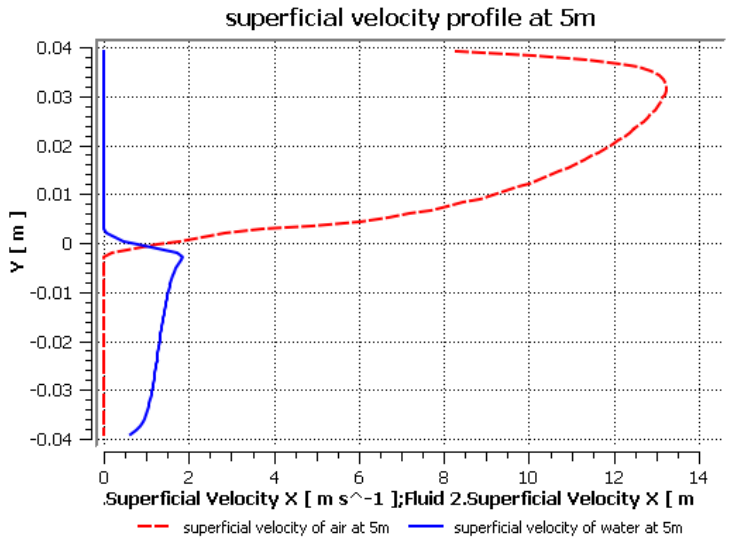

Figure 3.34: Transversal gas and liquid velocity profiles at test-section.

However, during the 15s of the simulation, the interface remained as stratified and none of the surface instabilities grew into large waves or slugs. Therefore the simulation with the chosen combination of models was failed to reproduce experimental results. Frank (2003) carried out a systematic study of numerical simulation of horizontal slug flow using CFX. He pointed out the formation of slug flow regimes strongly depends on the perturbation of the inlet boundary conditions. The simplified inlet boundary in the present study has neglected the inlet disturbances introduced to the flow, and leads to the underproduction of the free surface instabilities. Furthermore, Frank showed that the length of the computational domain plays an important role in slug formation, therefore a full pipe should be modeled. However, due to the restricted time frame and limited computation resource, further investigation was not possible.

3.4 Conclusion

In this chapter, CFD results concerning a benchmark for two-phase slug flow conducted in WASP facility are discussed. Time traces of liquid hold-ups and slug frequency at various probe locations are provided as reference for comparisons against the simulations. For this benchmark exercise, six different codes have been tried out. The conditions in terms of meshing, run time, boundary conditions applied in various CFD codes are summarised in Table 3.5.

Table 3.5: Simulation conditions used in various CFD cases.

Code	Domain length	Mesh size	Time step	T_{CPU}/ T_{real}	PC	Boundary condition
TRIOMPH 1D	36m	1250	0.0001s	-/300s	Single CPU	Inlet: fluid velocity & phase fraction specified Outlet: pressure controlled
LedaFLow quasi-3D	30m	10x2440	-	2.3 days/ 52.5s	4CPUs	Inlet: fluid velocity & phase fraction specified Outlet: pressure controlled
FLUENT 3D	12m	322560	-	18days/ 23s	4CPUs	Inlet: fluid velocity & phase fraction specified Outlet: pressure controlled Symmetric boundary at the pipe center
	12m	1008000	-	18days/ 40s	8CPUs	
	37m	1989120	-	-	-	
STAR-CD 3D	37m	568512	0.0008s	10days/ 100s	20 CPUs	Inlet: fluid velocity & phase fraction specified Outlet: pressure controlled Symmetric boundary at the pipe centre
TransAT 3D	17m	1200000	Self-adaptive	53hrs/20s	18 nodes IBM multi-core	Inlet: fluid velocity specified at feed stream inlets Outlet: pressure controlled
CFX 3D	8m	910,000	0.0001s	40days/ 15s	2CPUs	Inlet: fluid velocity specified Outlet: pressure controlled

1D prediction was performed by using TRIOMPH code, which is based on the two-fluid slug capturing technique. The modelling domain is the 37 meters long test-section with simplified plane inlet. The slug frequency trend predicted by the code is similar to the measurement, including a peak in the slug initiation site and an asymptotic value in the developed region. However, it was noticed the initiation of the slug flow is sensitive to the inlet conditions such as inlet liquid fraction.

2D prediction was performed using TransAT code. The modeling domain includes separate gas liquid inlet streams and stratification blade, the length of the domain is 17 meters. The IST/BMR meshing approach was applied to the domain. The LEIS (Large Eddy & Interface Simulation) model implemented in the code is used in conjunction with VLES turbulence model. The simulation is able to capture slug flow in terms of the intermittency feature. However, it has failed to predict the stratified flow regime close to the inlet, large surface perturbations were predicted instead.

Quasi 3D prediction was performed by using LedaFlow Q3D model. The modelling domain is the 37 meters long test-section. The Q3D model slices averaging the domain, and use multi-fluid approach to model the physics at the Large Scale Interface. The code is able to produce slug flow from initial stratified flow without introducing any disturbance. However, the slug initiation process is delayed in the prediction; the reason can be partially attributed to the simplification of the inlet geometry which is expected to trigger instabilities and waves.

3D FLUENT prediction used the VOF approach together with the k-ε turbulence model. The code has shown its ability to predict the transition from stratified flow to slug flow. The results reveal the pressure controlled outlet is more robust than the open outlet; and the pipe length is influential in the slug flow predictions. The peak in the slug frequency was captured in the simulation and the value agreed with measurements. However in further downstream, the simulations failed to predict the asymptotic trend of the frequency.

3D STAR-CD prediction used VOF approach to track the interface; the turbulence model was k-ω based SST model and turbulence damping was also applied at the interface. An initial disturbance was applied in the flow domain. Different to FLUENT which used liquid hold-up threshold to identify slug, STAR-CD used velocity discrimination method to identify the presence of the slug. Full pipe length was modeled, however symmetry was assumed at the vertical center of the pipe, as a compromise to the computation resource. A qualitatively agreement with experiments were obtained in terms of continuous development of the slug length and slug flow development structure along the pipe. However, the code failed to reproduce the slug initiation process, the reason is attributed to the simplification of the inlet boundary.

The physical model applied to the 2D TransAT prediction was also tried out in the 3D TransAT simulations. The 3D result is improved comparing to the 2D results, the stratified flow regime near the inlet is reproduced in the 3D calculation, and the subsequent slug initiation and developing process is also well captured. However the code failed to reproduce the asymptotic trend of the slug frequency in the developed region. Furthermore, prediction was also made on a simplified geometry, with body-fitted mesh, the model was found inappropriate due to convergence problem.

The 3D CFX simulation was performed with inhomogeneous multi-fluid Euler-Euler approach. Turbulence was modeled with SST turbulence model. No slug was captured within the 15 seconds of real time.

Overall, the simulation of transition from stratified flow to slug flow and subsequently slug flow development is a sensitive benchmark case for the model setup. Different CFD codes have applied various CFD models to simulate the slug flow, the numerical simulation was performed by using phase-averaged multi-fluid models, such as the homogeneous VOF model (STAR-CD, FLUENT) and the two-fluid approaches (TRIOMPH, CFX, LedaFlow) or non–phase averaged variants, such as interface tracking methods (TransAT). The behavior of transition from stratified flow to slug flow was captured by various models, however the comparisons against the measurements were not satisfying, the main reasons may attributed but not limited to the following aspects:

1. In the simulation without any transient perturbation of the interface between water and air, a very fine mesh and long pipe is necessary in order to observe the formation of liquid slugs. However it is almost impossible to experimentally create completely undisturbed inlet boundary conditions. The geometry of the inlet section in the laboratory usually introduces certain fluctuation. Therefore it's important to model the details of inlet geometry in order to reproduce the physics in reality. The introduction of artificial disturbances to the flow domain may possibly create numerical effects which are not desirable.
2. It was found the computational domain plays an important role in slug development. The reason may be partially attributed to the pressure fluctuation created by liquid

slug exiting the pipe; the longer pipe should reduce the downstream pressure fluctuation.

3. The interpretation of the slug frequency is important for a quantitative comparison between the experiment and numerical simulations. The use of liquid hold-up threshold should be combined with velocity discrimination method to identify slug from large waves. Moreover, the convergence and the accuracy of simulations have to be assessed; the appearance of large wave structure can be a result of numerical diffusion.
4. The time frame of the numerical simulation should be long enough to generate sufficient number of slugs in order to produce a better slug statistics.
5. The uncertainty in the experimental measurements should be precisely controlled to a minimum standard. If the perturbations introduced by the experimental set-up, such as the pump surge and vibration of the test-section, it creates a difficult task for CFD benchmark.

Chapter 4

TRIOMPH-steady/unsteady inlet

4.1 Summary

The TRIOMPH (TRansient Implicit One-dimensional Multi-PHase) code (Issa & Woodburn, 1998) is based on the "slug capturing" technique in which the slug flow regime is predicted as a mechanistic natural outcome of the solution of the conservation equation system. This method solves the one-dimensional two-fluid model (see Section 4.2.1), in order to capture the initiation and growth of the slugs. However, the equations of the model are only conditionally well-posed for horizontal pipes. The mathematical classification of the system of equations can be defined by the characteristics analysis (Montini, 2011): if the characteristics are real the equations are hyperbolic and the system is well-posed; if the characteristics are complex the equations are elliptic and the initial value problem is ill-posed (see Section 4.2.2). The numerical model of the code is discussed in Section 4.2.3. A validation study of well-posedness of the system was carried out in the present study, simulations of a well-posed case and an ill-posed case, with steady inlet conditions were performed, and the results are given in Section 4.3.1. To remedy the ill-posedness of the equations which mainly occurs in the stratified region, the output of the TRIOMPH calculation was recycled and feed at the domain inlet, running the simulation with unsteady inlet boundary condition (Section 4.3.2.1), and a converged solution was obtained for an originally ill-posed case. An alternative method is to generate trains of slugs using slug tracking code, and feed them at the TRIOMPH inlet (Section 4.3.2.2), similarly a unique solution was obtained regardless of the difference at the inlet.

4.2 TRIOMPH code

The ability of the TRIOMPH code to predict the process of slug initiation and development is discussed in this section. The code is based on the "slug-capturing" technique, where slugging is automatically captured as a natural outcome of flow instabilities giving rise to perturbation growth in stratified flows leading to the formation of slugs. This method uses an Eulerian approach to solve the one-dimensional two-fluid model. The same set of equations are retained regardless of the local flow pattern (slug or stratified) that generates in the pipe.

In slug capturing, no external excitation is needed to generate a perturbation of the solution. The inception of slugs from a stratified condition is due to the disturbances in the solution continually being generated by round-off and discretisation errors: these disturbances are of random nature and therefore have different wave spectra. This leads to different wave lengths which give different wave growth rates, hence varying wave structures and eventually slugs that are of different characteristics. As a consequence, a slug capturing computation takes advantage of the random-like nature of the round-off errors and uses it as the engine to reproduce the experimentally observed random nature of slug flow.

4.2.1 Two fluid model

The one-dimensional two fluid model (Ishii, 1975; Ishii & Hibiki, 2006) represents a system of partial differential equations used to mathematically describe and reproduce the main properties of the different flow regimes. Although the two phase flow has a clear three-dimensional nature, being related to phenomena such as turbulence and the presence of slugs, the one-dimensional approach still is the most appropriate for modelling the flow in long pipelines in light of the current computational capabilities.

The one-dimensional form of the model is obtained by integrating over the cross sectional area of the pipe. By area averaging, the variations occurring in the radial direction are lost. For this reason the effect of the interactions (mass and momentum transfer) between the phases must be modelled with appropriate closure relations.

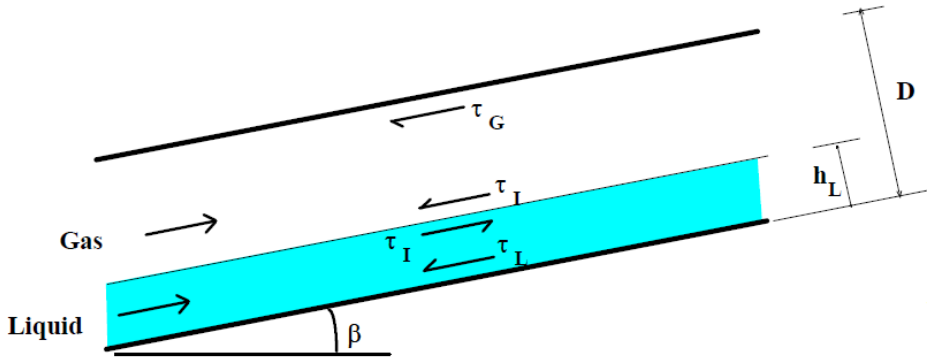

Figure 4.1: The stratified flow system under consideration.

Using the isothermal one-dimensional two-fluid model to describe the gas-liquid two phase flow in a pipe as shown in Figure 4.1 , the area-averaged liquid and gas continuity equations are given by:

$$\frac{\partial \varepsilon_G \rho_G}{\partial t} + \frac{\partial \varepsilon_G \rho_G u_G}{\partial x} = 0 \qquad [4.1]$$

$$\frac{\partial \varepsilon_L \rho_L}{\partial t} + \frac{\partial \varepsilon_L \rho_L u_L}{\partial x} = 0 \qquad [4.2]$$

where ε_K , ρ_K and u_K (k is either gas or liquid) represent phase volume fraction, density and viscosity, respectively.

The momentum equations for each phase are given by:

$$\frac{\partial \rho_G \varepsilon_G u_G}{\partial t} + \frac{\partial \rho_G \varepsilon_G u_G^2}{\partial x} = -\varepsilon_G \frac{\partial p}{\partial x} - \rho_G \varepsilon_G g \sin\beta - \frac{\tau_{wG} S_G}{A} - \frac{\tau_i S_i}{A} \qquad [4.3]$$

$$\frac{\partial \rho_L \varepsilon_L u_L}{\partial t} + \frac{\partial \rho_L \varepsilon_L u_L^2}{\partial x} = -\varepsilon_L \frac{\partial p}{\partial x} - \rho_L \varepsilon_L g \frac{\partial h_L}{\partial x} \cos\beta - \rho_L \varepsilon_L g \sin\beta - \frac{\tau_{wL} S_L}{A} - \frac{\tau_i S_i}{A} \qquad [4.4]$$

where p is the interfacial pressure and h_L is the liquid height above the pipe bottom, β is the inclination of the pipe. S_G, S_I and S_L are the respective lengths of the gas-wetted perimeter, the interface and the liquid-wetted perimeter. τ_{wG}, τ_{wL} and τ_i represent the liquid-wall, gas-

wall and interfacial shear stresses respectively. The second term on the right hand side of Eqn.4.3 and 4.4 is the hydrostatic term; it is negligible for the gas phase at atmospheric conditions, since the liquid-gas density ratio is reasonably high.

The gas-wall and liquid-wall shear stress τ_{wk} are defined by:

$$\tau_{wk} = f_{wk} \frac{\rho_k u_k |u_k|}{2} \qquad [4.5]$$

and the interfacial shear stress is defined by:

$$\tau_i = f_i \frac{\rho_G (u_G - u_{L)} |u_G - u_L|}{2} \qquad [4.6]$$

In the TRIOMPH code, the following closures for the friction factors f_{wG} f_{wL} f_i are employed which were recommended by Rippiner (1998).

The gas-wall and interfacial friction factors are based on the standard Blasius model where the expression for the gas-wall friction factor is:

$$f_{wG} = C_G \, \mathrm{Re}_G^{-n_G} \qquad [4.7]$$

where the Reynolds number is defined as

$$\mathrm{Re}_G = \frac{D_{hG} u_G \rho_G}{\mu_G} \qquad [4.8]$$

and D_{hG} is the gas hydraulic diameter

$$D_{hG} = \frac{4 A_G}{S_i + S_G} \qquad [4.9]$$

The coefficient C_G and n_G respectively have values of 0.046 and 0.25 if the flow is turbulent ($Re_G > 2100$), or 16 and 1 if the flow is laminar ($Re_G \leq 2100$).

The interfacial friction factor is expressed as:

$$f_i = C_i \, \mathrm{Re}_i^{-n_i} \qquad [4.10]$$

where Re_i is defined as:

$$\mathrm{Re}_i = \frac{D_{hG} u_{rel} \rho_G}{\mu_G} \qquad [4.11]$$

The velocity u_{rel} represents the gas-liquid slippage ($u_{rel} = |u_G - u_L|$) while C_i and n_i have the same expressions as those for the gas friction factor. The correlation used for calculating the liquid-wall friction factor f_{wL}, is that from Spedding & Hand (1997). It is defined as:

$$f_{wL} = \frac{24}{\mathrm{Re}_L^s} \quad (Re_L \leq 2100) \qquad [4.12]$$

$$f_{wL} = 0.0262(\alpha_L \, \mathrm{Re}_L^s)^{-0.139} \quad (Re_L > 2100) \qquad [4.13]$$

where

$$\mathrm{Re}_L = \frac{D_{hL} U_{SL} \rho_L}{\mu_L} \qquad [4.14]$$

The hydraulic diameter for the liquid phase D_{hL} is given as $D_{hL} = \frac{4A_L}{S_i}$.

The liquid Reynolds number Re_L^s is based on the liquid superficial velocity

$$\mathrm{Re}_L^s = \frac{D\, U_{SL} \rho_L}{\mu_L} \qquad [4.15]$$

The above liquid-wall friction factor is retained in the present version of the TRIOMPH code regardless of the gas-liquid flow pattern (stratified or slug).

4.2.2 Well-Posedness of the system

The two-fluid model represents a system of first order partial differential equations, the equations are only conditionally well-posed for horizontal and nearly horizontal pipes. The mathematical classification of the system of equations can be defined by the characteristics analysis: if the characteristics are real, the equations are hyperbolic and the system is well-posed; whereas if the characteristics are complex the equations are elliptic and the initial value problem is ill-posed (Montini, 2011). In horizontal stratified flow, Wallis (1969) found the term accounting for the hydrostatic pressure distribution in the liquid phase makes the two-fluid model well-posed with real characteristics for certain flow conditions. There conditions are given by:

$$(u_L - u_G)^2 \le (\frac{\varepsilon_L}{\rho_L} + \frac{\varepsilon_G}{\rho_G})(\rho_L - \rho_G) g \cos\beta \frac{dh}{d\varepsilon} \qquad [4.16]$$

where ε_G=1-ε_L. Assuming the value of ε_L is given by the equilibrium state of a stratified flow; a single curve can be obtained on a flow regime map as shown in Figure 4.2. The continuous line represents the limit of the well-posedness as given by a characteristics analysis. All the cases below this line are well-posed and the solutions of the model are legitimate from a mathematical point of view, while the cases above the limit are ill-posed and the numerical results are unreliable. Therefore, the well-posedness line on the flow pattern map clearly defines the limitation of the standard mathematical model.

From a numerical prospective, simulations are always subject to machine round-off and these errors in the specific case of an ill-posed system may grow sometimes to such an extent so as to dominate the solution and render the final result meaningless. This is due to the fact that

the instabilities predicted by the two-fluid model are not always physically-realisable solutions reflecting the real flow conditions, but could also be a manifestation of the mathematical or numerical instability of the model (Issa & Kempf, 2003).

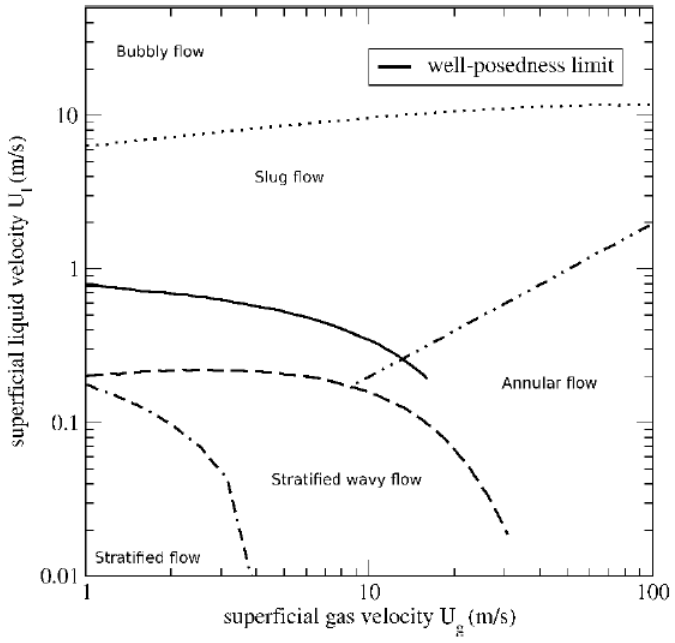

Figure 4.2: Flow pattern map for horizontal pipes (Taitel & Dukler, 1976) with the well-posedness limit.

4.2.3 Numerical solution

The TRIOMPH code applies a finite volume methodology to discretise the two fluid model equations whereby the solution domain is subdivided into a finite number of contiguous control volumes. The grid arrangement is staggered (Harlow & Welch,1975), in this configuration the pressure and densities are stored at ordinary grid whereas the velocities are stored at a staggered grid.

The code solves for one of the phase volumetric fractions ε_G, the two phase velocities (u_L and u_G), and the gas-liquid interfacial pressure p. The liquid phase is regarded as incompressible, the compressibility effects in the gas phase is accounted for using the perfect gas law. As illustrated by Issa & Abrishami (1986), if the gas and liquid continuity equations are weighted by a related reference density, the form of the overall continuity obtained is:

$$\frac{\partial \varepsilon_L}{\partial t} + \frac{\partial (\varepsilon_L u_L)}{\partial x} + \frac{1}{\rho_G^{ref}} \left[\frac{\partial (\varepsilon_G u_G)}{\partial t} + \frac{\partial (\rho_G \varepsilon_G u_G)}{\partial x} \right] = 0 \qquad [4.17]$$

The velocities u_L and u_G are replaced by expressions which are derived from the discretised momentum equation. The pressure equation is solved using the PISO algorithm (Issa, 1986). The boundary conditions imposed in the calculations of the code are as follows: at the inlet, the liquid hold-up, the liquid and gas superficial velocities are fixed; at the outlet the absolute pressure is also fixed. The initial condition assumes a uniform stratified flow field, where hold-ups, gas and liquid velocities, and the pressure are uniform throughout the pipe.

When a slug forms, the gas volume fraction tends to zero and consequently the discretised gas momentum equation becomes singular. A criterion was therefore adopted when the liquid volume fraction exceeds a certain threshold value (α_L > 0.98) the cell is considered slugged (Montini, 2011). From this instant, the gas momentum equation is suppressed and the gas velocity is forced to zero. An ideal numerical model should avoid numerical diffusion, captures small instabilities and obtains an accurate solution within a reasonable computational cost. Sensitivity analyses (Bonizzi, 2003, Issa & Woodburn, 1998) suggested that the grid size should be about one third of the diameter of the pipe ($dx/D \approx 0.3$) in order to meet these requirements.

4.3 Validation of TRIOMPH code

Over the past years, researchers extensively assessed the TRIOMPH methodology for slug flow against available experimental data obtained from the Imperial College WASP facility. The validation was favourably carried out for slug characteristics such as hold-up, slug velocity, slug length and etc, with a maximum error bound of 30% (Montini, 2011) . However, as discussed earlier, the numerical prediction of this one-dimensional code is reliable only if the flow condition is well-posed.

Bonizzi (2003) performed an investigation to exam the effect of the well/ill-posed nature of the system for two WASP slug flow test cases. One case is above the well-posed limitation line whereas the other is below it. The location of the two points also suggests slugging is

expected for both flow rates. The computed time-averaged slug frequency was plotted against the size of the grid spacing: for a well-posed system, a unique solution exists and the average slug frequency converges to the same value which is in agreement with the measurement. On the other hand, for the ill-posed case, a unique solution no longer exists and values of the frequency computed subsequently diverge as the mesh is refined. Bonizzi (2003) analysed the differences between two cases with the aim of understanding the origin of the ill-posedness case. In regards to the ill-posed case, Bonizzi checked the well-posedness of the system locally for each grid cell and found out that the equations are mainly ill-posed in the initial stratified region where slugs initiate, whereas in the fully developed flow area towards the pipe exit the equations are mainly well-posed. He then proceeded to replace the steady state inlet conditions, which are responsible for the ill-posed stratified region, with unsteady boundary conditions. The inlet conditions are the velocities of the two phases and the liquid volume fraction, which stored during a previous simulation from a probe at the end of the pipe (well-posed region).

To verify Bonizzi (2003)'s finding, two WASP slug flow cases were chosen to be numerically investigated in present study, the experiments were performed by Ujang (2003), one case is in the well-posed region and the other is in the ill-posed region of Figure 4.2.

4.3.1 Steady inlet boundary condition

The steady inlet boundary condition is defined by constant phase velocity and volume fraction at the inlet. In experiment, a stratification plate was placed in the middle of the test section inlet, therefore the phase fraction for gas and liquid is defined as 0.5 for both cases. The superficial gas and liquid velocities are summarised in Table 4.1. In the simulation, the gas phase was treated as compressible and the liquid phase was treated as incompressible; the gas entrainment was not accounted for in the current code version. Each simulation runs for 300 seconds of real time. A slug was assumed if the liquid holdup of an object is bigger than 0.98 and the length of this object is more than twice the pipe diameter.

Table 4.1: Superficial gas and liquid phase velocity for case 1 and 2.

	CASE 1 well-posed case	**CASE 2** ill-posed case
U_{SL}	0.41m/s	1.003m/s
U_{SG}	2.36m/s	4.259m/s

To examine the mesh dependency, for each case, four different mesh spacing Δx were studied (Δx = 0.09D, 0.186D, 0.37D and 1.15D), the finest mesh is 0.09D and the coarsest is 1.15D. Figure 4.3 and Figure 4.4 show the slug frequency as a function of mesh spacing (the red dots represent measured slug frequency which is independent of the mesh spacing, and is included in the diagram as a reference). For case1(well-posed case), refining the mesh from the coarsest meshing spacing of 1.15D to 0.37D results in an increased slug frequency, however, the slug frequency remain constant if further refines the mesh from 0.37D to 0.186D and 0.09D, indicating the numerical result is independent of mesh spacing. Compared with the measurement, the numerical prediction slightly underestimates the slug frequency, with an error of 28%. In the simulation, only the long waves generated by Kelvin-Helmholtz type of instabilities can be captured, whereas in reality disturbance can be introduced by pump, inlet device and etc., therefore it is more likely that the initiation process of the slug maybe damped out, giving an under-prediction of the slug frequency. On the other hand, the simulation results of case 2 (ill-posed case) have shown a strong dependence on the mesh spacing, the slug frequency kept increasing from the coarsest to finest mesh, this appears to be the manifestation of the ill-posedness of the system, which is in agreement with Bonizzi (2003).

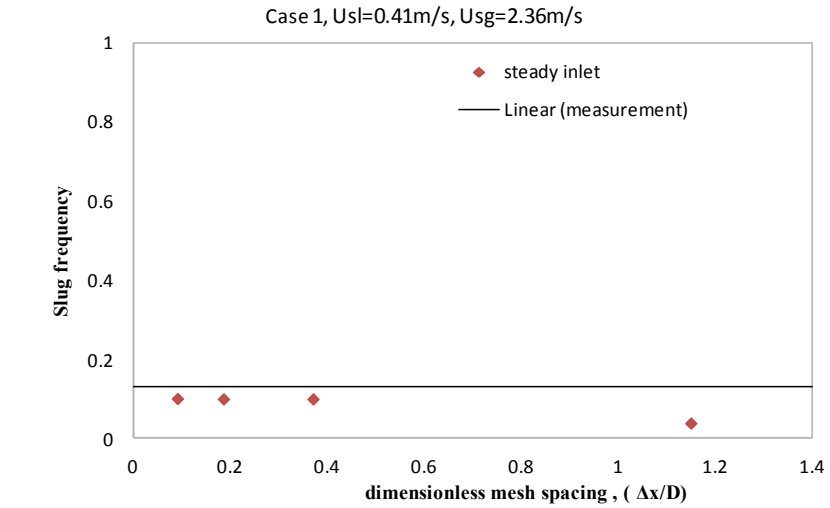

Figure 4.3: Predictions of slug frequency plotted versus the dimensionless mesh size for case 1. Steady inlet bounday conditions.

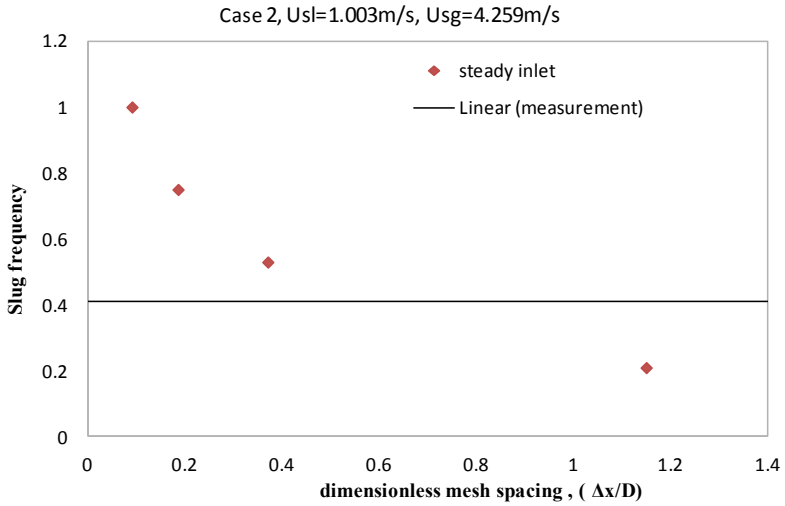

Figure 4.4: Predictions of slug frequency plotted versus the dimensionless mesh size for case 2. Steady inlet bounday conditions.

4.3.2 Unsteady inlet boundary condition

As suggested by Bonizzi (2003), the ill-posedness of the system was due to the ill-posed equations at the stratified flow where slug initiate. In order to replace the steady state inlet conditions, which are responsible for the ill-posed initial region, unsteady inlet boundary condition were introduced by imposing trains of slugs. The transient inlet conditions are

defined by time traces of unsteady phasic velocities and liquid fraction, this information can be generated through the TRIOMPH code or obtained via the slug tracking code.

4.3.2.1 Inlet flow condition obtained by TRIOMPH

As discussed above, the ill-posed case 2 is mesh dependent when using the steady inlet condition, by varying the mesh spacing ($\Delta x/D$ = 0.09D, 0.186D, 0.37D and 1.15D), four sets of slug flow information can be obtained in the domain exit, and then feed each set at the inlet to repeat simulation with unsteady inlet condition. As illustrated in Figure 4.5, the slug frequencies predicted from transient simulations converge towards a unique solution regardless of the origin of the inlet condition, and it is in a good agreement with Bonizzi (2003). He explained the new well-posed behaviour is mainly played by the pressure along the pipe. The pressure was set at the outlet boundary only, whereas the inlet pressure is an outcome of the solution of the conservation equations, and consequently changes as a function of time. When the steady boundary conditions are applied, the pressure waves that propagate downstream at any location of the pipe are unphysical due to the ill-posed stratified region close to the inlet. Once that region is removed, by feeding into the pipe inlet with new unsteady boundary conditions corresponding to the well-posed phase velocity and liquid fraction, the pressure that is generated in the pipe downstream is then well-posed.

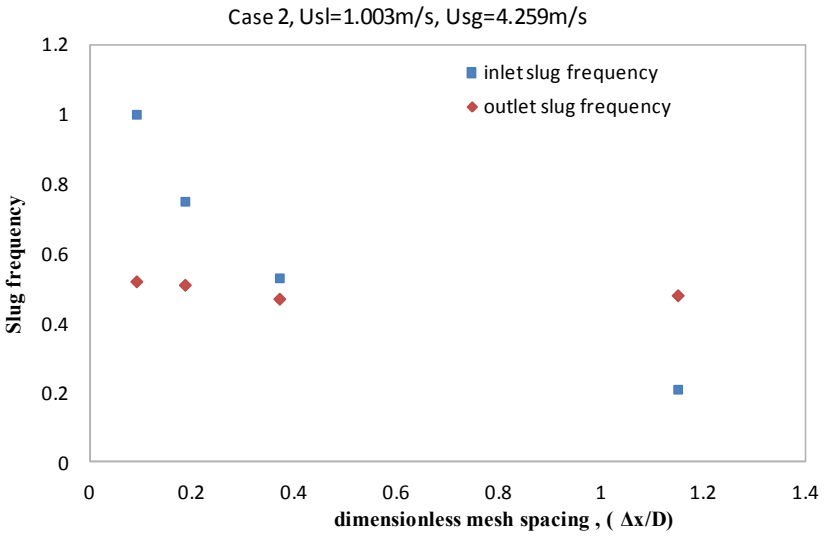

Figure 4.5: TRIOMPH computed slug frequencies versus dimensionless mesh size for case 2. Slug frequency feed at the inlet (blue marker) and predicted slug frequency near the exit. (red marker).

4.3.2.2 Inlet flow condition obtained by slug tracking code

In addition to the recycling of the flow time traces obtained by TRIOMPH, attempts were also made to feed the inlet with flow information obtained by slug tracking code. Slug tracking models have been implemented in one-dimensional numerical codes using a Lagrangian frame of reference in order to follow the time development of the slugs. (Zheng, 1991, Nydal & Banerjee, 1994, Taitel & Barnea,1998, King, 1998, Manfield, 2000 and Ujang & Lawrence 2004). These models are based on the idea of following and controlling the formation and decay of individual slugs of a certain slug distribution. A slug tracking transient simulator often needs to assume the initiation of a predetermined train of slugs in the pipe as an initial condition, therefore much reliance on empiricism is still retained.

The in-house Incompressible Conservative Slug Tracking Model (ICSTM) was developed by Ujang & Lawrence (2004) in Imperial College Chemical engineering department. The algorithm conserves mass exactly, and uses the first order differential equations for the mass and position of each object. The pipeline is taken to be filled with an ordered sequence of slug and stratified film regions. Each object is characterised by two quantities, the mass of gas it contains and its length. The governing equations define the mass and lengths rates of change within the slug body and the film region. Gas entrainment is modelled by using the Manolis correlation (1995). The slug injection time can be either exponentially distributed or the slug arrival time measured from experiments. In particular, if a stochastic initiation method is applied, the nominal length of each slug object and the slug fraction at the inlet need to be defined.

The initial condition for slug tracking simulation is taken to be a stratified flow. The condition at the pipe inlet is more complex. In the current model, the inlet conditions are specified as a series of entry times, Tk, with $T_0 = 0$, so that

$$\lambda_N(t) = \frac{1}{2}(1 + (-1)^k), T_{k-1} < t < T_k \qquad [4.18]$$

The values are chosen to simulate short slugs ($\lambda_N = 0$, odd k) separated by stratified region ($\lambda_N = 1$, even k). When a slug object is introduced, the inlet flow is set to pure liquid, so that the

mass flow rate $F_N = 0$. When a stratified region is introduced, the gas flow rate is set to be somewhat higher than F_G to compensate. Hence the inlet boundary condition is given by

$$F_N(t) = -\lambda_N(1+\beta)F_G \qquad [4.19]$$

where β represents the slug fraction at the inlet. In order to achieve the desired overall inlet gas flow rate, the time interval of the stratified region following each slug is set to a constant multiple ($1/\beta$) of the time interval for that slug. The length of each slug object as it is introduced is chosen to be of order 2D. Hence the time interval for a slug object (odd k) is given by

$$T_k - T_{k-1} = \left(\frac{L_s}{U_M}\right)\xi \qquad [4.20]$$

where U_M is the mixture velocity which is the sum of gas and liquid superficial. ξ is a pseudo-random variable with unit mean and an exponential probability distribution.

$$P(\xi_1 < \xi < \xi_2) = \int_{\zeta 1}^{\zeta_2} e^{-\xi} d\xi = e^{-\xi_1} - e^{-\xi_2} \qquad [4.21]$$

The time interval for the following stratified region is then given by

$$T_{k+1} - T_k = (T_k - T_{k-1})/\beta \qquad [4.22]$$

Hence the time interval between slugs is also given by an exponential distribution in the form

$$\Delta T = T_{k+1} - T_{k-1} = \frac{L_s(\beta+1)}{U_M\beta}\xi \qquad [4.23]$$

it can then be verified that the total mass of gas introduced into the pipe during this time interval is

$$\Delta M = (1+\beta)F_G(T_{k+1} - T_k) = (1+\beta)F_G\frac{L_s}{\beta U_M}\xi = F_G\Delta T \qquad [4.24]$$

so that the correct average mass flow rate of gas is achieved for each slug unit.

The nominal inlet slug length *Ls* and β can be either guessed value or determined from the experimental data. The model has been implemented in FORTRAN, the program also keeps a history of each object that it has injected. This history is used to obtain the flow evolution and slug frequency at several measurement positions. Based on this information, every object that passes through a given probe for the entirety of the calculation can be determined by post processing.

In the present study, the stochastic initiation method was applied; different time traces of phasic velocities and liquid holdup can be obtained by varying the nominal length of each slug object. The slug fraction at the inlet was kept constant for each case; the conditions are summarized in Table 4.2.

Table 4.2: Summary of nominal inlet slug length and inlet slug fraction imposed in the slug tracking simulations.

CASE	nominal inlet slug length ***Ls***	slug fraction at the inlet $\boldsymbol{\beta}$
1a	6D	0.2
1b	14D	0.2
1c	45D	0.2

Time traces of liquid holdup predicted by slug tracking code are shown in Figure 4.6, which corresponding to case 1a, 1b and 1c. For a fixed value of inlet slug fraction, the flow characteristics are strongly influenced by the nominal inlet slug length. Accordingly, three unsteady inlet TRIOMPH simulations were performed using a mesh spacing of $\Delta x/D = 0.37D$, results are given in Figure 4.7. Regardless of the difference in liquid holdup fed at the inlet (Figure 4.6), the holdup time traces predicted by the TRIOMPH simulations near the exit have shown a similar appearance (Figure 4.7). Comparison of the slug frequencies are given in Figure 4.8, at the domain inlet, the slug frequencies given by slug tracking code have shown a large variation among the three cases, however, a similar value was obtained from the TRIOMPH simulations, showing the prediction is independent of the origin at the inlet.

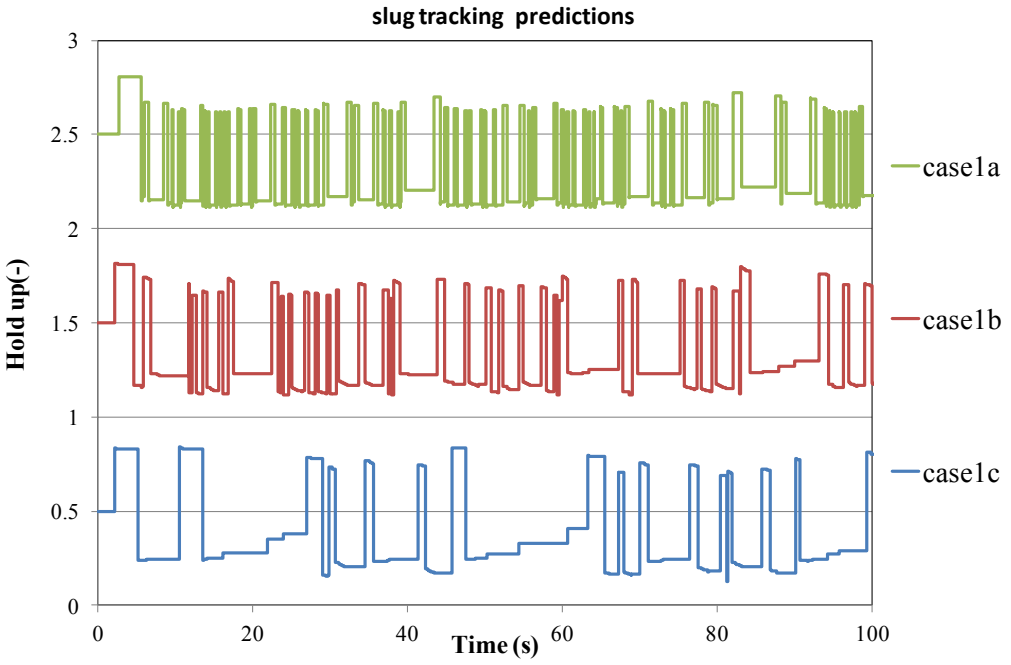

Figure 4.6: Liquid holdup time traces computed from slug tracking code, for case 1a,1b,and 1c.

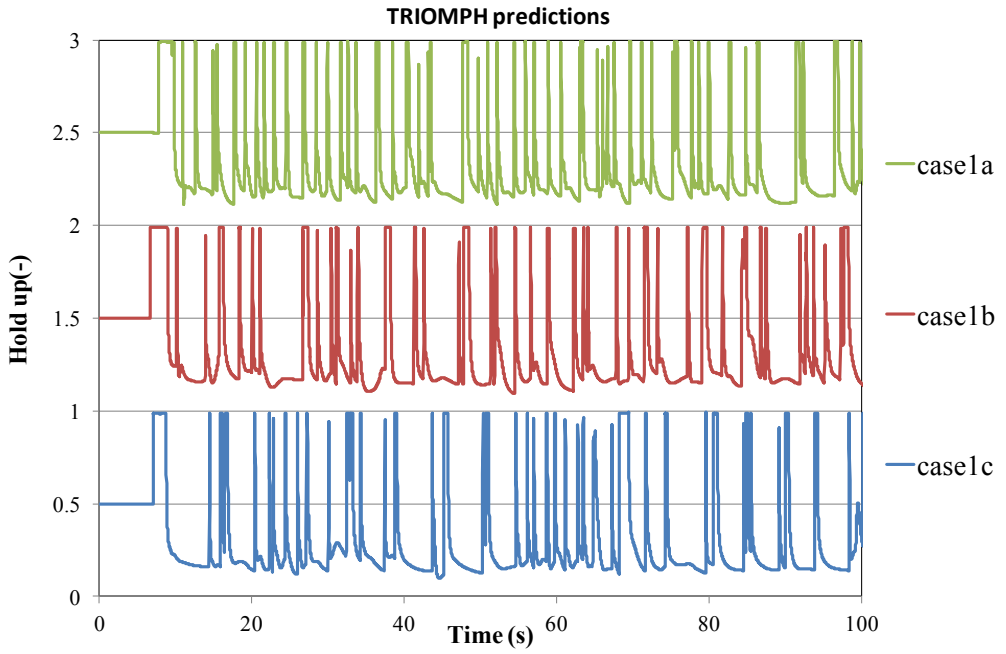

Figure 4.7: Liquid holdup time traces computed from TRIOMPH code, by imposing the unsteady inlet condition obtained from slug tracking code of case 1a,1b, 1c.

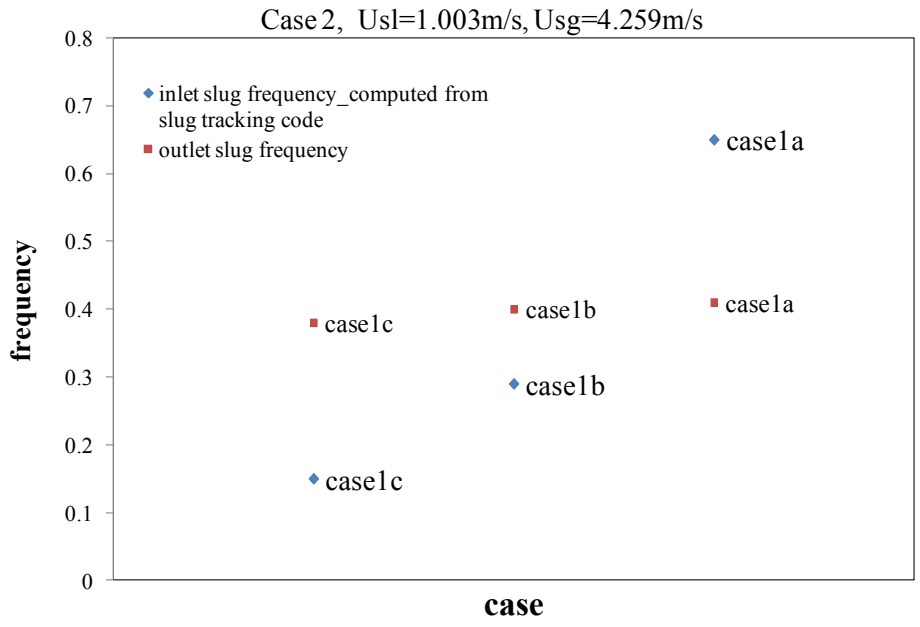

Figure 4.8: Slug frequency feed at the inlet (blue marker, computed from slug tracking code) and predicted slug frequency near the exit (red marker).

The evolutions of the flow structure at various locations along the pipe obtained from TRIOMPH simulations for case1a, 1b and 1c are given in Figure 4.9 to Figure 4.11. The flow structure at 0.1m was strongly influence by the inlet condition, however, when slugs propagate along the pipe, some of the short slugs were merged, some of the large slugs decay into shorter slugs, and some large waves evolve into new slugs and also grow in length as they travel along the pipe. These features are highlighted in red circles. The merge and collapse mechanisms of the slugs were captured in the TRIOMPH simulation, and eventually, the slug flow in the fully developed region among three cases have shown a similar trend.

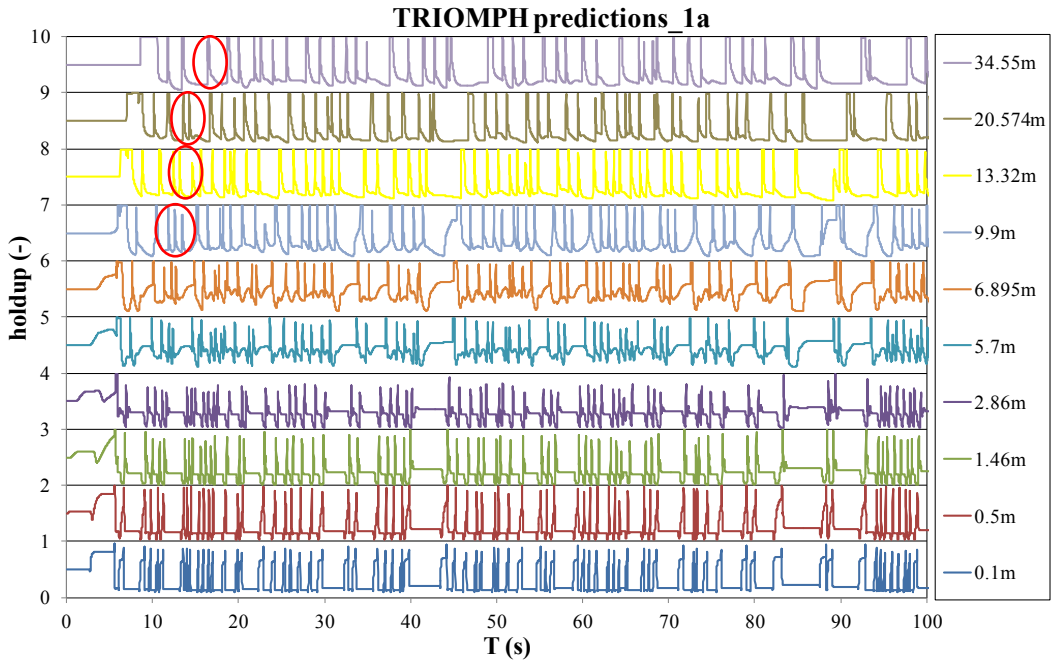

Figure 4.9: TRIOMPH computed flow evolution at variosu locations along the test section, case 1a.

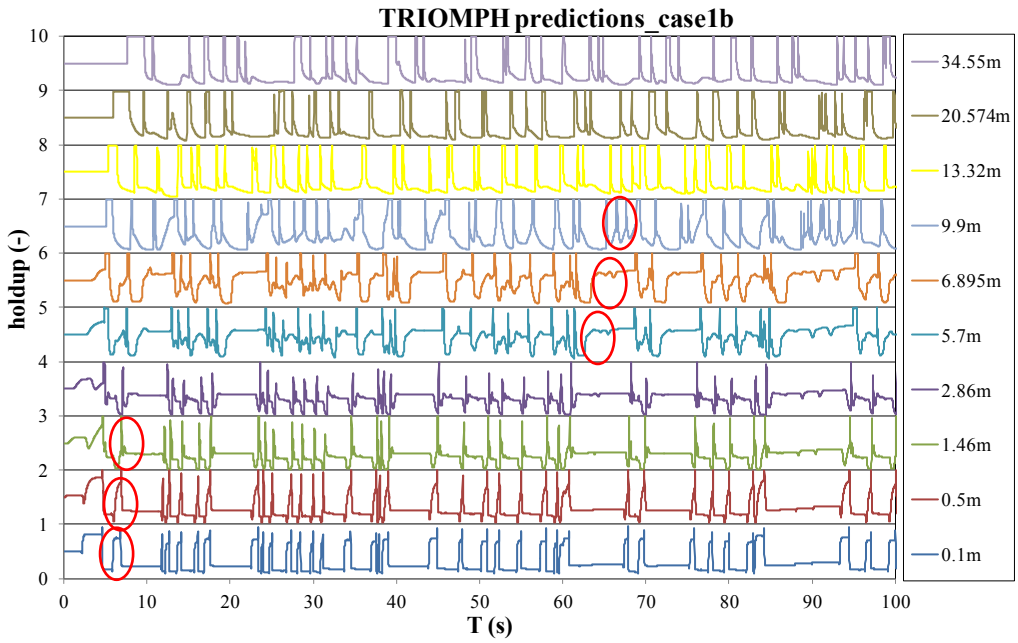

Figure 4.10: TRIOMPH computed flow evolution at variosu locations along the test section, case 1b.

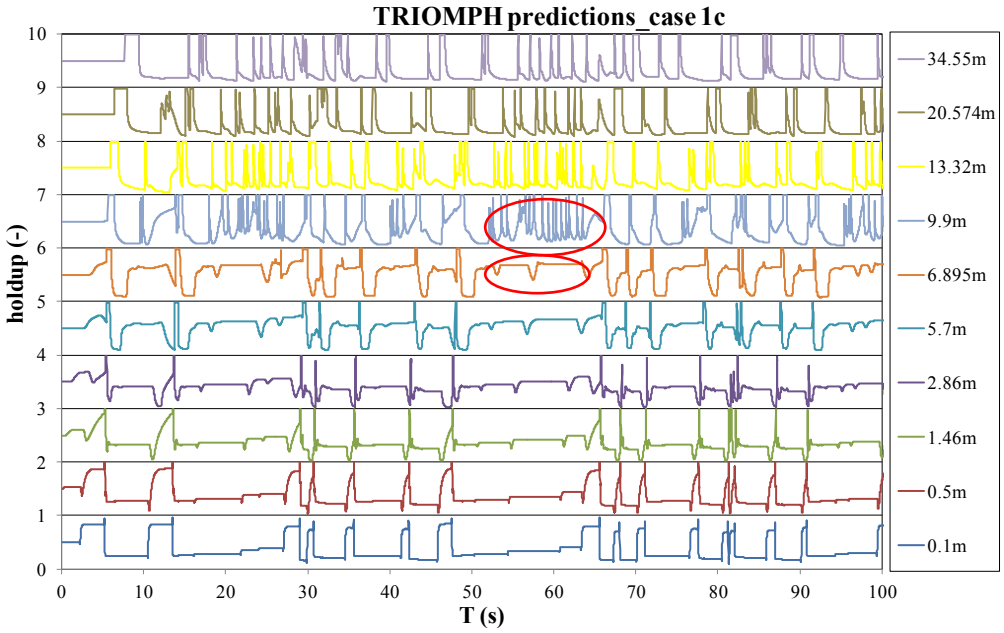

Figure 4.11: TRIOMPH computed flow evolution at variosu locations along the test section, case 1c.

4.4 Conclusion

In this chapter, the well/ill posed nature of the two-fluid equations employed in the TRIOMPH code were reviewed and studied. The two-fluid model for stratified and slug flow is well-posed, if and only if the relative velocities of the two phases obey the certain condition as discussed in Section 4.2.2. For a well-posed system, the information propagates in the real domain starting from a number of initial data corresponding to the number of characteristics of the system (initial value problem), as a result, a unique solution exists and the computed slug frequency is independent of the mesh density. For an ill-posed system, some of the characteristics are complex, as a result, a unique solution no longer exists and consequently the computed slug frequency diverges as the mesh is refined. The lack of uniqueness of the solution is the manifestation of the ill-posed equations in the stratified region, whereby random unphysical disturbances occur in the flow due to the assumption of the steady inlet condition. In latter case, the boundary conditions must be prescribed in space and time in order to account for the unsteadiness at the inlet. The unsteady inlet condition can be computed from steady inlet TRIOMPH simulation or slug tracking simulation, in the

subsequent TRIOMPH simulation, although originally ill-posed, the system became well-posed leading to a unique solution independent of the origin at the inlet.

Chapter 5

Numerical simulation of slug flow in rectangular channel

5.1 Summary

This chapter presents computational fluid dynamics (CFD) predictions of two-phase slug flows conducted in a horizontal air/water channel with a rectangular cross-section. The experimental data was provided by Forschungszentrum Dresden-Rossendorf (FZD). A slug flow case of a superficial water velocity of 1.0 m/s and a superficial air velocity of 5.0 m/s has been chosen as the reference test for the simulation. An introduction of the experiment performed on the HAWAC facility at FZD is given in Section 5.2. A brief summary of the previous CFD work on HAWAC slug flow predictions is given in Section 5.3. The commercial code STAR CCM+ was employed in the present calculation to carry out the numerical simulations. The methodology used in the present work is discussed in Section 5.5 together with the results of the numerical simulations. Finally, Section 5.6 provides a summary of the work described in this Chapter.

5.2 Introduction to the FZD HAWAC slug flow experiments

As already discussed in chapter 3, the slug flow case performed at Imperial College WASP facility provides a benchmark for the validation of various CFD codes. However, due to the large geometry of the WASP test section, the calculations require large computation resource, hence very expensive. The slug flow experiment performed in the horizontal air/water channel (HAWAC) at Forschungszentrum Rossendorf (FZD) provide a good optical access to the local stratified air/water flow phenomena, and an appropriate source of data for CFD model validation. The test-section is 8 m long and its cross-sectional dimensions are 100mm×30mm (height x width), giving a length-to-height ratio, L/H, of 80. Alternatively, the dimensionless length of the channel L/D_h is 173 if related to the hydraulic diameter.

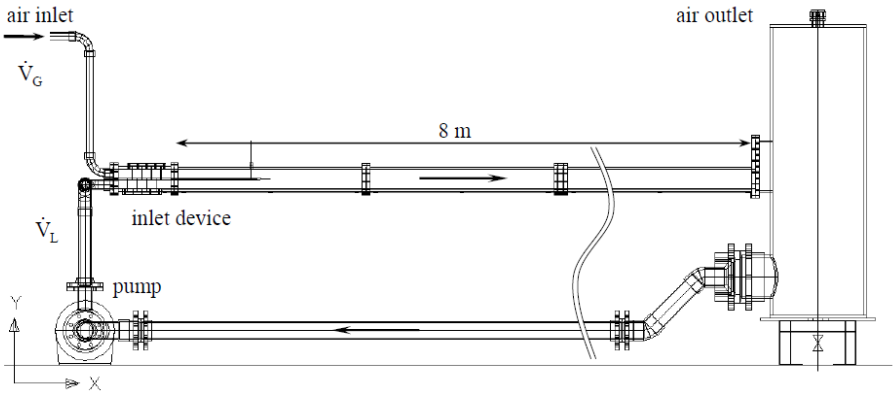

Figure 5.1: Schematic diagram of horizontal air water channel (HAWAC).

An inlet device provides well-defined inlet boundary conditions through the use of a separate injection of water and air into the test-section. As can be seen in Figure 5.2, air and water flow through the upper and lower parts of this device, respectively. Because the inlet geometry produces perturbations, 4 stainless steel wire mesh filters are mounted in each part of the inlet device to provide homogenous velocity profiles at the inlet of test-section. Moreover, the filters produce a pressure drop that attenuate the effect of the pressure surge created by slug flow on the fluid supply systems. Air and water come in contact at the final edge of a 500mm long blade that divides both phases downstream of the filter segment. This inlet blade is equipped with a pivot located at its connection with the filter segment. Therefore, the free inlet cross-section for each phase can be controlled by adjusting the incline of the blade (Vallée, 2010).

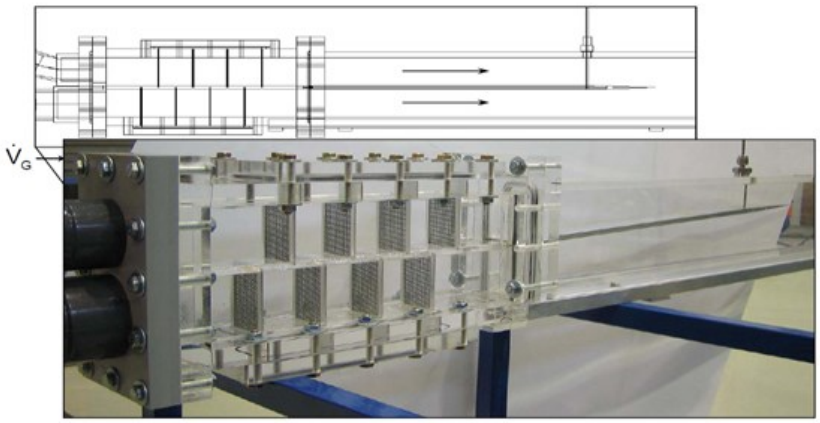

Figure 5.2: Schematic diagram of the inlet device for gas liquid.

The water flow rate is measured with a paddle-wheel flow transmitter and the air flow rate is measured with thermal mass flow meters. The case studied in this chapter was performed at the following superficial velocities: U_{SG}=5.0 m/s and U_{SL} = 1.0 m/s. The inlet blade was orientated horizontally, and therefore the cross-section opening at the vertex of the inlet blade was 50mm for each phase. Optical measurements were performed at different locations along the channel, with a high-speed video camera operating at 400 frames per second.

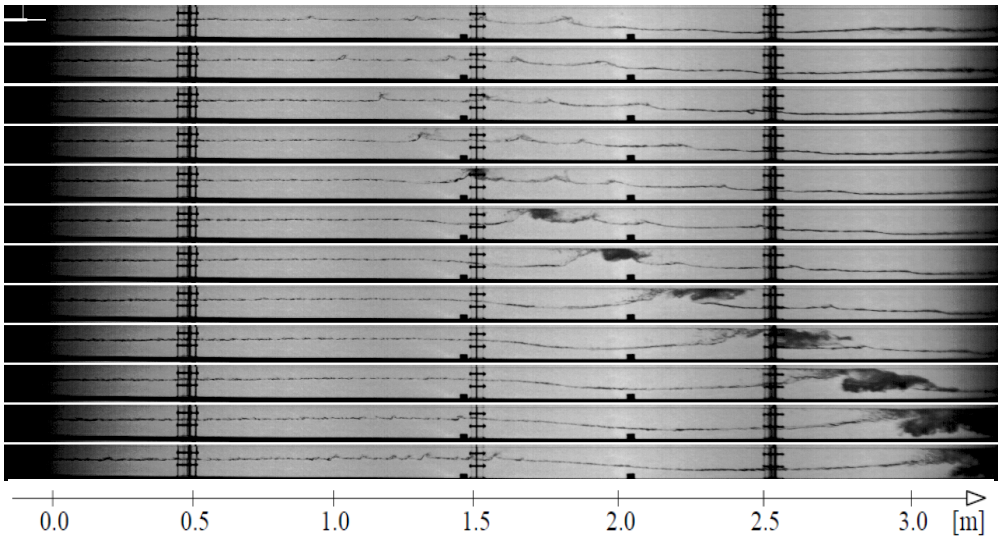

Figure 5.3: Recorded sequence of slug flow over the first 3.2m, Δt = 50 ms, U_{SG} =5.0 m/s and U_{SL}=1.0 m/s.

Figure 5.3 shows a time sequence of a slug over the first 3.2m of the test-section. This sequence shows that the flow is stratified downstream of the inlet blade; however, the interface is slightly wavy due to the supercritical flow condition imposed at the inlet. One of

the waves grows rapidly from 1.0m and bridges the cross-section at around 1.5m, forming a slug. This slug travels along the channel, picking up liquid ahead of it and growing in length. The gas entrainment is clearly observed from the picture sequence, forming a bubble jet at the slug front. Following the passage of the slug, the liquid level drops in the slug tail region.

Figure 5.4 shows an example of the measured water level history for six chosen positions. The water level was measured with a frequency of 400Hz. It can be seen that an approximately constant water level develops into a wavy flow at a distance of around 1.0 m. Downstream of the 1.5 m location, slugs are generated quasi-periodically. Further downstream from the inlet, evidence of slug coalescence and dissipation is found.

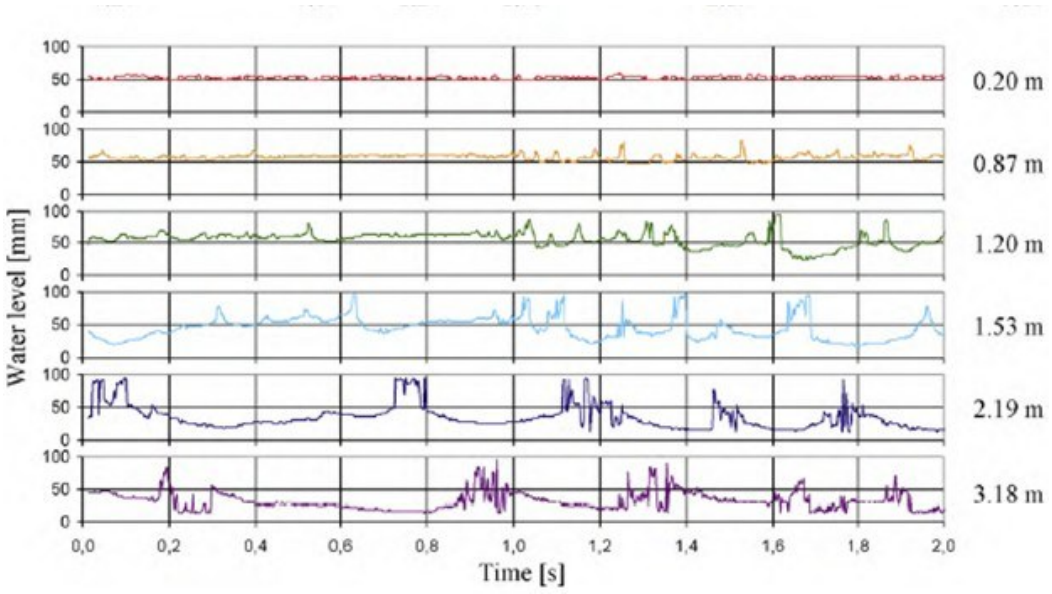

Figure 5.4: Time-dependent water level at chosen cross-sections during slug flow, U_{SG} =5.0 m/s and U_{SL} = 1.0 m/s.

In order to provide a statistical reference for comparison with the CFD results, a time-averaged water level was calculated at each cross-section and bounded by a standard deviation; this resulted in a mean water level profile along the channel (see Figure 5.5). The standard deviation quantifies the spread of the measured values which originates from the complex interfacial dynamics.

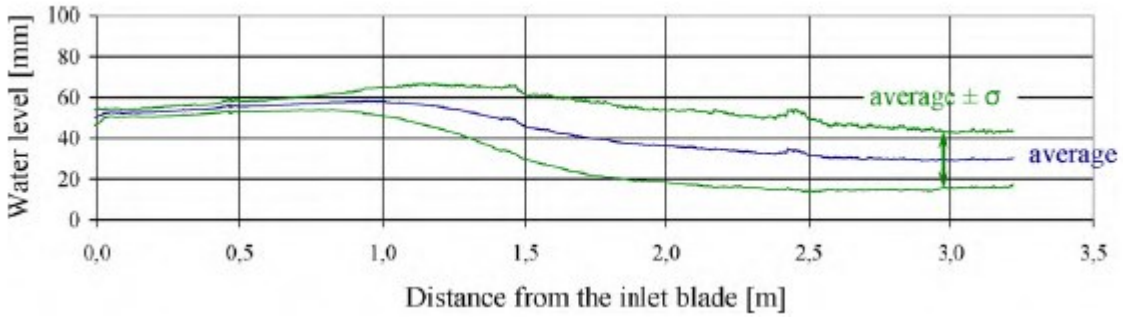

Figure 5.5: Spatial variation of the time-averaged water level during slug flow generated for the same parameter values as in Figure 5.4.

In the first part of Figure 5.5, a slight increase of the mean water level was observed to occur between 50mm and 58mm; this was accompanied by a low standard deviation. Around the 0.9m from the inlet, a maximum of the mean water level reached, the standard deviation increased due to the rapid wave growth induced by the high air velocity in this zone. In the downstream region, where the slugs are generated and propagate, the mean water level decreases to an asymptotic value of about 30mm.

5.3 Introduction to previous CFD work

Two different CFD codes have been tested, namely CFX and FLUENT. A brief overview of the work associated with each test is given below.

5.3.1 CFX

CFX simulations of this test were investigated at FZD by Vallée *et al.* (2005). The three dimensional model dimensions are $8000\times100\times30mm^3$ (length×height×width). The grid consists of 1.2×10^5 hexahedral elements. In the simulation, both phases were treated as isothermal and incompressible. The inlet was divided into two parts: water was injected in the lower half of the inlet cross-section, and air in the upper half. An initial water level of y_0 = 50mm was assumed for the entire computational domain. The inner surface of the channel walls was defined as hydraulically smooth with a no-slip boundary condition applied to both phases. The channel outlet was modelled using a pressure-controlled outlet boundary condition. In the simulation, the two-fluid model was used with an interface-capturing

method using a compressive advection scheme for surface sharpening. Vallée *et al.* (2005) suggest the high velocity gradients at the free surface, especially in the gaseous phase, generate excessively high levels of turbulence throughout the two-phase flow when using *k-ω* type models. Therefore, in order to mimic turbulence damping near the interface, a turbulence correction was applied. It took the form of a source term applied to the ω equation of the *k-* ω model, and is mesh-dependent:

$$A \cdot \Delta y \cdot \beta \cdot \rho_i \left(B \cdot \frac{6 \cdot \mu_i}{\beta \cdot \rho_i \cdot \Delta n^2} \right)^2 \qquad [5.1]$$

where A is the interface area density, Δn is the typical grid cell size across the interface, ρ_i and μ_i are the density and viscosity of the phase i. The factor A activates this source term only at the interface, where it cancels the standard ω-destruction term of the ω-equation $\left(-r_i \cdot \beta \cdot \rho_i \cdot \varpi_i^2\right)$ and enforces the required high value of ω_i and thus the turbulence damping.

The parallel transient calculation of 15.0 s of simulation time on 4 CPU took 20 days. The advection scheme was set to High Resolution, a hybrid scheme between first-order upwind and higher-order methods. For time integration, the fully-implicit second-order backward Euler method was applied with a constant time-step of dt = 0.001 s and a maximum of 15 coefficient loops. A convergence in terms of the root mean square values of the residuals to be less than 10^{-4} was assured most of the time.

The calculated phase distribution during slug generation was visualized (see Figure 5.6). The first slug developed spontaneously at approximately 1.65s after the beginning of the simulation, induced by instabilities. In comparison to the experimental data, the initiation and propagation of the slugs were qualitatively captured in the simulation, though quantitative comparison was less satisfactory The required entrance length for slug generation was 3.5m in the calculation, whereas it is about 1.5m in the experiment; this can be explained by appealing to the fact that inlet disturbances are prevalent in experimental settings, which can promote the formation of waves and slugs. In the numerical simulation, no such disturbances were modelled; instead, the slug evolved naturally via growth from perturbations associated with round-off errors in the computations. Consequently, the development length for the slugs in the simulation was larger than that observed in the experiment.

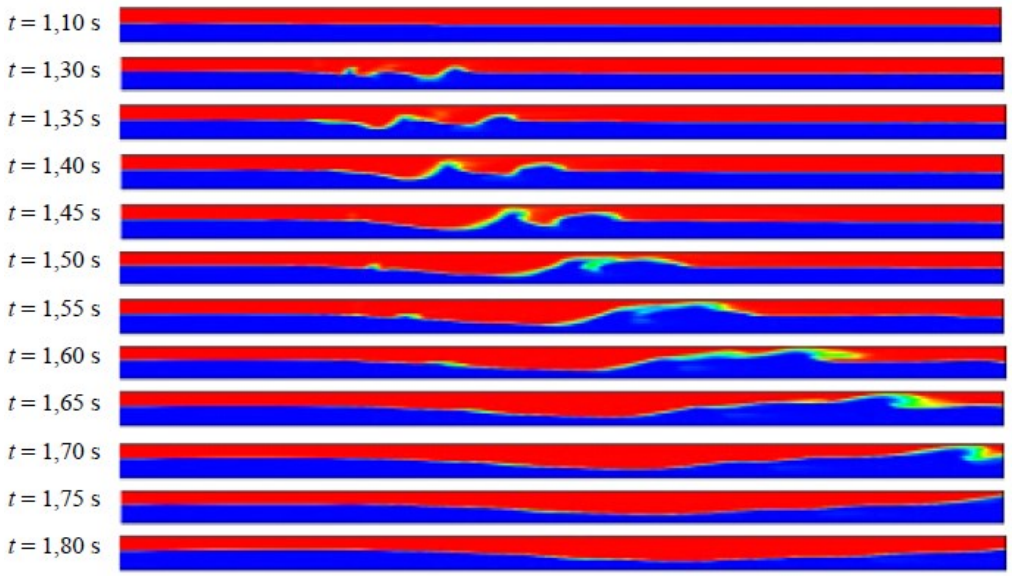

Figure 5.6: Picture sequence calculated by CFX at U_{SL} = 1.0 m/s and U_{SG} = 5.0 m/s (depicted part of the channel: 1.4 to 4 m after the inlet).

5.3.2 FLUENT

The simulation of the HAWAC test case was also investigated using FLUENT at Universite Catholique de Louvain (UCL) by Bartosiewicz et al.(2008). The volume-of-fluid (VOF) model was used for the simulation; this model is typically used to simulate the dynamics of interfaces separating two (or more) immiscible phases (similar to those shown in Figure 5.3). In VOF models, a single momentum equation is solved for the respective fluids and the volume fraction of each fluid in every computational cell is tracked throughout the domain. VOF models typically account for the presence of interfacial tension and are ideal for simulating stratified rather than dispersed flows. In a previous study by Bartosiewicz *et al*. (2008), the VOF method provided good results for instabilities in free surface flow, therefore this method was chosen to simulate the HAWAC test case. Different viscous models including k–ε model, k–ω model and k–ω based Shear Stress Transport (SST) model (Fluent User Manual, 2008) were tested but without success: there was no slug observed in the simulations and the interface remained smooth at all times. The author suggested that this may be due to the volume-of-fluid (VOF) model being incapable of simulating stratified flow when the slip velocity between the phases at the interface is too high (the slip between the phases is approximately equal to 8m/s in the test), and interfacial tension effects are weak.

5.4 STAR-CCM+ modeling of HAWAC slug flow

The objective of the present study is to build up predictive models for the evolution of air-water slug flow. The multiphase flow model adopted is briefly described in this section, together with the chosen turbulence model to account for the turbulent features and interactions at the interface. The geometry is set up to mimic the experimental configuration with appropriate initial and boundary conditions. The details of this study are described below.

5.4.1 Simulation methodology

Two primary multiphase models are considered: the Lagrangian and Eulerian models. The former is typically used to model systems comprising a single continuous phase carrying a relatively small volume of discrete particles, droplets, or bubbles. This approach is often applied in particle-tracking studies characterised by a low volume fraction (< 5-10%) of the discrete phase. For larger volume fractions, the Eulerian model is used. In this approach, two different models are distinguished: Multiphase Segregated Flow and Volume of Fluid (VOF) models. The former model solves conservation equations for mass, momentum, and energy for each phase. Phase interaction models are provided to define the influence that one phase exerts upon the other across the interfacial area (STAR-CCM+ user guide).

As already discussed in Chapter 3, the VOF method was employed in the STAR-CD and FLUENT predictions of the WASP slug flow benchmark case. In those simulations, interface instabilities were captured which developed into slugs, even though the slip velocity across the two phases s relatively high (about 8 m/s). Moreover, among the other multiphase models, the VOF method is also the most computationally efficient approach. Therefore, in the present STAR-CCM+ study it was decided to use the VOF method with a High Resolution Interface capturing (HRIC) scheme to simulate the HAWAC slug flow test. The HRIC scheme is designed to mimic the convective transport of immiscible fluid components, suited for tracking sharp interfaces. Nevertheless, it is important to note the following limitation of the VOF method:

- The VOF method is not able to solve momentum equations and turbulence models for each phase; it assumes that the two fluids in the channel can be represented with only one set of those equations.

- Entrainment and deposition are not considered and the momentum exchanges between two fluids are neglected.

Turbulence models need to be applied for this case due to the fluctuating features when the flow is unstable and exhibits stochastic characteristics. There are a number of available turbulence models in the STAR CCM+ code. For example, the Detached Eddy Simulation (DES) or Large Eddy Simulation (LES) approach involve three-dimensional simulations and could provide accurate results but are computationally expensive. In the present study, the Shear Stress Transport (SST) k-ω model is used with a combination of the standard k-ω model in the near wall region and the standard k-ε model far from the wall. This is highly recommended for flow separation since its prediction of real flow separation is more accurate than those obtained from the standard k-ε model (Tu *et al*., 2008). The transport equation of the SST k-ω model is presented as:

$$\frac{\partial}{\partial t}(\rho k)+\frac{\partial}{\partial x_i}(\rho k u_i)=\frac{\partial}{\partial x_j}\left(\Gamma_k \frac{\partial k}{\partial x_j}\right)+\widetilde{G}_k-Y_k \qquad [5.2]$$

$$\frac{\partial}{\partial t}(\rho \varpi)+\frac{\partial}{\partial x_i}(\rho \varpi u_i)=\frac{\partial}{\partial x_j}\left(\Gamma_\varpi \frac{\partial \varpi}{\partial x_j}\right)+G_\varpi-Y_\varpi+D_\varpi \qquad [5.3]$$

where, $\widetilde{G}_k$ and G_ϖ represent the generation of kinetic energy, k, and specific dissipation rate, ϖ, Γ_k and Γ_ϖ are the effective diffusivity of k and ϖ, respectively. Y_k and Y_ϖ are the dissipation of k and ϖ. D_ϖ is a modified term which is the additional consideration for adapting model for far area from the wall, differently from the standard $k-\varpi$ model.

5.4.2 Flow domain and mesh

In the present work, the geometry was built to mimic the channel configuration used in the experiments; assuming symmetry over the central xy plane, half channel cross-section with full pipe length was simulated. The domain dimension is 8000mmx100mmx15mm (length x height x width). The inlet blade was not modelled, accordingly the domain inlet was divided into two parts; water and gas with constant velocities are injected in the bottom and upper half of the cross-section, respectively.

5.4.2.1 Grid dependency

Creating sufficiently fine meshes is important to capture the onset and evolution of slugs, as well as the small-scale features of the flow. This, however, comes at a large computational cost. STAR-CCM+ contains different types of meshing models that can be used to generate a volume mesh, mainly are tetrahedral mesh, hexahedral mesh and polyhedral mesh. In terms of general accuracy for a given number of cells, the hexahedral and polyhedral cell type meshes produce more accurate solutions when compared to a tetrahedral mesh. Therefore a grid dependency study was performed in order to choose a suitable grid for slug flow test case. Table 5.1 summaries mesh density of the four cases tested in the grid dependency study, the corresponding mesh for each case are given in Figure 5.7 and Figure 5.8.

Table 5.1: Mesh density of 4 cases.

Case	Mesh type	Base size	Cell number	Face number
1	Hexahedral	1.4mm	2217984	6499104
2	Hexahedral	2mm	928672	2709604
3	Polyhedral	2mm	1682023	11011621
4	Polyhedral	3mm	591649	3715232

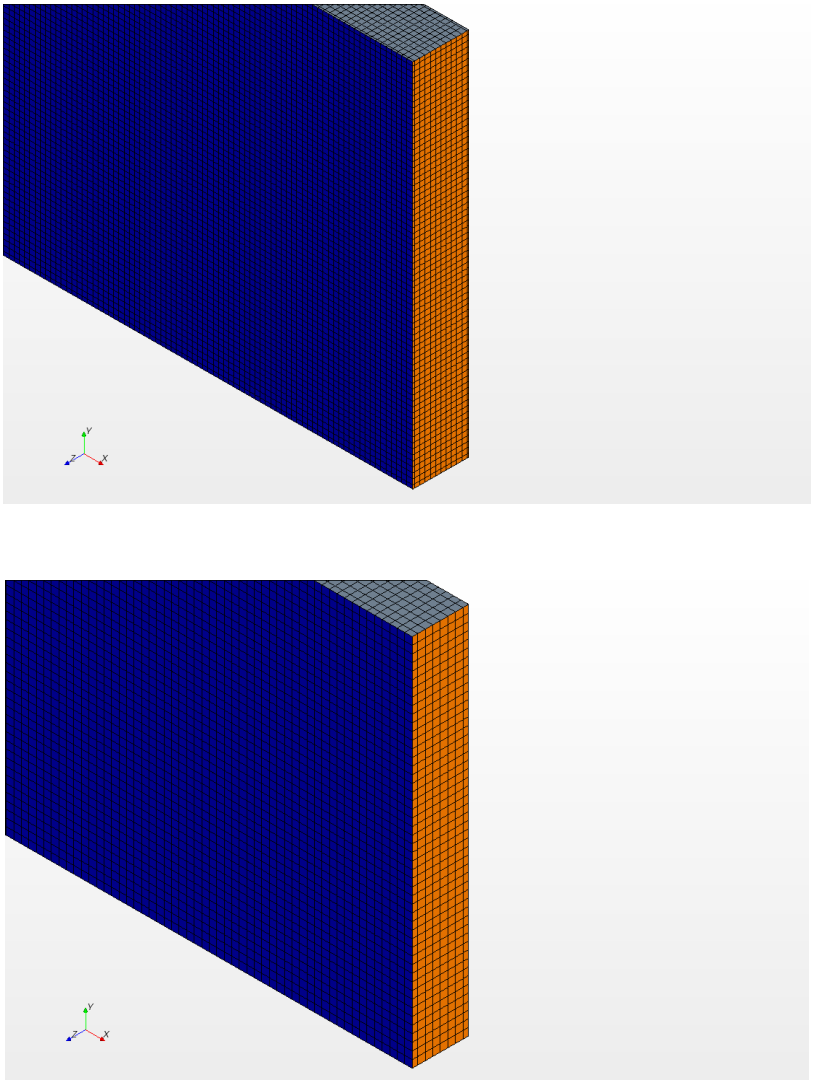

Figure 5.7: Hexahedral grids. (Above: base size = 1.4mm, 2217984 cells, case 1, Below: base size = 2mm, 928672 cells, case 2).

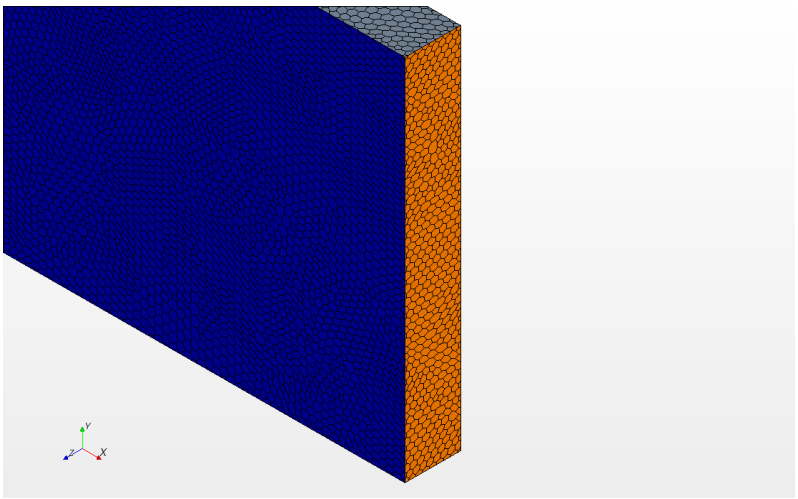

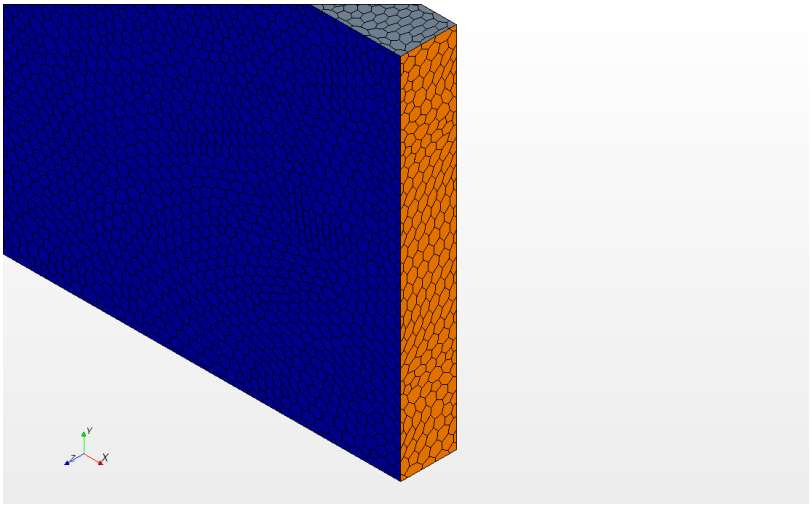

Figure 5.8: Polyhedral grids. (Above: base size =2mm, 1682023millison cells, Below: base size = 3mm, 591649millison cells).

In terms of hexahedral mesh, slugs were captured with both coarser and refined mesh density, however considerable smearing of the interface due to excessive numerical diffusion was observed and it persist with refined mesh (see Figure 5.9). The "water residual" representing the residual for the volume fraction transport equation of the water always above 1, indicating the calculation convergence is not satisfactory (see Figure 5.11). Further refinement of the hexahedral mesh was not conducted since a higher density of the mesh would significantly increase the computation time and resource. In contrast, the numerical diffusion problem was considerably improved with polyhedral mesh (see Figure 5.10), a satisfactory residual convergence less than 10^{-4} is assured with the coarser polyhedral mesh at the end of each time-step (see Figure 5.12). The reason is that each polyhedral cell has on average 12 or 14 neighbours and this result in the flow information propagates much more quickly through a polyhedral mesh. It allows for reasonable predictions of both gradients at cell centers and local flow directions and leading to an increased rate of convergence (Afgan, 2008). Between the cases with coarser and finer polyhedral mesh, the calculated integrated liquid volume fractions were not changing appreciably. However a perfect agreement was not obtainable as because finer mesh grid would results in finer scale turbulence structures. Based on the above analysis, a grid consists of 1.68×10^{6} polyhedral elements was considered to be suitable for HAWAC slug flow test case.

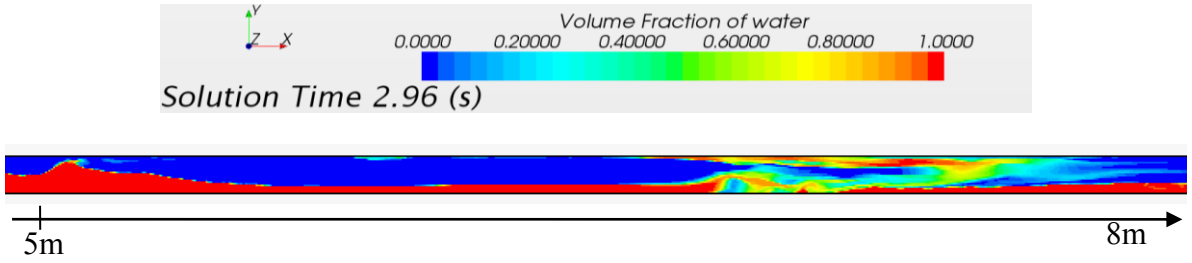

Figure 5.9: Liquid volume fraction contours at *x*= 5-8m and *t*=2.96s, hexahedral mesh (case1).

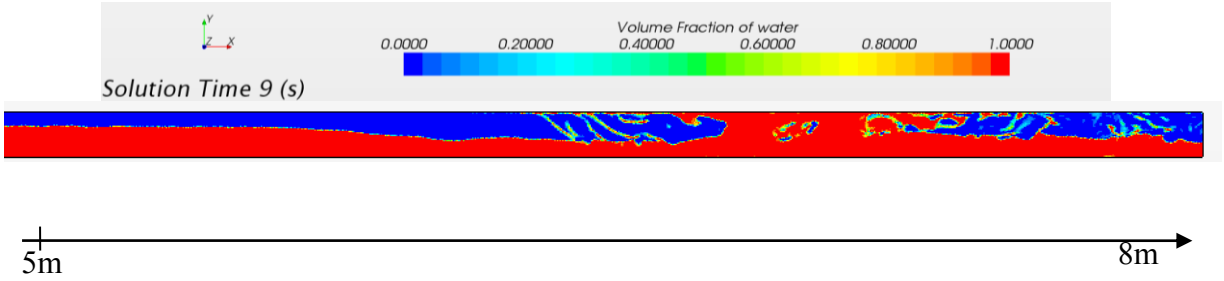

Figure 5.10: Liquid volume fraction contours at x=5-8m and t=9.0s, polyhedral mesh (case3).

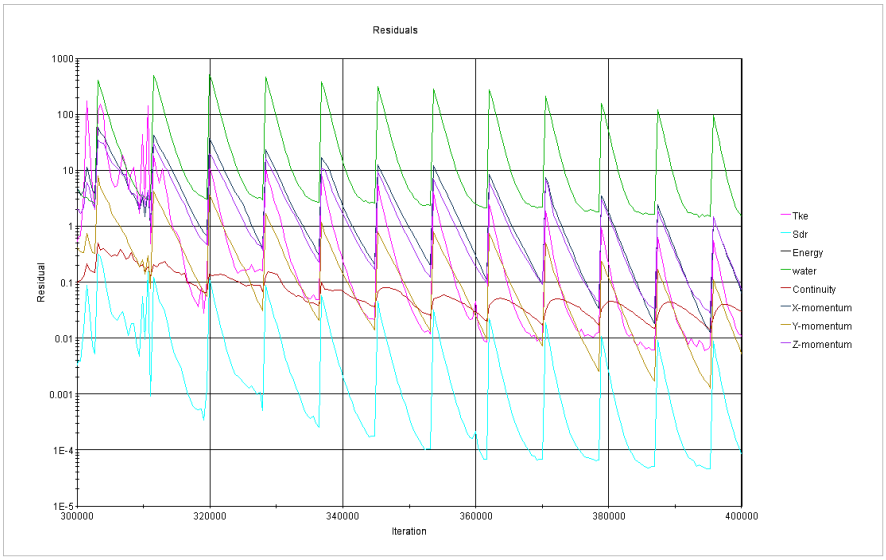

Figure 5.11: Simulatinon convergency residual plot of case1, hexahedral grid.

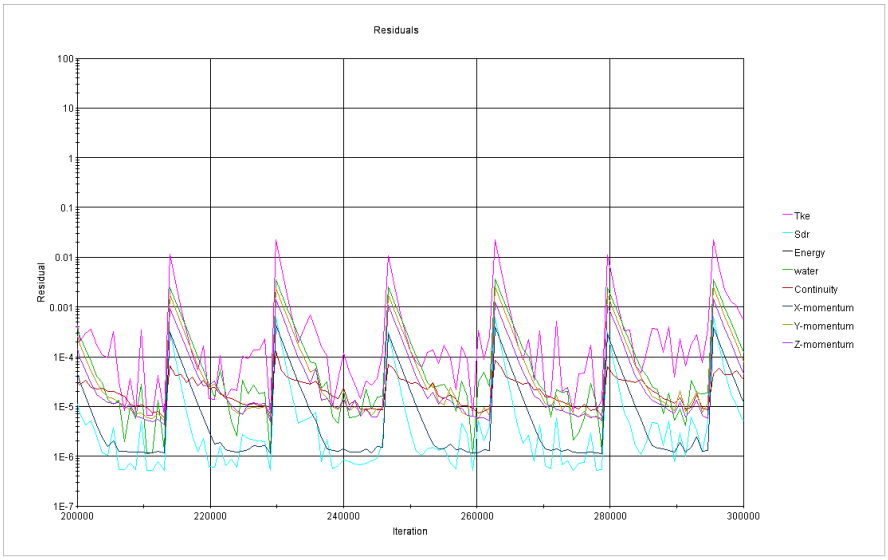

Figure 5.12: Simulation convergency residual plot of case3, polyhedral grid.

5.4.3 Initial and boundary condition

User defined functions were used to define the inlet boundary conditions. At the inlet, the upper half of the channel cross-section is filled with air and a constant superficial air velocity of 5.0m/s was defined. Similarly, the bottom half of the channel cross-section is filled with water and a constant superficial liquid velocity of 1.0 m/s was defined. In the simulation, both phases have been treated as isothermal at 25°C, while the gas and liquid phases were considered compressible and incompressible, respectively. Buoyancy effects between the two phases are taken into account and the no-slip boundary condition is imposed at the pipe wall. At the pipe outlet, a pressure outlet boundary condition (set equal to the atmospheric pressure) is used. An initial water level of y_0 = 50 mm for the entire computational domain length was assumed.

5.4.4 Solution and convergence criterion

A first order temporal discretisation scheme was selected. For complex slug flow, a very small time-step is usually required to ensure the accuracy; an initial fixed time-step of 0.0004s was chosen and the number of inner iterations was set to 20. A convergence criterion that the root mean square values of the residuals should not exceed 10^{-4} was set. Output files

were produced at intervals of 0.02s, and 20 seconds of real time simulation was performed. Before running the simulation, measuring planes were placed at various locations along the channel which correspond to the experimental set-up where the visualisations were recorded. Useful information can be restored and extracted; for example, the area averaged liquid volume fraction, the average liquid level and velocity distribution. Hence inferences can then be made regarding how the flow develops.

5.4.5 CPU requirement

A sensitivity analysis was carried out to determine the suitable number of processors to simulate the present CFD case. Figure 5.13 illustrates the parallel performance of STAR-CCM+ simulations on Imperial College High Performance Computer (HPC) in terms of speed-up as a function of number of processors. As shown in this figure, MPI parallel simulations with 8 processors were found to be eight times faster than serial simulation. Further increase in the number of processors, up to 64, resulted in a decrease of the speed-up ratio from 1 to 0.2; this is due to the concomitant increase in time taken to exchange data between the processors. Beyond 64 processors, the speed-up ratio decreases further as the time associated with data exchange becomes a dominant factor. Therefore, 64 processors were used in all simulations in this study. As reported by CD-Adapco, the parallel performance is also dependent on the type of mesh employed, the domain with 1.68×10^6 of polyhedral meshes is studied in this particular analysis.

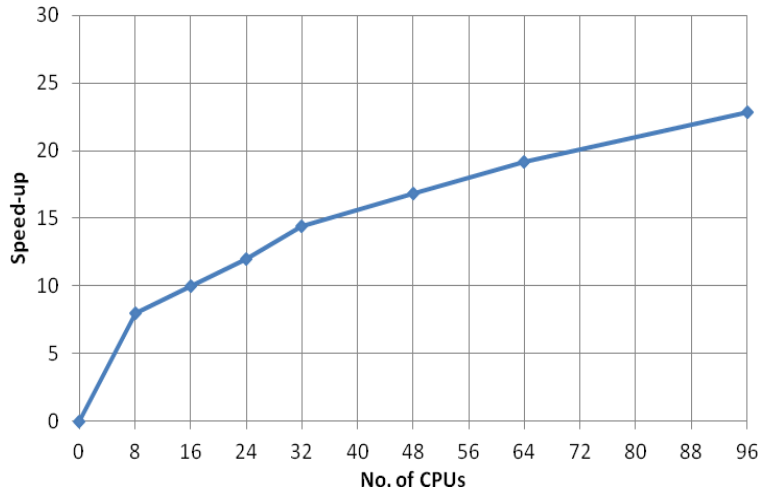

Figure 5.13: Parallel performance of STAR CCM+ simulation STAR-CCM+ simulations on Imperial College High Performance Computer (HPC).

5.4.6 Parametric study

The results of a parametric study are presented next. In all cases, the simulations were performed using STAR CCM+ version 7.02 using the Imperial College HPC facility, the hardware of this system is predominantly Dell and Viglen.

5.4.6.1 Interface treatment

As discussed in Section 5.3, in CFX simulation, a turbulence correction was applied by Vallee *et al*. (2005) in their CFX simulation. We have investigated the effect of this damping function in the present CFD predictions, which we implemented into the STAR CCM+ package via a user defined function (see Appendix A).

Figure 5.14 illustrates a comparison of the Cartesian *x*-component velocity profiles of gas and liquid phase at a cross-sectional plane located at the middle of the channel with and without interface treatment in the early stages of the simulation where the flow is still stratified; the reduction in the interface drag has changed the gas and liquid velocity profile. Notably, the profile near the interface is no longer linear but parabolic, which is more physically realistic.

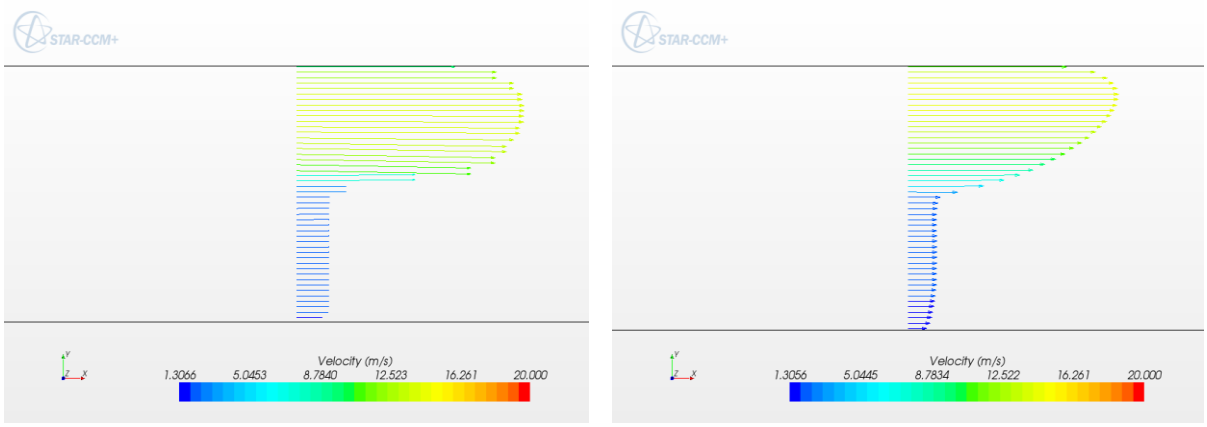

Figure 5.14: Cartesian x-component velocity profiles without interface treatment (left) and with interface treatment (right), after running simulation for 0.5s, at x=4m.

Nonetheless, the prediction of the slug evolution indicates the interface damping treatment does not have a strong effect on the appearance of waves and slugs. This is because when the mesh is very fine, the turbulence correction is applied to a very thin region near the interface, and there is negligible numerical diffusion.

5.4.6.2 Inlet boundary condition

As mentioned in Section 5.4.3, the velocities for gas and liquid phases are defined at the inlet. In this parametric study, two sets of velocity profiles were investigated. One corresponds to a flat velocity distribution (case A) as illustrate in left-hand-side graph of Figure 5.15. The other condition was guided by the inlet conditions in the experimental setup in which the rectangular channel has a blade close to the inlet separating the phases which means each phase is bounded by solid walls along the length of the blade in the inlet region. This length of the blade is too short for fully developed velocity profiles to be obtained; however, data regarding the velocity profiles near the inlet were not provided from the measurements, hence fully-developed profiles were assumed and imposed in the simulations. In order to obtain the fully-developed profiles, prior to their imposition as inlet conditions, simulations were carried out in a channel with cross-section area that is half the cross-section of the actual channel (as the horizontal blade divides the cross-section into two equal portions). In this channel, a steady state single phase flow of the gas and of the liquid was simulated in turn. A plane section sufficiently far from the inlet, where the flow would be fully-developed, was placed,

and the phase velocity profile in the plane section was recorded in each simulation. Two tables which tabulate the velocity profile for the gas and liquid phases were merged into a single file with simple manipulation on the vertical coordinate. This file can be loaded in the two-phase simulation to specify the inlet velocity profile. As illustrated in right-hand-side graph of Figure 5.15, a fully developed velocity profile for gas-liquid phases was imposed in case B.

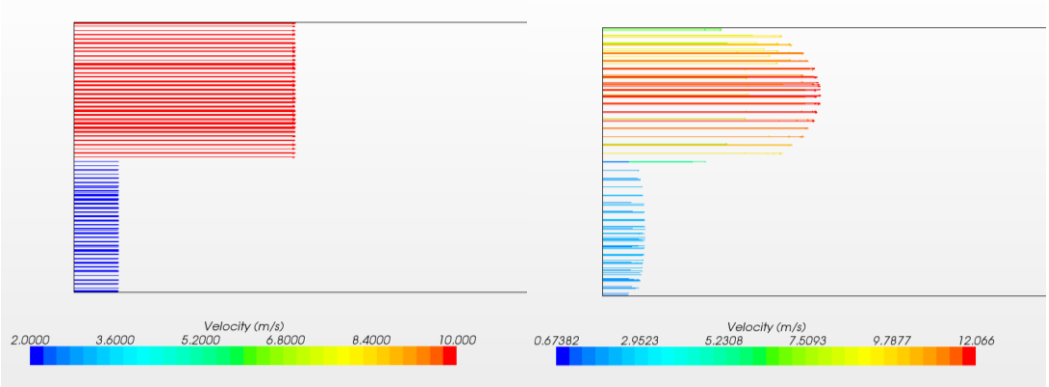

Figure 5.15: The x-componet of the velocity distribution imposed at the inlet. Flat (left, case A) and fully-developed velocity profile (right, case B).

According to the simulation results, the effect of the inlet gas-liquid velocity profile was not significantly noticeable, though the fully developed gas-liquid velocity profile has slightly shift the needed entrance length of the first slug towards the inlet. As illustrate in Figures 5.16 and 5.17, the initial slug appeared at 3.45m in case B while that appeared at 3.78m in case A. However, this length was found to be 1.5m in the experiment, means initial position where the first slug appeared was not successfully reproduced in the simulations.

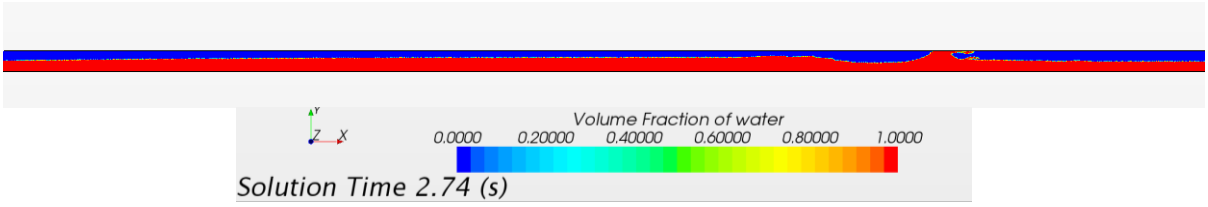

Figure 5.16: Liquid volume fraction contours at x=0-5.5m, t=2.74s, simulation with flat gas-liquid velocity profile defined at inlet (case A).

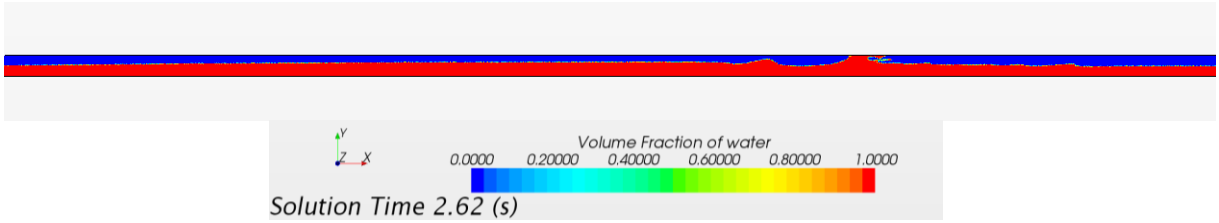

Figure 5.17: Liquid volume fraction contours at x=0-5.5m, t=2.62s, simulation with fully-developed gas-liquid velocity profile defined at inlet (case B).

In addition, a simple test was carried out to investigate the effect of gas velocity on the slug initiation. In this simulation (case C), a flat gas-liquid velocity profile was imposed, the liquid velocity remain the same as the one provided from the experiment (U_{SL}=1.0m/s), but the gas velocity was increased by 5%, gives U_{SG}= 5.5m/s. Comparisons of the liquid holdup time traces predicted in case A and case Care illustrated in Figure 5.18 to Figure 5.21. In the upstream of the channel where the flow regime is stratified flow (x=2.19m and 3.18m), the liquid level is slightly decreased and the interface appears wavier with higher gas velocity. Though a direct comparison cannot be made against HAWAC data, this finding is consistent with the experimental observations made in the present study in a circular pipe, as discussed in chapter 7 (a higher gas flowrate leads to a decrease in the liquid level, but more waves at the gas-liquid interface).

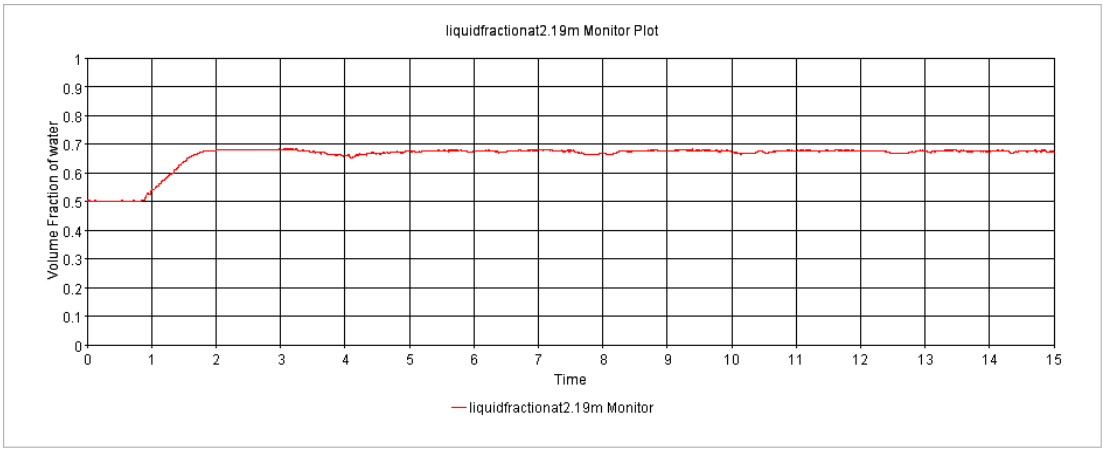

Figure 5.18: Calculated liquid holdup traces at x=2.19m, Usl=1.0m/s and Usg=5.0m/s.

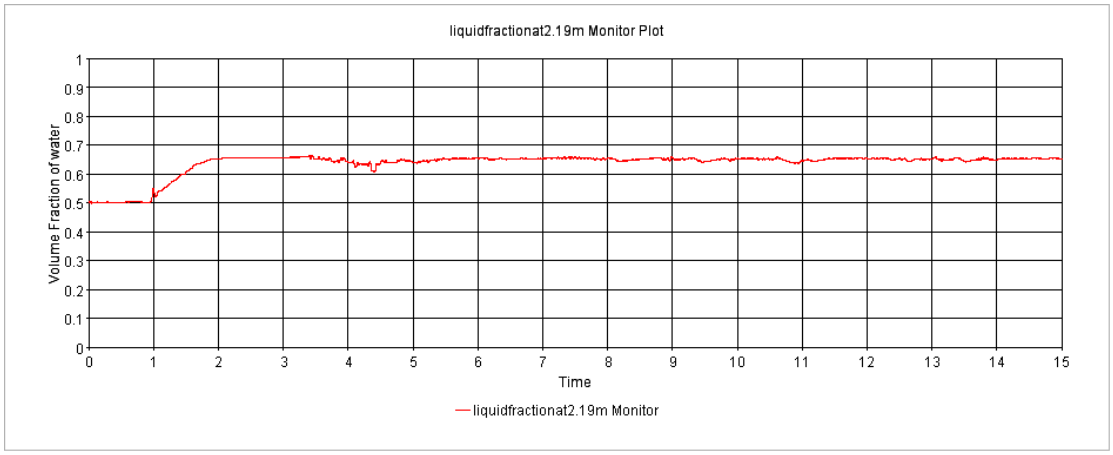

Figure 5.19: Calculated liquid holdup traces at x=2.19m, Usl=1.0m/s and Usg=5.5m/s.

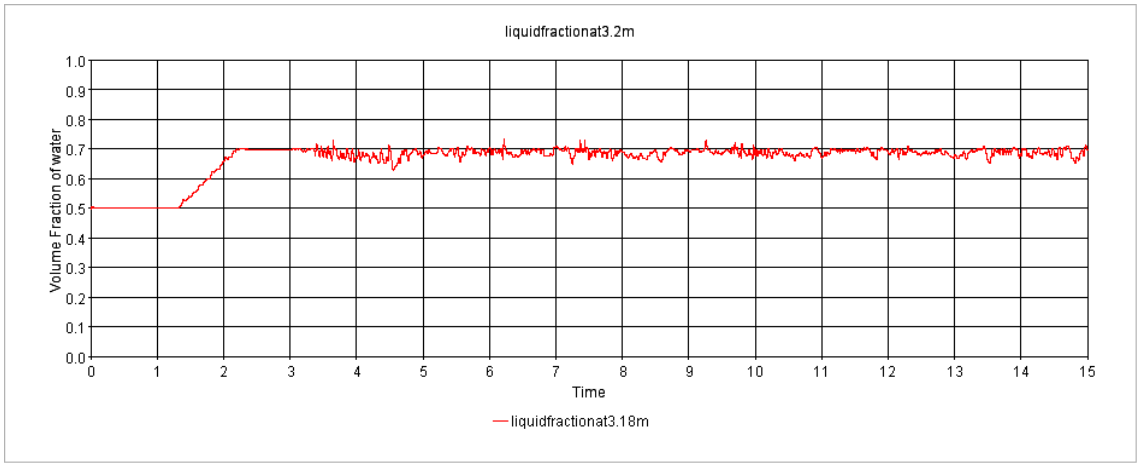

Figure 5.20: Calculated liquid holdup traces at x=3.18m, Usl=1.0m/s and Usg=5.0m/s.

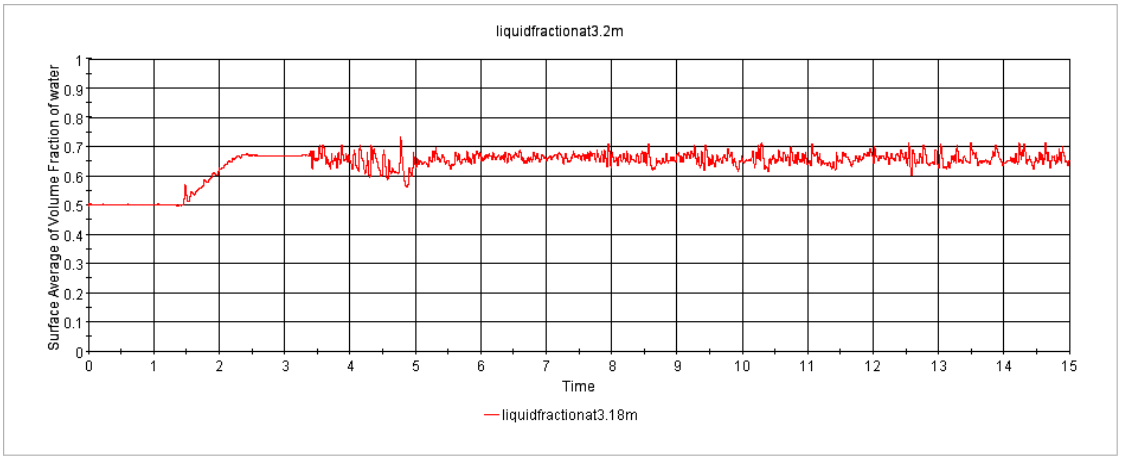

Figure 5.21: Calculated liquid holdup traces at x=3.18m, Usl=1.0m/s and Usg=5.5m/s.

5.4.7 Prediction of flow characteristics

In the following section, simulation results with respect to flow development and slug characteristics are illustrated. To validate the model, slug initiation mechanism, liquid holdup time traces, slug velocity and average liquid level were compared to experimental measurements.

5.4.7.1 Slug generation and propagation phenomenon

The picture sequence in Figure 5.22 is the calculated phase distribution at time interval of 0.04s; it shows the qualitative behaviour of the slug generation and propagation is similar to the experimental measurement (see Figure 5.23). Initially, one of the waves grow larger in amplitude as can be seen at t=2.66-2.70s. The bigger wave rolls over and can bridge the channel cross-section, thereby forming the first slug at approximately t= 2.74s. The slug can catch up waves and merge with them, develop into a larger slug. Behind the slug, the water level decreases. Figure 5.23 illustrate the three-dimensional configuration of a typical slug observed in the simulation.

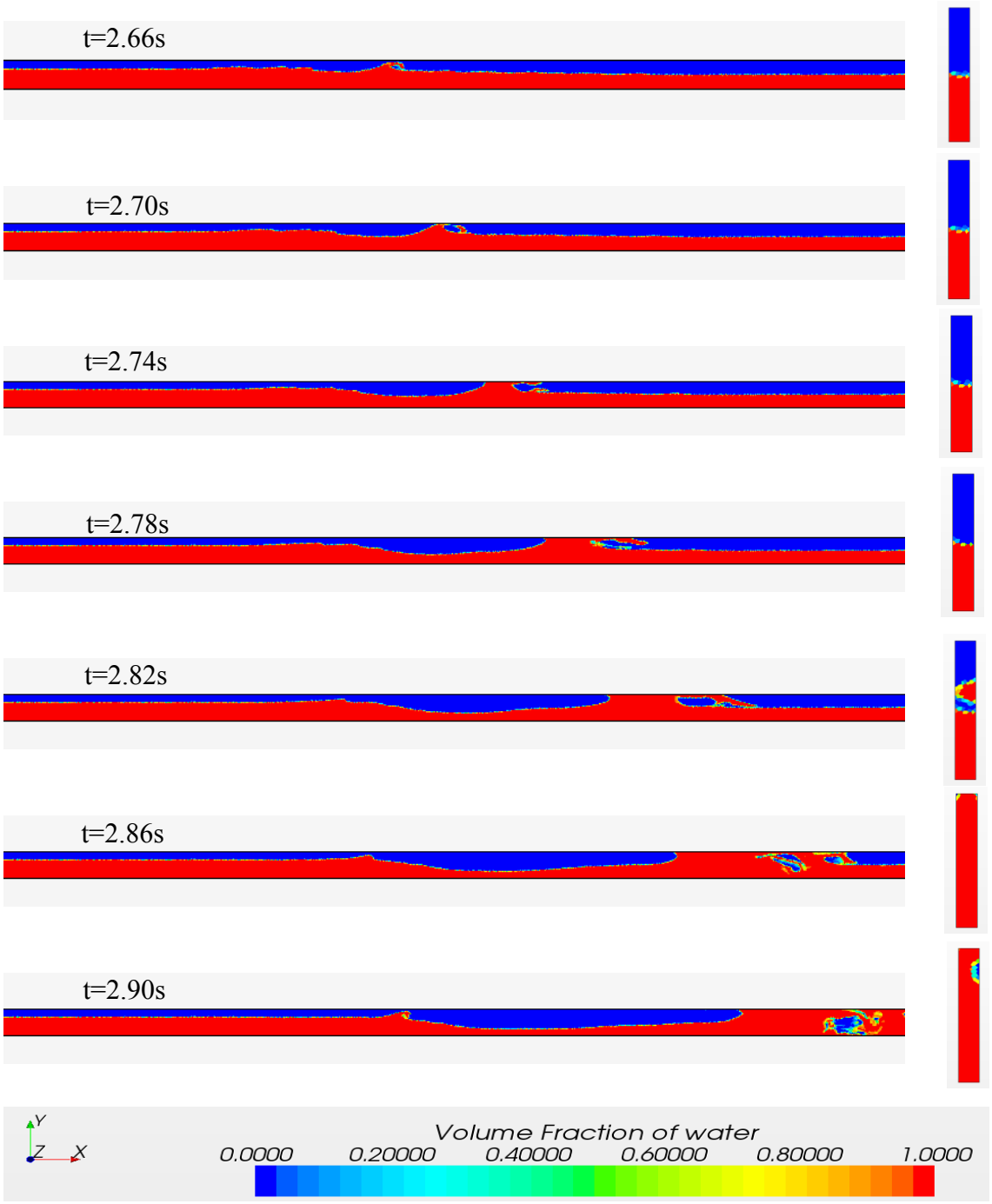

Figure 5.22: Calculated time sequence of slug initation and progation. For horizontal section, Z=2.0-6.5m, the cross-sectional plane at Z=6m.

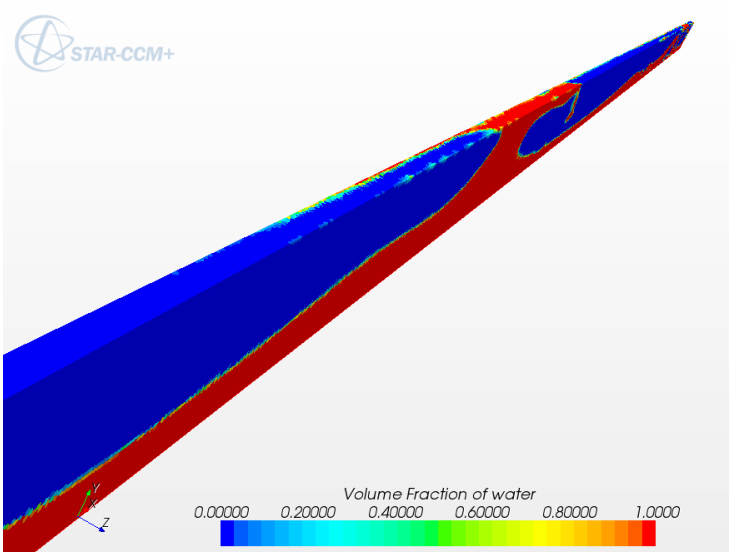

Figure 5.23: Three-dimensional confifiguration of a typical slug observed in the simulation.

5.4.7.2 Liquid holdup traces

Integrated liquid volume fractions at various cross-sectional planes are plotted when running the simulation (see Figure 5.24), a slug or large roll wave is detected when the volume fraction is close to unity. At 0.53m, the gas and liquid interface is rather flat, indicating a smooth stratified flow regime close to the inlet. The interface become wavy at 1.53m and develops in to a clear wavy flow at 3.2m. Downstream at 5m, slug flow is generated spontaneously; and further downstream at 6m and 7m, the numbers of water peaks decreases illustrating that some slugs merge together while some collapse. A fraction (2.5s) of liquid volume fraction at various locations is plotted in Figure 5.25, in order to compare with the experimental data plotted in Figure 5.26 (rearrange the H_L/D time traces in Figure 5.4). In the experiment, a clear wavy flow was observed very close to the inlet (0.2m and 0.53m), indicting the simulation has underestimated the development of the interface instabilities. Some of the waves become larger at 1.2m and slugs are irregularly generated at 1.5m. Further away from the inlet, the behaviour of the slug development including the merge and collapse processes is qualitatively in agreement to CFD predictions. The discrepancy can be explained with the flow regimes observed close to inlet. In the experiment, small disturbances of the interface were observed from the inlet which provides a more efficient momentum transfer

from the air to the water and consequently induce more rapid wave growth and slug generation. Whereas in the simulation, initially close to the inlet, the gas-liquid interface is rather flat, interfacial waves are grown due to the velocity difference between the two phases, and consequently a longer channel length is required for the spontaneously generation of the slug. This result is found to be in agreement to CFX simulation. It is difficult to apply the boundary conditions to the CFD model to accurately reproduce the small disturbances observed in the experiment, which have important influence on the generation of gas-liquid slug flow.

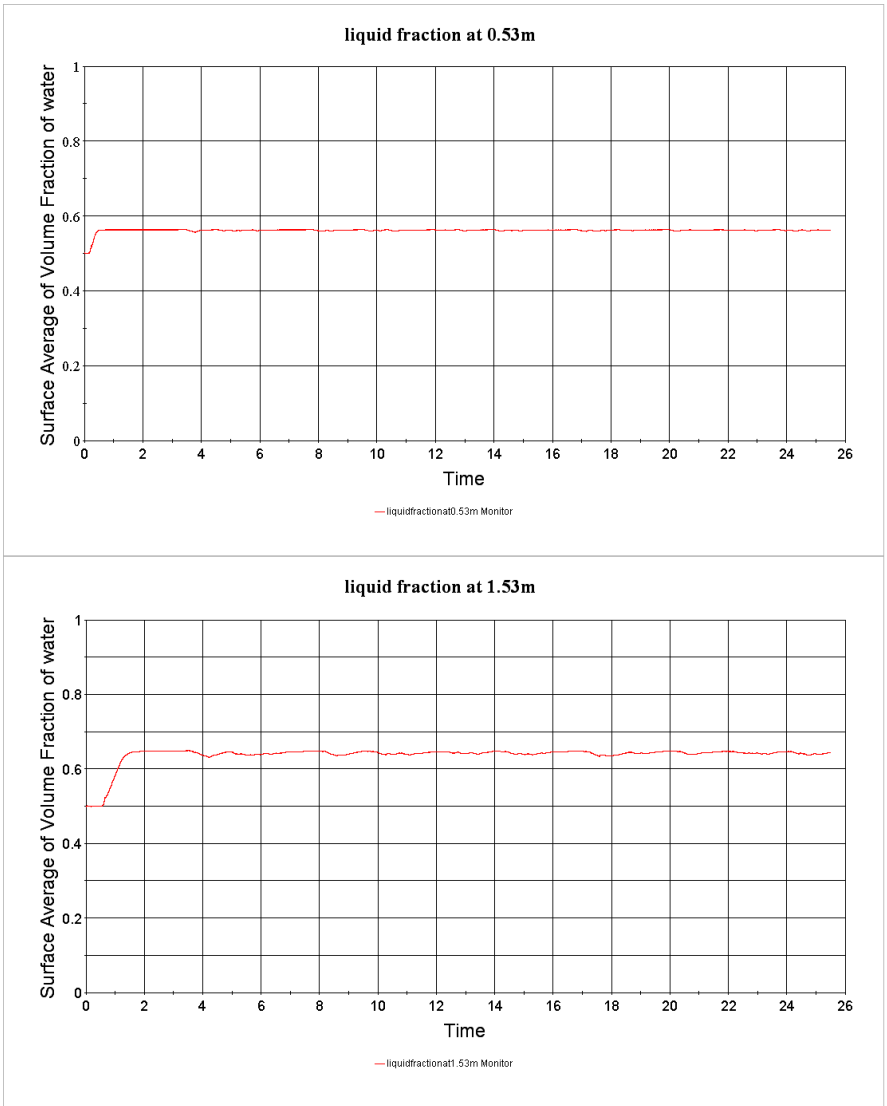

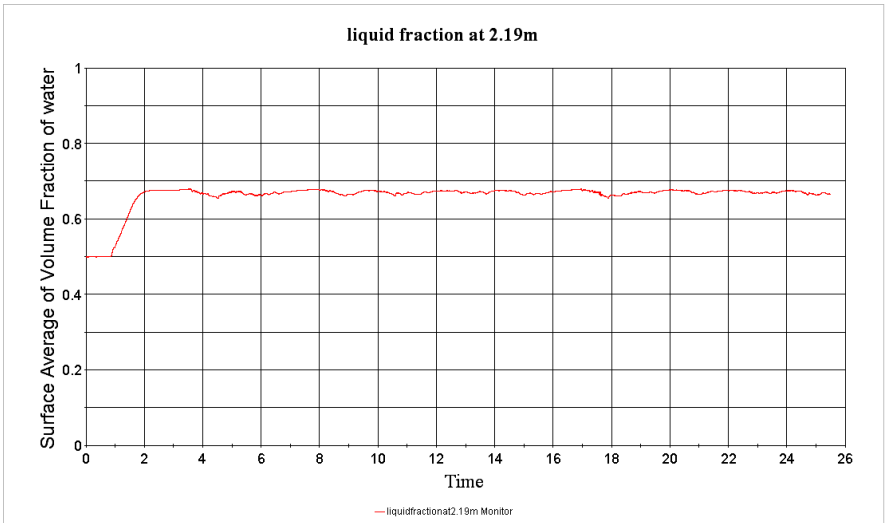
liquid fraction at 2.19m
Surface Average of Volume Fraction of water
Time
liquidfractionat2.19m Monitor

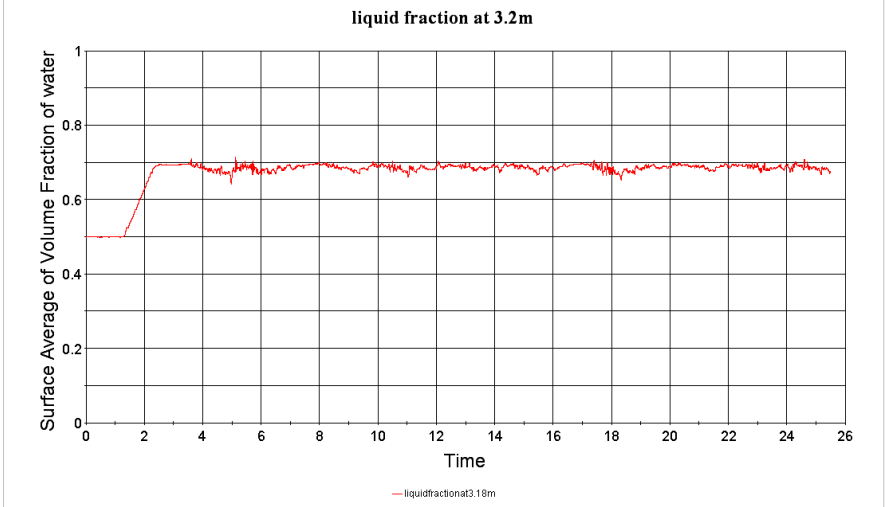
liquid fraction at 3.2m
Surface Average of Volume Fraction of water
Time
liquidfractionat3.18m

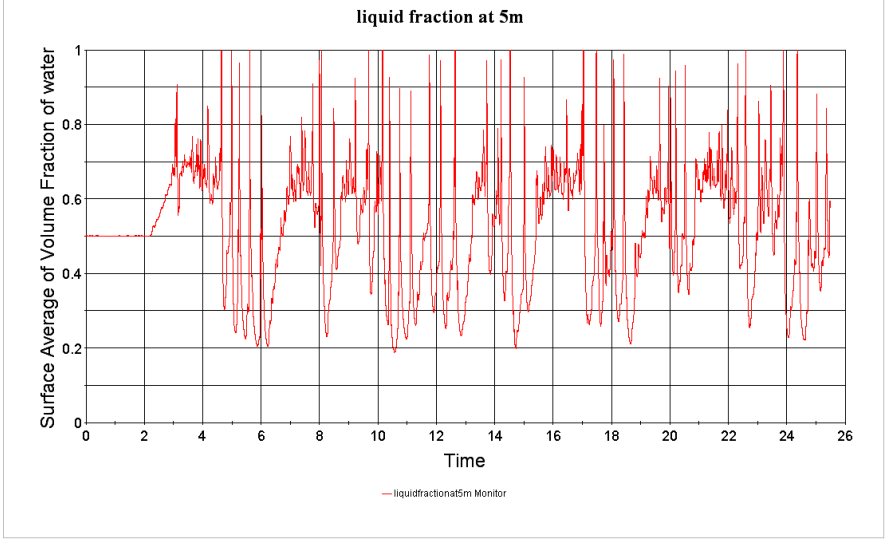
liquid fraction at 5m
Surface Average of Volume Fraction of water
Time
liquidfractionat5m Monitor

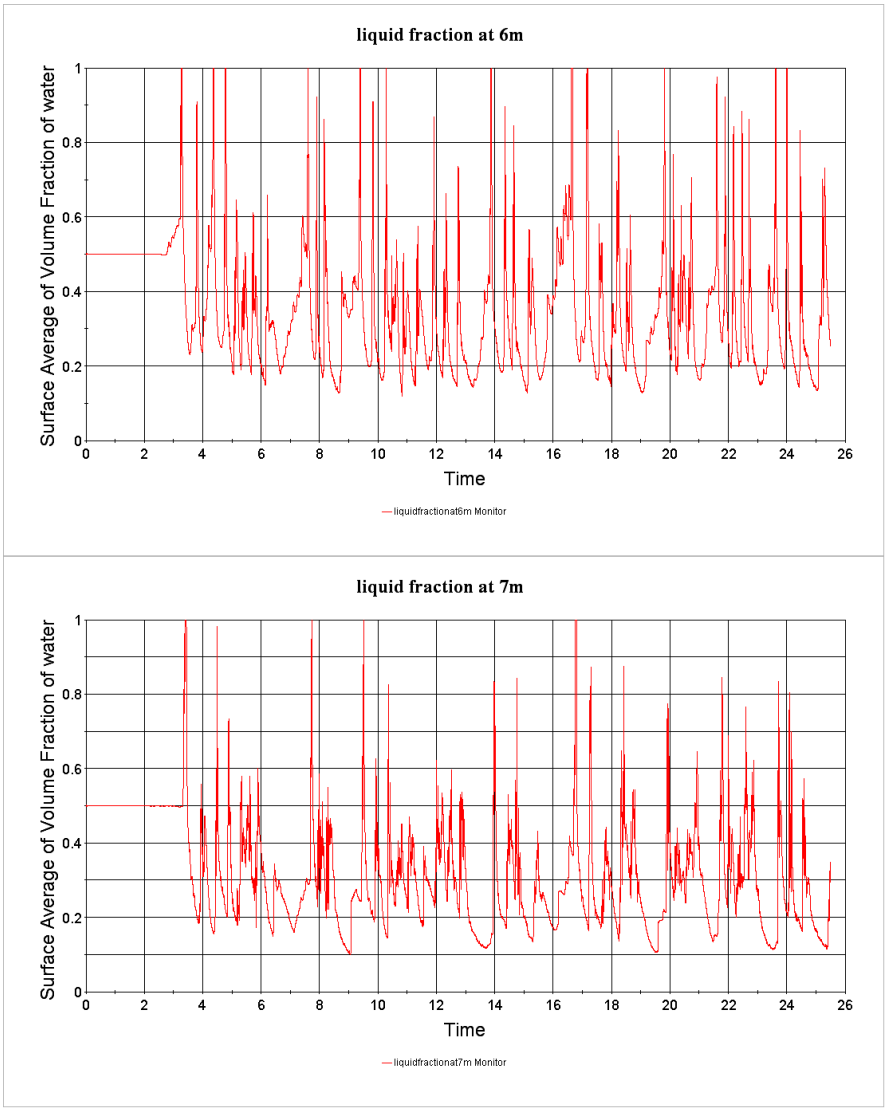

Figure 5.24: Plots of liquid volume fractions at various locations, x= 0.5m, 1.53m, 2.19m, 3.20m, 5m, 6m, 7m.

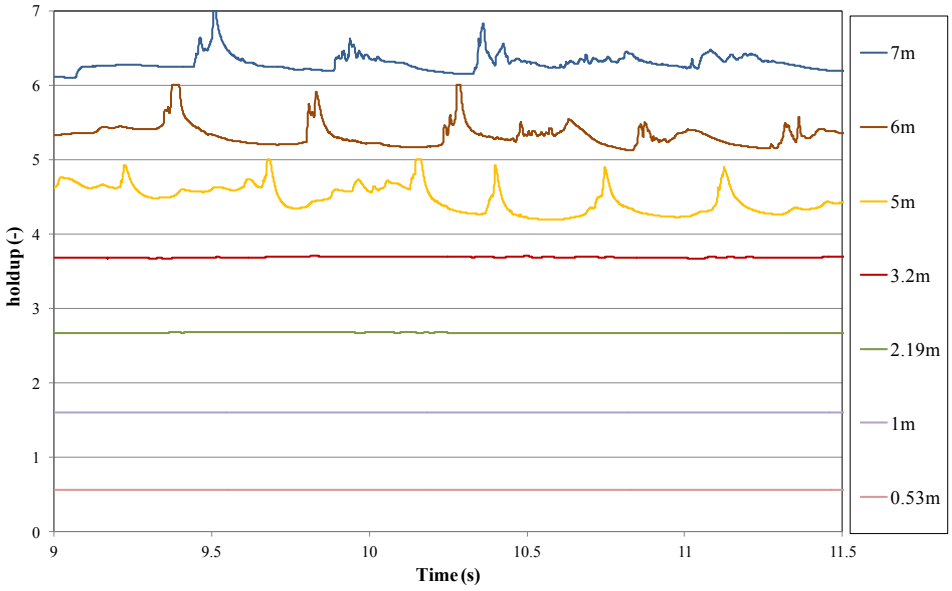

Figure 5.25: Plots of liquid volume fraction time trace at various locations, as computed from simulation. (Note: For clarity of presentation of the respective traces in this Figure the plots show the holdup values plus 1, 2 , 3,4,5,6 for the probe positions 0.53, 1, 2.19, 3.2, 5, 6 and 7 respectively).

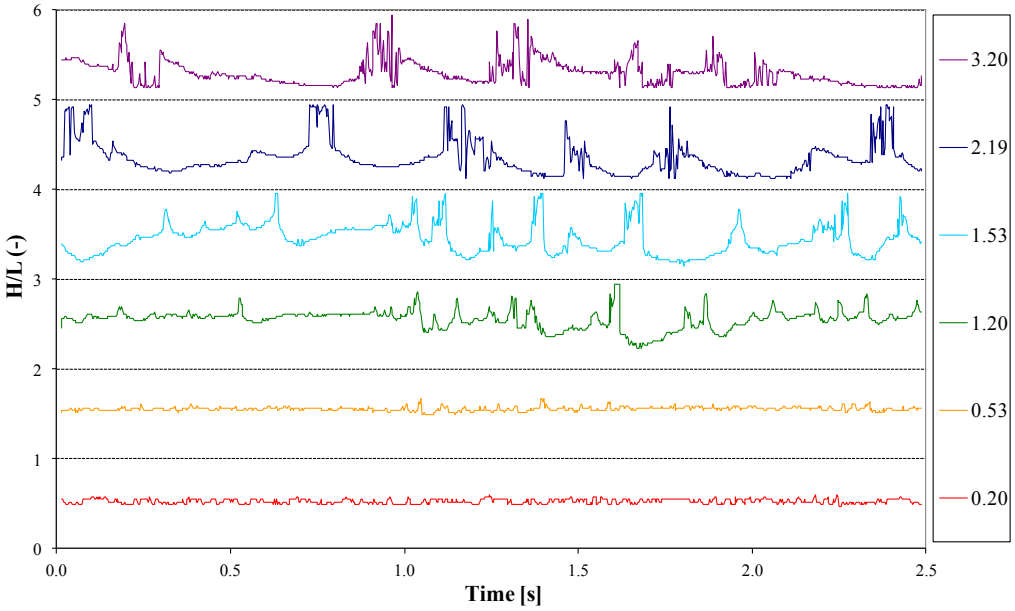

Figure 5.26: Plots of h_L/H time trace at various locations, as measured from experiment. (Note: For clarity of presentation of the respective traces in this Figure the plots show the h_L/H plus 1, 2 , 3,4,5 for the visualisatin position 0.2, 0.53, 1.20, 1.53, 2.19 and 3.20 respectively).

5.4.7.3 Slug velocity

Figure 5.27 plots the x-component of velocity vectors for one slug unit at different sections along the channel. Three location of x = 5.42 m, 5.42 m and 5.67 m were chosen to plot different velocity vectors for slug tail, slug body and slug front respectively. It is observed that velocity profile varies with gas-liquid flow configurations.

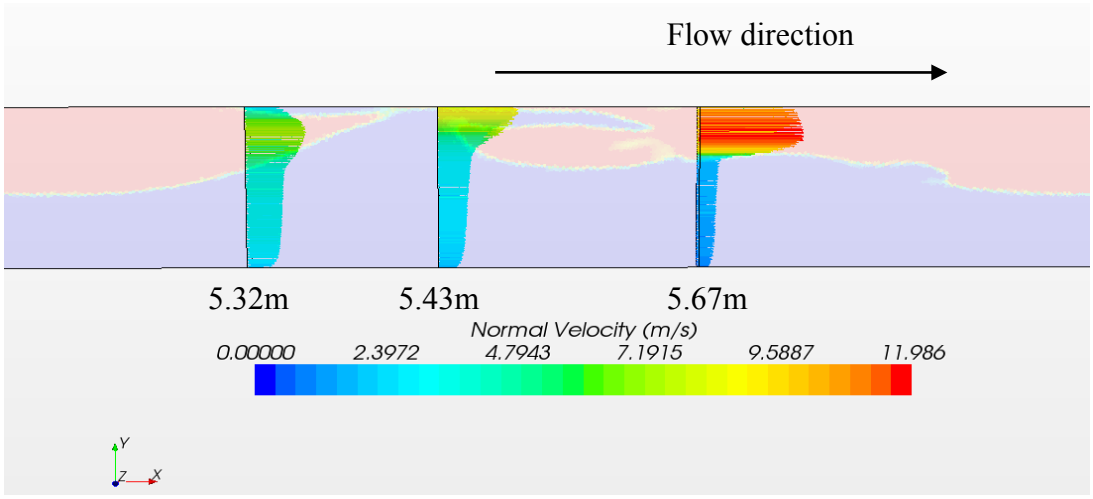

Figure 5.27: Cartisian x-component of velocity vectors for one slug unit at 5.32m (slug tail), 5.42m (slug body) and 5.67m (slug front).

Figure 5.28 illustrate the radial velocity profiles plotted at the locations of 5.32m, 5.42m and 5.58m. The corresponding turbulence kinetic energy profiles are plotted in Figure 5.29. At the slug front, high degree of turbulence is observed, an upward inclining shape of velocity indicating a high gas flow rates. The velocity in the gas phase is much higher than the liquid phase, the liquid velocity increase slightly towards the interface due to the drag force of the gas exerted on the liquid. In liquid slug body, the velocity profile is similar to single phase liquid velocity profile, the maximum velocity is observed towards the top wall. However, very close to the wall, the velocity decreases due to the shear stress exerted by the wall inner surface. In the slug tail, the parabolic shape of velocity profile in the gas phase presents laminar features. Considering the slug unit, at the slug tail, gas velocity has a high value, but it decreases in the liquid slug body; at the slug front, gas phase tends to accelerate again. However comparison against experiment was not performed due to the lack of velocity measurement data.

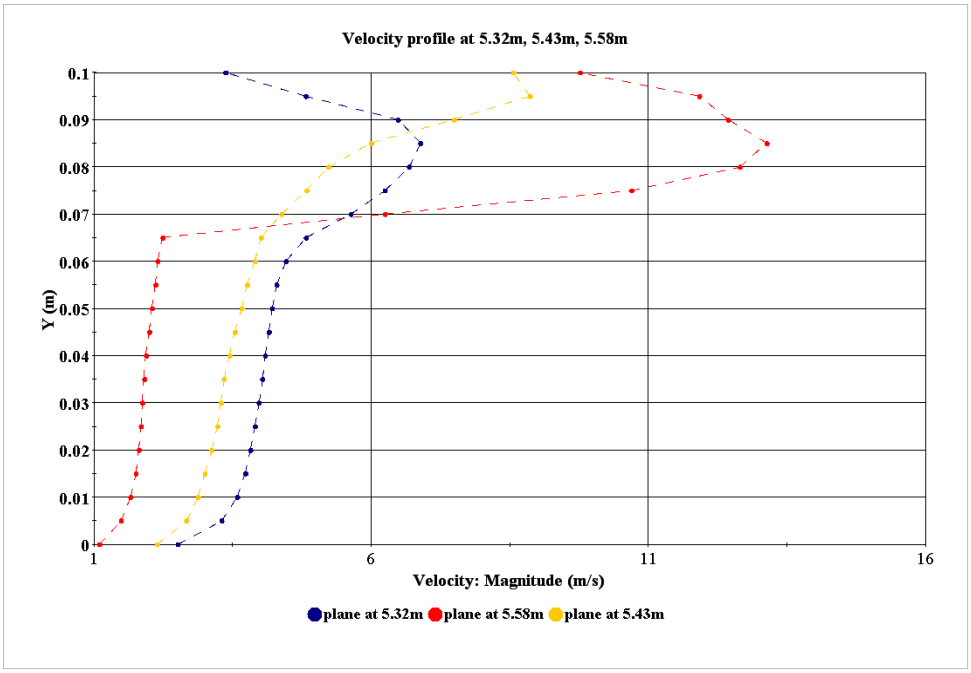

Figure 5.28: Radial velocity profiles obtained in the simulation at 5.32m (blue line), 5.43m (red line) and 5.58m(yellow line).

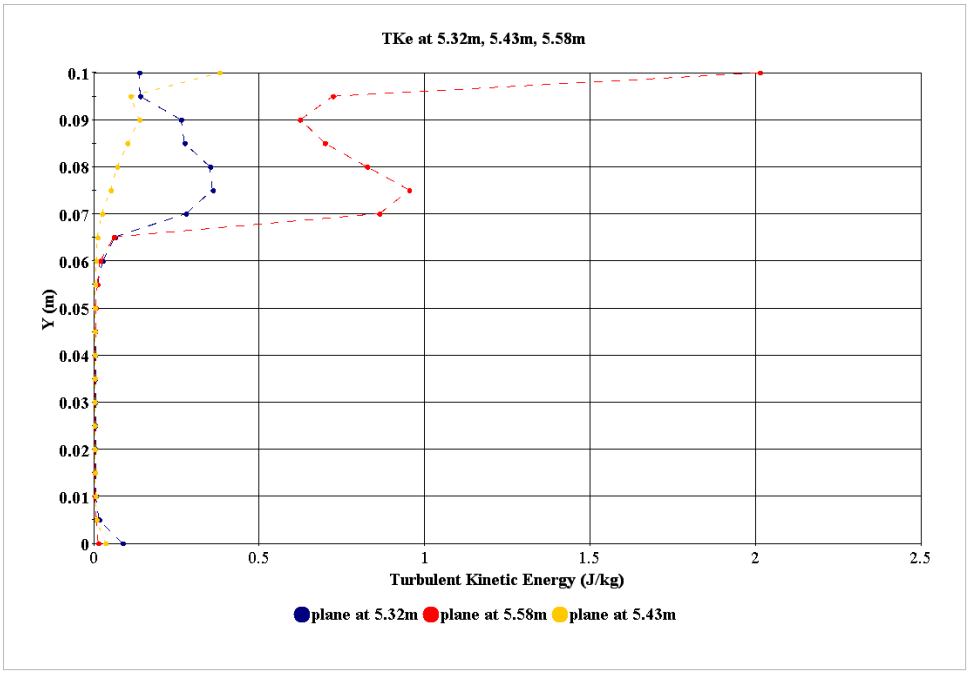

Figure 5.29: Radial turbulence kinetic energy (TKE) profiles obtained in the simulation at 5.32m (blue line), 5.43m (red line) and 5.58m(yellow line).

5.4.7.4 Average Liquid level

As already introduced in Section 5.2, a mean water level profile along the channel which reflects the structure of the interface was extracted from the high speed video recording in the experiment, the time-averaged water level at various cross sections was bounded by the standard deviation as shown in Figure 5.5. Similarly, the data restored in the simulation at each cross-section was processed to give the time averaged water level profile, as shown in Figure 5.30.

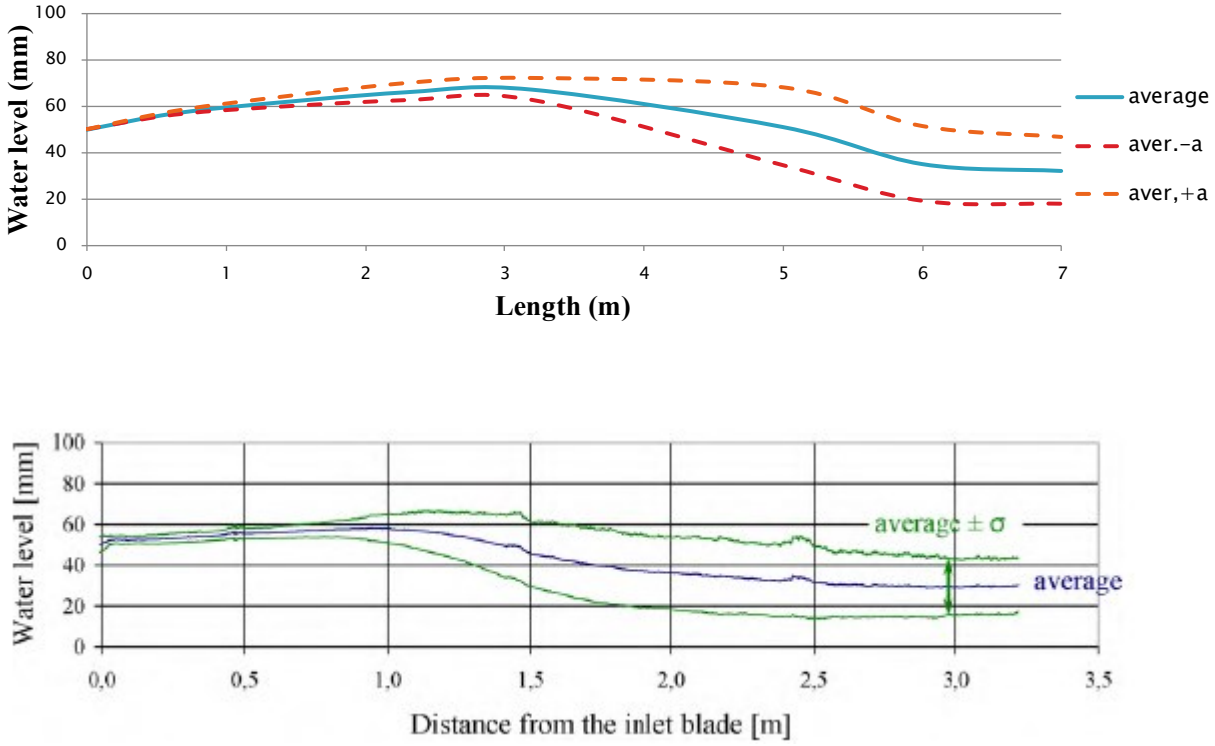

Figure 5.30: Comparision of time- averaged water level profiles obtaiend from STAR-CCM+ calculation(above) and experiment (below).

Similar trends were obtained in the simulation and measurement. As shown in Figure 5.30, the mean water level profile increases after being injected over a height of 50 mm at the inlet. Further downstream, the water levels decrease simultaneously with an increase of the standard deviation due to the presence of the irregular slugs. In the last part of the channel, the mean water levels converge to an asymptotic value, at about 35mm. However, in the

simulation, wave growth starts from 3.2 m, revealed by a rapid increase of the standard deviation, whereas rapid wave growth starts from 0.9 m in the experiment.

5.5 Conclusion

In this chapter, a three dimensional CFD simulation of water-air two phase slug flow in the horizontal rectangular channel was performed using a commercial software package, STAR-CCM+. In this simulation, the biggest challenge is to find a good combination of the geometric, boundary and initial conditions for the experimental set up. From the exercise of modelling the slug initiation and development in the horizontal channel, the following conclusions can be drawn:

- The choice made for the physical model is crucially important and should be well justified. In this case study, the free surface was tracked by a VOF model together with a HRIC scheme; the behaviour of interface instability, wave growth and slug generation processes were qualitatively captured.

- The polyhedral mesh was found to yield a better residual convergence than hexahedral mesh, since each cell has 10-14 faces which can propagate flow information more efficiently. For the same type of mesh, the liquid volume fraction trace at certain locations was plotted for different grid size until the variation is minimised.

- In present study, the SST k-ω model was applied and has shown its capacity to simulate slug flow. The effect of applying turbulence damping functions in the interfacial area was also investigated. The interface damping treatment has certain effect on the gas-liquid velocity profile in the stratified flow regime; however, it did not show a particularly strong effect on the appearance of waves and slugs, providing the mesh grid are sufficiently fine.

- Though the behaviour of slug initiation and propagation was captured qualitatively, a quantitative comparison against experiment was complicated by the deviation in the slug initiation site. At the inlet, a fixed gas-liquid velocity with either flat or parabolic

velocity profile leads to a similar results. The longer length needed for the initiation of the slug in the simulation is likely due to the simplification of the inlet geometry. The presence of the stratification blade can introduce the disturbance due to the flow jump at the blade end, which may have significant influence in the wave growth.

- The outlet boundary condition was defined as pressure controlled outlet. However, when pressure waves leave the domain through a pressure boundary, back waves can be generated towards the interior of the domain due to discretization reason. Unfortunately, a non-reflecting boundary is not available in the STAR-CCM+ platform. One possible solution is to extend the pipe length by adding a region of very coarse mesh before the outlet in order to kill the numerically generated back waves. However, there are too many aspects to cover in this numerical test, due to the constrained time, a further investigation of the outlet boundary condition is recommended in future work.

In regards to the points above, the process of CFD-experiment integration is a difficult and long term task. In order to achieve a best practice, it's recommended to set up the experimental and modelling work from the beginning. The measurement should be taken with relevant quantities and at relevant locations according to the computational domain.

Chapter 6

Experimental facilities and methods

6.1 Summary

This chapter describes the basic facilities and procedures employed throughout the experimental work. The low pressure rig, LOWPRESS, is described in detail, with special attention to the key pieces of instrumentation such as the high-speed photography (Section 6.2.4) and conductivity probe (Section 6.2.5). To study the entrance effect on the slug initiation and development, special inlet sections were designed and manufactured as discussed in Section 6.2.3. Following the description of the instrumentation used, the basic operating procedures are outlined in Section 6.2.6; the measurement error is discussed in Section 6.2.7.

6.2 LOWPRESS Rig

LOWPRESS Rig is located in room 111 in the Department of Chemical Engineering. It is designed to enable investigation of gas liquid flows at atmospheric pressure and ambient temperature. The test-line is 7.5m long and comprises several pipe sections that are joined together by using tongue and groove flanges. These are machined to the exact internal diameter of 32 mm to ensure geometric continuity so that disturbances to the flow are

minimised. The pipe line is supported by ring supports attached to a steel framework, which is inclinable. A sketch of the LOWPRESS facility is shown in Figure 6.1.

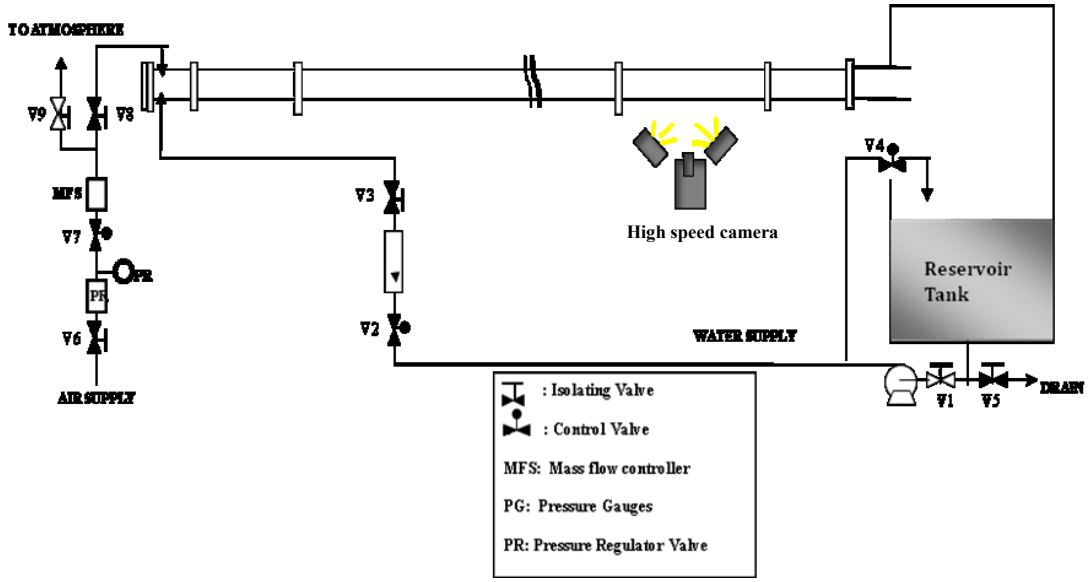

Figure 6.1: Schematic of the LOWPRESS 32mm rig.

6.2.1 Fluids storage and flow metering

Liquid is introduced into the test-section from a $1m^3$storage tank. From the base of this tank, the water passes via isolation valve MV1 into a Beresford PV122 pump which is capable of delivering a maximum flowrate of 350 l/min. Most of the water is then pumped into the inlet section, via control valve V1. The water flow is measured using a Series 2000 KDG MOBREY rotameter (range: 1.5 l/min to 16 l/min with accuracy of 0.5%), see Figure 6.2. A fraction of the water is allowed to flow through the recycle loop via control valve V4 and back into the tank, so that the flow can be easily regulated. The liquid flows into the rotameter through V2 and the liquid height in the rotameter is proportional to the liquid flowrate hence the superficial velocity. Calibration curves for liquid have been developed in order to deduce the superficial velocity from the liquid height in the rotameter.

Air is obtained from the low-pressure departmental supply (up to7 bar). It passes through an isolating valve (V6) and an IMI Norgren pressure regulator and filter, enabling fixed upstream pressure, before passing through a mass flow controller. The mass flow controller is

connected with a PC, enabling the air flowrate to be monitored and controlled from computer during the experimental runs. The isolating valve combination V8 and V9 enables air to either vent to atmosphere (V8 closed, V9 open) or pass directly along the test line (V9 closed, V8 open). The air flow rate is controlled and measured using a mass flow controller (MFC) which is supplied by Bronkhorst and calibrated for 100-3000 l(s)/min as seen in Figure 6.2. It has an inlet port, an outlet port, a mass flow sensor and a proportional control valve. The MFC is fitted with a closed loop control system. It is provided an input by the PC so that it compares to the value from the mass flow sensor and adjusts the proportional valve accordingly to achieve the required flow. The flow rate is a specified percentage of its calibrated full scale flow and is supplied to the MFC as a voltage signal. A typical MFC signal can be seen in Figure 6.3.

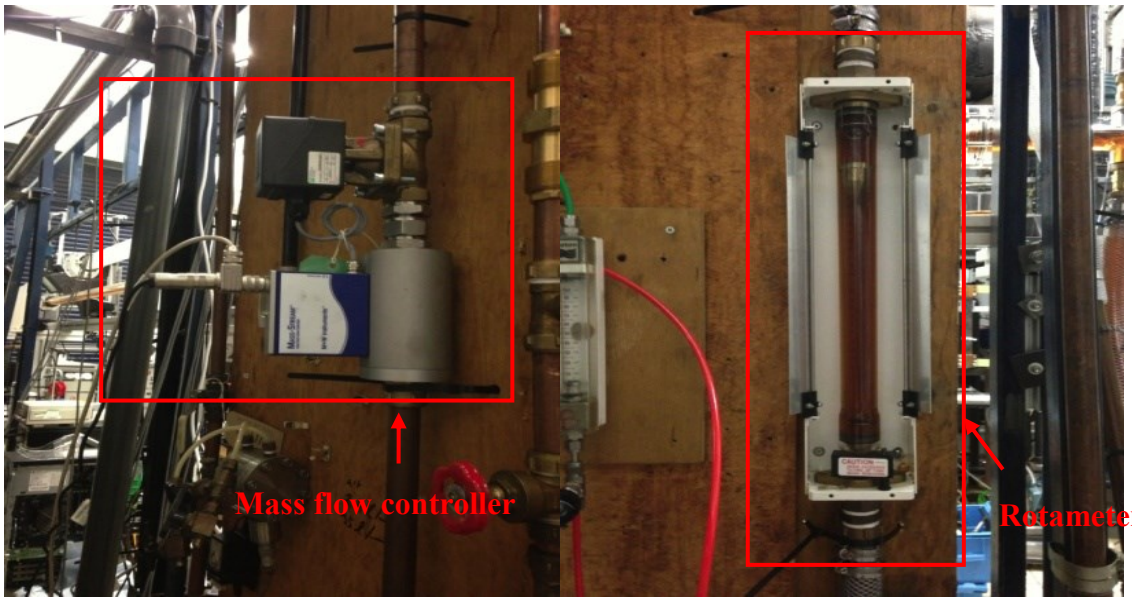

Figure 6.2: Photograph of the LOWPRESS mass flow controller and rotameter.

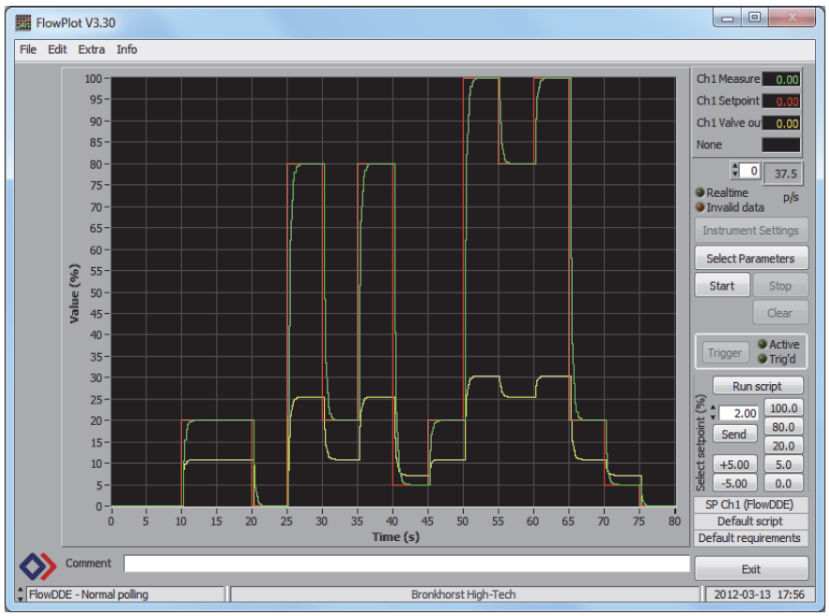

Figure 6.3: Typical signal of mass flow controller.

6.2.2 Fluid properties

In all cases the LOWPRESS rig operates at local ambient temperature. The typical operating temperature is about 15°C. The fluids used in the LOWPRESS facility for this series of experiments were air, water and oil. Their physical properties at atmospheric pressure are given in Table 6.1.The surface tension of the oil and water in the rig was measured using Kruss Tensiometer K100, and viscosity was measured using Anton Paar viscosity meter.

Table 6.1: LOWPRESS fluid physical properties (1 bar).

	Air	Water	Shell Tellus 22 oil
Density (kg/m^3)	1.18	998.3 (15° C)	860 (15° C)
Viscosity(Pa s)	0.0000183(20° C)	0.00098(15° C)	0.06(15° C)
Surface tension(N/m)	--	0.072(20° C)	0.03(20° C)

6.2.3 Inlet Configuration

Gas and liquid are injected into the test section via an inlet section. In order to study the effect of inlet configuration on slug initiation and development, two types of inlet sections were designed and manufactured.

6.2.3.1 Inlet section with stratification plate

Gas and liquid are introduced into the test section via feed streams which are perpendicular to the pipe. In order to reduce the interaction in the vertical plane between the two fluids, a plate is mounted parallel to the tube axis hence a co-current stratified flow of two fluids are obtained before they came into contact Davies (1992).

The inlet configuration is shown in Figure 6.4. Each feed stream is connected with a non-return check valve to prevent the back flow. To mount the stratification plate horizontally at various levels, four groove slots are created on the internal surface of the pipe and the blanking flange. They are evenly spaced with a distance equal to the pipe radius. Accordingly, plates with different width are made for each level, as can be seen in Figure 6.5. By rotating the inlet 180 degrees, it can possibly give a total of seven different channel sizes for the respective phases.

Three different inlet plate configurations were studied for this research, of which the plates were inserted at heights of 8mm, 16mm and 24mm from the base of the pipe. To change the plate, the entrance section has to be detached from the rest of the test section by disconnecting it at the flanges, the first plate is removed then another plate is inserted into the appropriate groove slot. The entrance section is then re-attached to the test section.

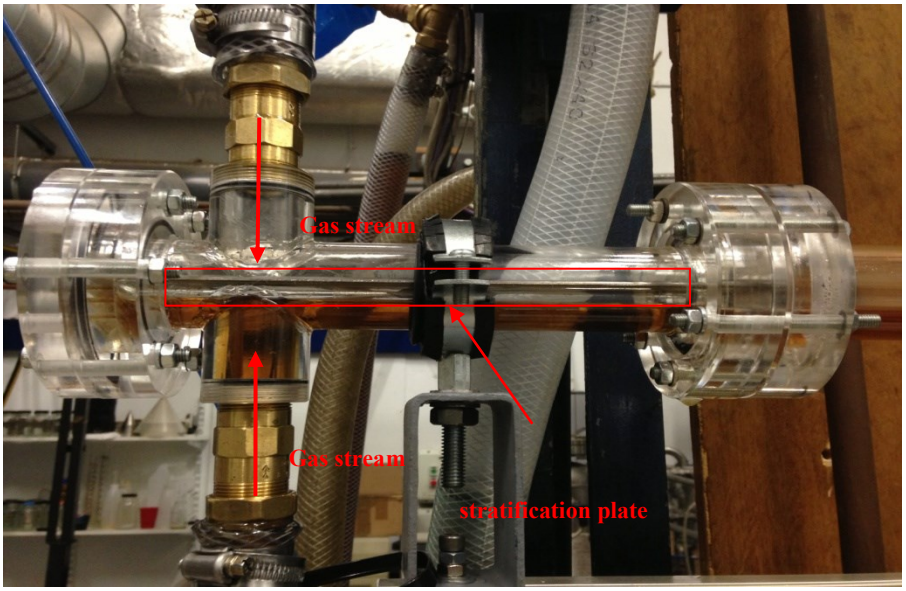

Figure 6.4: Photograph of LOWPRESS inlet section with stratification plate being inserted.

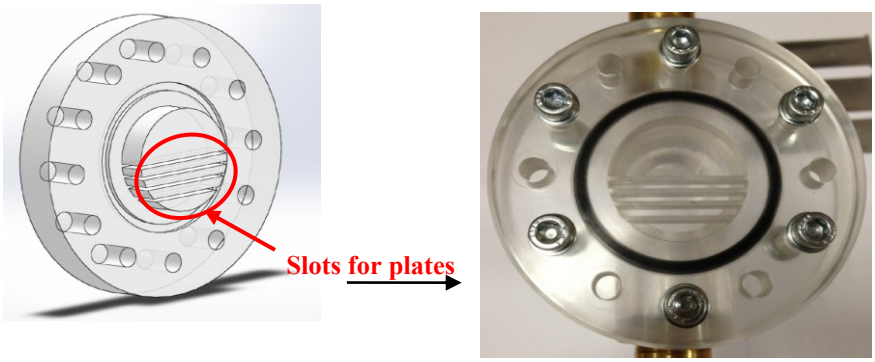

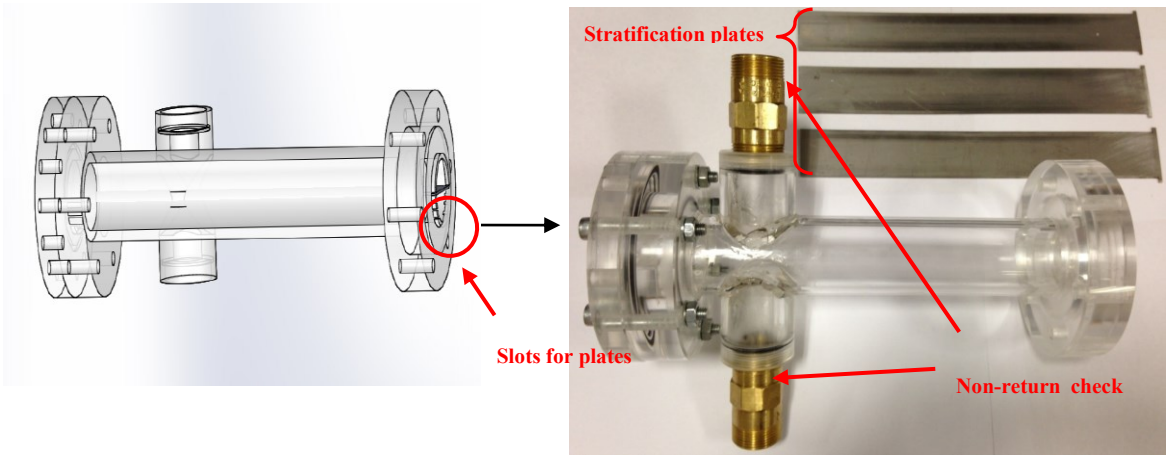

Figure 6.5: Photograph of LOWPRESS inlet section parts.

6.2.3.2 Inlet section with conical reducer

The design of inlet with conical reducer enables the gas and liquid to gradually accelerate into the test section. The entrance consists of a 74 mm ID "T-configuration" pipe section and a conical reducer section (Figure 6.6). The inner diameter of reducer reduces from 74 mm to 32mm, and the section length is 260 mm which gives a reducing angle of 4.6 degree（Figure 6.7）. Gas is injected from top of the front section and liquid is injected from the bottom. Fluids are mixed and continue to develop over the 400 mm length pipe. Then the pipe size gradually decreases over the conical reducer section when introducing the fluids into the test section. The fraction of gas liquid entering the test section is not fixed and varies with different fluids velocities.

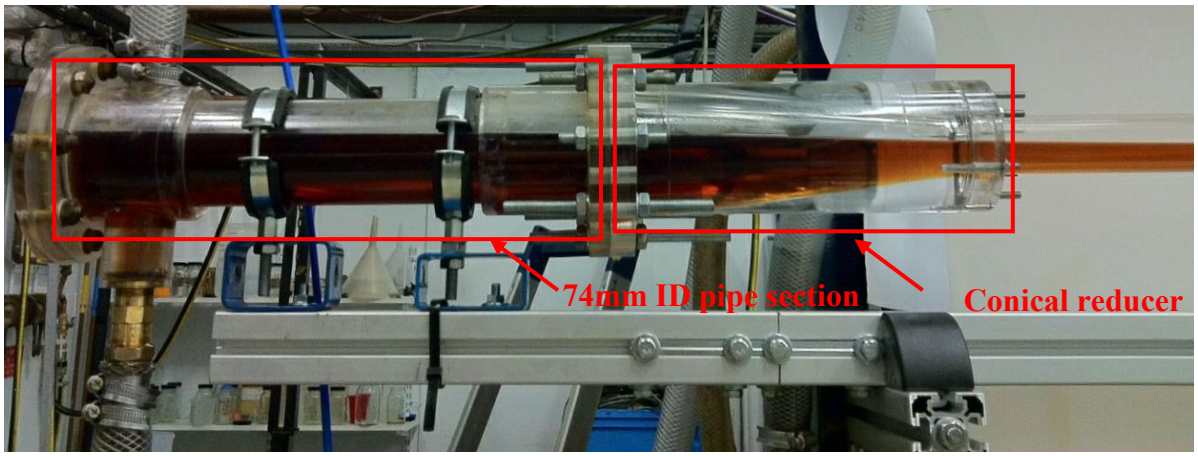

Figure 6.6: Photograph of the LOWPRESS conical entrance system.

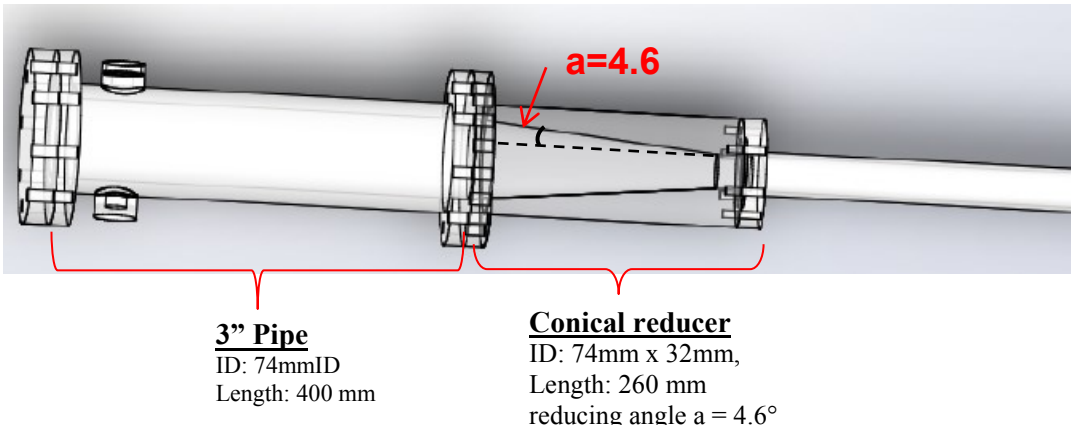

Figure 6.7: Schematics of the LOWPRESS conical entrance system.

6.2.4 High Speed visualisation

In present study, high speed cameras were used in series to capture the slug initiation and development processes.

The videos were recorded using in-house Olympus high speed I-SPEED 2 and I- SPEED 3 cameras. Both high speed video cameras provide high resolution and light sensitivity. The I-SPEED 3 camera can record up to 150,000 fps with a pixel resolution of 1280x1024, and I-SPEED 2 camera can record up to 33,000fps with a pixel resolution of 800x600.

To mount the cameras, supporting frames were assembled using aluminum profiles. Each camera can be stabilised on the frame which is perpendicular to the test section. In order to provide sufficient lighting, two flood lights were attached to the frame and a third light was placed above the test section, as seen in Figure 6.8. Two cameras were connected with two adjacent PC respectively and both controlled by I-SPEED software suite interface. The I-SPEED software suite does not contain synchronization function therefore two cameras cannot be controlled synchronously. The trigger is pressed to start the recording, and once the recording was completed the video length could be trimmed to specific frames of interest. In the present study 60 fps for 150s would give 9000 pictures. The pictures were downloaded in JPEG format on to computer and then assembled into movies using MATLAT imaging processing routine. The playback rate could be adjusted to speed up or slow down the viewing of movies.

The prime measurement parameter is slug frequency which can be achieved by counting the number of slugs appeared in the images over a certain recording time, therefore a sufficiently long period is required to give statistical results. When the frame rate is at its maximum, the recording period is shorter and lighting requirements are higher, and resolution is reduced. A frame rate of 60 fps with an exposure of 1500 was decided for the present study. Accordingly 150s sampling time could be recorded for each run in which 30-100 slugs are visualised for different combinations of fluid velocities.

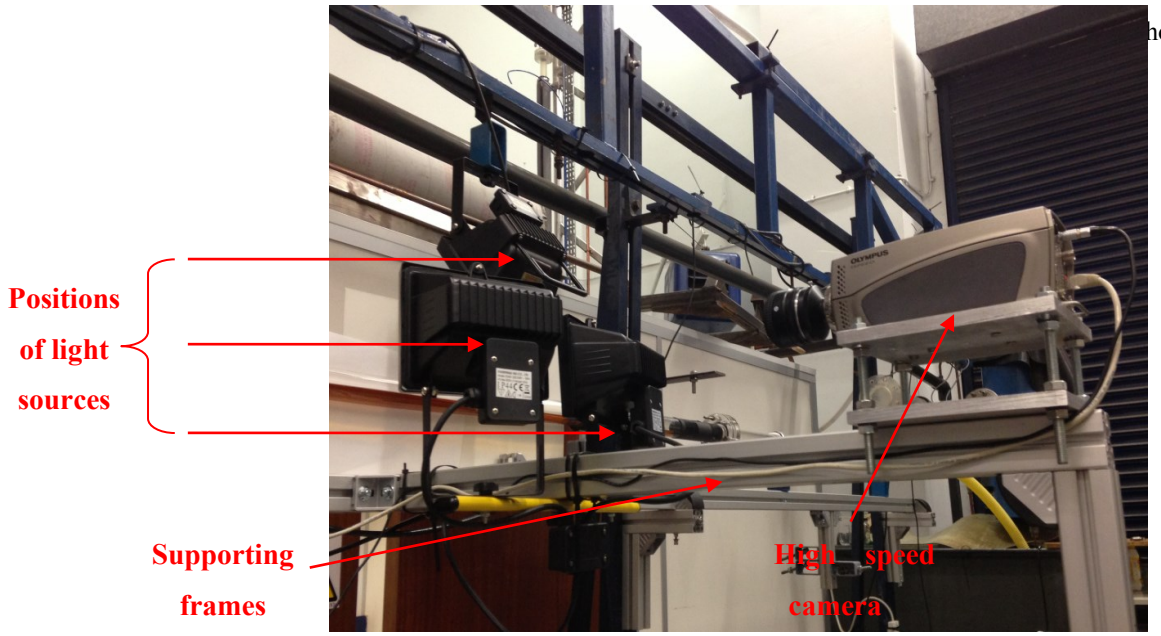

Figure 6.8: Photographs of camera and lighting set-up.

6.2.5 Conductivity probe measurement

Twin-wire conductance probes provide a convenient way of measuring the local liquid film height, provided that the liquid electrical conductivity is sufficiently high (Davies, 1992 and Manolis, 1995). The design of probes used in the LOWPRESS facilities is illustrated in Figure 6.9 and Figure 6.10. Each probe has two parallel 0.125mm 99.99% purity platinum wires, which are spaced 2mm apart and passing vertically from the top to the bottom of the pipe. In order to fix the wires in place the protruding ends were held between locking nuts on screws attached to saddles fitted to the external pipe wall. From these saddles the platinum wires connect to the conductivity measurement system. When two parallel, vertical, closely spaced thin wires are dipped into a conducting liquid the length of wire immersed can be inferred by measuring the resistance between the wires. This provides a nearly instantaneous measurement due to the speed of electricity transmission. The device is particularly suitable for air-water experiments because water is a good conductor and instantaneous measurement can be obtained for the fast moving slug.

The LOWPRESS facility has four pairs of conductivity probes inserted in the replacement acrylic pipe sections, as can be seen in Figure 6.11. Two of them were inserted in two separate short sections and each section is 0.25m long. The other two probes were inserted in

a 1m long pipe section; the distance between these two probes is 0.8m. During the present air-water experiments, one short section was inserted next to the inlet section; another section was inserted at a location where the probe was 2.5m from the entry. One of the test sections downstream was replaced by the long replacement section which contains a pair of probes. Hence two probes were located 6m and 6.8m from the entry.

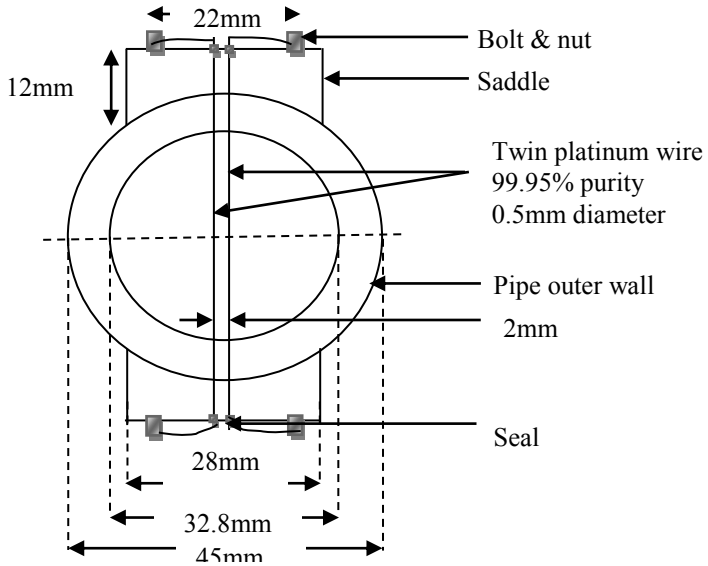

Figure 6.9: Schematic representation of the twin-wire conductivity probe as used on the LOWPRESS facility.

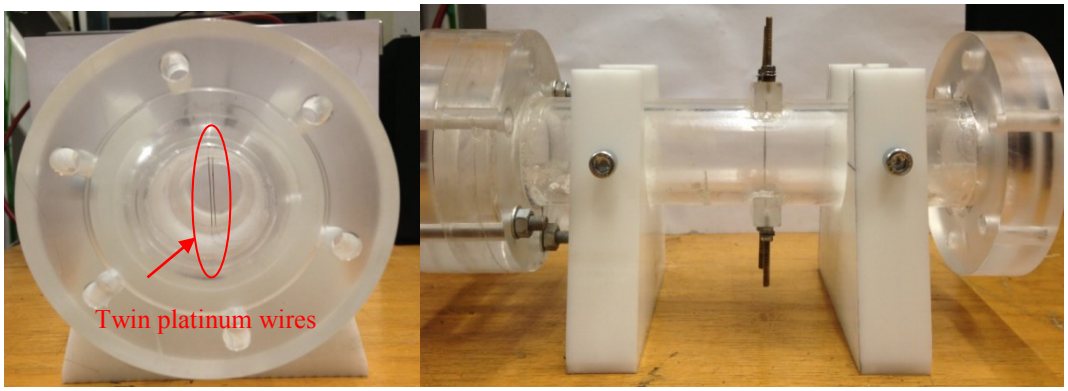

Figure 6.10: Photos of the twin-wire conductivity probe as used on the LOWPRESS facility.

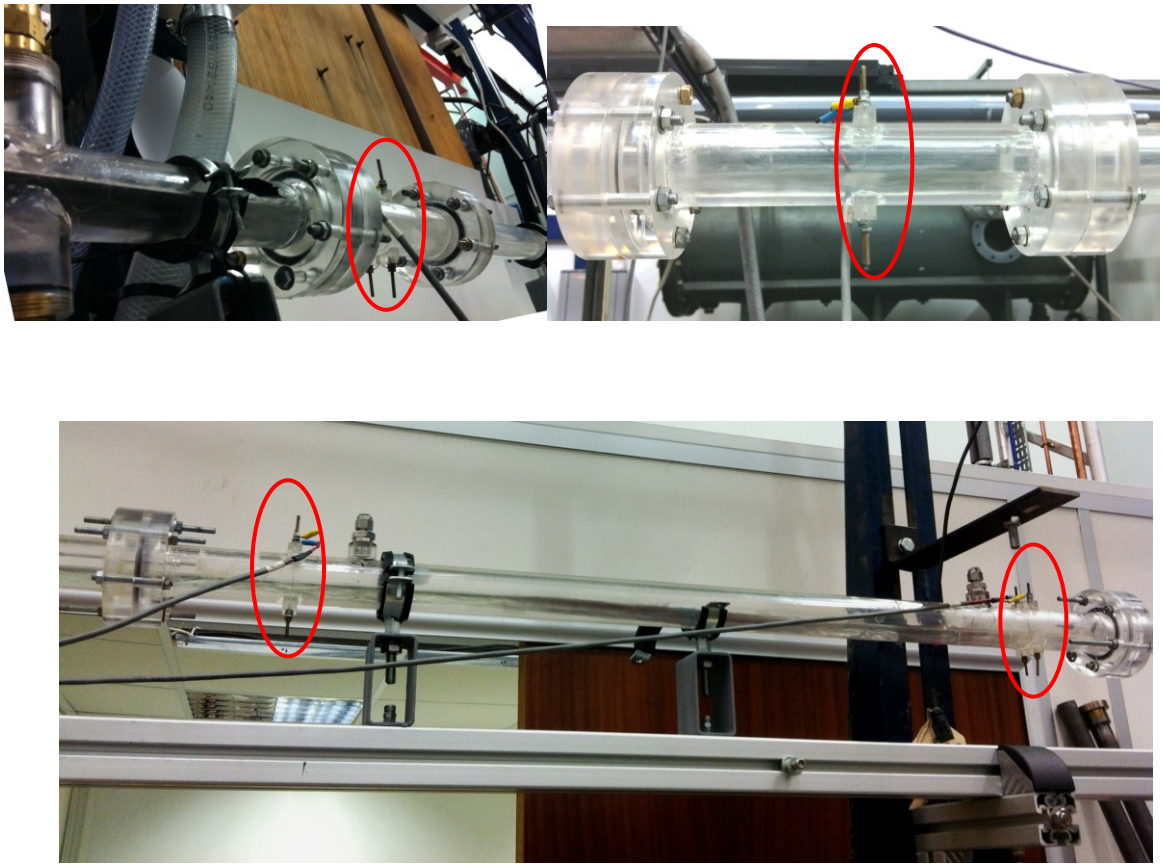

Figure 6.11: Four conductivity probes located at various locations along the LOWPRESS test-section.

The electronic circuit systems for the probe are in Figure 6.12 and Figure 6.13 (Mohammed, 2012). The clock generator (A) produces a square wave which is fed through a potentiometer to an amplifier (B) which in turn provides the driving signal for the probe. The clock generator is also fed to an adjustable pulse delay (C) which is used to drive the synchronous detector (E). One of the parallel wire probes is driven by the amplifier (B) and the other wire probe is the 'pick-up' which feeds an AC current, proportional to the conductivity of the fluid is now applied to the synchronous detector (E) to produce a steady DC voltage. Finally, a buffer amplifier provides signal level adjustment and drive for data acquisition system.

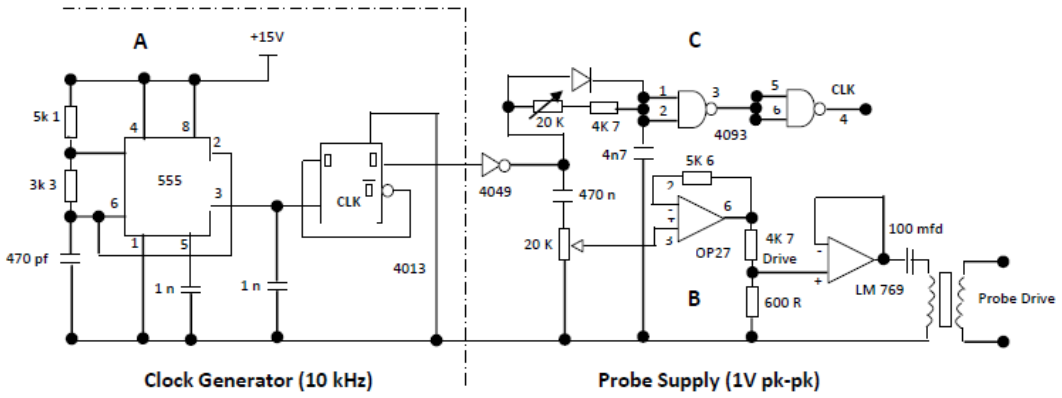

Figure 6.12: Conductivity probes electronic circuits (Part 1).

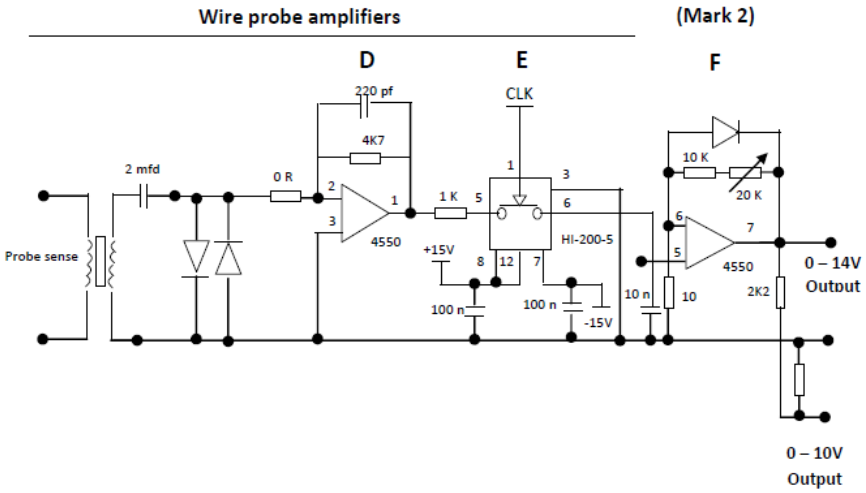

Figure 6.13: Conductivity probes electronic circuits (Part 2).

The output signals produced from conductivity probe electronic circuit is then feed into a rapid acquisition system. This system uses an Amplicon-Liveline PC30AT analogue to digital conversion card installed in the expansion slot of a PC. It enables rapid acquisition of signals from up to 16 channels. To control the A/D conversion and record the converted data, a program is written in LABVIEW, see Figure 6.14. On the user controlled interface, the range of output signal and the sampling frequency can be specified. A signal range of-10V to10V was set to correspond with the output from the conductivity probes. A sampling frequency of 500Hz is generally chosen for the experiments as a compromise between the necessity for high sampling rates and the ease of handling large data files. Each experimental run was

sampled for 300 seconds. A real-time display of conductivity signals can be monitored at the meantime as shown in Figure 6.15.

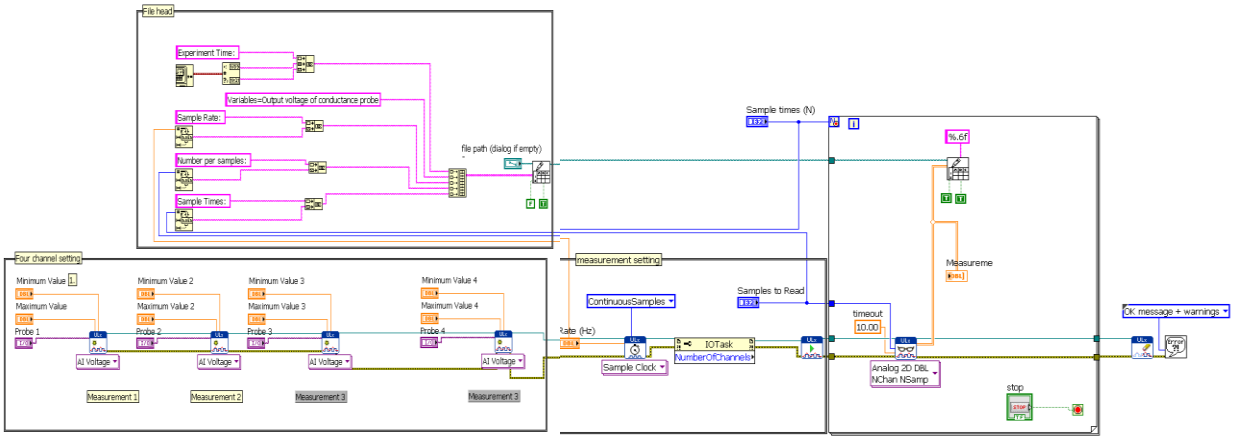

Figure 6.14: LABVIEW program of data acquisition.

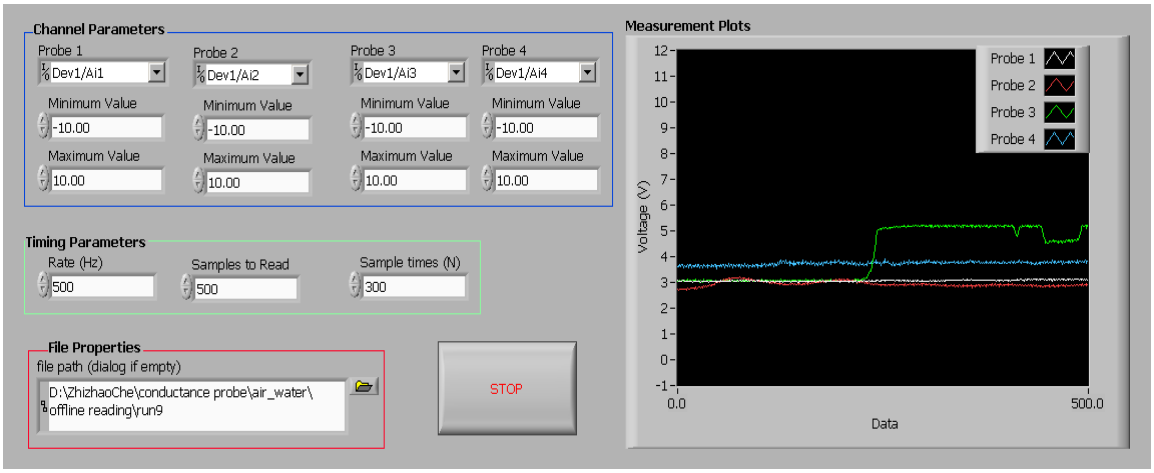

Figure 6.15: LABVIEW user input interface and display of real-time conductivity signals.

The twin wire conductance probes need to be calibrated offline with the water used in LOWPRESS facility, so the voltage reading can be correlated to the liquid height. Each probe was therefore calibrated offline. Each calibration was performed by taking a reading for a dry pipe first. One end of the replacement section was blanked off with a blind flange, a known volume of water was introduced into the section and then another end of the pipe section will be sealed as well and moved to a supporter to ensure the pipe section is orientated horizontally as shown in Figure 6.10. A conductivity reading was taken after a sufficient

settling time. These procedures were repeated until the pipe was full of liquid. Because the liquid was evenly distributed in the horizontal pipe, therefore for a known volume of liquid, both the equivalent cross-sectional area and liquid height can be calculated. Correlation of liquid height against voltage signals were plotted for four probes in Figure 6.16, the error bars were assumed to be +/- 1.5 mm. It was also noticed although the construction of each probe was exactly the same, the settings on the gains and drives of the output signals were slightly different, and as a result the correlations of voltage signal to liquid height were slightly different for four probes. Therefore it reasonable to assume a linear relationship for conversion of voltage signals to liquid height for each probe.

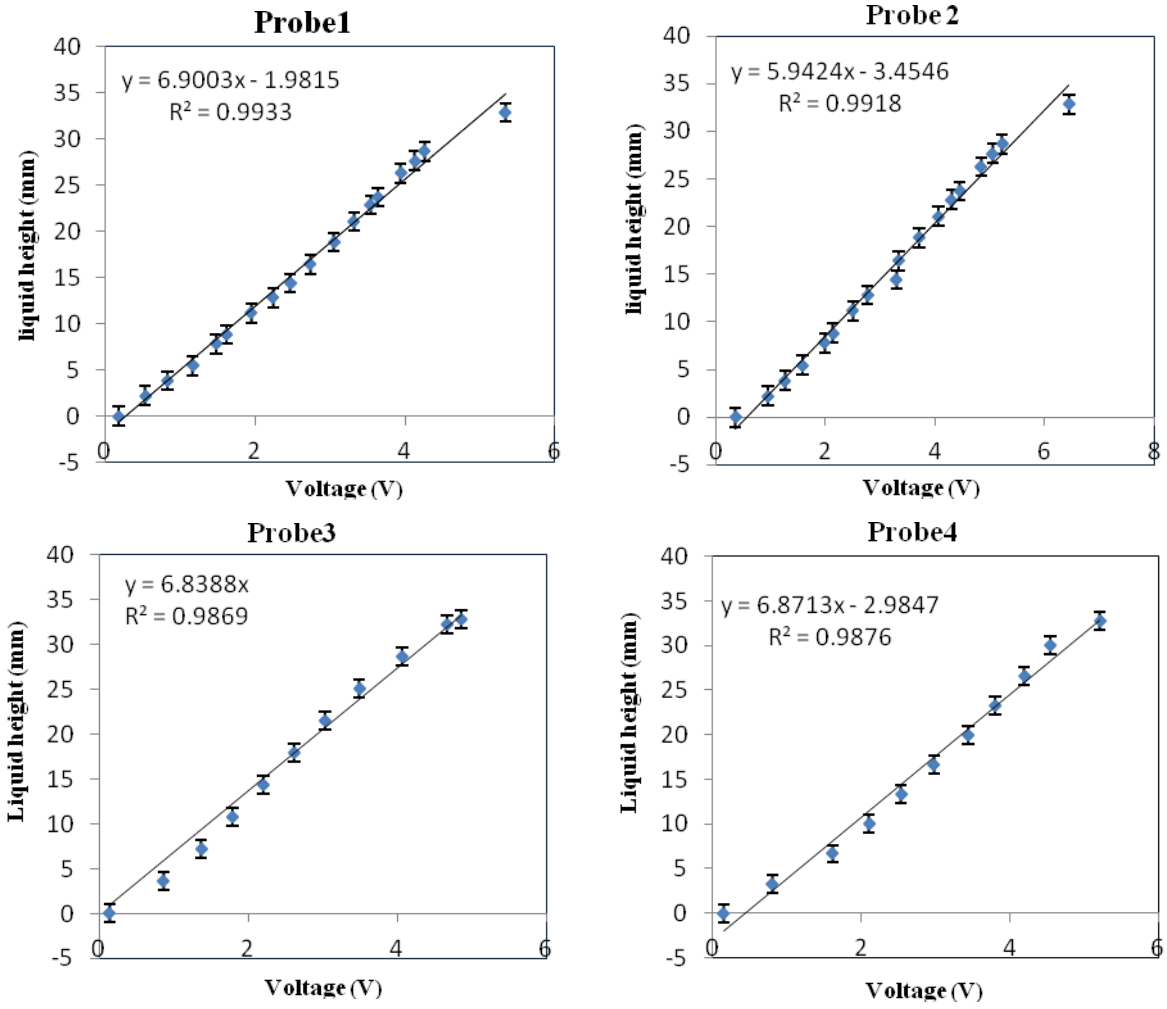

Figure 6.16: LOWPRESS conductivity probes calibration curves.

6.2.6 Slug flow experimental procedures

Three sets of experiments were conducted with different inlet configurations. One set is air-oil slug flow with stratification plate inserted at three different heights (low-plate, mid-plate and high-plate), another set is air-oil slug flow with conical inlet, and the last set is air-water slug flow with stratification plate inserted at middle of the pipe (mid-plate). Prior to each set of experiments, the test line level was adjusted as necessary to ensure it was orientated horizontally. This can be achieved by changing the distance of the ring supports from the steel framework. Once the test line was leveled, the experiment can be started. Initially air was introduced into the test-line before the liquid. Doing this could prevent the liquid from flooding the test section as would be the case if the liquid is introduced first. The mass flow controller provides an automatic control of the air velocity according to the set value. The liquid velocity needs to be kept as steady as possible by adjusting the control valve. For air-oil system, after the flow become steady, turn on the lighting systems and set up the high speed cameras. Once the recording was done, images were viewed on the I-SPEED software suite and if satisfactory, the recording was downloaded on to the computer. For air-water system, after the flow become steady, start to record the conductivity probe signals via LABVIEW user interface, in the meantime, the real-time display of the signals can be viewing from the screen.

6.2.7 Measurement error

The instrumentation measurement errors on the Low Pressure Rig (LPR) are summarized in Table 6.2.

Table 6.2: Measurement errors on the LOWPRESS rig (FS = full scale).

Measured parameter	Measurement error	Instrument
Superficial gas velocity, U_{SG}	± 0.1 %	Bronkhorst mass flow controller
Superficial liquid velocity, U_{SL}	± 0.5 %	2000 KDG MOBREY rotameter
Liquid holdup(water), ε_L	±3 % FS (1mm in measured liquid height)	Conductivity probes

Chapter 7

Slug initiation and development in horizontal pipes: results and discussions

7.1 Summary

This chapter describes a set of horizontal air-oil and air-water slug flow experiments performed on the LOWPRESS rig by the present author. The facilities and the physical bases for the LOWPRESS experiments are described in Chapter 6; the tube used was 32 mm internal diameter. All the experiments were performed with atmospheric pressure at the end of the tube and ambient temperature. The Chapter also presents previously unpublished data on horizontal slug flow obtained by Dr. Colin Hale (Imperial College) on the Imperial College WASP facility which has a 78 mm internal diameter tube; the WASP experiments were also performed at atmospheric outlet pressure. In the LOWPRESS experiments, data were obtained for both air-oil and air-water flows; the WASP data were for air-water flows. The objectives of the experiments were to improve the understanding of the slug initiation and development phenomena.

In what follows, Section 7.2 describes the LOWPRESS experiments and Section 7.3 gives a brief description of WASP facility (used by Dr. Colin Hale in obtaining the data for the 78 mm diameter tube). Section 7.4 illustrates the regions of occurrence of present slug flow data in the horizontal flow regime transition maps of Weisman et al. (1979) and Taitel & Dukler

(1976). The major mechanisms of air-oil slug initiation observed at different superficial gas and liquid flow-rates with two type of inlet arrangement are illustrated in Section 7.5. Section 7.6 discusses the development of air-oil and air-water slug flow in the LOWPRESS test-section. Section 7.7 analyses the influence of varying the inlet arrangement on slug initiation and development. It was observed that the developed slug flow exhibits a very weak dependence on the inlet geometry for the range of system parameters investigated. Section 7.8 is focused on the slug frequency in the developed region and presents a comparison between the measurements and the predictions of empirical correlations. The influence of inlet boundary condition on the prediction of slug flow using the one-dimensional two fluid model code TRIOMPH is discussed in Section 7.9, and a comparison is made between the WASP measurement data and TRIOMPH predictions.

7.2 Experiments on the LOWPRESS facility

In previous experiments on slug flow development on Imperial College WASP facility, Ujang (2003) used a series of conductance probes to track the slugs along a pipe, the experiments were for air-water only as the use of conductance probes is not feasible for air-oil flows. Ujang (2003) made distinction of slugs from waves by measuring the velocity of the slugs and waves; the slugs had a much higher velocity. Measurement of the velocity was difficult, especially close to the inlet at the first few upstream probes, the very short developing slugs were often preceded by a wave which was of the same height, so it was decided to manually record the arrival and exit times of each wave and slug, which is very time consuming.

In order to improve the understanding of slug initiation and development mechanisms, a set of experiments were conducted on the LOWPRESS facility involving air-oil flows at atmospheric pressure using high speed photography. The air-oil flow characteristics were obtained by analyzing high-speed video pictures of the flow at various locations along the channel, each video clip was recorded for a length of 150s. Two high-speed cameras were employed to capture the images at 60 frames per second, with exposure of 1500 ms. Compare to the earlier experiments, the use of high speed video recordings offered another advantage; thus, slugs could be distinguished visually from large waves on the stratified layer. The influence of inlet geometry on the slug flow characteristics was investigated. Two types of inlet arrangements were tested on the LOWPRESS rig:

(1) In the first type of injector, the gas and liquid phases were injected at the top and bottom of the pipe respectively, the two streams being separated initially by a flat plate mounted horizontally at a fixed distance from the bottom of the tube. Three positions of the separator plate were used. At the end of the plate the two streams came into contact; and were both travelling in the axial direction. The stratification plate was placed at one of three positions namely at 0.25. 0.5 and 0.75 tube diameters from the bottom of the tube.

(2) In the second type of injector, the gas and liquid phases were injected respectively at the top and bottom of a 3 inch pipe section, the two fluids develop as a mixture and then enter the 32 mm ID tube via a conical reducer section.

In addition, for the purpose of comparison, a set of air-water experiments were conducted using first type of injector, with stratification plate placed at the centre of the tube. Slugs were tracked by four conductivity probes operating in series at 500Hz. Table 7.1 and 7.2 summaries the experiments performed on the LOWPRESS facility.

Table 7.1: Experimental conditions and equipments used to study horizontal two-phase slug flows with first type of injector on the LOWPRESS facility.

System	Pressure (bar)	U_{sl} (m/s)	U_{sg} (m/s)	Inlet stratification plate height h_L/D
Air-Oil	1	0.1- 0.2	1.0-8.5	0.25, 0.5, 0.75
Air-Water	1	0.1-0.3	1.0-8.5	0.5

System	Equipment	Sampling sections (distance from inlet, m)	Sampling frequency
Air-Oil	OLYMPUS I-SPEED 3 camera (monochromatic)	0.6,2.5,6.5	60 fps
Air-Oil	OLYMPUS I-SPEED 2 camera (color)	1.3,4.5	60 fps
Air-Water	Conductance probe	0.5, 2.5, 6, 6.8	500 Hz

Table 7.2: Experimental conditions and equipments used to study horizontal two-phase slug flows with second type of injector (conical reducer) on the LOWPRESS facility.

System	Pressure (bar)	U_{sl} (m/s)	U_{sg} (m/s)
Air-Oil	1	0.1- 0.2	1.0-8.5

System	Equipment	Sampling sections (distance from inlet, m)	Sampling frequency
Air-Oil	OLYMPUS I-SPEED 3 camera (monochromatic)	0.4, 3.5	60 fps
Air-Oil	OLYMPUS I-SPEED 2 camera (color)	1.3, 6.5	60 fps

7.3 A brief introduction to the WASP experiments

This thesis presents (for the first time), new data on air-water slug flow obtained in the Imperial College WASP facility. This data was obtained (though not analyzed) by Dr. Colin Hale (of Imperial College) whose contribution is gratefully acknowledged. The WASP facility has a 37 m long, 78 mm internal diameter tubular stainless steel section that can be used in horizontal or slightly inclined (+2 degree to -2 degree) orientations, it allows investigation of flow of up to four phases at different inclinations with a wide range of flow rates. The operation of the WASP facility is based on the 'blow-down' mode in which air from high pressure supply tanks flows through the test section and is released into the atmosphere. A schematic diagram of the facility is presented in Figure 7.1. Liquid feed is passed to the section by pressurizing the liquid tanks with high pressure air or by pumping. Air feed to the test section can also be obtained either from high speed pressure tanks or from the low-pressure departmental supply. At the exit of the test section, the "slug catcher" acts as a primary separator of the gas and liquid phases. The air is discharged through a silencer while the liquid phases are returned to the dump tank where they are separated under the gravity. In the experiments for which the results are presented here, the liquid phase used was water.

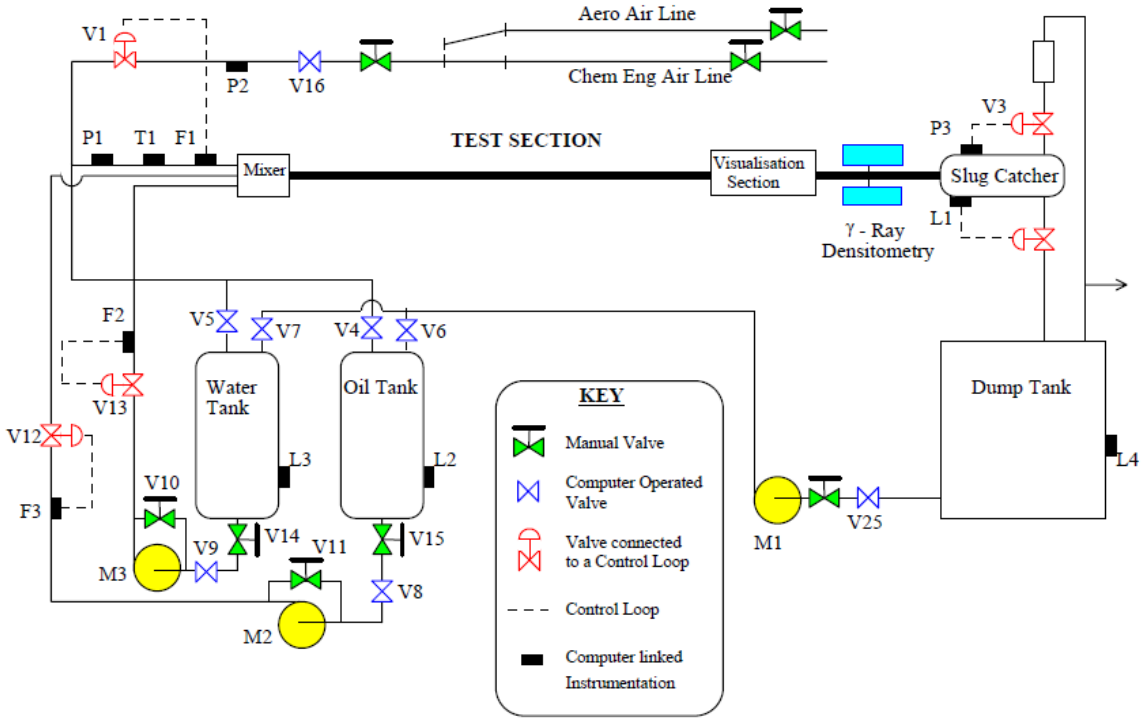

Figure 7.1: Schematic diagram of the WASP facility.

Air and liquid (water for the results presented here) are fed into the test section through a short length of inlet section which connects smoothly into the main test section (see Figure 7.2). The inlet streams of air and water are separated at the inlet using a flat stratification plate (the gas flowing between plate and the upper surface of the test section and the water between the plate and the lower surface of the test section). By this means co-current stratified layers of the phases are established before they come into contact (see Figure 7.3). In the past, most of the gas-liquid two-phase experiments conducted on WASP facility had the stratification plate mounted at the centre line. In order to study the effect of altering the stratification plate level on the development of slug flow, a replacement inlet flange was manufactured which a 2 mm thick stratification plate had welded into a position 18 mm from the centre line of the tube. When the plate was in the lower position, the height of the liquid layer at inlet was 20 mm. By rotating the inlet flange 180 degree, liquid can be introduced into the test section with an initial liquid height of 56 mm (see Figure 7.4).

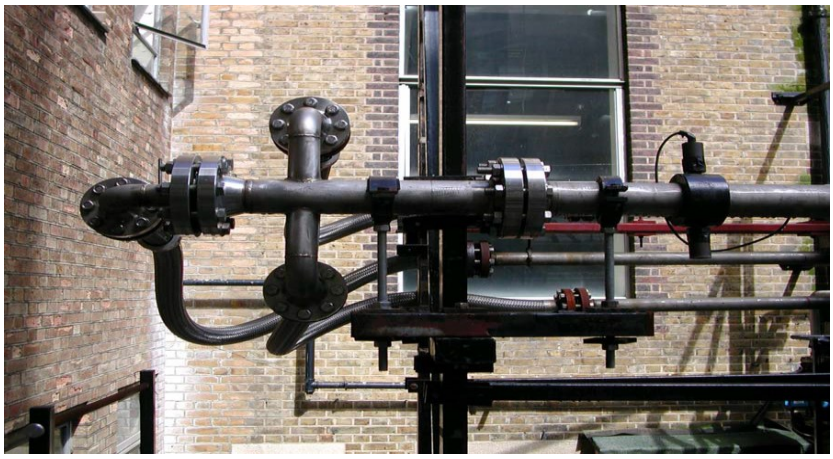

Figure 7.2: The inlet section to WASP facility test section.

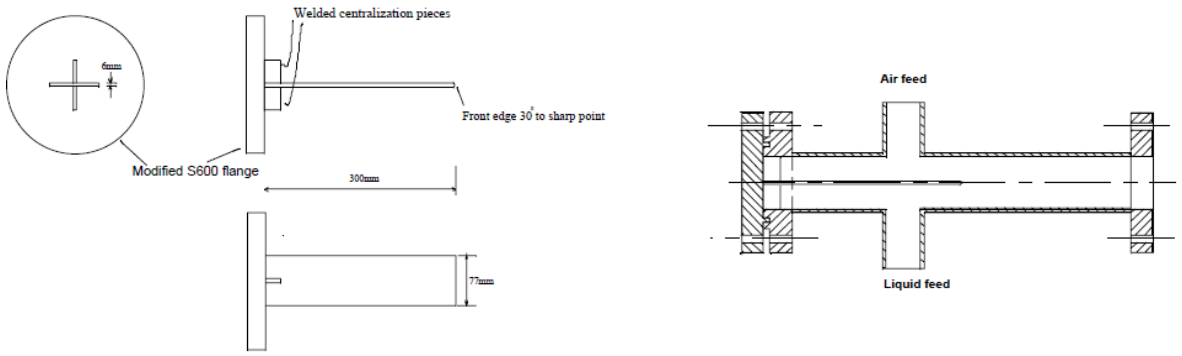

Figure 7.3: The inlet section for a two-phase gas-liquid flow with stratification plate incorporated at center line (Hale, 2000).

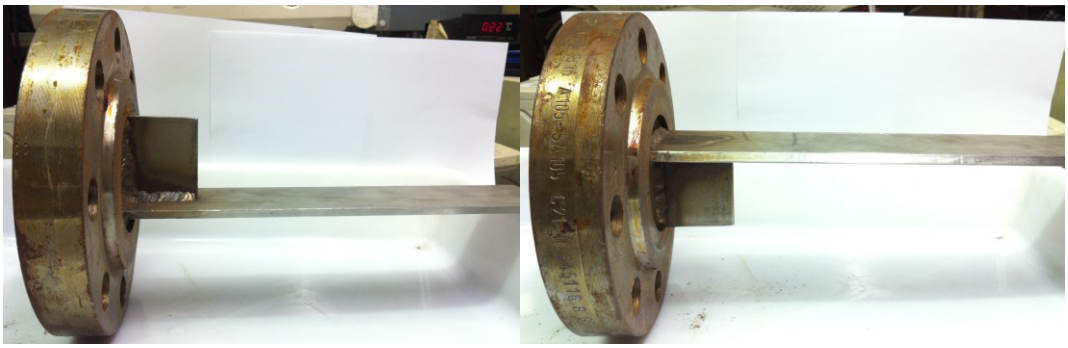

Figure 7.4: The inlet blanking flange with wielded low-plate and high plate configuration.

In the WASP experiments, slug frequencies could be determined from both video photography and from the output of a gamma ray densitometer. Videos of slug flow were obtained through the visualisation section. This section consists of a 0.8 m long polycarbonate tube. Images are recorded by using a Panasonic MV-10VHS video camera recording at 24fps and then fed to a television monitor and a video recorder. For each experimental run, a video sampling time of 300s was used and the number of slugs that passed along the visualization section within the sampling time was counted. Hence the slug frequency can be analysed.

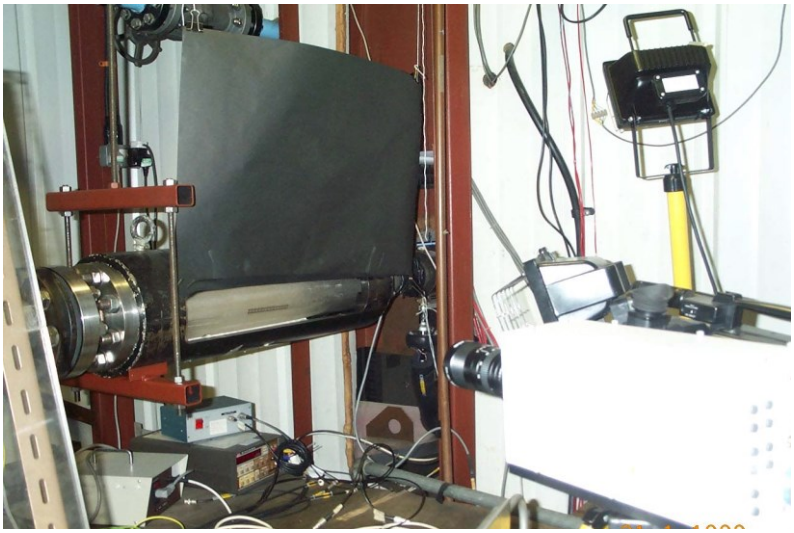

Figure 7.5: WASP facility visualisation section.

The variation of liquid holdup with time was measured using a dual energy traversing gamma densitometer developed by Pan (1996), see Figure 7.6.

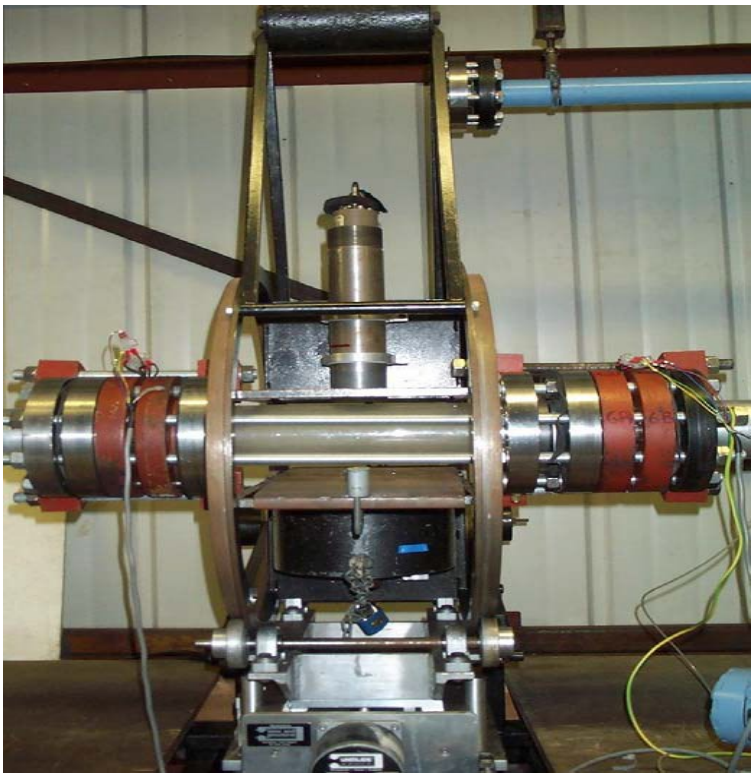

Figure 7.6: The traversing dual-energy gamma densitometer.

For the two-phase flows studied in the experiments, the energy used is 81keV from the two energies (31 keV and 81 keV) available from the barium source and the attenuation law for a mono-energy gamma beam passing through an absorbing medium:

$$I = I_0 \exp(-\mu\rho x) = I_0 \exp(-\gamma x) \qquad [7.1]$$

I_0 is the initial intensity of the gamma beam, I is the transmitted intensity of the gamma beam, μ is the mass absorption medium and ρ is the density of the absorbing medium, γ is the linear absorption coefficient and x is the thickness of the absorbing medium traversed. Eqn.7.1 can be also written as:

$$x = \frac{1}{\gamma} \ln\left(\frac{I_0}{I}\right) \qquad [7.2]$$

If the incident intensity I_0 and the transmitted intensity I are known, the medium thickness x can be determined by Eqn. 7.2.

In the experiments described here, the beam was fixed to pass through the centre line and the chordal phase fractions are then given as:

$$\varepsilon_L = \frac{\ln I - \ln I_G}{\ln I_L - \ln I_G} \qquad [7.3]$$

$$\varepsilon_G = 1 - \varepsilon_L \qquad [7.4]$$

where ε_L and ε_G are the local chordal phase fractions of the liquid phase and gas phase respectively. I_L and I_G are obtained by calibration tests where the test-section is completely filled with liquid or gas phase.

At a given chordal location the gamma photon count is measured during the specified counting time. As a result, the count rate I can be calculated as the ratio of the counts over the sampling time. Combining this value with the values of I_L and I_G which are obtained by

calibration tests, the chordal phase fraction can be estimated using Eqn. 7.3 and 7.4. The error in the measurement of the liquid holdup is approximately ±5% of full scale. This error arises because of the random nature of photon emission from the source. The measurements obtained by both gamma densitometer and high speed videos were analysed in present study and results will be discussed in the following sections. Table 7.3 summaries the experiments performed on the WASP facilities.

Table 7.3: Experimental conditions and equipment used to study horizontal air-water slug flows on the WASP facility.

	Air	Water
Density (kg/m^3)	1.18	998.3 (20°C)
Viscosity(Pa s)	0.0000183(20° C)	0.0009787(20°C)
Surface tension(N/m)	--	0.037 (20°C)

System	Pressure (bar)	U_{sl} (m/s)	U_{sg} (m/s)	Inlet separating plate height h_I/D
Air-water	1	0.2-0.6	2.0-8.0	0.25, 0.75

Equipment	Visualization sections (distance from inlet, m)	Sampling frequency
PANASONIC MV-10VHS camera	36	24fps
Gamma densitometer	35	25Hz

7.4 Regions of occurrence of slug flow

All the data points examined in present study are compared to the flow regime maps of Weisman et al. (1979) and Taitel & Dukler (1976) for horizontal flows. For the air-oil flow experiments performed on the LOWPRESS facility, the identification of flow regime was achieved by examination of high speed video records. The observed regime for these air-oil experiments was usually slug flow. However, for certain cases with low liquid velocity and high gas velocity, the flow characteristics were observed to oscillate between the slug flow

and annular flow regimes, indicating that the flow condition lay on the transition boundary. The flow pattern map of Weisman et al. (1979) shown in Figure 7.7, fails to predict the correct trends. The transition map of Taitel &Dukler (1976) as displayed in Figure 7.8 more successfully captures the data.

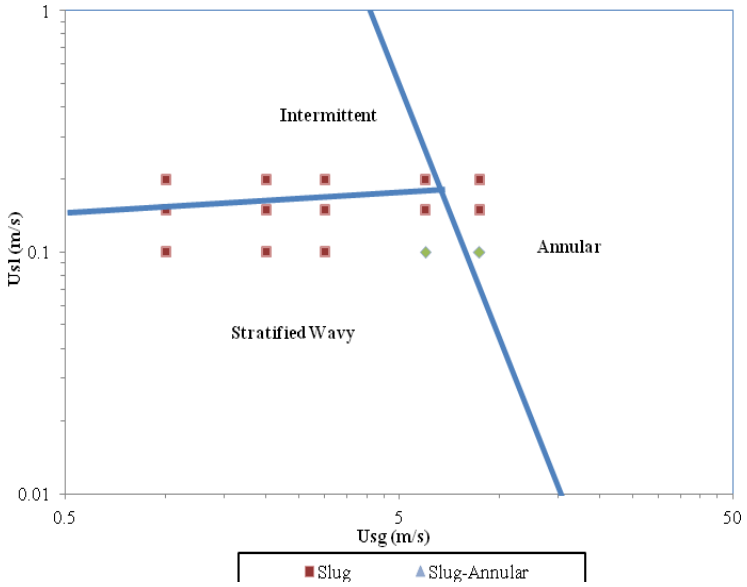

Figure 7.7: Comparison of the Weisman et al. (1979) transition map to LOWPRESS air-oil data.

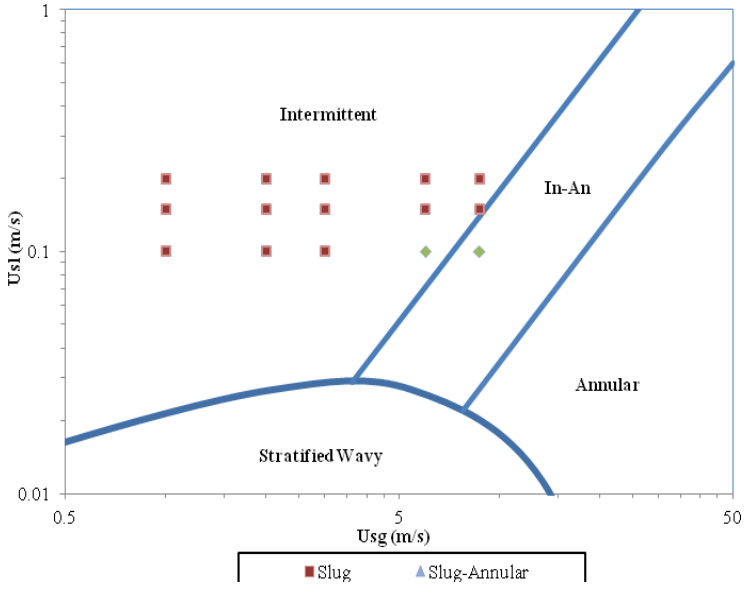

Figure 7.8: Comparison of the Taitel & Dukler (1976) transition map to LOWPRESS air-oil data.

For the air-water system, the stratified smooth, stratified wavy, slug and slug/annular transition flows were observed. The identification of flow regimes was obtained by examining the holdup time trace signals from conductivity probes with confirmation made by visual observations. Figure 7.9 show signals for a constant liquid velocity of 0.1m/s and with increasing gas velocity. With low gas velocity, the flow regime is smooth stratified flow. Increasing the gas velocity, slug flow is observed and further increase the gas velocity, the flow regime becomes stratified wavy flow. The flow pattern maps of Taitel & Dukler (1976) and Weisman et al. (1979) as seen in Figure 7.10 and Figure 7.11 capture the basic trends; however both of them predict the stratified-slug transition occurs at slightly higher superficial liquid velocities than those observed for the experimental air-water data.

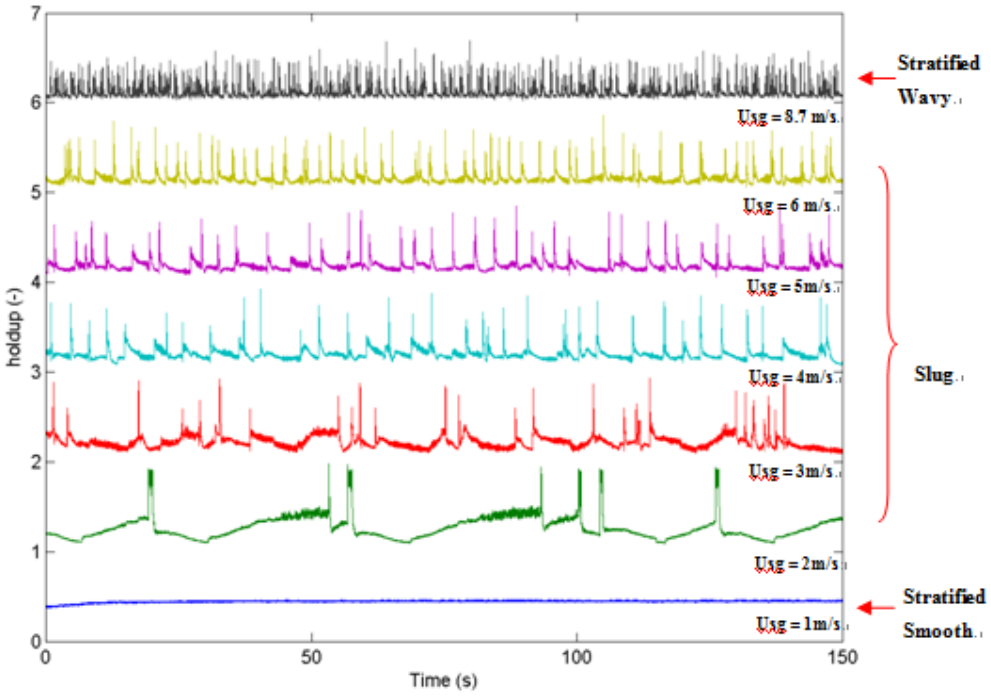

Figure 7.9: Flow regime identification based on the plots of liquid holdup time traces. Usl = 0.1m/s and Usg=1-8.7m/s.

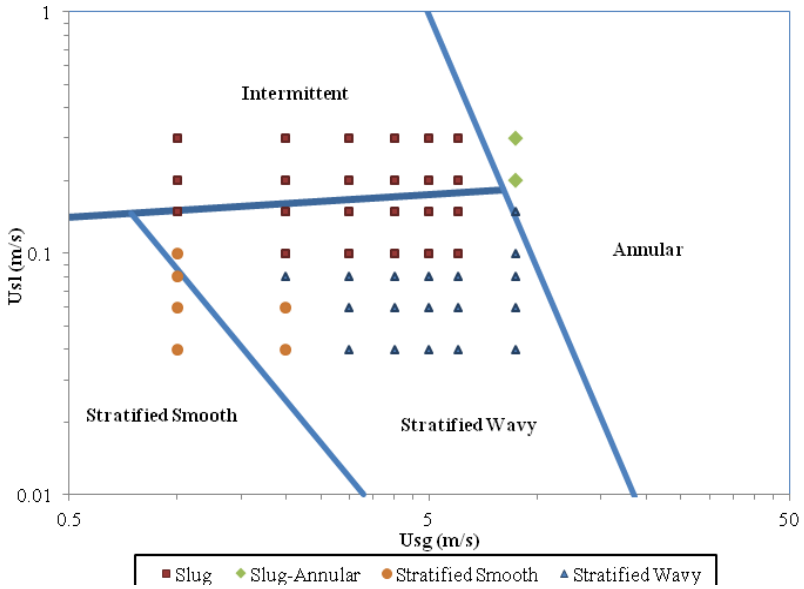

Figure 7.10: Comparison of the Weisman et al. (1979) transition map to LOWPRESS air-water data.

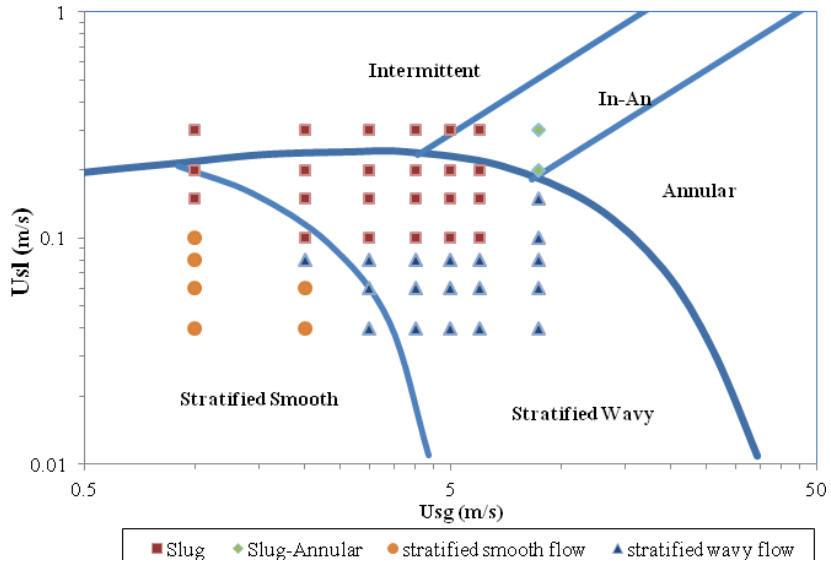

Figure 7.11: Comparison of the Taitel & Dukler (1976) transition map to LOWPRESS air-water data.

For the experiments performed on the WASP facility the regime observed was mainly slug flow. The flow pattern map of Weisman et al. (1979) as seen in Figure 7.12 predicts that the slug-annular transition occurs at lower superficial gas velocities than those observed for the experimental data.The flow pattern maps of Taitel & Dukler (1976) captures the basic trend but slightly over predicts the slug/stratified and slug/annular transition boundaries for the WASP data.

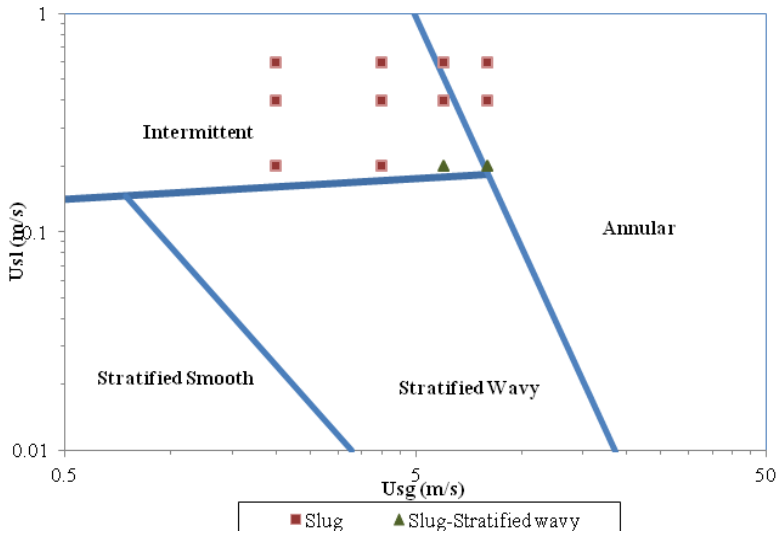

Figure 7.12: Comparison of the Weisman et al. (1979) transition map to WASP air-water data.

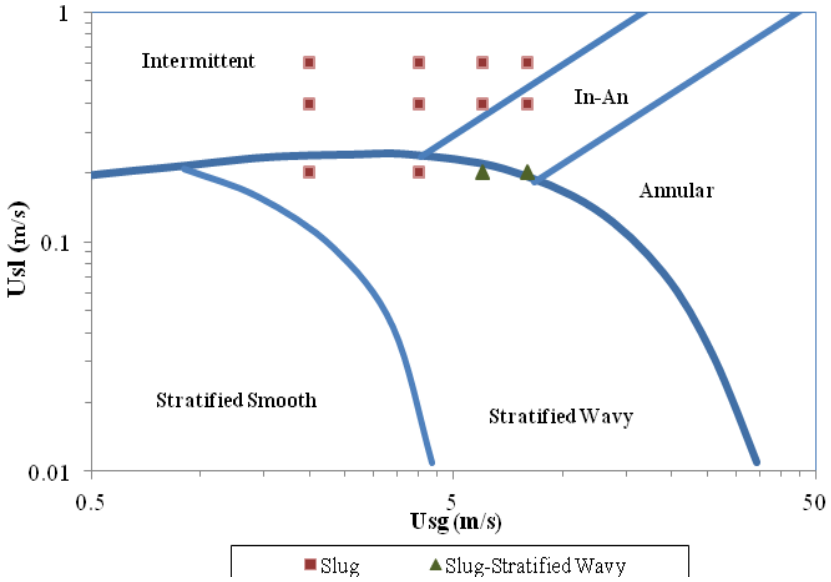

Figure 7.13: Comparison of the Taitel & Dukler (1976) transition map to WASP air-water data.

Overall, the Taitel & Dukler (1976) map is more successful in capturing the present experimental data. Though this map predicts the stratified wavy-slug flow transition for air-oil flow satisfactorily, it over predicts the transition for the air-water data obtained on both LOWPRESS and WASP. The discrepancy was also consistent with previous finding by Manolis (1995) and Pan (2010). Manolis (1995) suggested this discrepancy may be explained by the choice of friction factors used in the model.

7.5 Slug initiation

This section presents the results of slug initiation experiments obtained via direct observation of the air-oil two phase flows in the LOWPRESS facility using high-speed cameras. The aim is to use these results to elucidate the mechanisms underlying slug initiation. The effect of varying the gas and liquid flow-rates on the interfacial pattern will be described. Investigation of the entrance effects on slug initiation by altering the configuration of the inlet arrangement through which the fluids are introduced into the test-section will also be discussed.

7.5.1 Slug initiation mechanisms with a stratification plate at the inlet

This section summarises the slug initiation mechanisms observed in the series of experiments carried out with an inlet containing a stratification plate. Attempts are made to relate these observations to slug initiation mechanisms and characteristics proposed in the literature.

7.5.1.1 Effects of varying the liquid flow-rate at a constant gas flow-rate

This section will discuss the slug initiation mechanisms observed in a series of tests on the LOWPRESS facility; for these tests, the superficial gas flow velocity was maintained constant at 2 m/s and the liquid (oil) flow rate was increased in successive tests. The images illustrated in this section were obtained for the runs with an inlet stratification plate inserted in the middle of the pipe.

Images obtained in the first test (for a gas superficial velocity of 2m/s and a liquid superficial velocity of 0.1m/s) are shown in Figure 7.14. The gas-liquid interface is initially slightly wavy which is typical of the stratified-wavy regime (as shown in the first picture in Figure 7.14), but an instability grows on the smooth gas-liquid interface. When the aerodynamic lift forces outweigh the stabilising effects of gravity and surface tension, this wave lifts to approach the top of the pipe, forming a slug precursor. As the slug blocks the pipe, there is a build-up of pressure behind the slug, causing the gas to accelerate the slug in the axial direction. The slug length increases as more liquid is scooped up at the slug front than is shed from its tail. Behind the slug, the liquid level drops.

Time=0 s	
Time= $\frac{1}{30}$ s	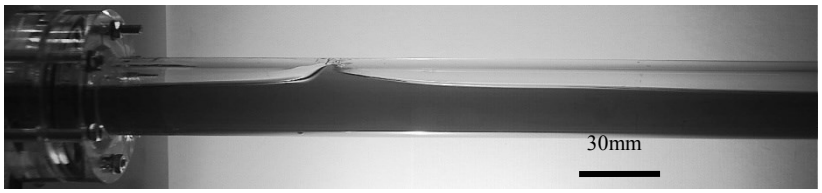
Time= $\frac{2}{30}$ s	
Time= $\frac{3}{30}$ s	

Figure 7.14: A series of images showing slug initiation at Usl=0.1m/s, Usg=2.0m/s.

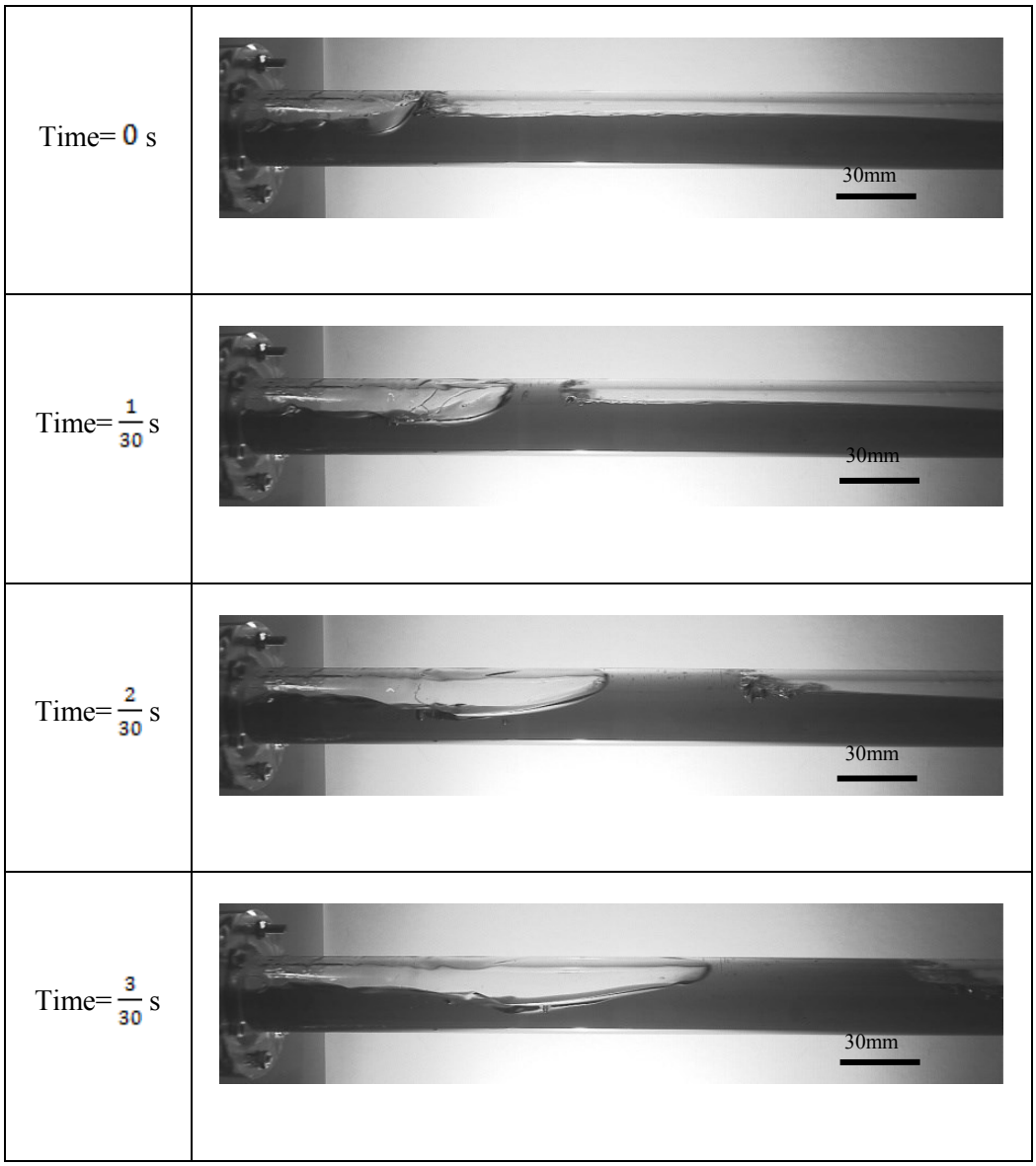

Figure 7.15: A series of images showing slug initiation at Usl=0.15m/s, Usg=2.0m/s.

With increasing liquid flow-rate, slug initiation occurs closer to the inlet, as shown in Figure 7.15 which was generated for a superficial liquid velocity of 0.15 m/s. As the liquid flow-rate is increased further to 0.2m/s, the gas-liquid interface is markedly wavier than that associated with lower liquid flow-rates (Figure 7.16), wave coalescence phenomena can be observed at higher flow-rates: a large wave catches up with a smaller one downstream and coalesces with it forming a slug that bridges the pipe. This coalescence event also leads to the entrapment of a gas pocket, which is transported downstream by the slug. Following the passage of the slug, the dip in the liquid level behind the slug is replenished and further slug initiation occurs as shown in Figure 7.16.

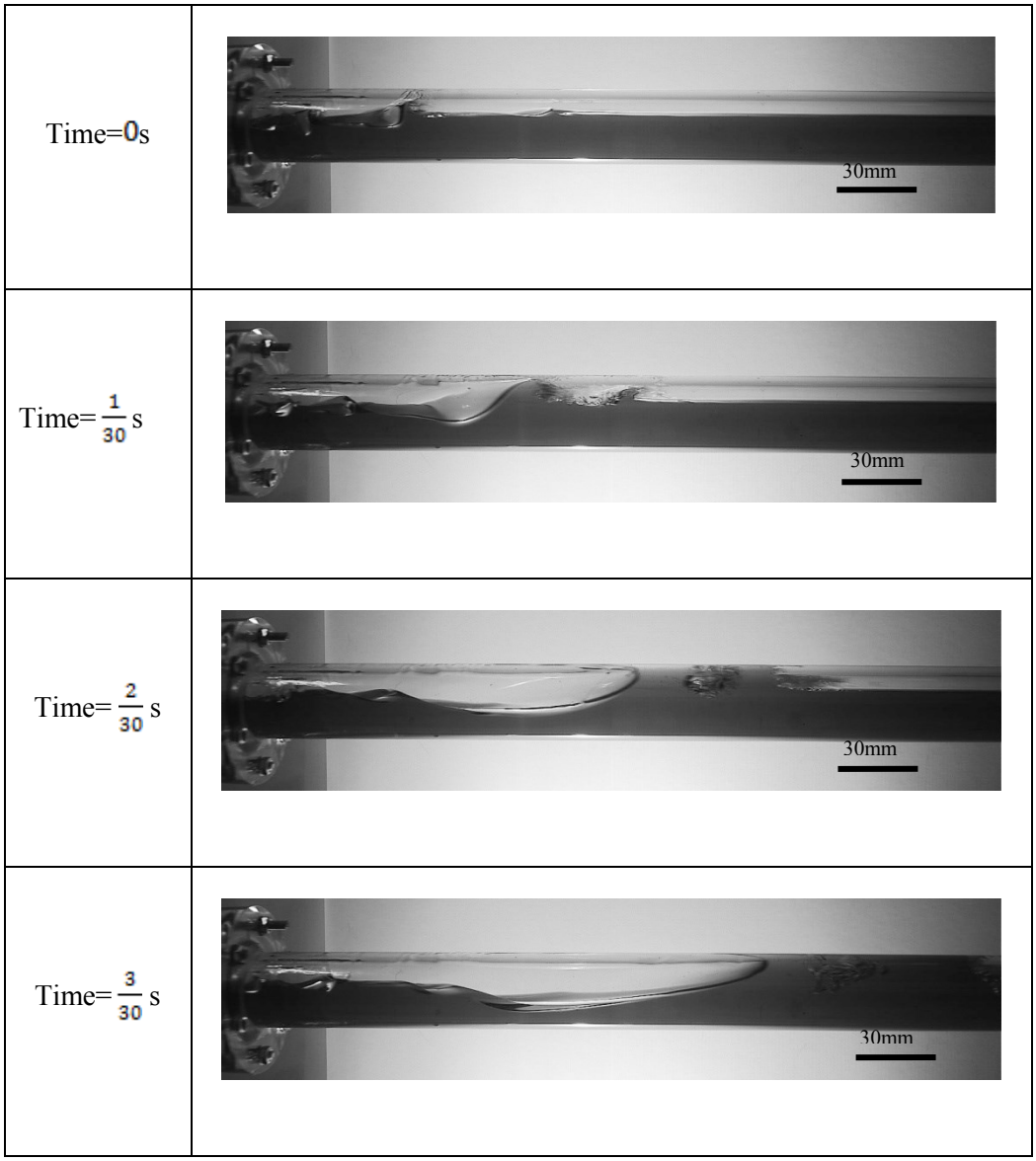

Figure 7.16: A series of images showing slug initiation at Usl=0.2m/s, Usg=2.0m/s.

Figure 7.17 illustrates how a wave is formed on the sloping interface behind the slug. The wave initially grows as it advances but then passes over a film with a height below the level necessary for wave to grow and so begins to dissipate. Figure 7.18 illustrates the case where a slug has passed and the wave behind this slug is advancing on the rebuilding liquid layer and quickly bridges the pipe, forming another slug. This case is in line with the work of Davies (1992) who reports cases in which waves grow on the rebuilding liquid layer and form "pseudo slugs" before the equilibrium level is reached.

Time= 0 s	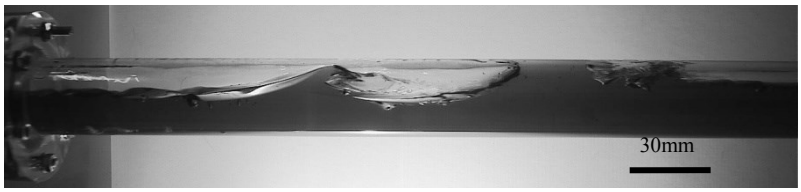
Time= $\frac{1}{30}$ s	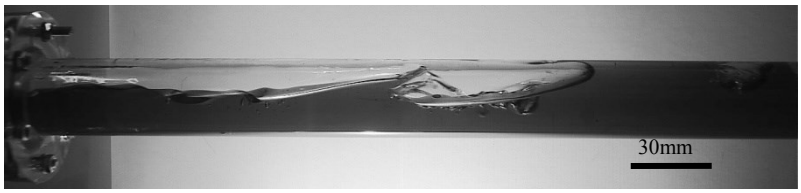
Time= $\frac{2}{30}$ s	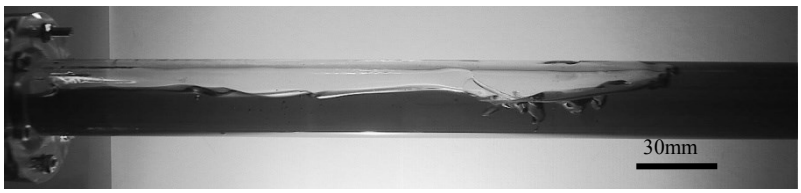
Time= $\frac{3}{30}$ s	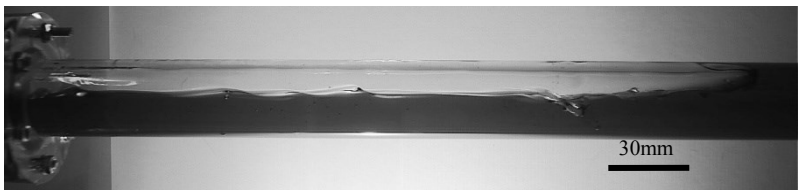

Figure 7.17: A series of images showing slug initiation at Usl=0.2m/s, Usg=2.0m/s.

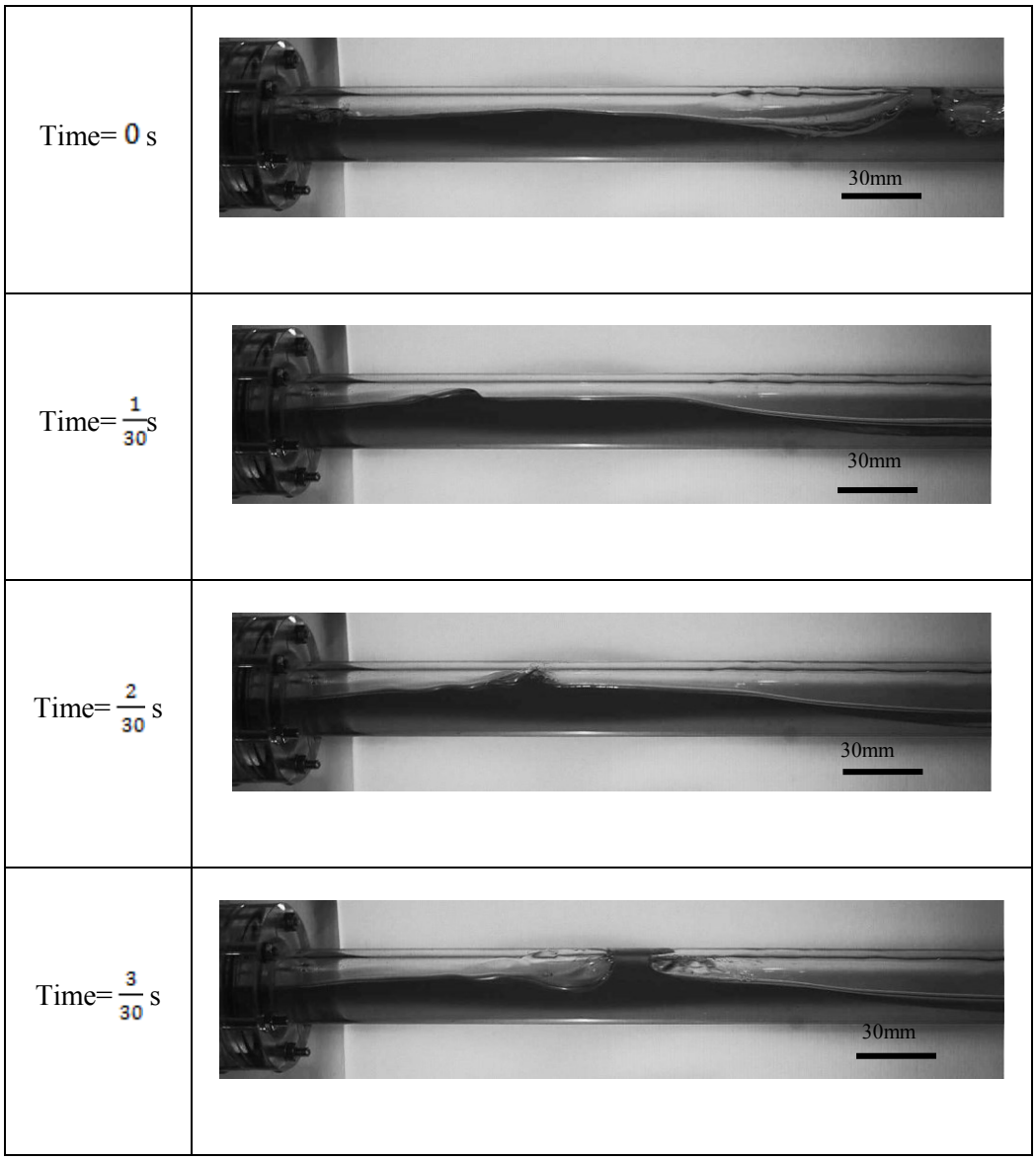

Figure 7.18: A series of images showing slug initiation at Usl=0.2m/s, Usg=2.0m/s.

In certain cases, the developing waves are large enough to reach the top of the pipe; however they collapse before the bridging event occurs. In Figure 7.19, we illustrate such case wherein a large-amplitude wave topples over to form a roll wave before bridging the pipe. This highlights the fact that the bridging event depends not only on the liquid level but also on the waves that form on the interface. If the instability that causes the disturbance on the interface is large enough to outweigh the stabilizing gravitational and surface tension effects, then the wave will continue to increase in amplitude and form a liquid slug.

Time= 0 s	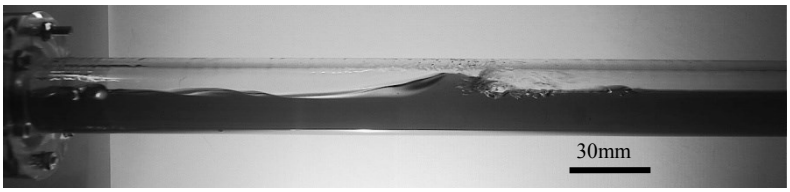
Time= $\frac{1}{60}$ s	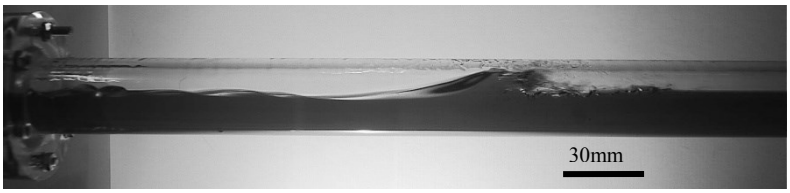
Time= $\frac{2}{60}$ s	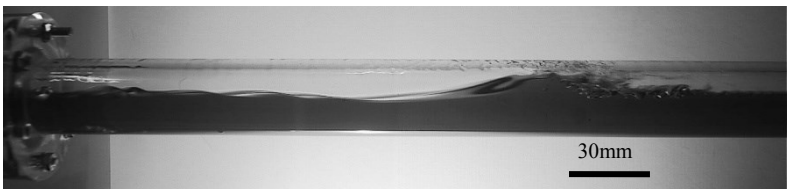
Time= $\frac{3}{60}$ s	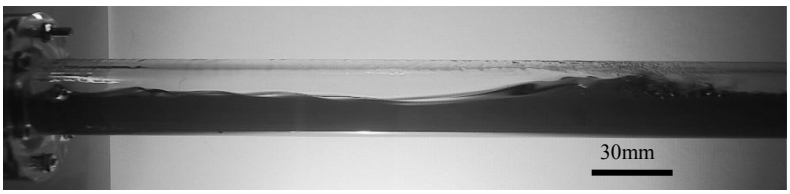
Time= $\frac{4}{60}$ s	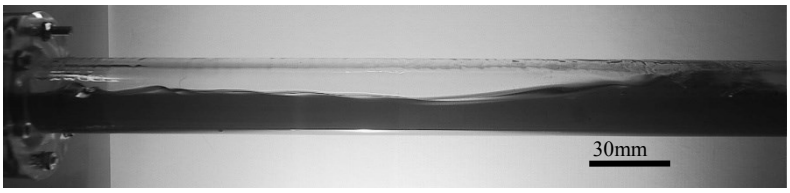
Time= $\frac{5}{60}$ s	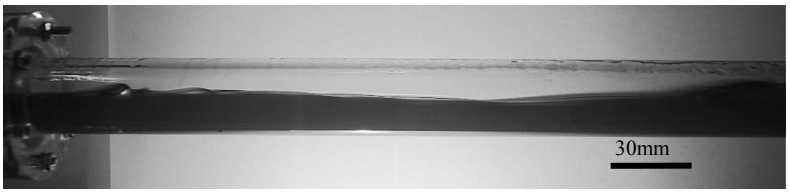

Figure 7.19: A series of images showing slug initiation at Usl=0.2m/s, Usg=2.0m/s.

The pictures shown above illustrate the great complexity of the slug formation process. The observations indicate that slug precursors developed from waves which arise from the instabilities of the gas-liquid interface. The slug increases in length if the rate of liquid intake at the slug front exceeds that of liquid shedding at its tail. For a constant gas flow-rate, an increase in the liquid flow-rate leads to an increase in the average film thickness, facilitating pipe-bridging, and leading to more frequent slug-formation.

7.5.1.2 Effects of varying the gas flow-rate at a constant liquid flow-rate

This section will discuss the slug initiation mechanisms observed at a constant liquid superficial velocity (0.15 m/s) with increasing gas superficial velocity. The images illustrated in this section are obtained for the runs with the inlet stratification plate inserted in the middle of the pipe.

At the lowest gas superficial velocity used (1m/s), liquid is observed to flow backward at the mixing point. Hence a layer of liquid sits on top of the stratification plate. As can be seen in Figure 7.20, the liquid level at the mixing point is much higher than the desired height. Initially the gas-liquid interface has a slightly wavy appearance indicating a stratified-wavy regime. A large wave approaches the top of the pipe and forms a slug front. No gas entrainment is observed in this case. Following the passage of this slug, the liquid level drops slightly.

Time= 0 s	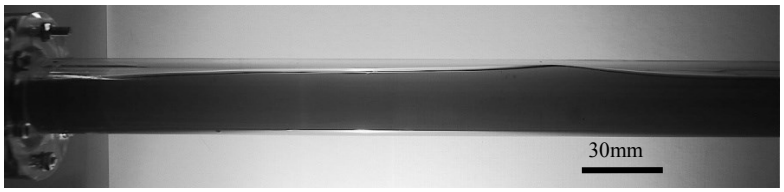
Time= $\frac{1}{30}$ s	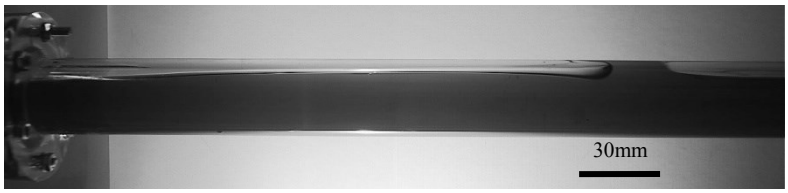
Time= $\frac{2}{30}$ s	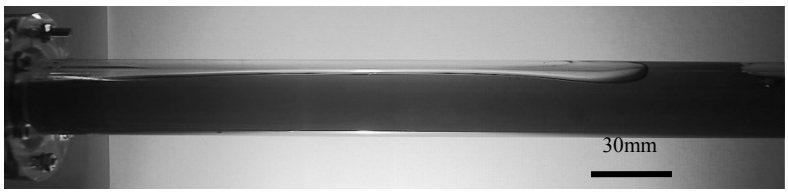
Time= $\frac{3}{30}$ s	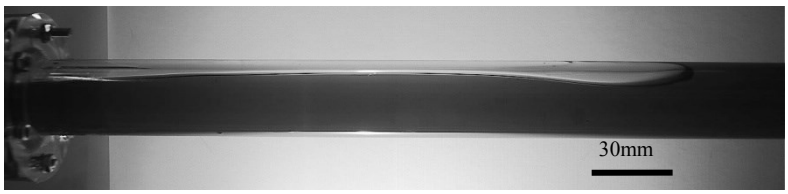

Figure 7.20: A series of images showing slug initiation at Usl=0.15m/s, Usg=1.0m/s.

Increasing the gas flow-rate to 2m/s, (see Figure 7.21) there is no backward liquid flow from the mixing point. The fast moving gas penetrates into the liquid phase and the slug front entrains gas bubbles. The slug increases in length while the liquid level behind the slug decreases by a significant amount.

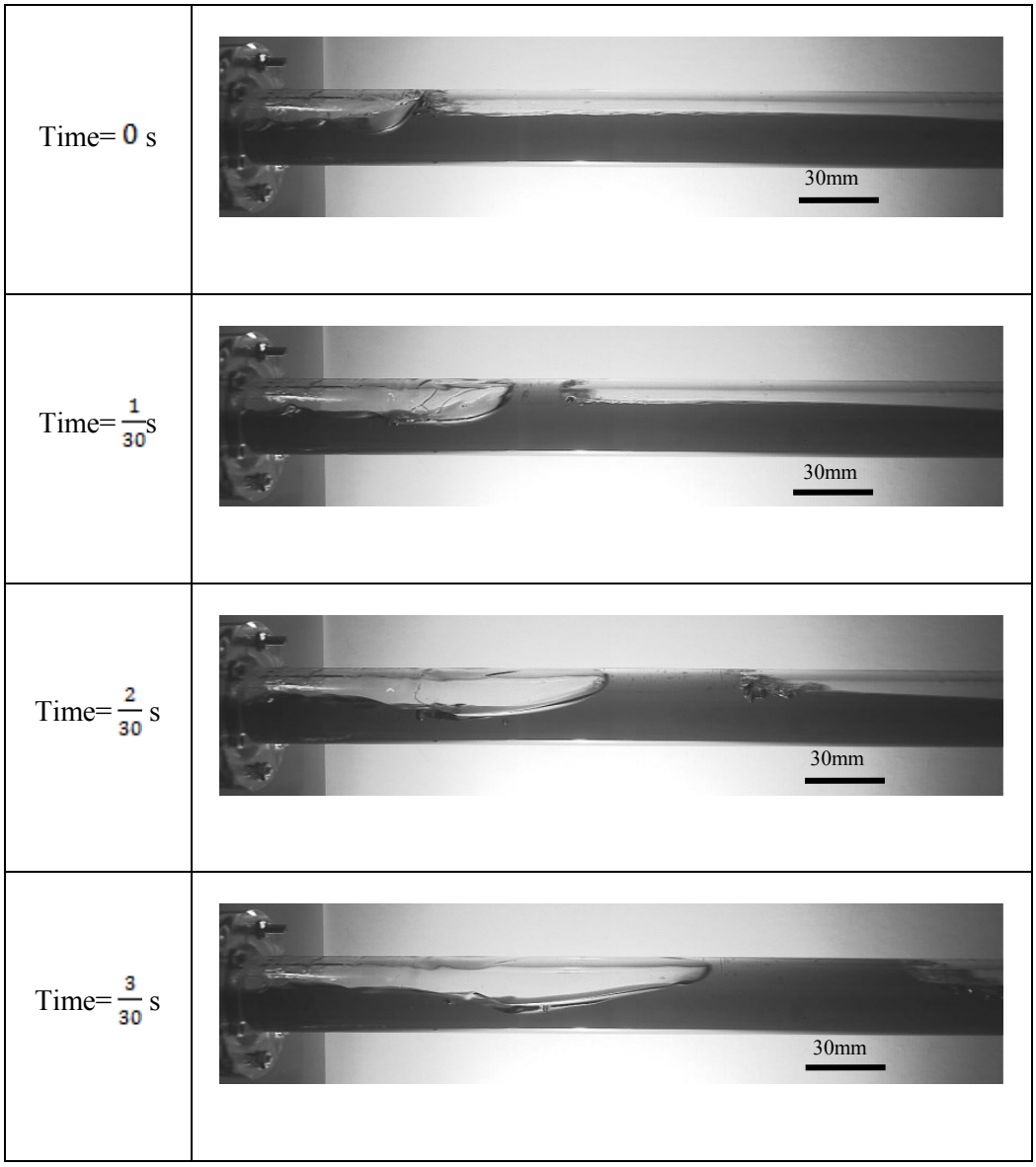

Figure 7.21: A series of images showing slug initiation at Usl=0.15m/s, Usg=2.0m/s.

For a further increase in the gas flow-rate to 3m/s (see Figure 7.22) the liquid level is lower. As can be seen in Figure 7.22, initially small-amplitude disturbances are observed at the gas-liquid interface which is driven by the gas to form waves. One of the waves grows larger in amplitude and coalesces with the waves downstream, subsequently bridging the pipe and

hence forming a slug. The liquid film behind the slug drops significantly and waves on this liquid film begin to dissipate.

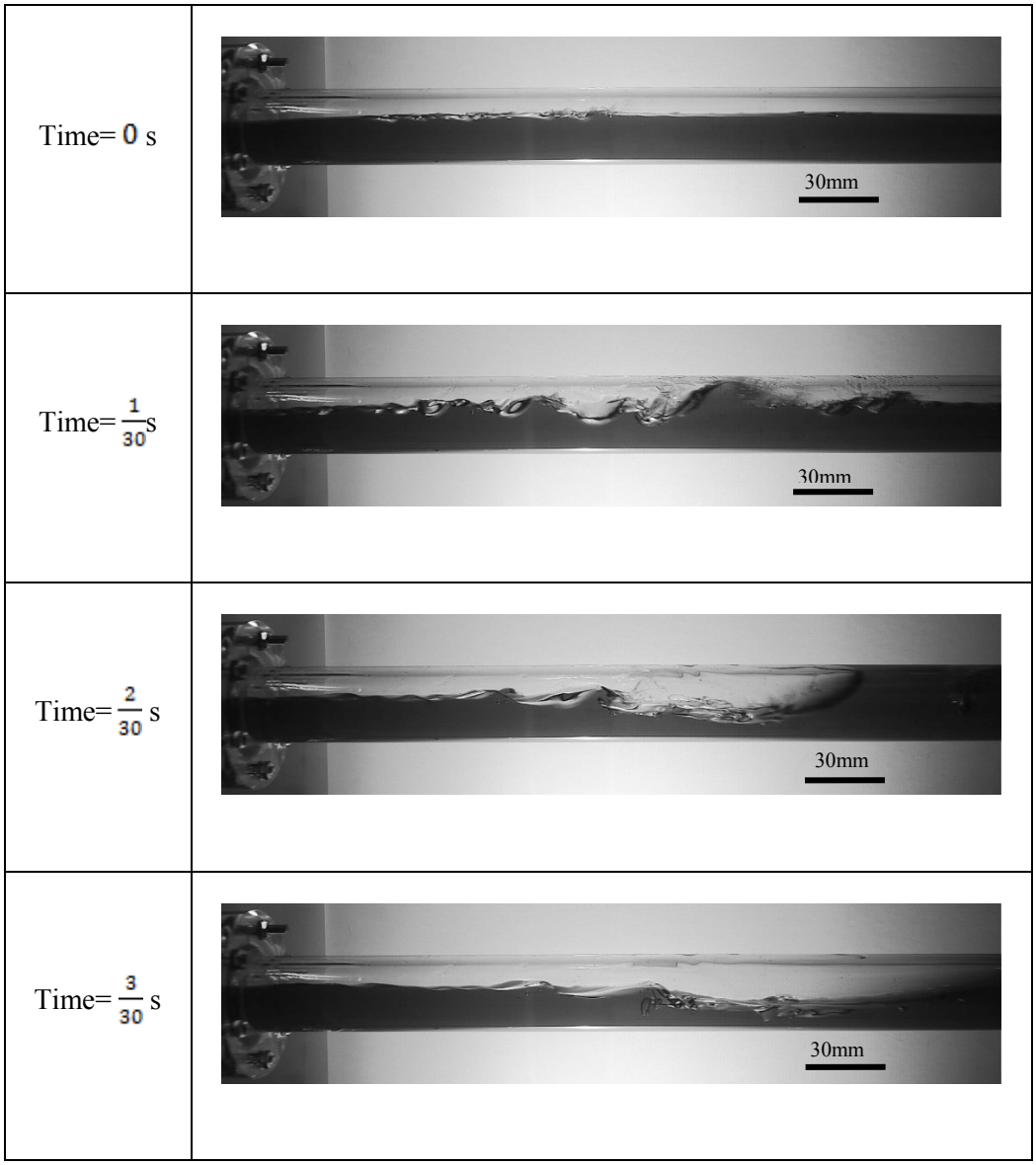

Figure 7.22: A series of images showing wave overtaking at Usl=0.15m/s, Usg=3.0m/s.

Increasing the gas flow-rate to 6 m/s (see Figure 7.23), small-wavelength waves are observed to dominate the gas-liquid interface. Slugs travel at a very high speed which makes them very difficult to capture with the high-speed camera used in the experiments. As can be seen in Figure 7.23 the slug is highly-aerated. Lin and Hanratty (1986) highlighted this fact in relation to high gas velocities where the aeration in slugs increases; this makes it difficult to differentiate between slugs and large roll waves which may touch the top of the pipe without forming a liquid bridge. Slugs and roll waves, however, can be distinguished by looking at

their shape and translational velocity. One characteristic of a slug precursor is that the liquid film drops sharply at its tail. In contrast, a large wave normally shows a much gradual decrease of liquid height in its tail profile. As can been seen in Figure 7.23, the liquid film immediately behind the slug almost disappears as the slug carries away a large amount of liquid. Another indicator of slug-formation is suggested by Ujang (2003) according to which the slug propagates at a velocity at least equal to the mixture velocity; a large-amplitude wave, on the other hand, tends to move with a slower velocity.

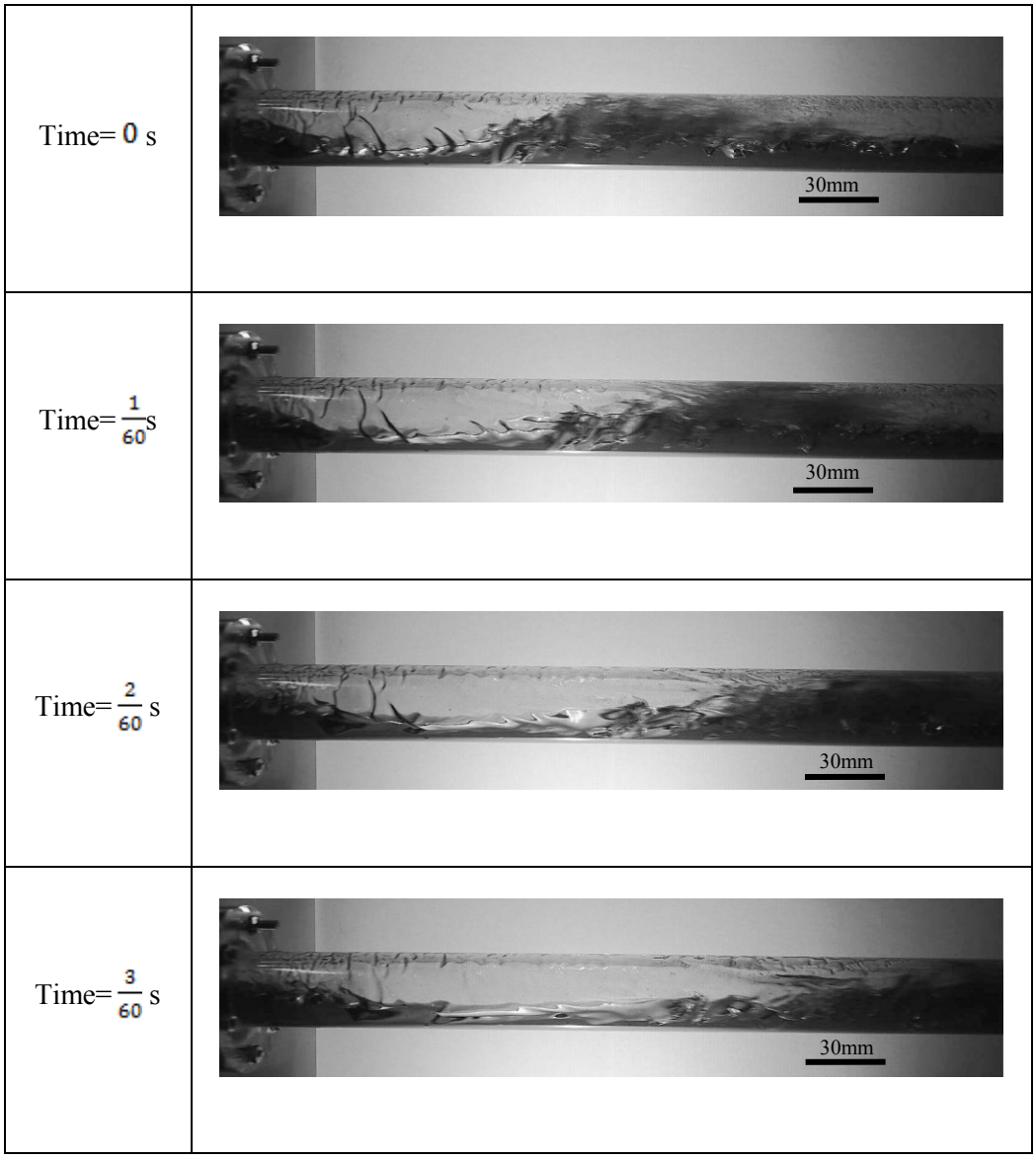

Figure 7.23: A series of images showing slug initiation at Usl=0.15m/s, Usg=6.0m/s.

Other nonlinear phenomena accompany slug flows. For instance, in Figure 7.24, wave-breaking is observed. Initially, a wave approaches the top of the pipe but does not bridge it, as

can be seen upon inspection of the time-sequence in Figure 7.24. Subsequently, the wave topples over to form smaller waves and droplets. In this case, the liquid level is not high enough to sustain wave growth; the fast moving gas penetrates into the wave and breaks it down into droplets.

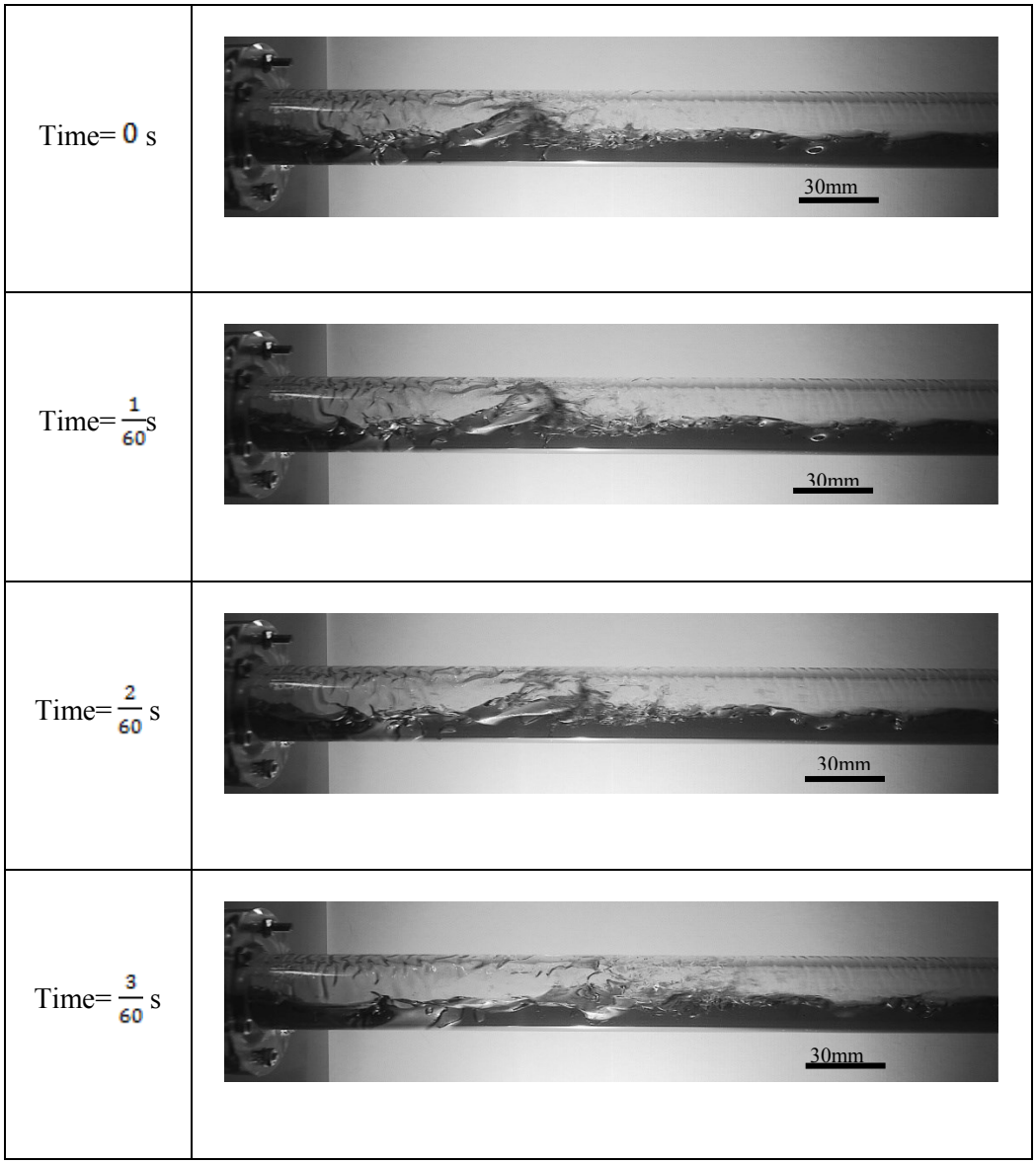

Figure 7.24: A series of images showing wave-breaking at Usl=0.15m/s, Usg=6.0m/s.

Figure 7.25 comprises enlarged views of a slug initiation time sequence in which it can be observed that as the liquid enters through the slug front, a jet which entrains gas bubbles is formed. This gas entrainment leads to a reduction in the slug average hold-up and interferes with the mechanism of liquid pick-up at the slug front, leading to the development of complex flow structures within the slug. This reinforces the point made above that

differentiating between slugs and large-amplitude waves are more difficult at such high velocities. It is also observed that after the slug has passed through the observation point, the top of the pipe wall is coated by a thin, liquid layer that exhibits the formation of waves of much shorter wavelength and lower velocity than the large-amplitude waves that are candidates for slug-formation.

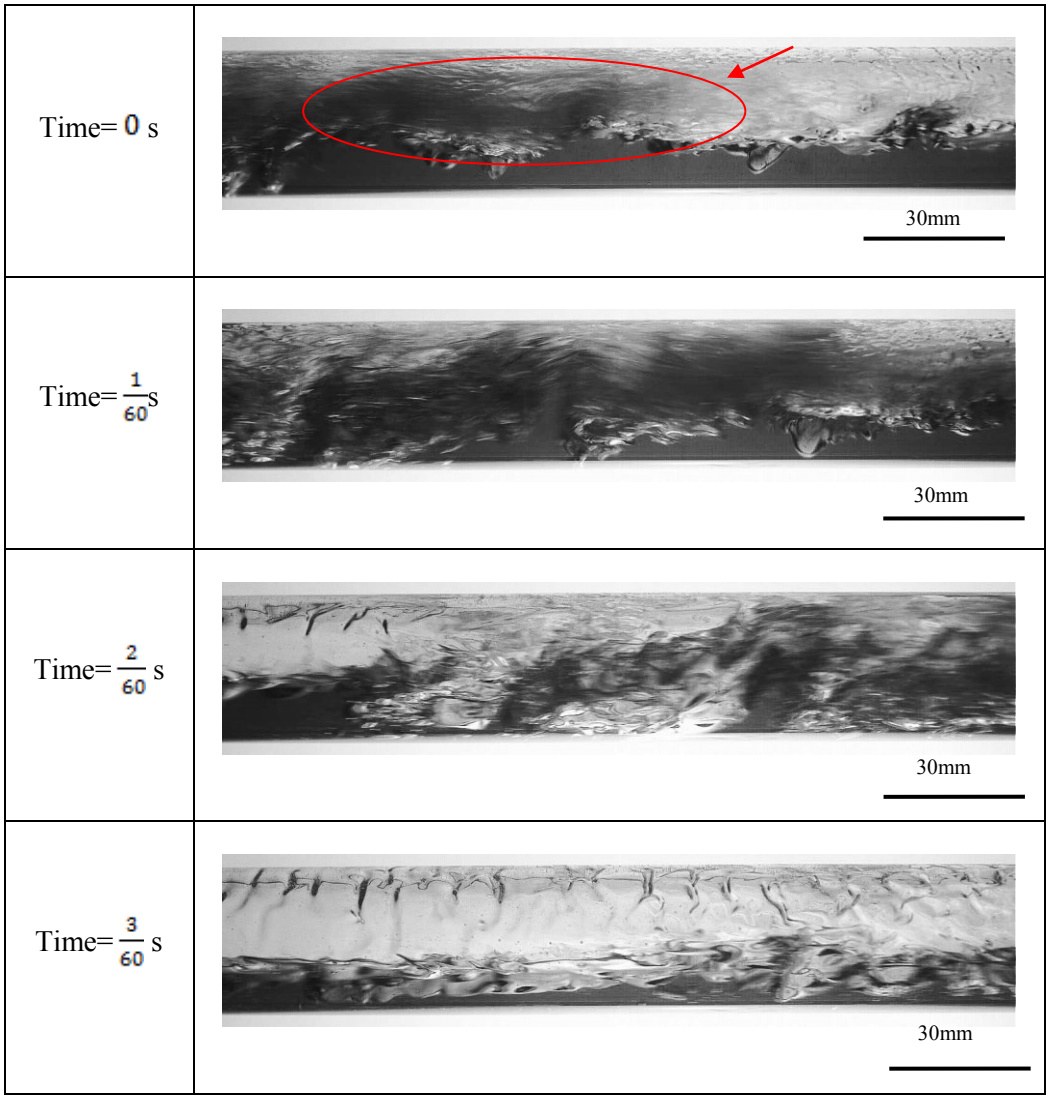

Figure 7.25: A series of enlarged images showing slug initiation at Usl=0.15m/s, Usg=6.0m/s.

In summary, increasing the gas flow-rate increases the interfacial shear stress which the gas exerts on the liquid interface, which causes a decrease in the equilibrium liquid level. With increasing gas flow-rate, the interface becomes more unstable giving more opportunities for large-amplitude waves to develop that can bridge the pipe and form slugs. Moreover, as the gas flow-rate increases, larger amounts of gas are entrained into slugs as can be seen in

Figure 7.26. The complex structures exhibited by the slugs can also be attributed to gas penetrating into the slug front.

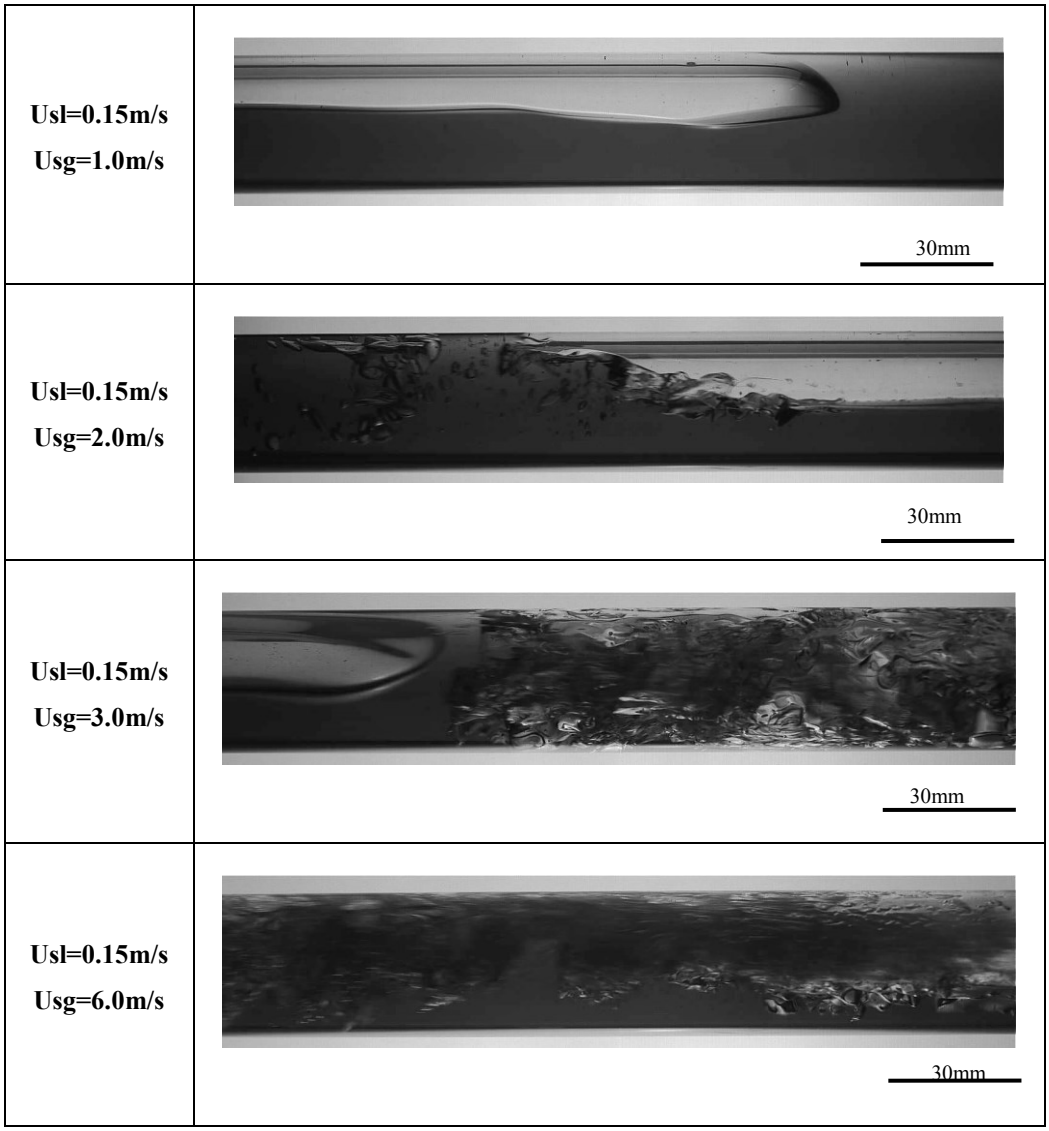

Figure 7.26: A series of enlarged images showing gas entrainment increased with increasing gas velocity.

7.5.2 Slug initiation mechanisms with a conical reducer inlet configuration

This section discusses the slug-formation mechanisms observed in the series of air-oil experiments carried out with 'Conical reducer' inlet configuration. As discussed in Chapter 6, the gas and liquid are initially introduced separately in the 75mm (3-inch) pipe and develop

as a mixture along the axial direction before they enter the 32 mm test-section via the conical reducer. Figure 7.27 shows the phenomena observed for the flow with liquid and gas superficial velocities of 0.1m/s and 2m/s, respectively. Though the gas liquid interface appears to be smooth in the reducer, many slugs are formed at the joint between the reducer and test-section. This is because the liquid at the outlet of the reducer is accumulated to a level that almost reaches the top of the pipe wall. The change in the pipe size accelerates the gas flow-rate which then pulls the liquid up towards the top of the pipe and a bridging occurs.

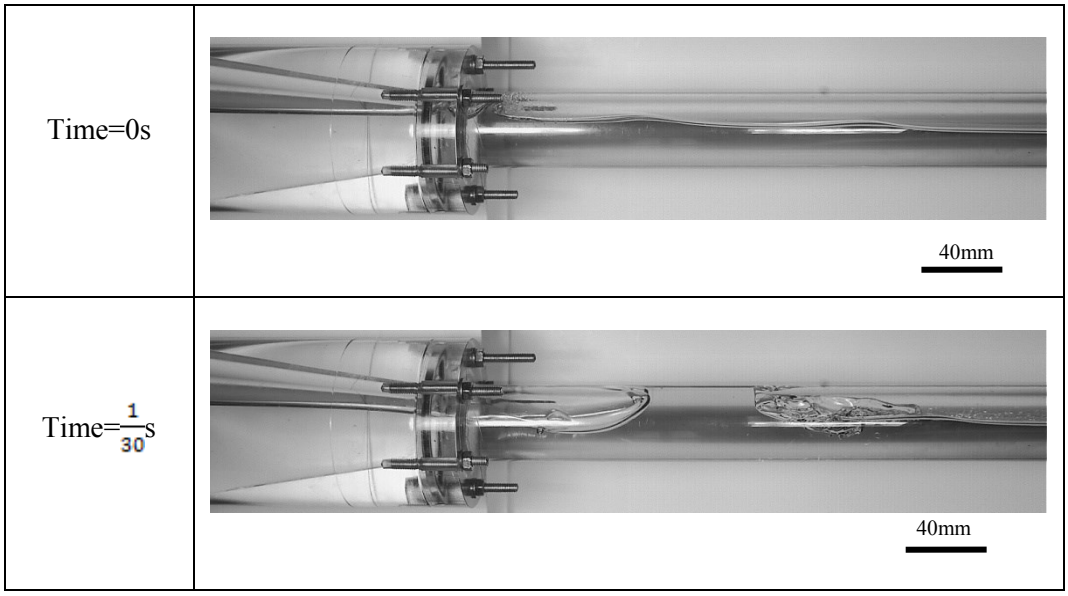

Figure 7.27: A series of images showing slug initiation at Usl=0.1m/s, Usg=2.0m/s, disturbances were induced at the pipe joint.

By keeping the gas superficial velocity constant and increasing the liquid superficial velocity to 0.2m/s, more liquid enters the entry and therefore the liquid level is increased, leading to the formation of the slugs in the cone reducer. When the gas and liquid accelerate through the reducer, the acceleration rate of the gas phase is higher than the liquid phase. The larger velocity difference increases the energy transfer between the fluids, and, as a result, the gas-liquid interface appears to be quite wavy in the reducer. Slugs are frequently formed in the reducer (see Figure 7.28) and propagate into the test-section. Some of them can develop further downstream and some are dissipated when they advance on the liquid level of varying heights.

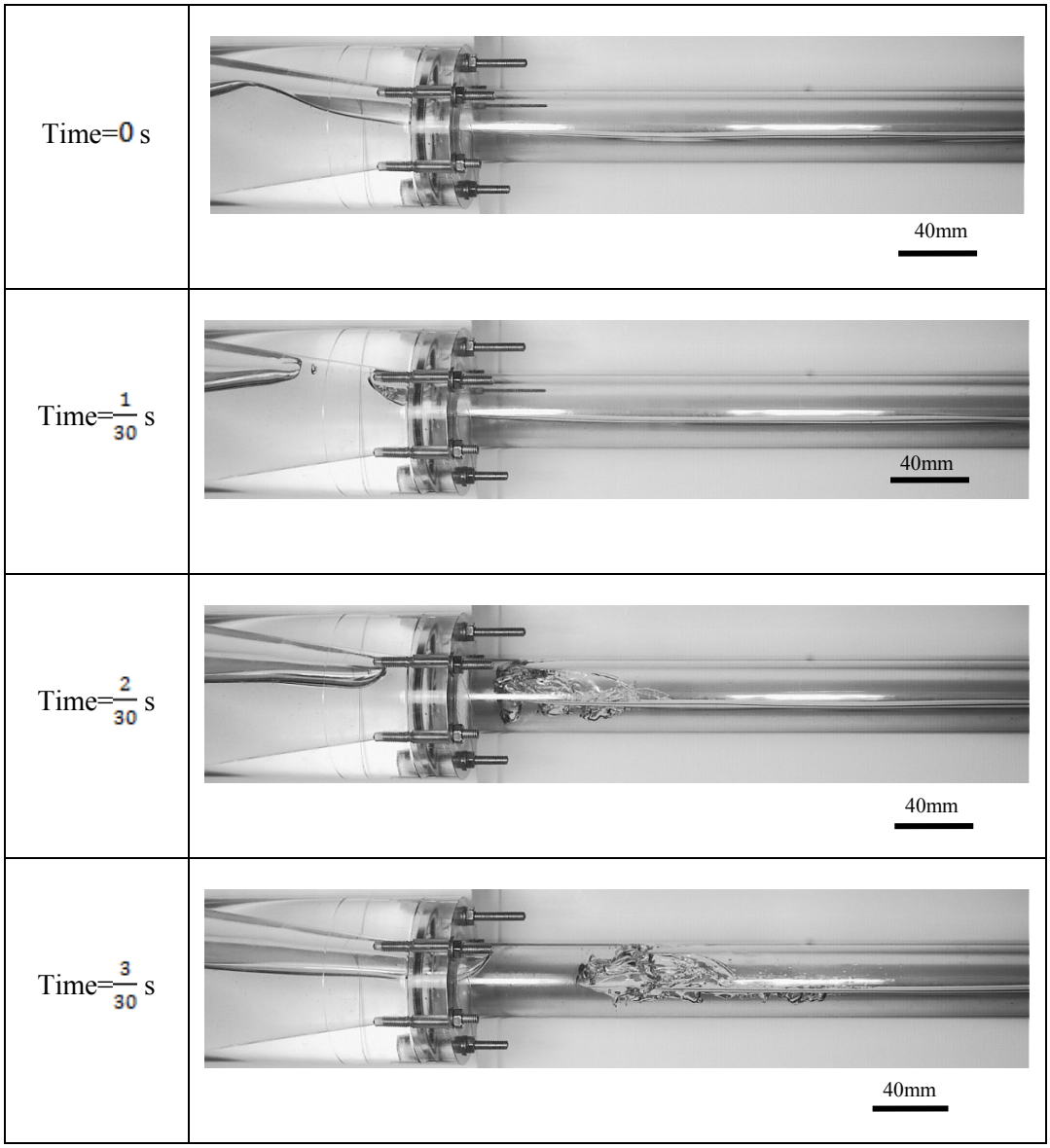

Figure 7.28: A series of images showing slug initiation at Usl=0.2m/s, Usg=2.0m/s, slug is formed at con reducer.

By keeping the liquid superficial velocity constant and increasing the gas superficial velocity to 6m/s, it can be seen from Figure 7.29 that the gas-liquid interface is dominated by small wavelength waves. The liquid level in the test-section is decreased due to the increased gas flow-rate. A large amount of gas is entrained at the front of the slug and a jet of gas bubbles is formed. In comparison to the case shown in Figure 7.28, most the slugs formed in the reducer are shorter and travel faster.

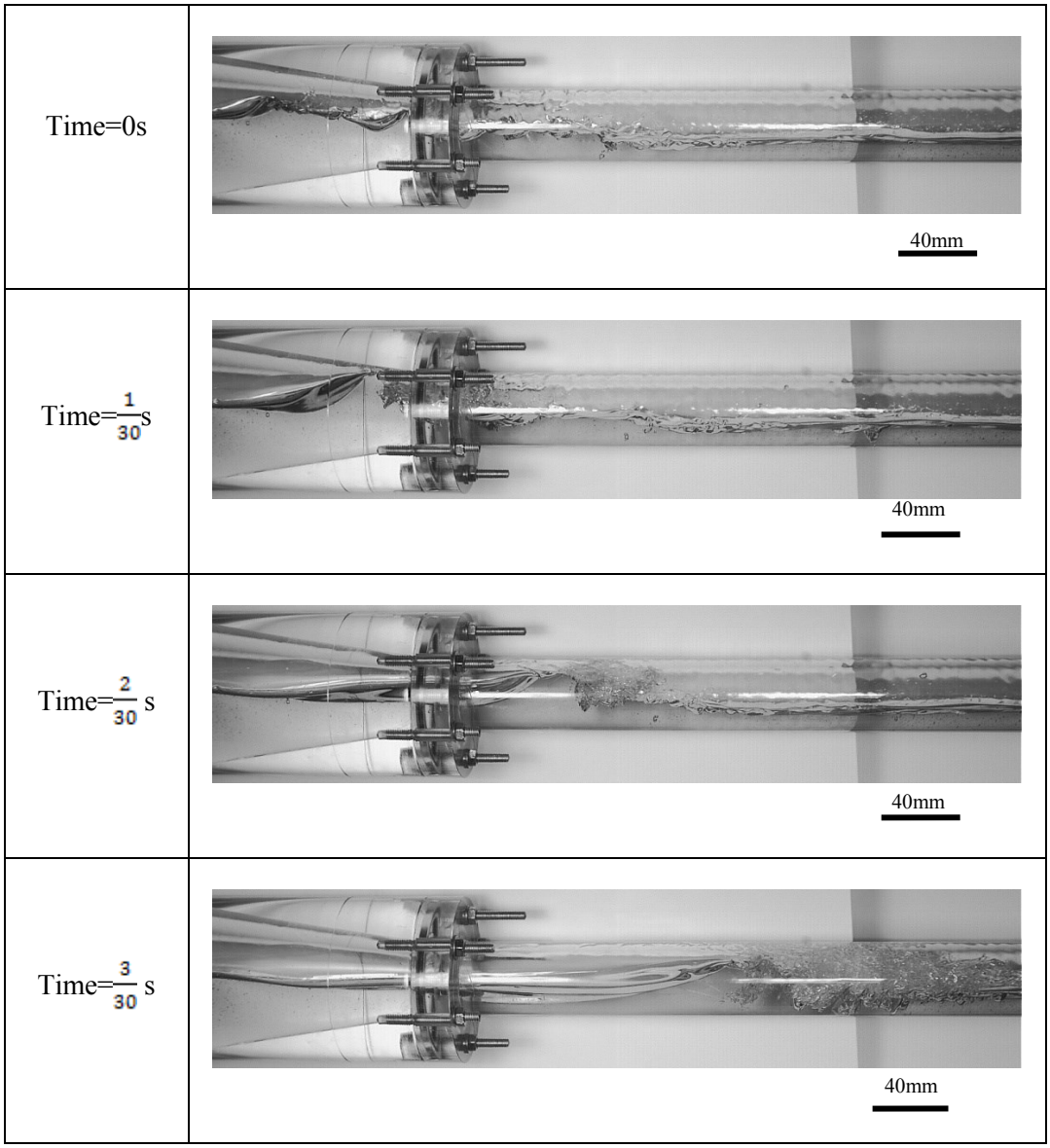

Figure 7.29: A series of images showing slug initiation at Usl=0.2m/s, Usg=6.0m/s, slug is formed at cone reducer.

7.5.3 Overview of LOWPRESS slug initiation experiments

Section 7.5 discusses slug initiation in the air-oil slug flow experiments performed on LOWPRESS facility with different inlet conditions and flow rates.

The experimental observations indicate that the slug initiation mechanisms are dependent on the liquid level and wave generation process. With low gas and liquid flow rates, the flow is initially stratified and the interface is smooth; the instabilities on the gas-liquid interface

gradually grow into larger amplitude waves and finally bridge the pipe, forming slugs. Increase liquid flowrate leads to an increase in the average film thickness, facilitating pipe-bridging. The rise of liquid level can also cause a higher relative velocity between gas and liquid leading to a wavier interface and hence more frequent slug-formation. Increasing the gas velocity, liquid level tends to be lower but waves grow more rapidly at the interface. Slug precursors tend to be shorter and highly aerated with higher gas velocity.

7.6 Slug development along the pipe

Two series of experiments on slug flow evolution were carried out on the LOWPRESS facility for horizontal air-oil flows and air-water flow: these are described in Sections 7.6.1 and 7.6.2 respectively.

7.6.1 High speed video observation of air-oil slug flow evolution in the LOWPRESS test-section

The aim of the experiments described in this Section was to monitor slugs from their initiation until their exit from the pipe. The progress of the slugs was monitored using high speed video cameras, namely the I-SPEED3 (monochromatic) and the I-SPEED2 (color) cameras. For each test, two cameras were used and the runs repeated 3 times. By this means, it was possible record images for each set of conditions at 0.6, 1.3, 2.5, 4.5 and 6.5 m from the inlet.

The number of slugs passing a camera was counted by reviewing the film footage over a measured sampling time. A slug is usually counted when the slug front passes through a line across the middle of image. It was noticed that at lower gas superficial velocities between 1m/s to 3m/s, it was possible to distinguish slugs from large-amplitude waves. The expected error is ± 3 counts over 150 seconds sampling time, which is approximately equivalent to ±0.02Hz error in frequency. However, with a further increase in the gas flow-rate, the slugs became more highly-aerated and travelled at greater speeds. As a result, it is more difficult to distinguish slugs from large-amplitude waves. Nevertheless, as the distance from the initiation position increases and the slugs grow, they become easier to identify. Therefore for

the cases with gas superficial velocities above 6m/s, at the locations of 0.6m and 1.3m, the expected error is ±6 counts over 150 seconds sampling time which is approximately equivalent to ±0.04Hz error in frequency. The error is reduced at the location of 2.5m, 4.5m and 6.5m with expected error of±3 counts over 150 seconds sampling time or approximately ±0.02Hz error in frequency.

For the inlet arrangement with a separating plate placed at mid-point of the pipe, a sample of the distribution of the slug frequency as a function of distance along the test-section is illustrated in Figure 7.30. Slugs are rarely formed immediately at the point when fluids are mixed together. A short distance is required for interface instability to develop into a slug, and therefore within this distance the slug frequency is zero. Once a slug precursor is formed, the liquid level behind this slug rebuilds, and waves that travel on the rebuilding film tend to grow more rapidly. It was observed that the region of most rapid initiation lies between the distance 0.6m to 1.3m from the mixing point, hence a maximum slug frequency is obtained at 1.3 m. After the initiation of slug precursors, the liquid pick-up rates at the front of the slug precursors change as they advance over a film of varying height. Consequently the slug frequency decreases at 2.5m, the ultimate survival of the slugs is related to the thickness of the liquid layer immediately downstream of them. If the level is too shallow, the front velocity of the precursor will be smaller than the tail velocity, leading to its collapse back into a wave. Eventually, the survived slugs will persist along the pipe towards the exit and the slug frequency approaches an asymptotic value after 4.5m, as shown in Figure 7.30.

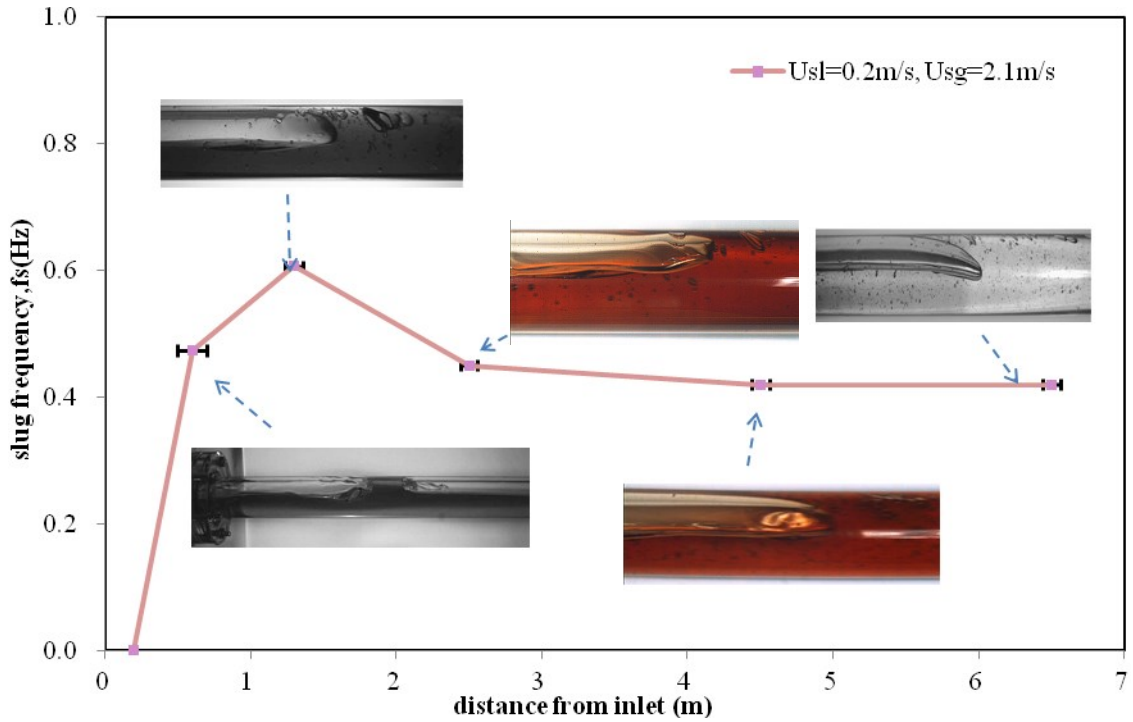

Figure 7.30: Slug frequency distribution at Usl=0.2m/s and Usg=2.1m/s for air-oil system. The insets show images of the slugs at various axial locations from the inlet.

Figure 7.32 and Figure 7.32 shows the effects of increasing the liquid superficial velocity on the slug development for constant gas superficial velocities of 2m/s and 3m/s. It can be seen that the peak due to the rapid slug initiation becomes more pronounced and the drop of the frequency to an almost asymptotic value becomes sharper with increasing liquid superficial velocity. As described earlier in this section, an increase in the liquid velocity increases the liquid level hence waves bridge the pipe with greater ease; as a result, the overall slug frequency at different locations along the pipe is generally higher with higher liquid superficial velocity. In the slug initiation region, the higher liquid velocity means liquid is quickly replenished after the passage of the previous slug, hence slugs are more rapidly initiated. However, the drop of slug frequency is sharper between 1.3 to 2.5m due to the slugs overtaking.

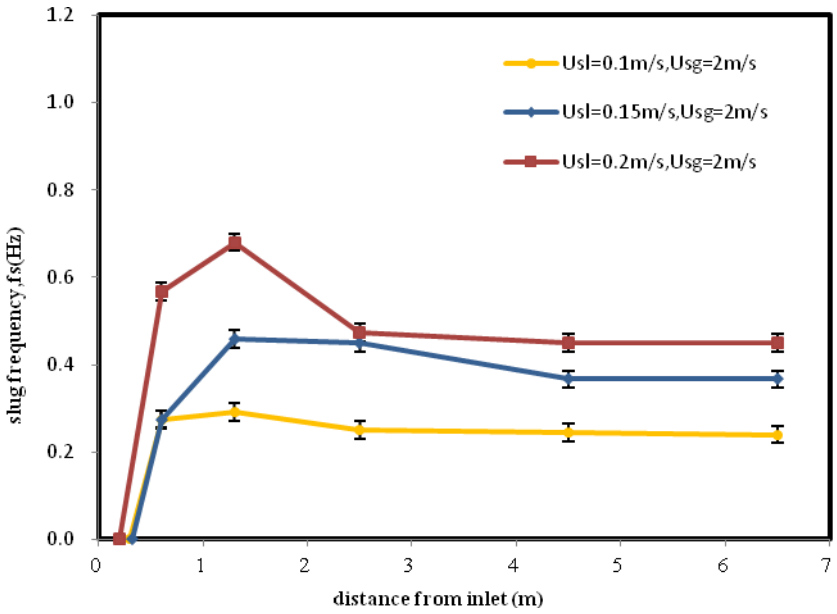

Figure 7.31: Effect of varying liquid velocity on the slug frequency distribution for Usg= 2m/s.

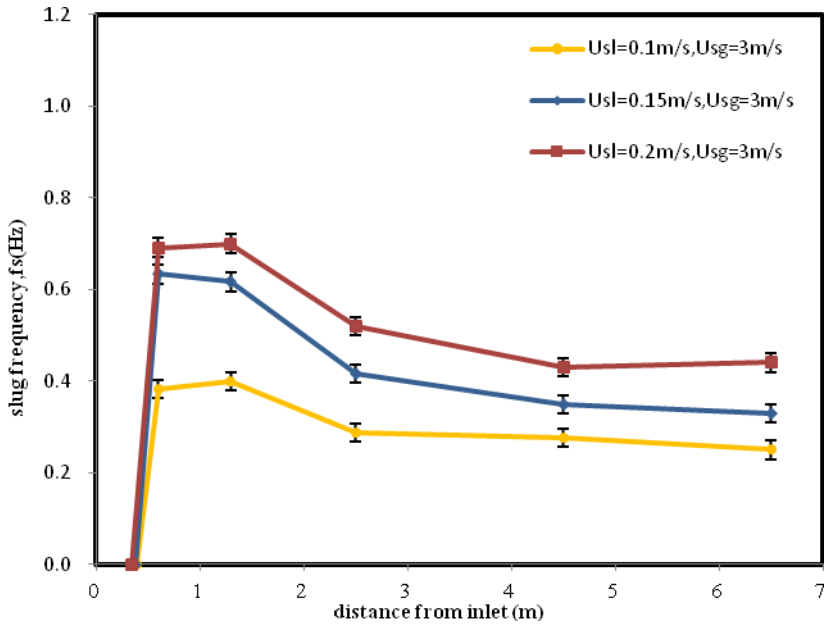

Figure 7.32: Effect of varying liquid velocity on the slug frequency distribution for Usg=3m/s.

Figure 7.33 and Figure 7.34 show the effects of increasing the gas superficial velocity on the slug development for a constant liquid superficial velocity of 0.1m/s and 0.2m/s respectively. Similar trends are observed with a peak in the slug frequency near the inlet and an approximately constant value at the test-section outlet. Between gas superficial velocities of 1m/s to 3m/s, the magnitude of the peak in frequency increases with this velocity up to a

value of 3m/s beyond which it decreases. In general, the frequency of developed slug is not strongly influenced by the gas velocity.

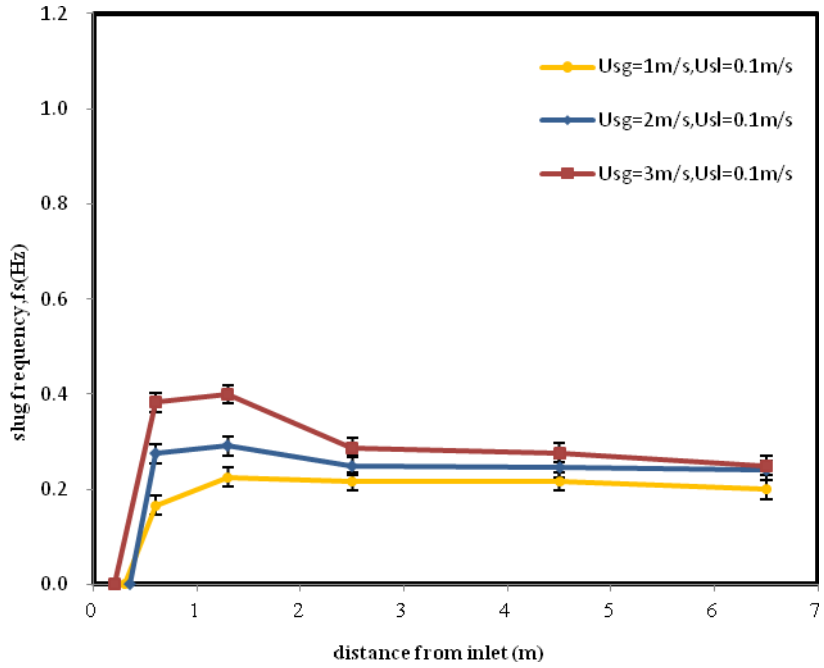

Figure 7.33: Effect of varying gas velocity on Slug frequency distribution for Usl=0.1m/s.

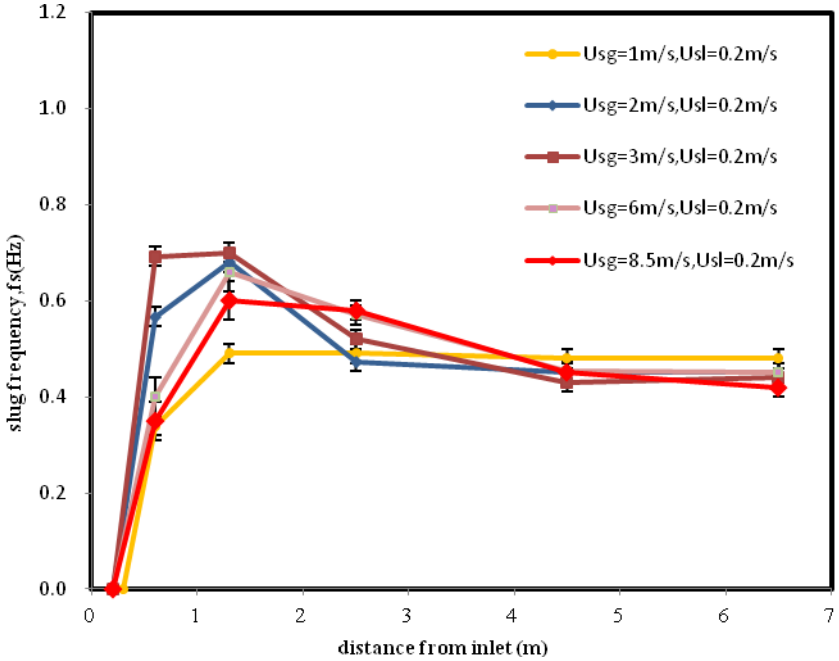

Figure 7.34: Effect of varying gas velocity on Slug frequency distribution for Usl=0.2m/s.

7.6.2 Monitoring of air-water slug flow evolution in LOWPRESS test-section using conductivity probes

In the experiments described in Section 7.6.1, video recording was used to study slug development in air-oil flows. For comparison purposes, slug evolution was also studied in the LOWPRESS facility for air-water flows; this more limited set of experiments was carried out with a separating plate placed at mid-point of the pipe at the entrance. Four twin wire conductance probes were placed at 0.5m, 2.5m, 6m and 6.8m from the entry of the test section respectively and were used to record instantaneous liquid height time traces. Each probe was calibrated offline and it was confirmed that the relationship between liquid height and the measured conductance was close to linear. Calibration of the probes inserted on the test-section, was conducted on a daily basis with the pipe dry and filled with water respectively. The liquid height value can be obtained by linear interpolation between the empty and full pipe conductivity signals. By assuming a flat interface, an estimation of the liquid holdup can be obtained by applying the following geometric relation (Taitel & Dukler,1977):

$$\varepsilon_L = \left(\frac{1}{\pi}\right)\left\{\pi - \cos^{-1}\left(2\frac{h_L}{D}-1\right)+\left(2\frac{h_L}{D}-1\right)\sqrt{1-\left(2\frac{h_L}{D}-1\right)^2}\right\} \qquad [7.5]$$

Figure 7.35 illustrates the development of the interfacial structures of the slugs with a gas velocity of 2m/s and liquid velocity of 0.1m/s. Slugs are observed at 0.5m from the entry where first probe was located, they periodically pass through the probe with time interval of approximately 25s. Between two slugs, the small amplitude waves occur on the gas liquid interface. At 2.5m from the entry where the second probe located, each slug has grown slightly longer, and liquid film behind each slug drops more sharply. Further downstream at 6m from the entry, a slug grows immediately behind the previously formed slug; slugs can be seen to propagate in successions of two as shown in Figure 7.35. At the location of 6.8m, a new slug is formed from the interface instability at the time of 8s, and the liquid film behind each slug drops more significantly, indicating slug is still growing as more liquid is absorbing into the slug body.

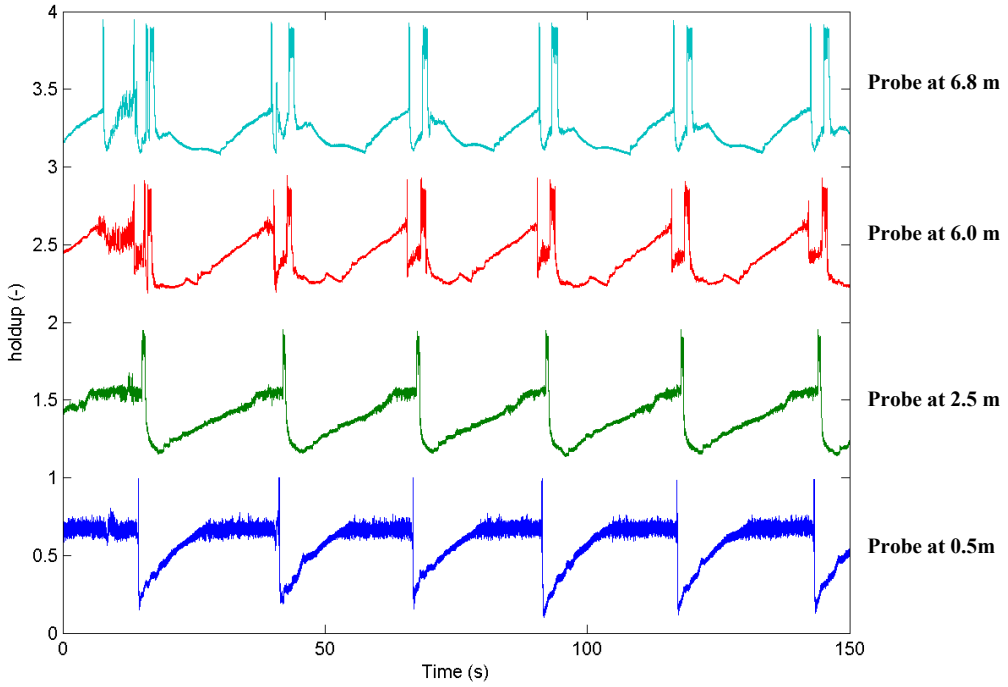

Figure 7.35: Plots of liquid holdup in a duration of 150s at different probe locations for U_{SL} = 0.1m/s and U_{SG} = 2.0m/s (Note: For clarity of presentation of the respective traces in this Figure and also in Figures 7.37, 7.38 and 7.39 the plots show the holdup values plus 1, 2 and 3 for the probe positions 2.5, 6.0 and 6.8 m respectively).

Figure 7.38 illustrates the development of the interfacial structures at the same gas velocity (2.0 m/s) but with a higher liquid velocity of 0.15m/s. At 0.5m from the entry, slugs occur periodically and, behind each slug, there appears to be a large wave building. Some of these waves have developed into new slugs at 2.5m, and these new slugs appeared to pair with the previously formed slug. At 6m and 6.8m, some slugs are observed to collapse back into waves.

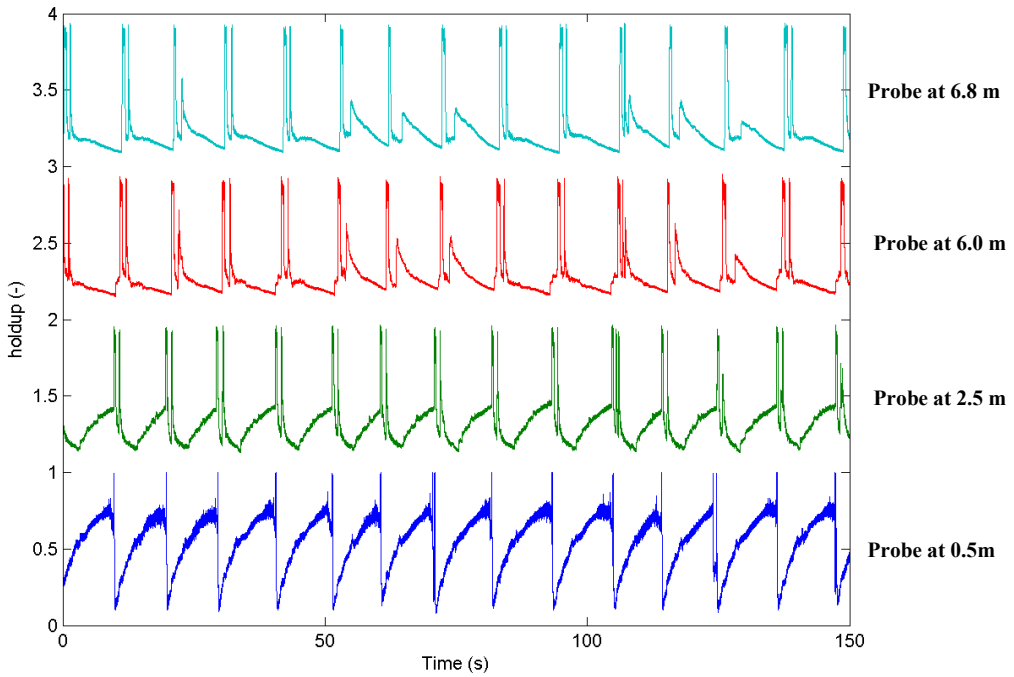

Figure 7.36: Plots of liquid holdup in a duration of 150s at different probe locations for U_{SL}= 0.15m/s and U_{SG}= 2.0m/s.

The results for the higher liquid rates of 0.2m/s and 0.3m/s are shown in Figure 7.37 and Figure 7.38 respectively. Again there are dramatic differences between the traces at 0.5 and 2.5m due to the slug initiation and growth process. Beyond 2.5m, though there are large waves propagate at the troughs of the liquid film behind slug precursors; most of the waves do not develop in amplitude and subsequently dissipate as can be observed at 6m and 6.8m. Comparing Figure 7.35 and 7.39, it is seen that, close to the entry, the average liquid holdup is around 0.65 when liquid velocity is 0.1m/s whereas the average liquid holdup increases to 0.75 when liquid velocity increase to 0.3m/s. The increase in the liquid level causes a higher relative velocity between gas and liquid, leading to a wavier interface and consequently there are many waves trailing behind slugs at 2.5m. However, most of these waves were merged or overtaken by slugs at 6m.

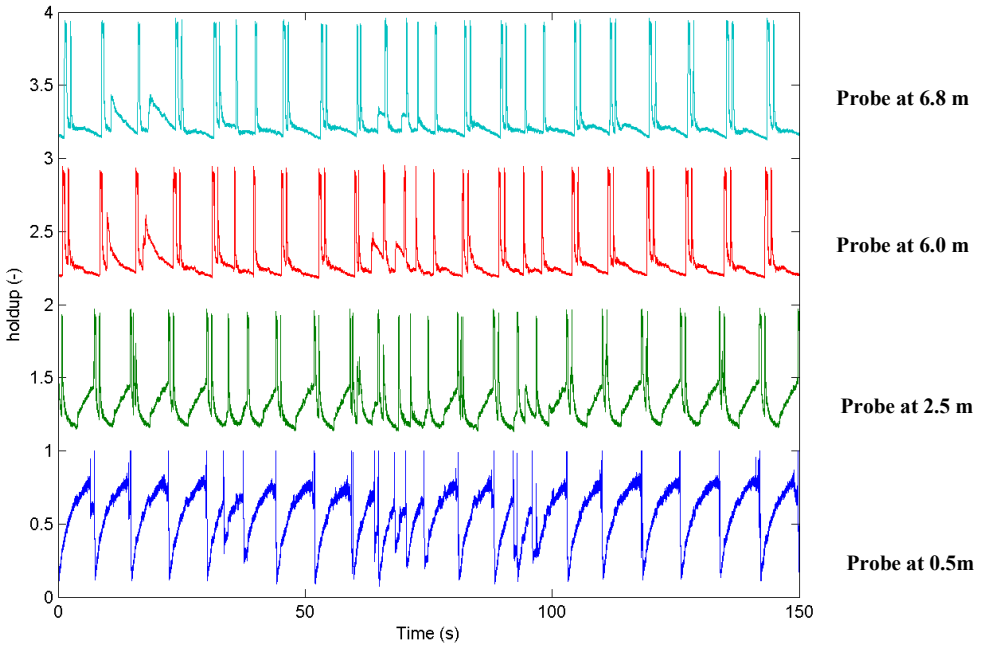

Figure 7.37: Plots of liquid holdup in a duration of 150s at different probe locations for U_{SL}= 0.2m/s and U_{SG} = 2.0m/s.

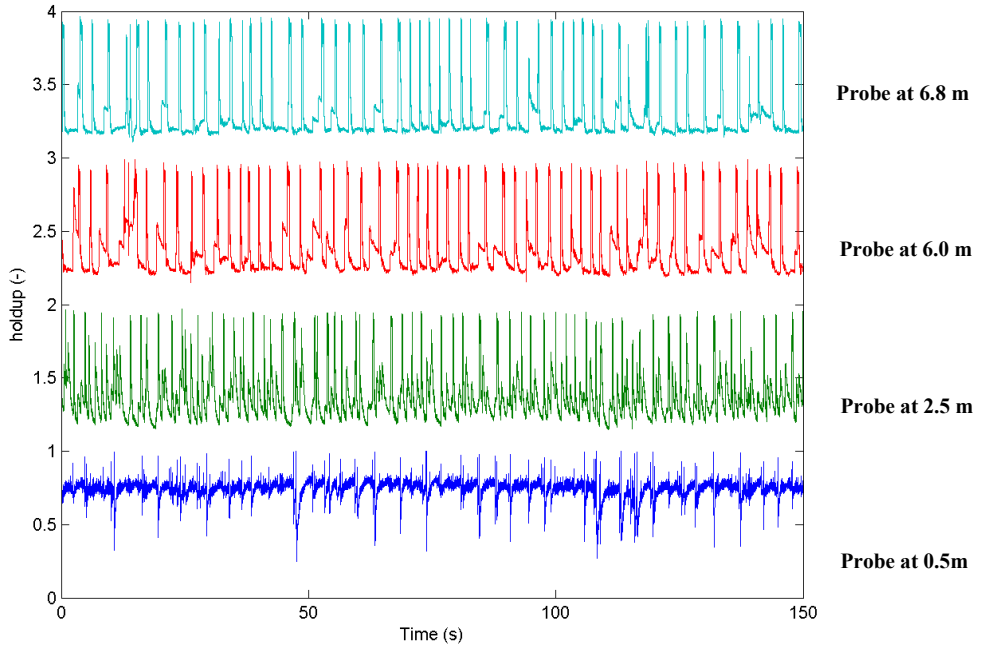

.

Figure 7.38: Plots of liquid holdup in a duration of 150s at different probe locations for U_{SL}= 0.3m/s and U_{SG} = 2.0m/s.

As observed in the above cases, increasing liquid velocity leads to an increase in the average liquid level, facilitating pipe-bridging and leading to more frequent slug-formation. The presence of large waves trailing a slug precursor indicates a combined effect of the phase velocities and the gradient in the liquid height. Beyond 2.5m, some slugs collapse back into the waves and some large waves dissipated or overtaken by slugs. However there is an exception for the lowest flow condition, new slug was observed to form at 6m, indicating the flow has not yet fully developed. Figure 7.39 shows the effects of increasing the liquid superficial velocity on the slug development for constant gas velocity. Slug frequency was estimated by counting the number of slugs in a 300s sampling time. As can be seen in Figure 7.35 to Figure 7.38, slugs were easily identified by looking at the holdup peaks with value almost to unity. For the lowest liquid velocity, slugs are still developing toward the pipe exit; therefore slug frequency keeps increasing downstream. Increasing the liquid velocity causes an upstream shift in the initiation site. For liquid velocities in the range 0.15m/-0.3m/s, slug frequency increases between 0.5m and 2.5m, then decreases between 2.5m to 6m, and remains constant at 6.8m.

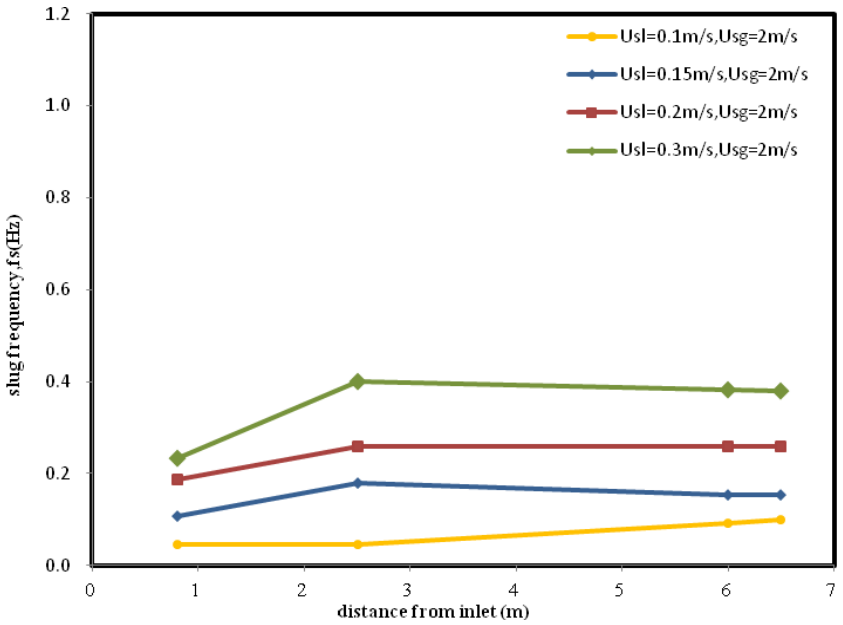

Figure 7.39: Effect of varying liquid velocity on the slug frequency distribution for constant gas velocity.

In contrast to air-oil flow (Figure 7.32), at the given liquid and gas flow rates, slug frequency is higher with air-oil system at each location along the pipe, and the peaks due to the rapid

slug initiation are also more pronounced with air-oil system which indicates that air-oil flow is more unstable than air-water flow under the same condition. The phenomena can be explained by viscosity contrast mechanism (Yih, 1967), the instability arises due to the jump in the viscosity across the interface. The higher liquid viscosity leads to a higher viscosity difference between the liquid and gas; consequently the interface is more unstable, and this manifests itself through higher slug frequency. A similar trend was observed by Manolis (1995) in his experiments on a 79 mm horizontal pipe. Manolis found that air-oil slug flow exhibited a higher slug frequency than air-water slug flow. Manolis (1995) explained this difference by noting that the liquid height in the stratified region near the pipe entrance is higher for the more viscous fluid, and that increased the ease of the pipe-bridging events; as a result slug frequency is higher. Moreover, the lower surface tension associated with air-oil flow can also lead to a more unstable interface. Because of the complexity and limited range of variables studied, no attempt has made to investigate which is the dominating mechanism.

Ujang (2003) studied the development of air-water slug flow in a 77.92 mm stainless steel internal diameter pipeline. Measurements of interfacial structures were made using conductance probes at 14 axial locations along the length of the 37m long test-section. Slugs were discriminated from waves by means of their velocities. Slugs move at a velocity above the mixture velocity, and therefore this criterion is used for the identification of all the slugs for the time series measured by each probe. Slug initiation began at 1.46m from the entrance and the slug frequency rose rapidly within the region 1.46 m to 5.01 m from the entry. Between 5.01 m and 13m, there was a rapid reduction in slug frequency due to overtaking and merging processes followed by a more gradual decline in slug frequency with the fully developed slug frequency being observed from 20m onwards. Ujang (2003) observed that the fully-developed slug frequency increases in proportion to the superficial liquid velocity, while the effect on the peak frequency appears to be stronger. Whereas the fully-developed slug frequency decreases in proportion to the superficial gas velocity, the latter has a much stronger effect on the slug initiation frequency. The experimental results in the present thesis for the evolution of slug frequency along the horizontal test-section have shown a qualitatively good agreement with Ujang (2003).

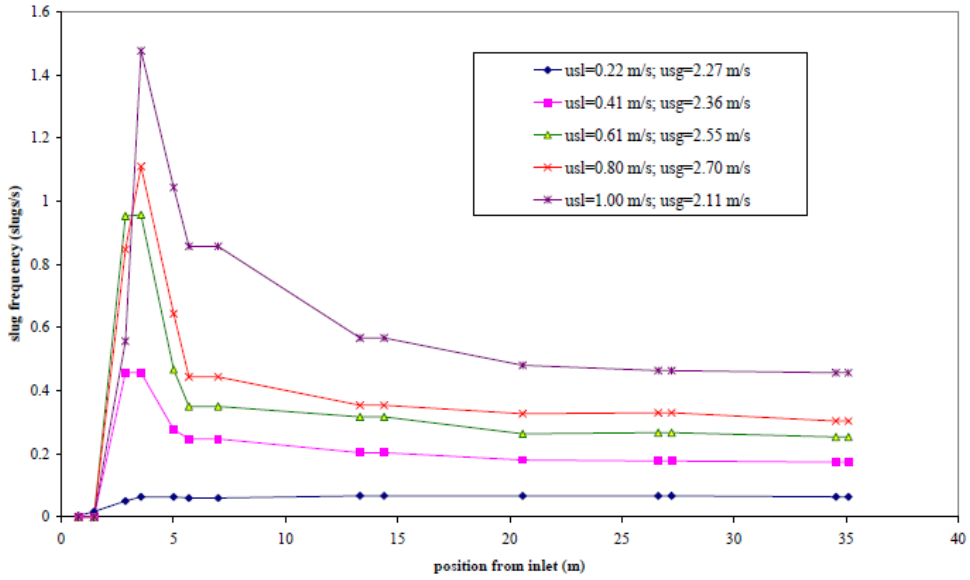

Figure 7.40: Effect of varying liquid velocity on the slug frequency distribution for constant gas velocity, as illustraed by Ujang (2003).

In the present measurements on the LOWPRESS facility for a liquid velocity of 0.3m/s, when gas velocity is 1m/s, there is no gas entrapped into the slug body, hence the liquid holdup of slug is unity as can be seen in Figure 7.41. If the gas velocity is increased to 2m/s, the gas liquid interface appears more unstable; many large waves are trailing behind slugs as observed at 2.5m though most of them have reduced in amplitude or dissipated at 6m. With further increase in the gas velocity, the rapid initiation site moves further upstream to 0.5m from the entry. As a result of this movement, the slugs become more aerated and this makes it more difficult to distinguish slugs from waves by looking at the holdup signal at each location, particularly those close to the entry. A characteristic of a slug precursor is that it propagates at a velocity at least equal to the mixture velocity whereas a wave tends to move slower. This criterion was used by Ujang (2003), slugs were discriminated from waves by means of their velocities. The arrival and exit times of each wave or slug at each probe location were manually recorded in her work and then matched to the times for the probe immediately downstream. These signals were then cross-correlated to obtain the average translational velocity. The velocity discrimination method has been adopted in present study to identify the slugs in the downstream end of the pipe where slug flow is more developed; details of the method are given below. However, close to the entry it was found very difficult to cross-correlate the signals between the first two probes as they are 2 meters away from

each other, slugs are rapidly collapsed or merged during that distance (see Figure 7.43 and Figure 7.44).

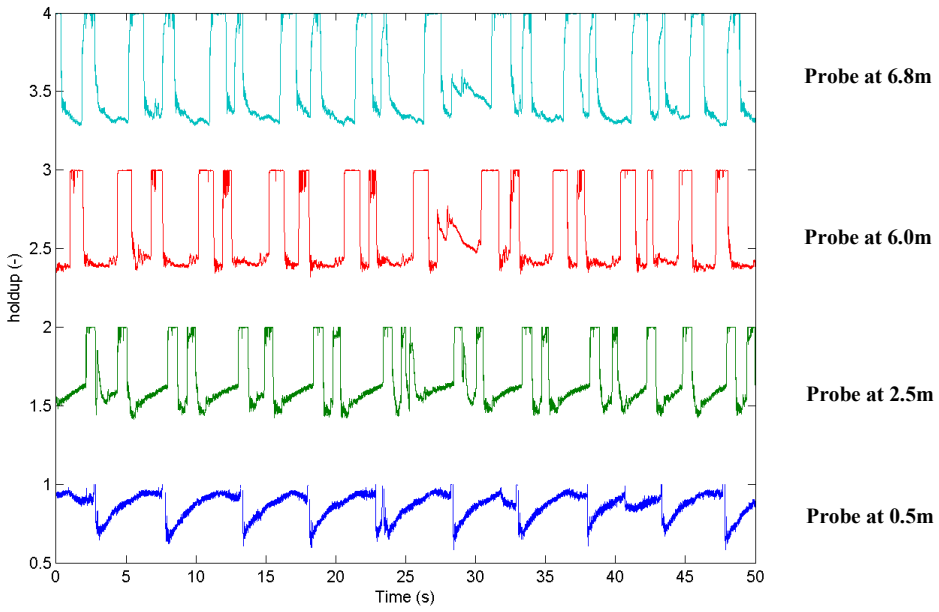

Figure 7.41: Plots of liquid holdup in a duration of 50s at different probe locations for U_{SL} = 0.3m/s and U_{SG} = 1.0m/s.

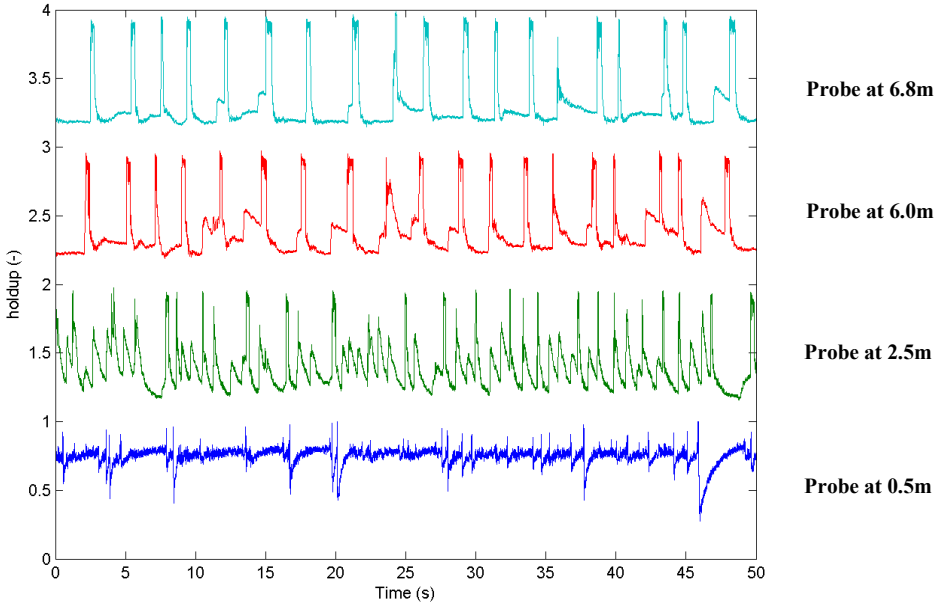

Figure 7.42: Plots of liquid holdup in a duration of 50s at different probe locations for U_{SL} = 0.3m/s and U_{SG} = 2.0m/s.

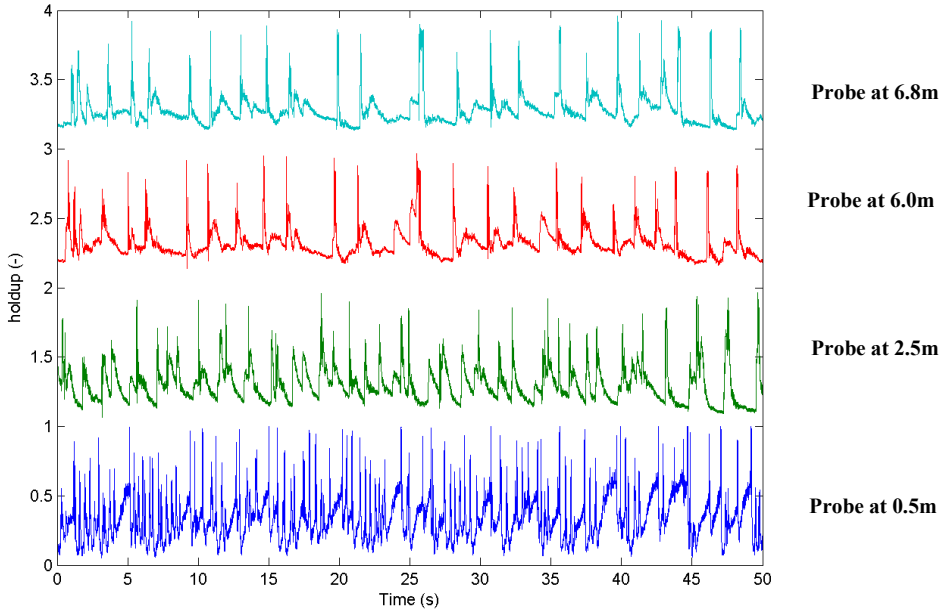

Figure 7.43: Plots of liquid holdup in a duration of 50s at different probe locations for U_{SL} = 0.3m/s and U_{SG} = 3.0m/s.

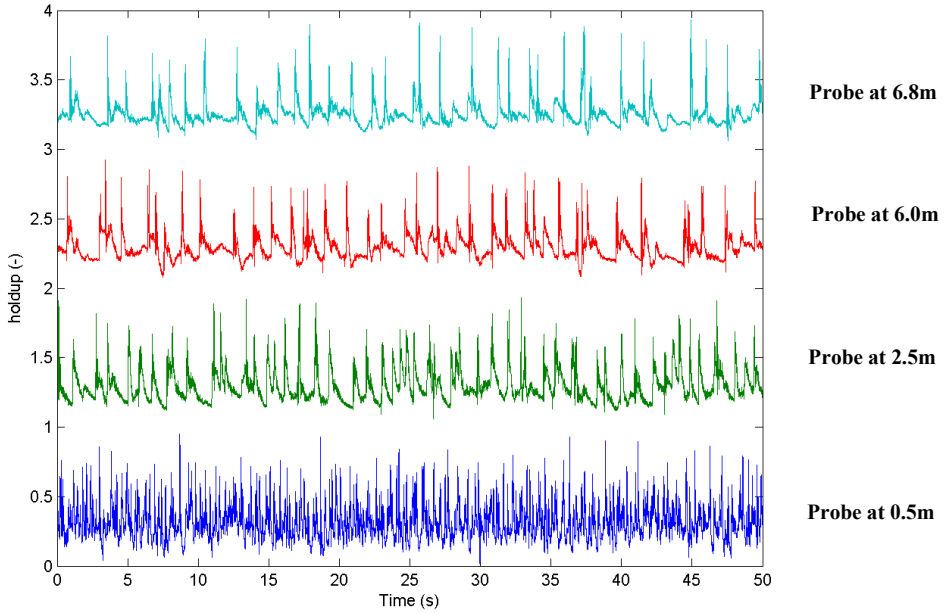

Figure 7.44: Plots of liquid holdup in a duration of 50s at different probe locations for U_{SL} = 0.3m/s and U_{SG} = 4.0m/s.

For evaluation of slug frequency at the downstream end of the pipe , the time evolution of the liquid holdup was measured using two conductance probes at two axial locations (x_1=6m, and x_2=6.8m). A peak in the signals from the conductance probes may correspond to a wave or a

slug so the identity of the moving object (slug or wave) was determined from the speed at which the peak travelled from the first probe to the second. As was stated above, slugs travel at much faster speeds than waves. The traveling speed was automatically obtained from the time lag using a customised MATLAB routine (see Appendix B) based on a cross correlation algorithm as follows：

1) Segmentation: The signal from the first probe f_1 was segmented to find major waves that could possibly be slugs. For this purpose, a threshold value ($f_{\text{threshold}}$) was selected which was 1.5 times of the time averaged liquid holdup, see Figure 7.45. A sample of peak segment is illustrated in Figure 7.46.
2) Smoothing: The digital signals from two probes were smoothed using a moving average filter to remove high frequency noises from the signal.
3) Cross correlation: Select a segment from f_1 above the threshold which is possible to be slug, $f_1(t_1, \Delta t)$, where t_1 is the starting time of the segment, and Δt is the length of the signal. Calculate the cross correlation of the segment $f_1(t_1, \Delta t)$ with second probe signal f_2.
4) Minimization: Find the best match to $f_1(t_1, \Delta t)$ in f_2 by minimizing the cross correlation, i.e. $f_2(t_2, \Delta t)$. See Figure 7.47.
5) Calculate the velocity of the wave $V=d/(t_2-t_1)$.
6) Justification: Determine whether the peak is a slug or a wave. If the translational velocity V is larger than the mixture velocity, the peak is counted as a slug; otherwise, it is counted as a wave.
7) Repeat steps (3)-(6) for the next wave in f_1 until all peaks are determined. See Figure 7.48.

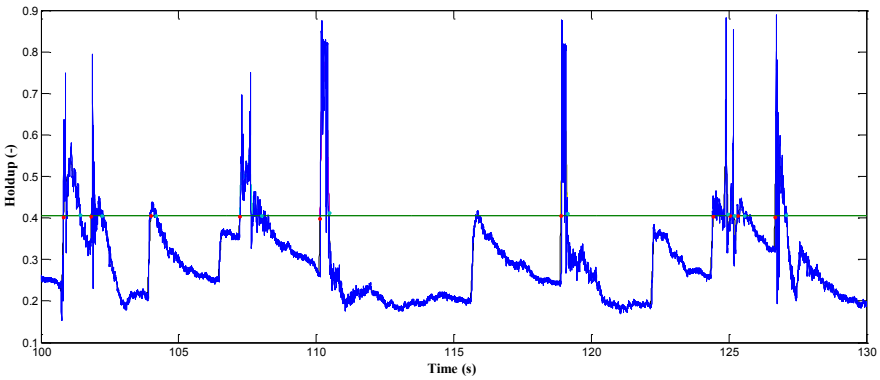

Figure 7.45: Green line represents the liquid holdup threshold to select the major peaks. Usl=0.15m/s, Usg=3m/s.

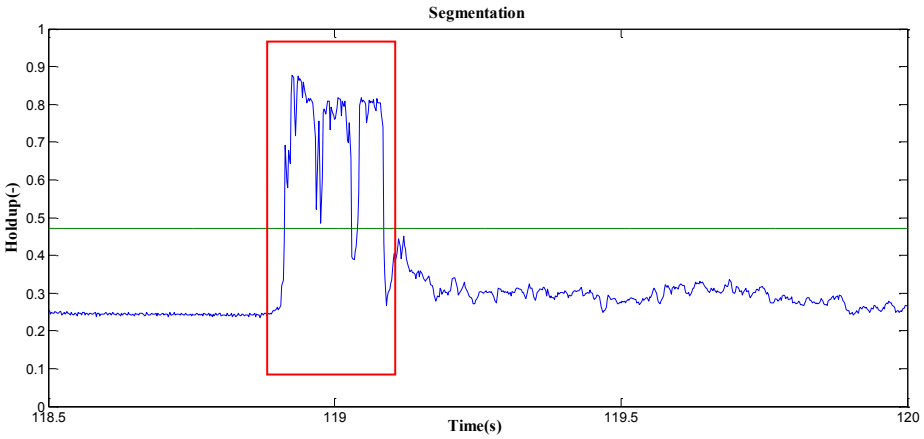

Figure 7.46: A sample of segment is highlighted in red color.

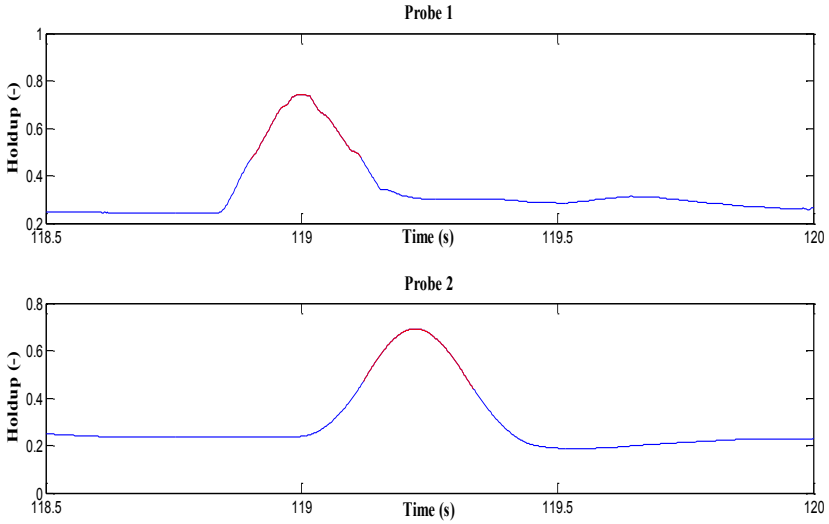

Figure 7.47: The cross-correlation between the holdup peak signals is highlighted in red color.

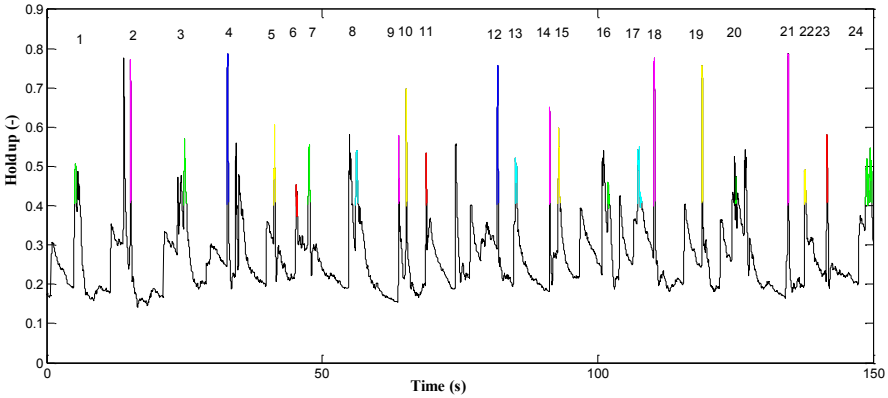

Figure 7.48: Identified slugs via velocity threshold method are highlighted for Usl=0.15m/s, Usg=3m/s.

Figure 7.49 to 7.51 show another two samples of identifying slugs from liquid holdup time trace signals via the velocity discrimination approach. The detail analysis of developed slug frequencies will be discussed in Section 7.8.

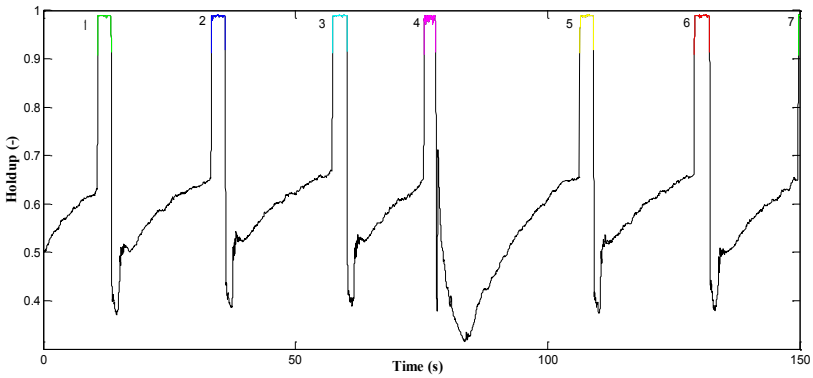

Figure 7.49: Identified slugs via velocity threshold method are highlighted for Usl=0.15m/s, Usg=1m/s.

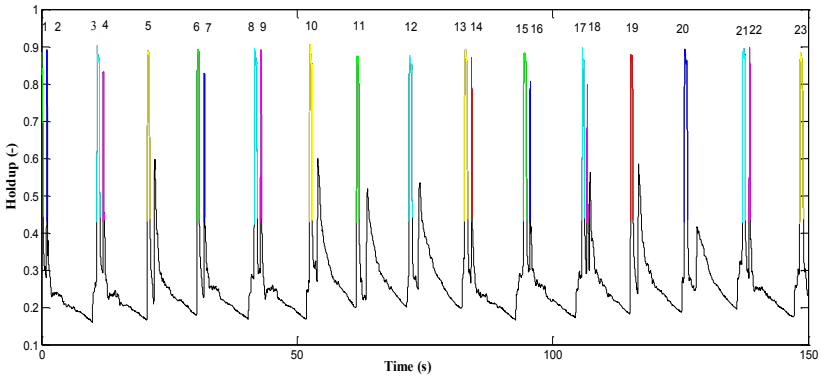

Figure 7.50: Identified slugs via velocity threshold method are highlighted for Usl=0.15m/s, Usg=2m/s.

7.7 Effects of inlet configuration on slug initiation and development

7.7.1 Effect of inlet geometry on LOWPRESS test-section

To study the effect of inlet stratified liquid level height on slug initiation and development, a set of air-oil experiments were carried out with the stratification plate introduced at three different heights namely at h/D of 0.5 (mid-plate), 0.25 (low-plate) and 0.75 (high-plate) respectively. Figure 7.51 shows three cases with the stratification plate inserted at different heights for a superficial liquid velocity of 0.2m/s and superficial gas velocity of 2m/s. A low-plate inlet configuration shifts the slug initiation position the furthest downstream because fluids enter the test-section with a lower liquid level, whereas the high-plate inlet configuration shifts the slug initiation position closest to the entry. These observations indicate that the liquid height is of central importance of slug formation, this is in agreement with the theory suggested by Kordyban and Ranov (1970) that slug precursors can be described as finite amplitude waves whose extent is determined by the proximity of the top wall of the pipe. Figure 7.52 shows the effect of increasing the superficial gas velocity to 3 m/s; with low-plate configuration, the stratified liquid film appears less wavy than the cases with the mid-plate and high-plate configurations. This is because the lower liquid level leads to a lower relative velocity between the gas and liquid, making the interface is more stable.

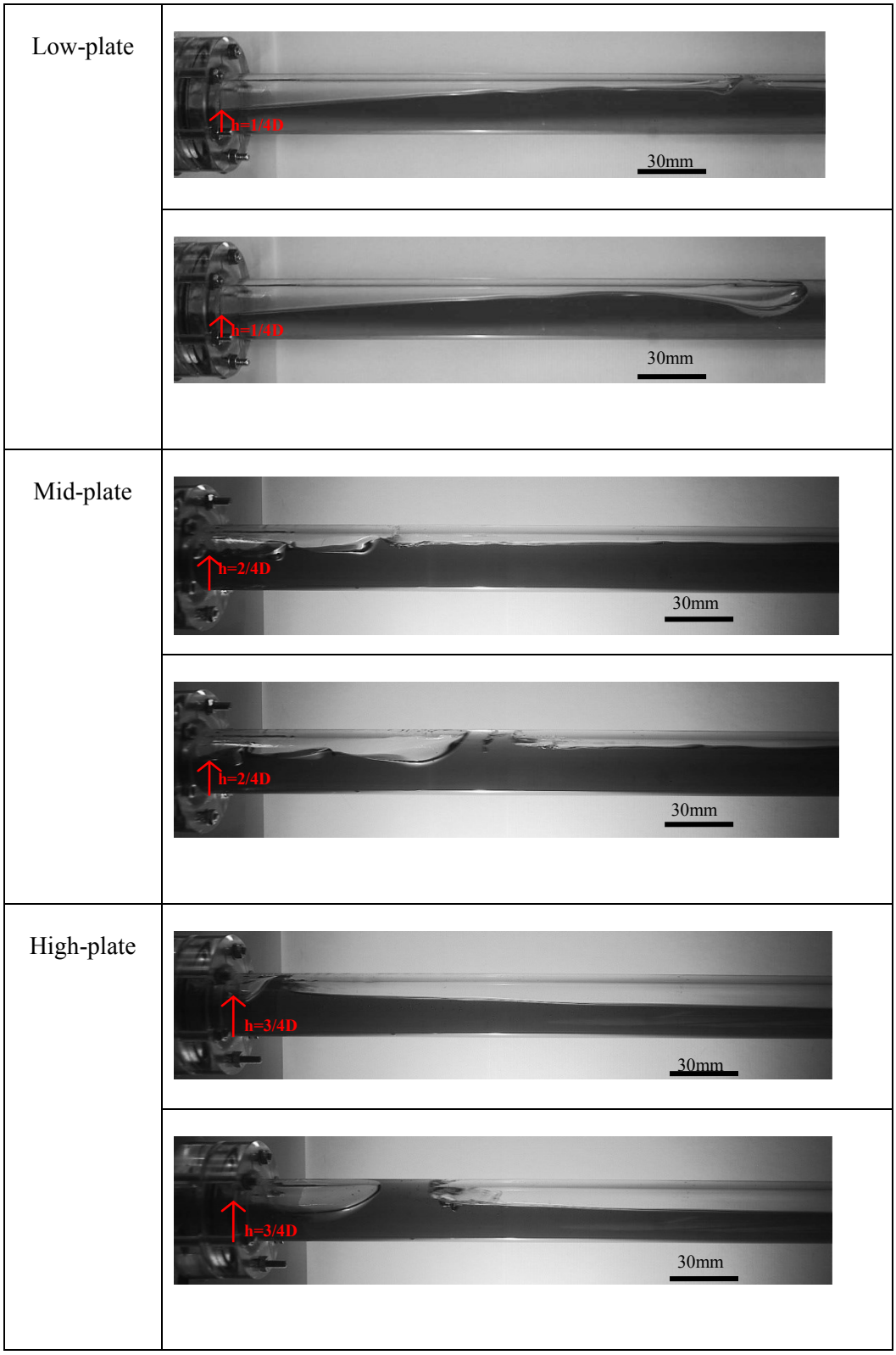

Figure 7.51: A series of images showing slug initiation at at Usl=0.2m/s, Usg=2.0m/s, with low-plate, mid-plate and high-plate.

Low-plate	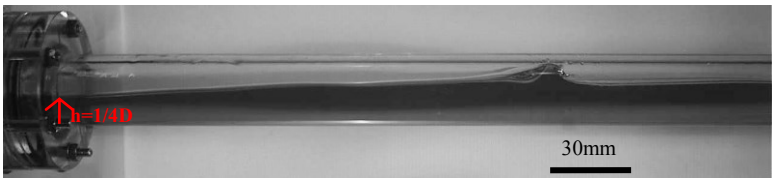
	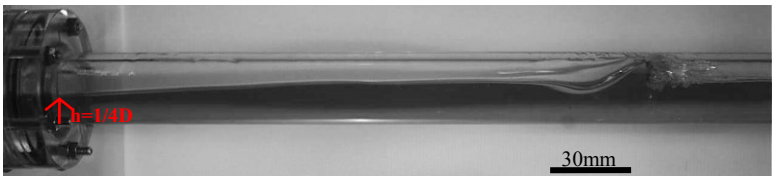
	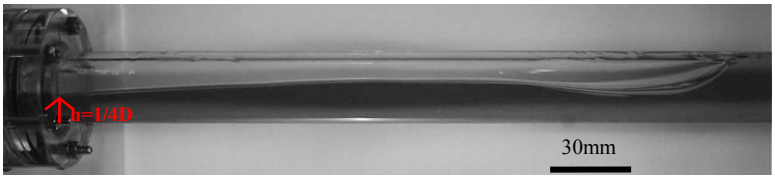
Mid-plate	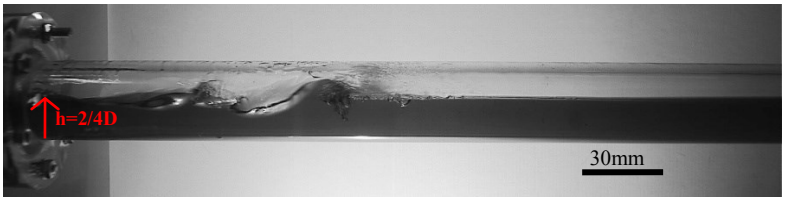
	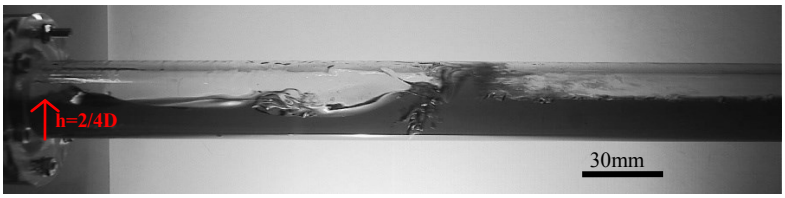
	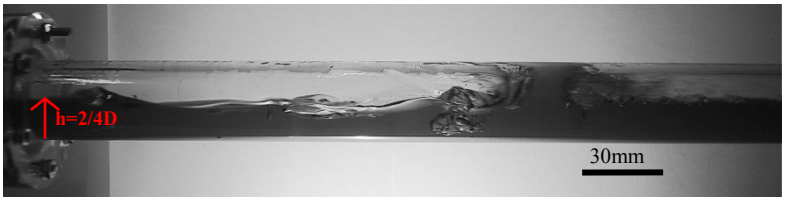

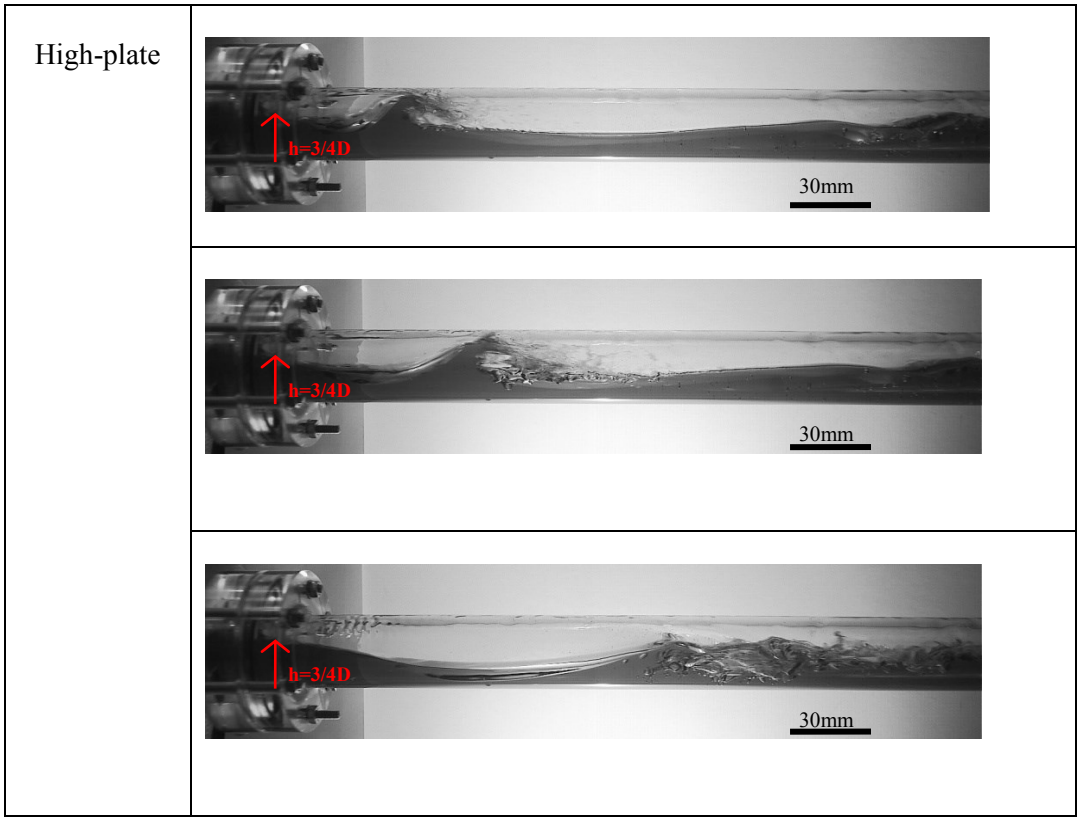

Figure 7.52: A series of images showing slug initiation at Usl=0.2m/s, Usg=3.0m/s, with low-plate, mid-plate and high-plate.

Figure 7.53 to Figure 7.56 shows the distribution of slug frequency along the test-section with different inlet configurations. For those cases in which the inlet contains a stratification plate, the maximum frequency near the pipe inlet is generally more pronounced for the high-plate configurations. As explained in the earlier sections, with higher liquid entry-level, waves can bridge the pipe with greater ease therefore slug precursors are more frequently initiated with high-plate inlet configurations. For cases that made use of a conical reducer at the inlet, the reducer section triggers many slugs in the reducer and at the joint between the reducer and test-section; as a result, a sharp peak in the slug initiation frequency is achieved near the inlet. However, slug precursors formed in the initiation region are not stable and collapse or coalesce fairly quickly with neighbouring waves. Although our results have demonstrated a strong dependence of the slug frequency on the inlet configuration, this dependence becomes progressively weaker with axial distance from the inlet. For sufficiently large axial distances, the eventually the slug frequency becomes fully-developed, asymptoting to approximately the same value regardless of inlet geometry.

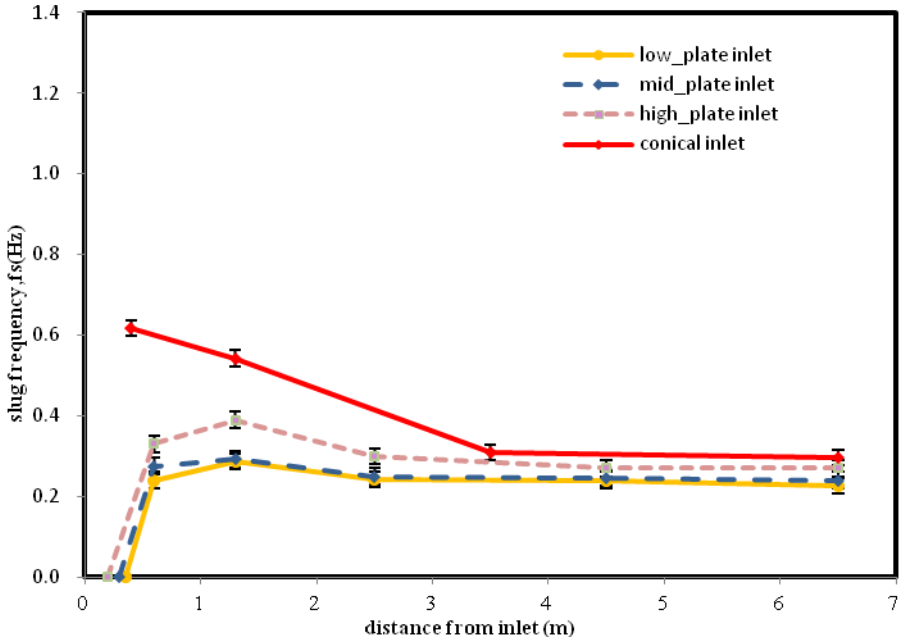

Figure 7.53: Slug frequency distributions with different inlet configurations at Usl=0.1m/s and Usg=2.1m/s, air-oil two-phase flow system.

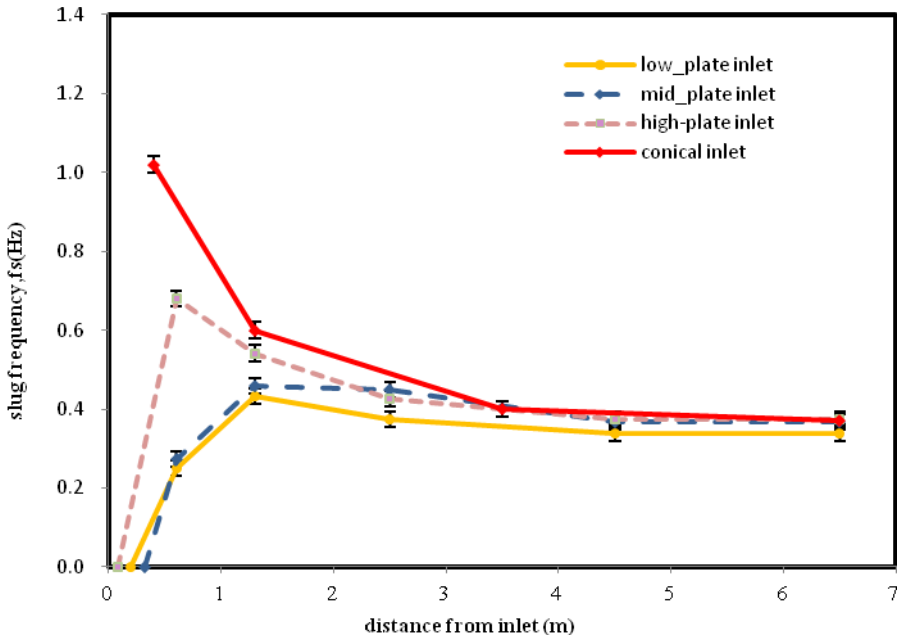

Figure 7.54: Slug frequency distributions with different inlet configurations at Usl=0.15m/s and Usg=2.1m/s, air-oil two-phase flow system.

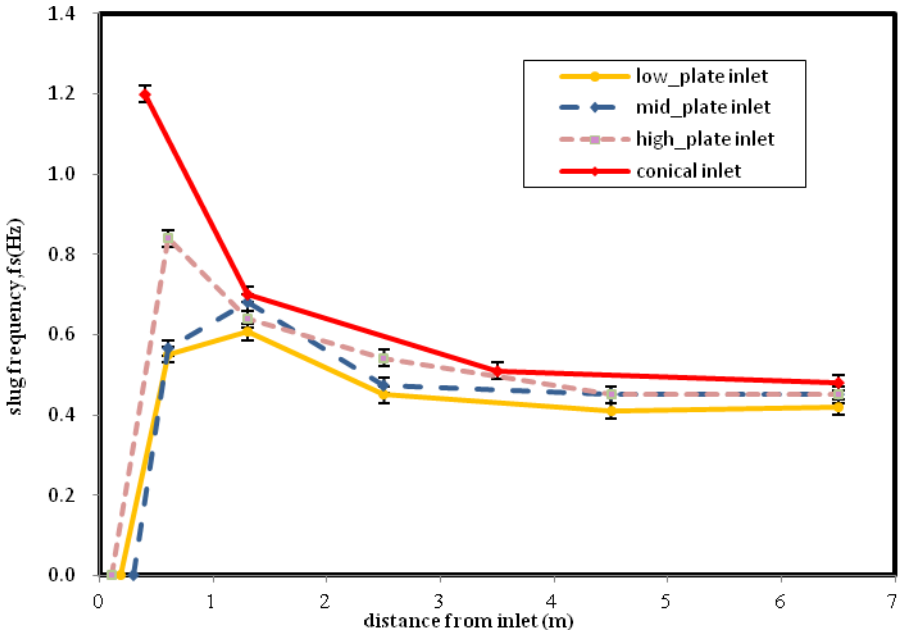

Figure 7.55: Slug frequency distributions with different inlet configurations at Usl=0.2m/s and Usg=2.1m/s.

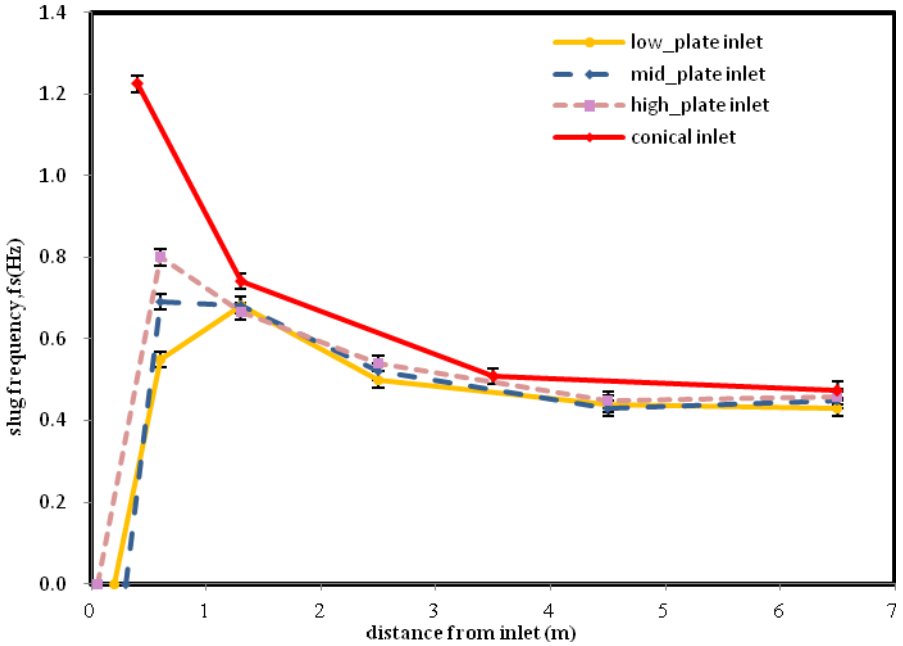

Figure 7.56: Slug frequency distributions with different inlet configurations at Usl=0.2m/s and Usg=3.1m/s.

7.7.2 Effect of inlet geometry on WASP test-section

Experiments on horizontal air-water slug flow were conducted on the WASP facility; as was explained above, these experiments were performed by Dr. C. P. Hale. However, the detailed analysis of the data was carried out by the present author and the data and its analysis are presented here for the first time. The WASP test section was 78 mm in diameter in contrast to the 32 mm test section used in LOWPRESS. For the WASP experiments, a modified separating plate was welded on a stainless steel blind flange at the height of 0.25 of the pipe diameter and then inserted into the WASP "T-junction" inlet. By rotating the blind flange by 180°, a low-plate or high-plate phase separation at the inlet can be obtained.

The output from the traversing beam gamma densitometer located at 35 meters from the inlet was employed to derive the slug frequency data. For a the length of 35 meters from the inlet one would expect the slug flow to become fully-developed hence its frequency should become essentially independent of length (Ujang, 2003). The gamma densitometer was set to record the centerline liquid height for continuous monitoring of flow in the study reported here. It was assumed that the liquid height was constant across the pipe and equal to its value at the tube centre. This assumption allows the calculation of liquid holdup using Eqn.7.5.This conversion of gamma densitometer data logger signals to liquid holdup was conducted using a MATLAB graphics tool, the instantaneous value of liquid height being measured every 40 ms over a sampling time of 300s. A typical slug flow liquid holdup time trace is given in Figure 7.57. When gas is entrained into slugs, the liquid peak is less than unity which means that peaks in signals can represent either a wave or slug. Since only one location has been monitored, the velocity discrimination approach cannot be applied in this case. A heuristic method was developed to overcome this problem. Manolis (1995) proposed a threshold value is calculated as a constant multiple of the value predicted by the slug body holdup correlation of Gregory et al. (1978), see Eqn. 2.160. The constant value of 2/3 was evaluated from his analysis of data from the WASP facility. This method has been proved to identify slugs reasonably accurately by several WASP operators (King, 1998; Hale, 2000, Pan, 2010). As mentioned earlier, a video was recorded for each experimental run from the transparent visualisation section located next to the gamma densitometer. The recording of the movie is synchronized with the gamma densitometer. To validate Manolis (1995) method, the number

of slugs were counted by looking at each video and compared to liquid peaks from holdup traces. A good agreement between two methods was obtained when the constant value previously employed by Manolis (1995) was replaced by 0.85. The expected error is ±6 counts over 300 seconds which means approximately ±0.02 Hz for slug frequency. Figure 7.58 illustrates the process of identifying the slug body from holdup traces.

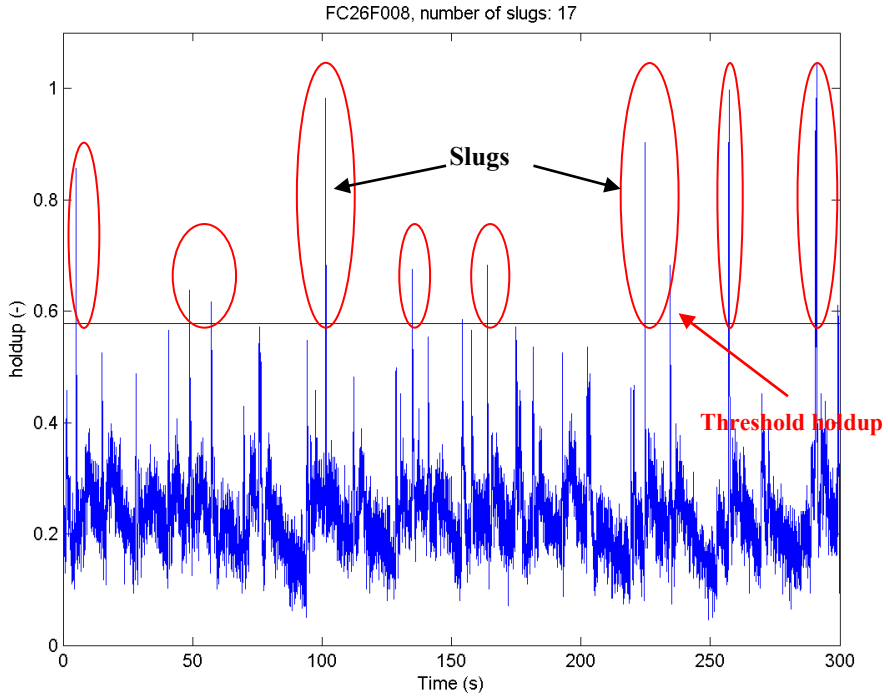

Figure 7.57: Liquid hold-up peaks above threshold holdup are considered as indication of slugs according to Manolis (1995) criterion.

Figure 7.58 shows WASP air-water slug frequency data plotted against superficial air velocity at superficial liquid velocities of 0.2, 0.4, 0.6 m/s. For each combination of fluid velocities, lines representing the measurements with low-plate and high-plate inlet configurations are more or less superimposed to each other, indicating slug frequencies at the developed region are not affected by the inlet phase separation height.

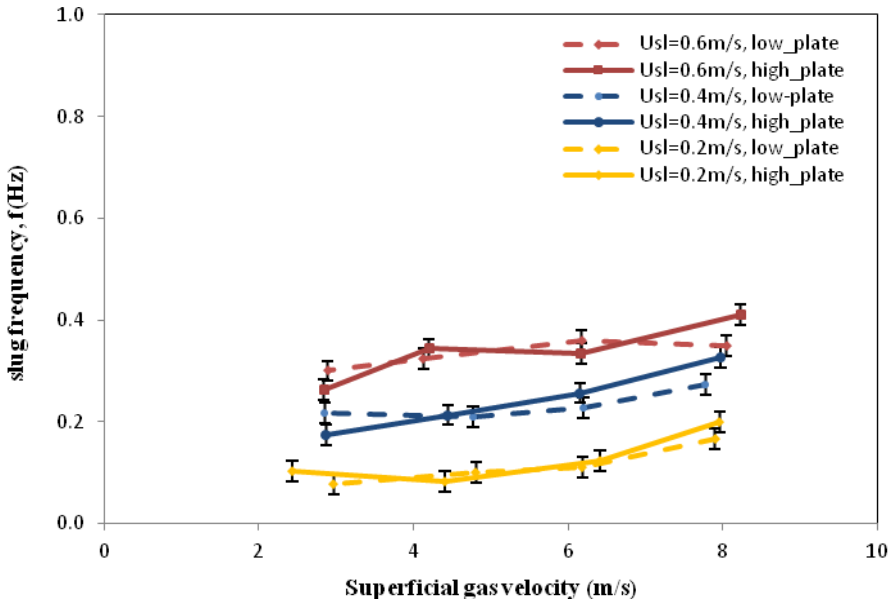

Figure 7.58: Comparison of the low-plate and high-plate slug frequency at constant superficial liquid velocities of 0.2m/s, 0.4m/s and 0.6m/s, with varying gas velocities.

The probability density functions (pdf) of the time intervals between slugs, as measured from the WASP data are illustrated in Figure 7.59 to Figure 7.61. For the same fluid velocities, the distributions of time intervals between slugs for low-plate and high-plate inlet configurations tend to a similar pattern. It can be seen that liquid superficial velocity has a stronger influence on the distribution of slug arrival intervals than the gas superficial velocity. For the largest liquid superficial velocities, more slugs are observed during the sampling time hence giving a better statistical evaluation of time interval distribution, time interval between slugs are mostly less than10s. For the smallest liquid superficial velocities, the time intervals between the slugs are more scattered, and longer time intervals are required between slugs due to the smaller liquid replenishment rate.

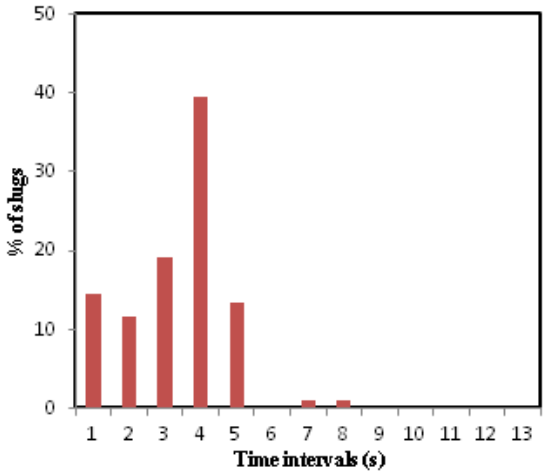

a) Usl= 0.57m/s, Usg=8.05m/s, low-plate

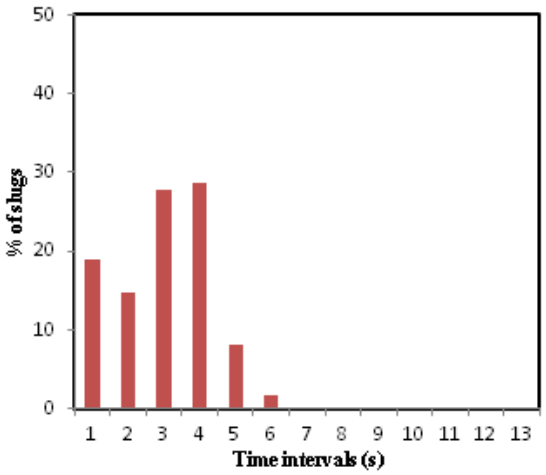

b) Usl=0.56m/s, Usg=8.23m/s, high-plate

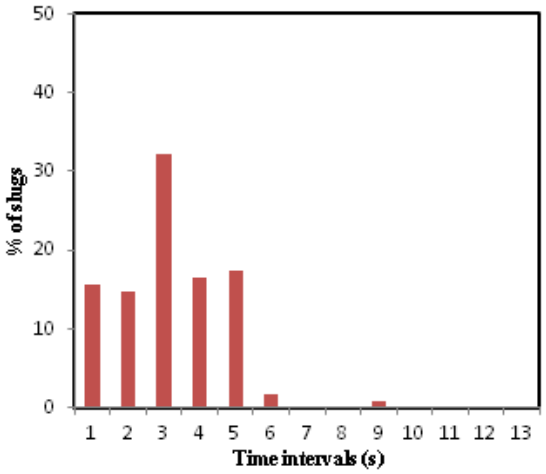

d) Usl= 0.59m/s, Usg=6.17m/s, low-plate

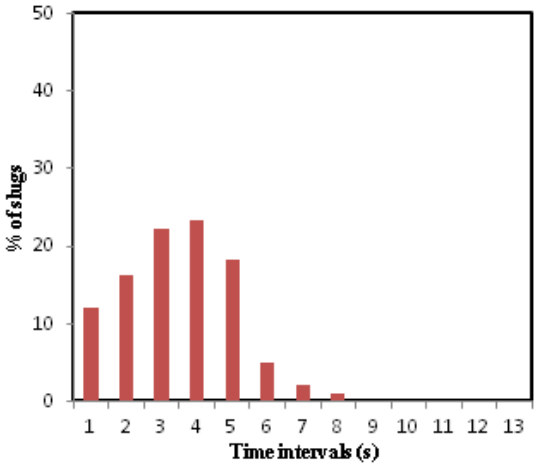

c) Usl= 0.55m/s, Usg=6.17m/s, high-plate

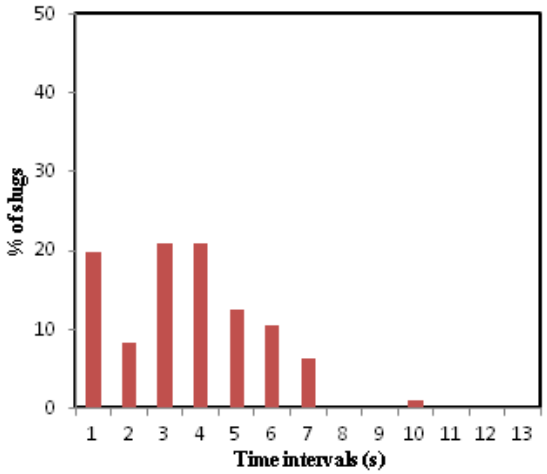

f) Usl= 0.56m/s, Usg=4.13m/s, low-plate

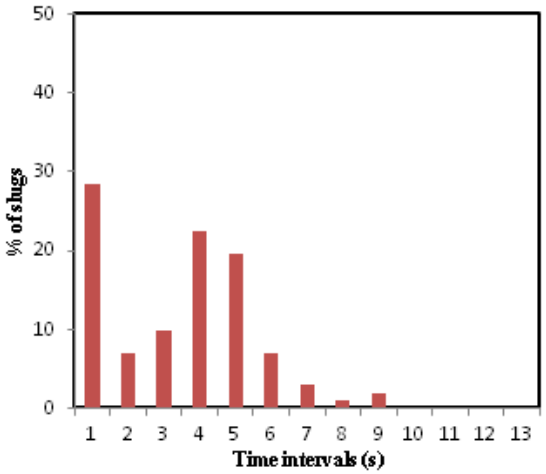

e) Usl= 0.57m/s, Usg=4.20m/s, high-plate

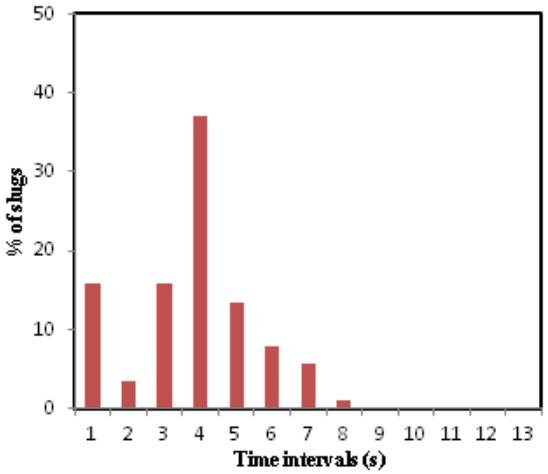

h) Usl= 0.57m/s, Usg=2.89m/s, low-plate

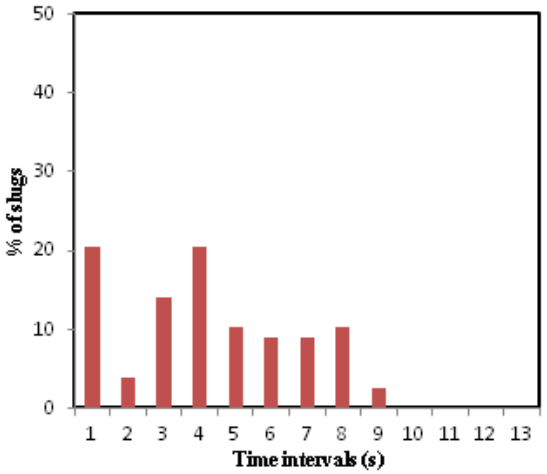

g) Usl= 0.54m/s, Usg=2.84m/s, high-plate

Figure 7.59: Distribution of time intervals between slugs for liquid superficial velocity around 0.6m/s, varying the gas superficial velocity and inlet configuration.

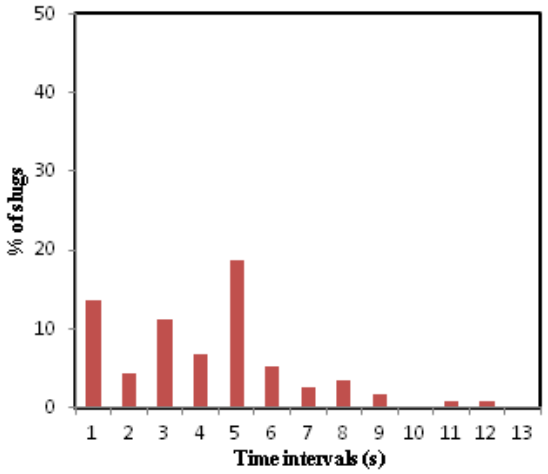

a) Usl= 0.40m/s, Usg=7.78m/s, low-plate

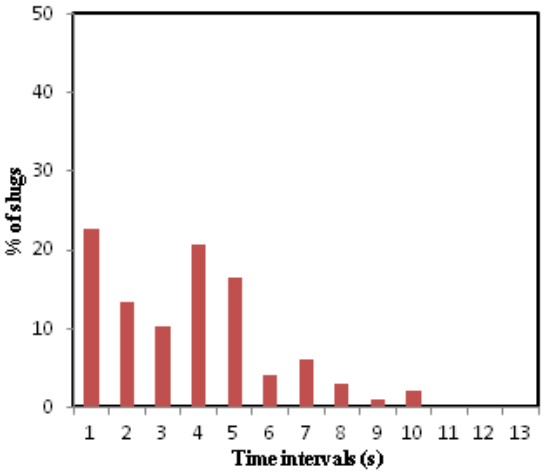

b) Usl=0.40m/s, Usg=7.94m/s, high-plate

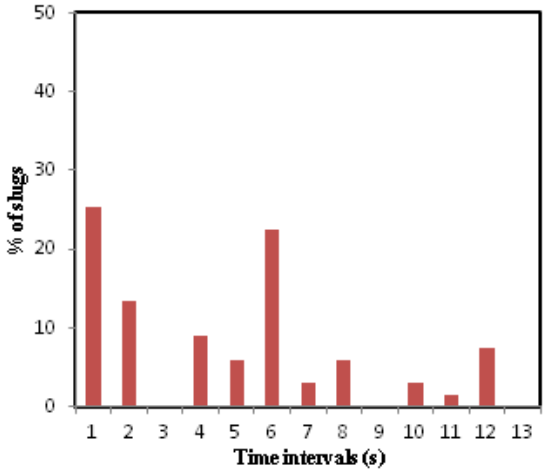

d) Usl= 0.39m/s, Usg=6.20m/s, low-plate

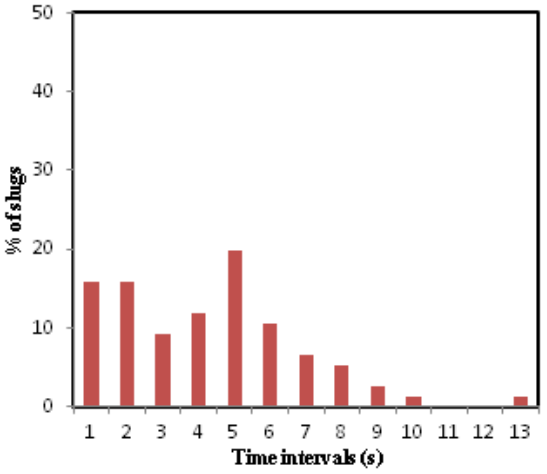

c) Usl= 0.41m/s, Usg=6.16m/s, high-plate

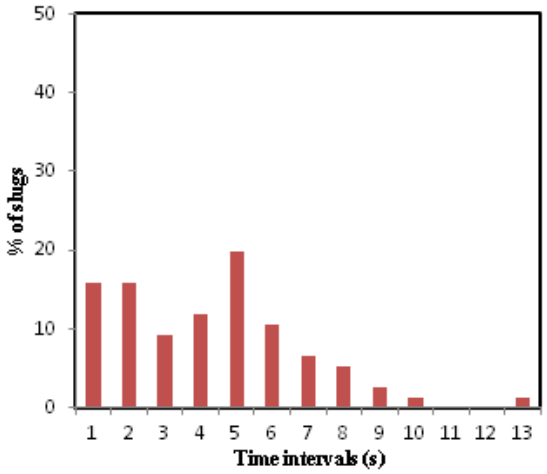

e) Usl= 0.37m/s, Usg=4.77m/s, low-plate

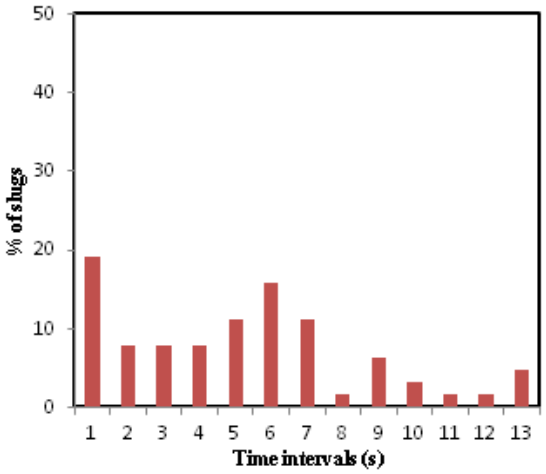

f) Usl= 0.39m/s, Usg=4.45m/s, high-plate

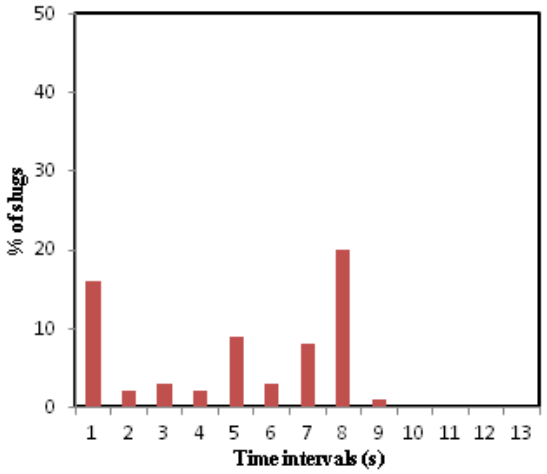

h) Usl= 0.41m/s, Usg=2.85m/s, low-plate

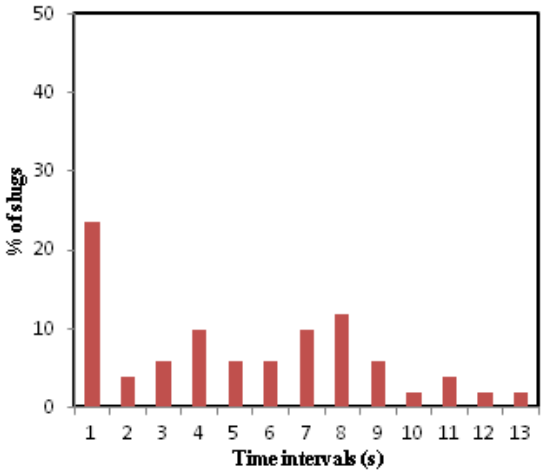

g) Usl= 0.38m/s, Usg=2.87m/s, high-plate

Figure 7.60: Distribution of time intervals between slugs at 35m from inlet for constant liquid superficial velocity of 0.4m/s, varying the gas superficial velocity and inlet configuration.

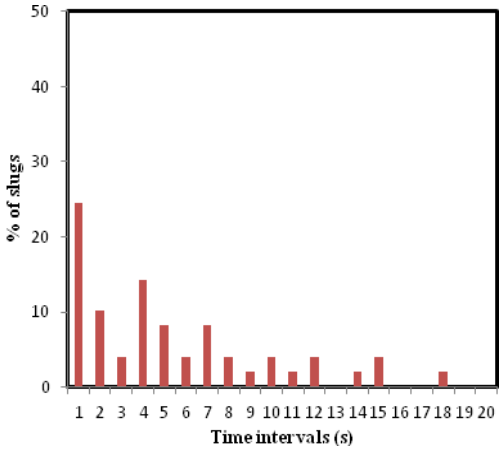

a) Usl= 0.22m/s, Usg=7.90m/s, low-plate

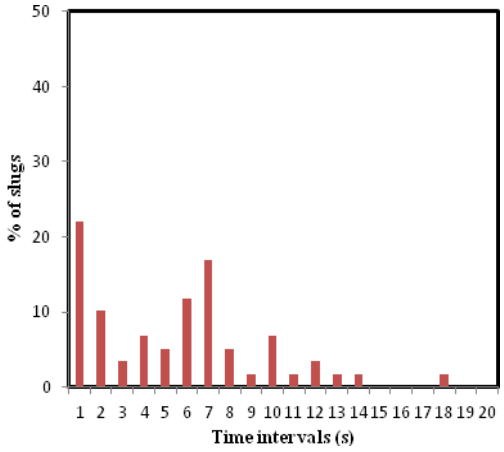

b) Usl= 0.21m/s, Usg=7.97m/s, high-plate

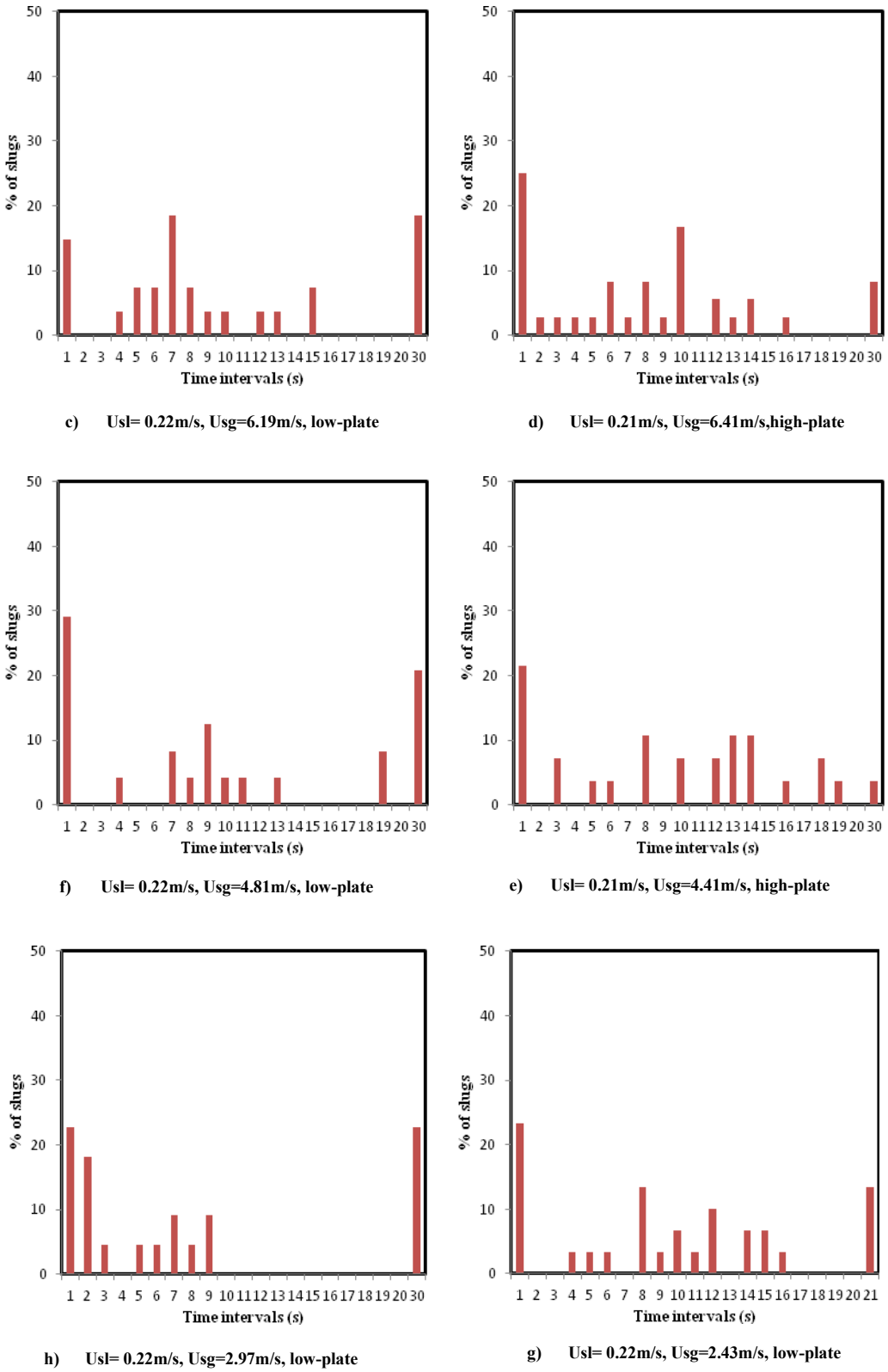

Figure 7.61: Distribution of time intervals between slugs at 35m from inlet for constant liquid superficial velocity of 0.2m/s, varying the gas superficial velocity and inlet configuration.

7.8 Mean liquid holdup

Liquid holdup values obtained in the fully-developed regions in both the LOWPRESS test-section and the WASP test-section will be discussed in this section.

7.8.1 Mean liquid holdup measurements obtained from the LOWPRESS facility

Images were obtained from a high-speed camera (I-SPEED 3, Olympus) which was placed at a position of 6.5m from the beginning of the test-section. The position of the liquid-gas interface at a defined axial location was obtained from the images using a MATLAB routine according to the pixel intensity, as shown in Figure 7.62. The spatial resolution of the images is 0.17 mm/pixel. The measured liquid height was then converted to a liquid holdup value using Eqn. 7.5 by assuming a flat, symmetric gas-liquid interface. The liquid holdup at this axial location is then averaged over time for 150s to yield a mean liquid holdup. At relatively high gas superficial velocities, i.e. above 3m/s, gas bubbles are entrained in the liquid and slug shapes are complex, which increases the measurement error of the liquid interface. However, this error is negligible because the time of slug event is short compared to the overall sampling time, as shown in Figure 7.63.

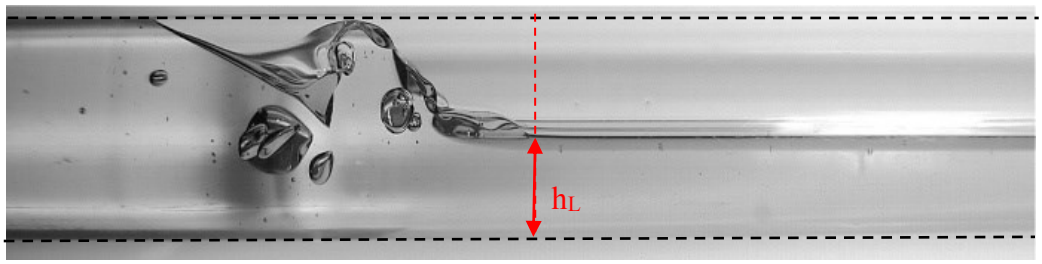

Figure 7.62: Measuring liquid height and holdup using MALTAB code.

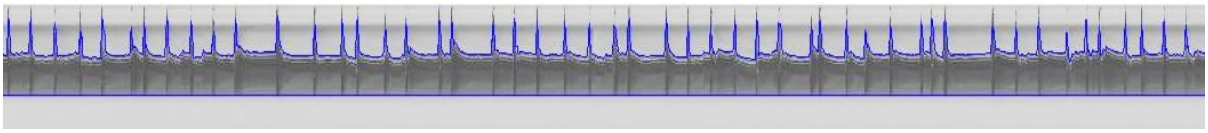

Figure 7.63: A time sequence of gas-liquid interface obtained using MALTAB code at a location of 6.7m from the inlet.

Figure 7.64 to Figure 7.66 show the comparisons of mean liquid holdup with the low-plate, mid-plate and high-plate inlet configurations at constant superficial oil velocity. In each graph, the lines representing different level of inlet phase separation are almost superimposed on each other, indicating the mean liquid holdup measured in the fully-developed region is independent on the inlet geometry. Figure 7.67 plots the mean liquid holdup data as a function of gas velocity for lines of constant superficial oil velocity. As expected, the mean liquid holdup decreases with increasing gas superficial velocity and it increase slightly with increasing oil superficial velocity. Figure 7.68 plots the mean liquid holdup data as a function of gas velocity for lines of constant superficial water velocity. For the same phase velocities, though similar trends are observed for both systems the mean liquid holdup is in general slightly higher with air-oil flow than air-water, as oil is the more viscous fluid.

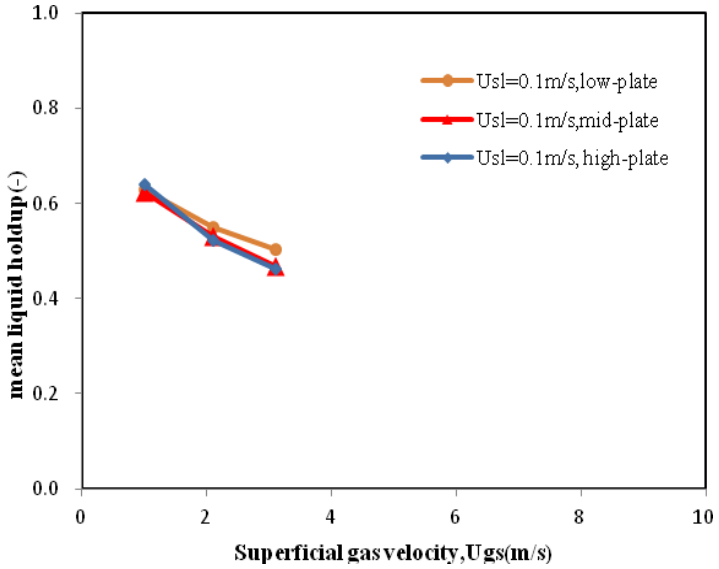

Figure 7.64: Comparison of mean liquid holdup for LOWPRESS air-oil slug flow with the low-plate, mid-plate and high-plate inlet configurations at constant superficial liquid velocity of 0.1m/s.

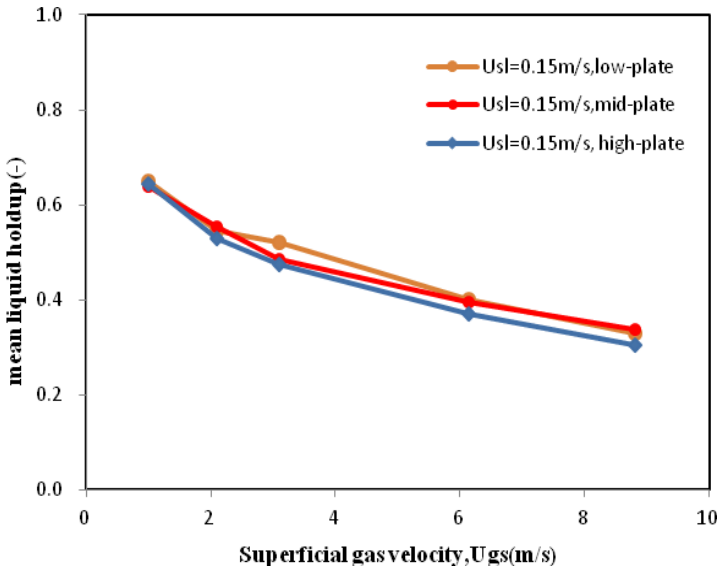

Figure 7.65: Comparison of mean liquid holdup for LOWPRESS air-oil slug flow with the low-plate, mid-plate and high-plate inlet configurations at constant superficial liquid velocity of 0.15m/s.

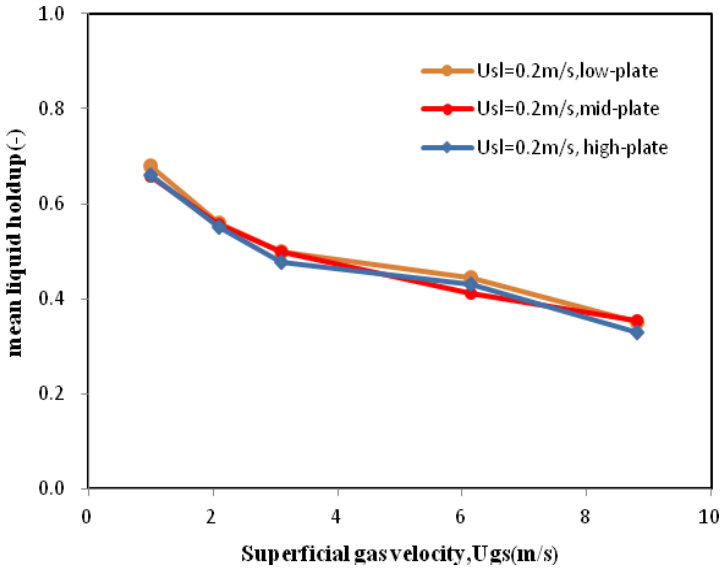

Figure 7.66: Comparison of mean liquid holdup for LOWPRESS air-oil slug flow with the low-plate, mid-plate and high-plate inlet configurations at constant superficial liquid velocity of 0.2m/s.

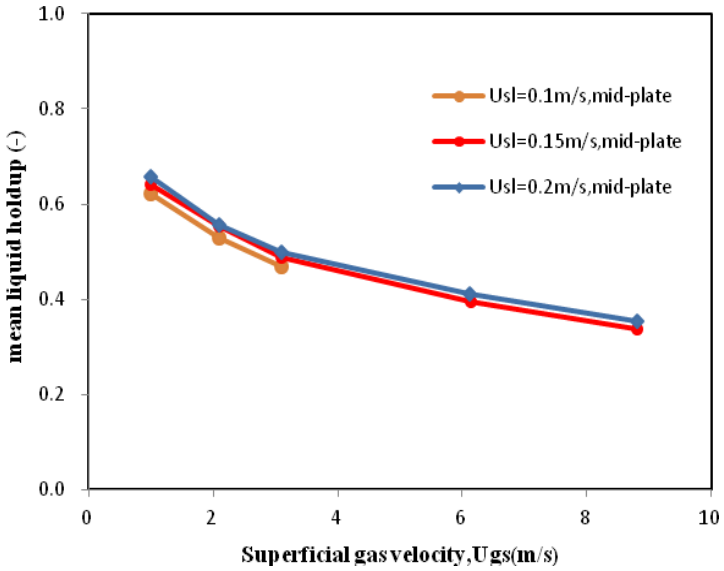

Figure 7.67: Variation of the mean liquid holdup for LOWPRESS air-oil slug flow as a function of the gas superficial velocity with the superficial liquid velocity varying parametrically.

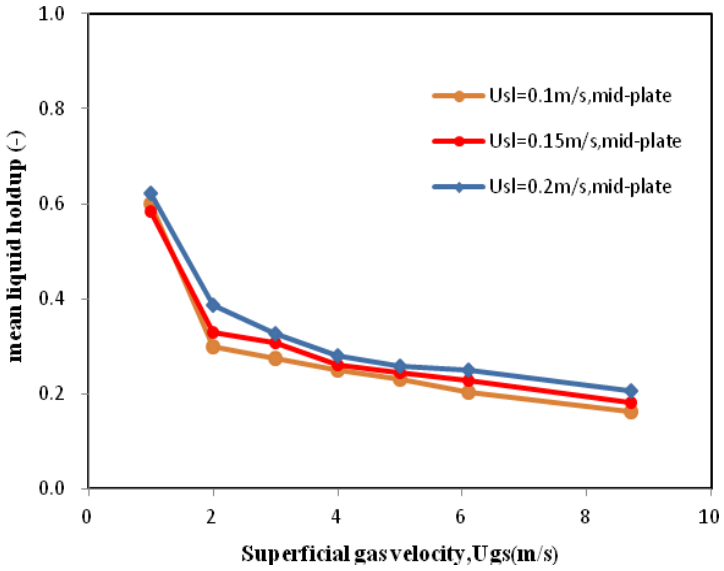

Figure 7.68: Variation of the mean liquid holdup for LOWPRESS air-water lug flow as a function of the gas superficial velocity with the superficial liquid velocity varying parametrically.

7.8.2 Mean liquid holdup measurements obtained from WASP facility

In order to obtain the mean holdup values from WASP measurements, gamma densitometer measurements were made at a fixed location, namely vertically through the centre of the pipe.

The measured liquid height was then converted to a liquid holdup value by assuming a flat, symmetric gas-liquid interface and applying the necessary geometric relation (Eqn.7.5). The time sequence of values of the holdup at the central position is then averaged to yield a mean liquid holdup. The measurement error in mean liquid holdup is estimated as ± 5 %.

Figure 7.69 to Figure 7.71 plot the mean liquid holdup data for WASP air-water slug flow as function of superficial gas velocity, with lines corresponding to low-plate and high-plate inlet configuration. The lines for the two plate positions are almost superimposed on each other, indicating the inlet configuration has no effect on the mean liquid hold up in the fully developed flow. Figure 7.73 shows the plots of mean liquid holdup as a function of superficial gas velocity for lines of constant liquid velocity. It can be seen that the mean liquid holdup decreases with increasing gas velocity due to increased gas content in the slugs and the thinning of the film between the slugs. On the other hand, it increases slightly with increasing liquid velocity.

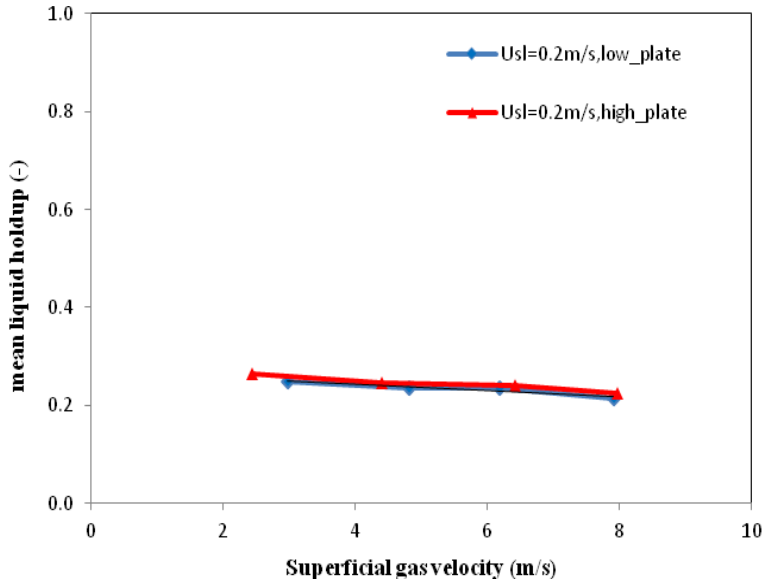

Figure 7.69: Comparison of mean liquid holdup for WASP air-water slug flow with the low-plate and high-plate inlet configurations at constant superficial liquid velocity of 0.2m/s.

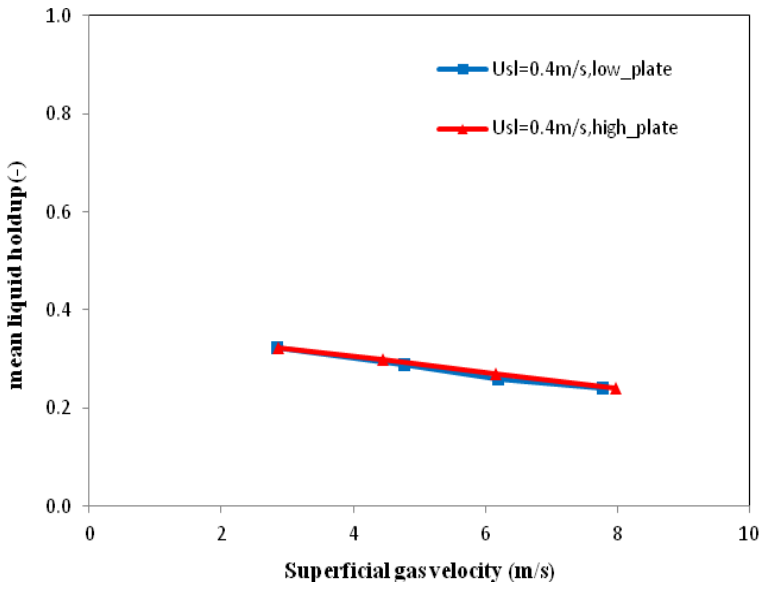

Figure 7.70: Comparison of mean liquid holdup for WASP air-water slug flow with the low-plate and high-plate inlet configurations at constant superficial liquid velocity of 0.4m/s.

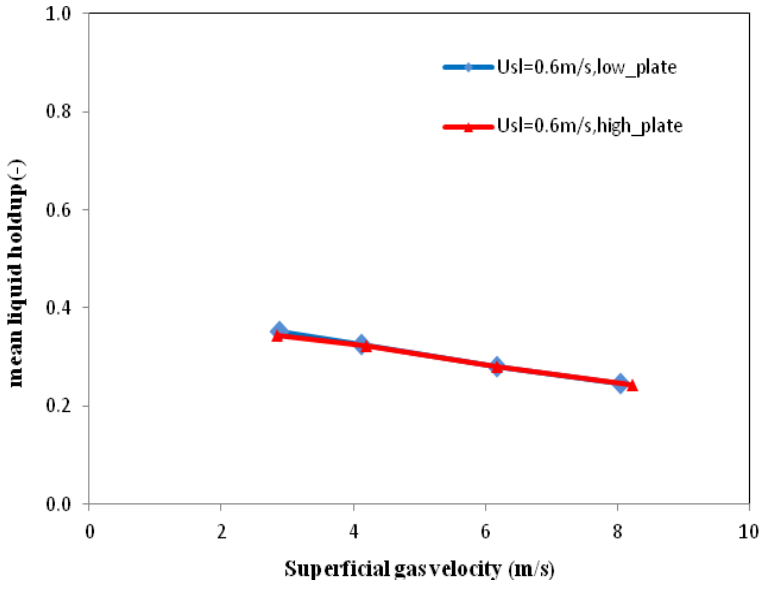

Figure 7.71: Comparison of mean liquid holdup for WASP air-water slug flow with the low-plate and high-plate inlet configurations at constant superficial liquid velocity of 0.6m/s.

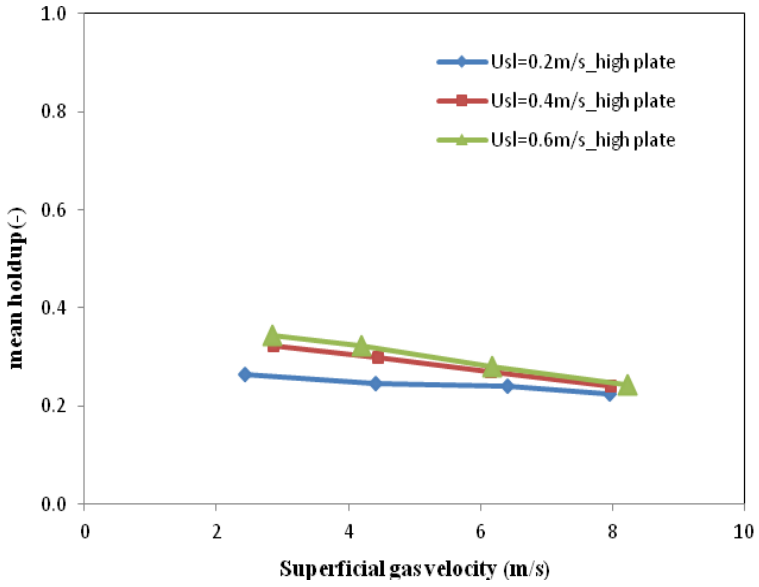

Figure 7.72: Variation of the mean liquid holdup for WASP air-water slug flow as a function of the gas superficial velocity with the superficial liquid velocity varying parametrically.

7.9 Fully-developed slug frequency

7.9.1 Slug frequency versus superficial liquid velocity and superficial gas velocity

In this section, slug frequency measured near the exit of the LOWPRESS and WASP test-sections will be discussed. Plots of slug frequency as a function of superficial liquid velocity for lines of constant gas velocity are shown in Figure 7.74 to Figure 7.76 for the LOWPRESS air-oil, the LOWPRESS air-water and the WASP air-water data respectively. It can be seen that the slug frequency increases with superficial liquid velocity, which is similar to the behaviour observed by several researchers investigating horizontal pipelines (Gregory & Scott,1969; Manolis,1995; Hale, 2000, Pan, 2010). For a constant gas velocity, as the liquid flow-rate increases, the volume of liquid passing through a given point in the channel per unit time will increase. Therefore, the level from which the wave would have to bridge the pipe is increased facilitating slug-formation.

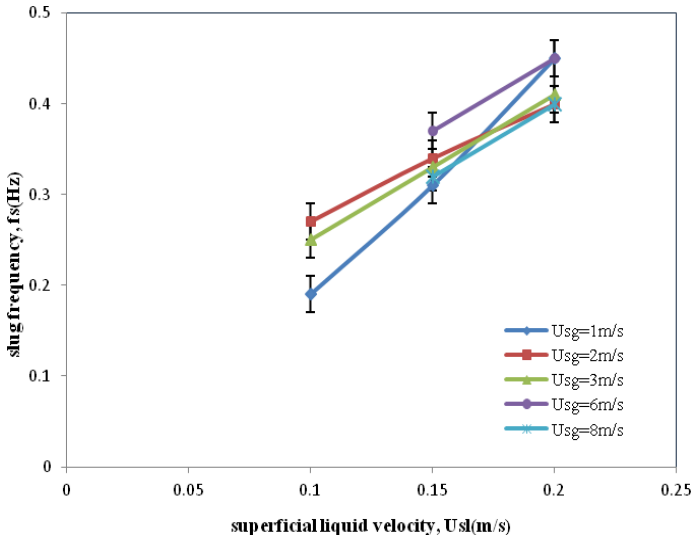

Figure 7.73: Slug frequency as a function of superficial liquid velocity for constant superficial gas velocity generated from LOWPRESS air-oil data.

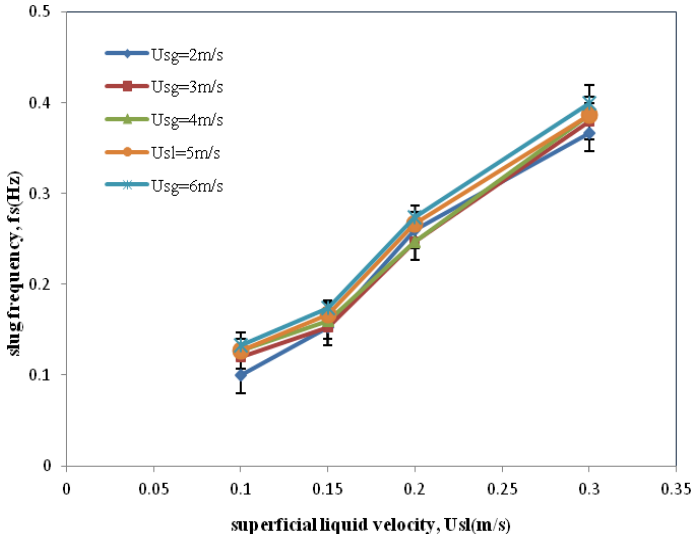

Figure 7.74: Slug frequency as a function of superficial liquid velocity for constant superficial gas velocity generated from LOWPRESS air-water data.

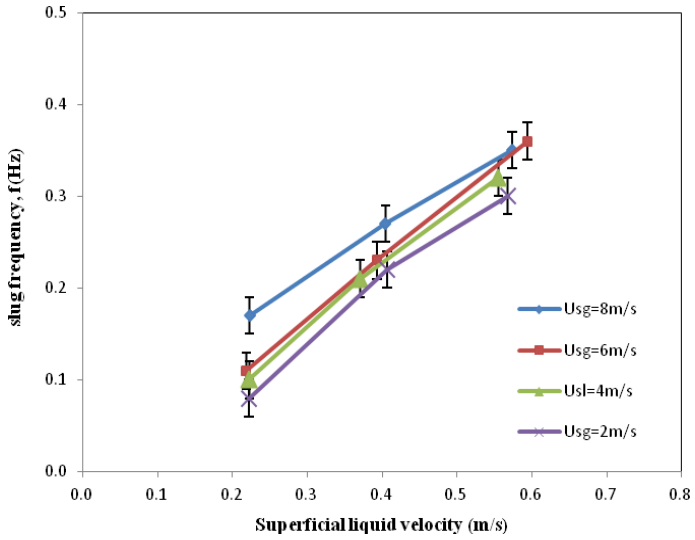

Figure 7.75: Slug frequency as a function of superficial liquid velocity with the for superficial gas velocity varying parametrically generated from WASP air-water data.

Figures 7.77, 7.78 and 7.79 show the LOWPRESS air-oil, the LOWPRESS air-water and the WASP air-water plotted against superficial gas velocity with the superficial liquid velocity varying parametrically. As will be seen, slug frequency can increase slightly or decrease slightly with superficial gas velocity depending on the gas and liquid superficial velocities but, in general, the effect of superficial gas velocity is rather small.

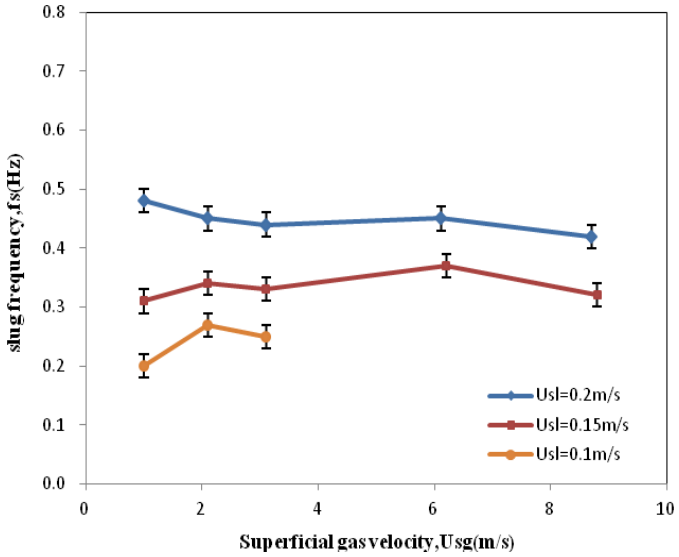

Figure 7.76: Slug frequency as a function of superficial gas velocity with the superficial oil velocity varying parametrically (generated from LOWPRESS air-oil data).

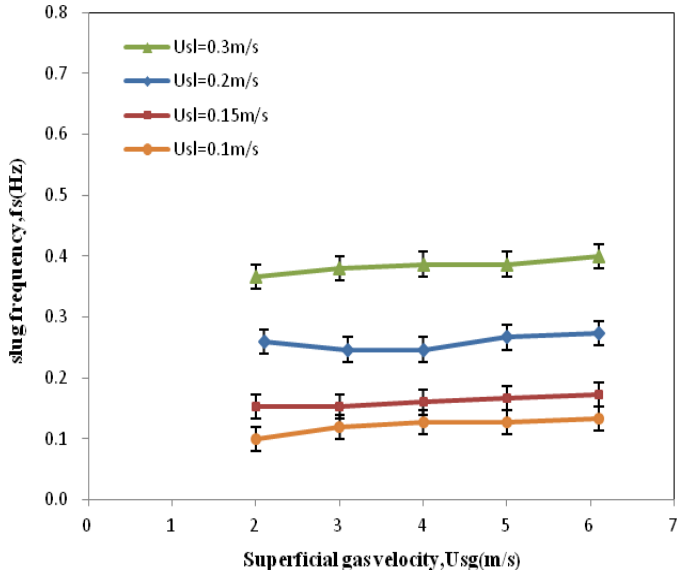

Figure 7.77: Slug frequency as a function of superficial gas velocity with the for superficial gas velocity varying parametrically (generated from LOWPRESS air-water data).

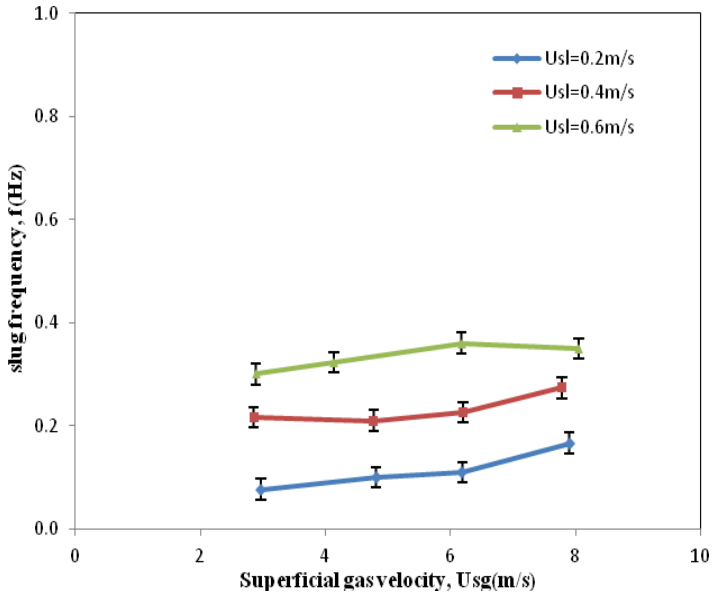

Figure 7.78: Slug frequency as a function of superficial gas velocity with the for superficial gas velocity varying parametrically generated from WASP air-water data.

7.9.2 Dimensionless slug frequency

According to previous work (Greskovich & Shrier, 1971; Heywood & Richardson, 1979; Manolis, 1995; Gokcal, 2009), the slug frequency, *f*, is a function of several parameters,

mainly the superficial phase velocities, liquid viscosity, pipe diameter and inclination and system pressure. The test-sections of the LOWPRESS and WASP facilities are horizontal and all the experiments were performed at atmospheric pressure. Therefore, the main variables for the two experiments are pipe diameter, liquid viscosity, and phase superficial velocities. A dimensionless frequency is introduced as $F = fD/U_m$ (Al-Safran, 2008; Schulkes, 2011) where U_m is the mixture velocity; the latter is chosen since it is known that the slug front propagation velocity is proportional to the this quantity (Bendiksen, 1984). Previous experimental observations indicate that the dimensionless frequency can be correlated as a function of non-slip liquid fraction which is equal to the ratio of superficial liquid velocity to sum of superficial liquid velocity and superficial gas velocity, U_{sl}/U_m (Woods, 2006). To illustrate this relationship, a plot of the dimensionless slug frequency as a function of non-slip liquid fraction is shown in Figure 7.80. It can be seen that the dimensionless slug frequency increases with increasing non-slip liquid fraction for both the LOWPRESS and WASP data. For the same non-slip liquid fraction, the dimensionless slug frequency values for LOWPRESS air-water data and WASP air-water data are similar, whereas the values for LOWPRESS air-oil date are generally higher than air-water data, indicating the dimensionless slug frequency increases with the increasing liquid viscosity. This is again highlights the importance of the liquid viscosity.

Gokcal (2009) studied the effect of liquid viscosity by performing horizontal slug flow at oil viscosities between 0.181-0.589 Pa.s. His experimental results reveal dimensionless slug frequency increases with increasing non-slip liquid holdup and liquid viscosity, and this is consistent qualitatively with the present data.

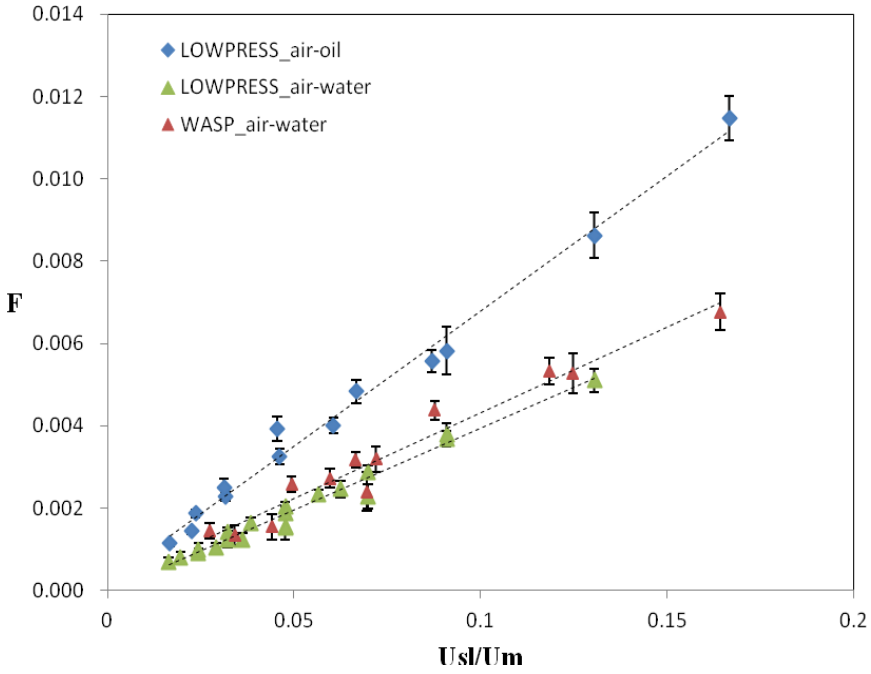

Figure 7.79: Plot of dimensionless frequency F as a function of non-slip liquid fraction.

7.10 Comparison of measured slug frequency with published correlations

The slug frequency data have been compared with a number of well-known empirical correlations which were summarized in Chapter 2. The correlations of Gregory & Scott (1969), Heywood & Richardson (1979), Tronconi (1990), Hill & wood (1990) 1, 2, Nydal (1991) and Manolis (1995), Zabaras (2000), Al-Safran (2008), Gokcal (2008) and Schulkes (2011) have been used in these comparisons. Table 7.4 gives the summary of the experiments for derivation of various slug frequency correlations.

Table 7.4: Summary of the slug frequency correlations and the corresponding experimental conditions. (see Chapter2).

Researcher	Correlation	Pipe diameter (mm)	Fluid system	Liquid Viscosity (cP)	Pressure (bar)
Gregory & Scott (1969)	$f_s = 0.0266\left[\frac{U_{SL}}{gD}\left(\frac{19.75}{U_{mix}} + U_{mix}\right)\right]^{1.2}$	19,35	CO_2/ Water	1	1
Heywood & Richardson (1979)	$f_s = 0.0434\left[\frac{U_{SL}}{U_{mix}}\left(\frac{2.02}{D} + \frac{U_{mix}^{\ 2}}{gD}\right)\right]^{1.06}$	42	Air/Water	1	1
Hill & Wood (1990) correlation 1	$f_s = \frac{0.275}{3600}\frac{U_{mix}}{D}e^{2.68H_L}$	50	Air/Water	1	1
Hill & Wood (1990) correlation 2	$f_s = \frac{2.74}{3600}\frac{H_L}{1-H_L}\frac{U_{GE}-U_{LE}}{D}$	150-590	Air/Water	1	1
Nydal (1991)	$f_s = 0.088\frac{(1.5+U_{SL})^2}{gD}$	31-90	Air/Water	1	1
Manolis (1995)	$f_s = 0.0037\left[\frac{U_{SL}}{gD}\left(\frac{25+U_{mix}}{U_{mix}}\right)\right]^{1.8}$	78	Air/water Air/Oil	1-50	1-14
Zabaras (1999)	$f_s = 0.0266\left[\frac{U_{SL}}{gD}\left(\frac{19.75}{U_{mix}} + U_{mix}\right)\right]^{1.2} \times\left(0.836 + 2.75\sin^{1/4}(\theta)\right)$	102	Air/water	1	1

Al-Safran (2008)	$Ln(f_s) = 0.8 + 1.53Ln(U_{SL}) + 0.27\left(\frac{U_{SL}}{U_{mix}}\right) - 34.1(D)$	50.8	Air/Oil	1	10.2
Gokcal (2009)	$f_s = 2.816\frac{U_{SL}}{D}N_\mu^{\ 0.612}$ $N_\mu = \mu_L / (D^{3/2}\sqrt{\rho_L(\rho_L - \rho_G)g})$	50.8	Air/Oil	181-589	1
Schulkes (2011)	$f_s = \frac{U_{mix}}{D}\Psi(a)\times\Phi(\mathrm{Re}_L)\times\Theta(\theta, Fr)$ $\Psi(a) = 0.016\frac{U_{SL}}{U_{mix}}(2 + 3\frac{U_{SL}}{U_{mix}})$ $\Phi(\mathrm{Re}_L) = 12.1\mathrm{Re}_L^{-0.37}\ for\ \mathrm{Re}_L < 4000$ $\Phi(\mathrm{Re}_L) = 1 for\ \mathrm{Re}_L \geq 4000$ $\Theta(\theta, Fr) = 1 + \frac{2}{Fr}\mathrm{sgn}(\theta)\sqrt{\lvert\theta\rvert}$ $for \lvert\theta\rvert \leq 0.17$ $\Theta(\theta, Fr) = \frac{1.8}{Fr}\times(0.6 + 2\theta - \theta^2)$ $for\ \theta > 0.17$	78	Gas/Oil	33-165	10-50

Figure 7.81 and Figure 7.82 show comparisons of the prediction of the Gregory & Scott (1969) correlation with the LOWPRESS air-oil and air-water slug frequency data respectively. For the case of constant superficial gas velocity, the correlation predicts that the air-water and air-oil slug frequency increases with increasing liquid superficial velocity, in agreement with the experimental measurements. For a constant superficial liquid velocity, the trend exhibited by the measured air-oil slug frequency versus superficial gas velocity is not properly captured by the correlation, whereas a better agreement is obtained for air-water slug frequency. Figure 7.83 shows comparisons of the predictions of the Gregory & Scott (1969) correlation with the WASP slug frequency data. This correlation manages to capture the basic shape of the experimental trend though it under-predicts the slug frequency for the range of superficial velocities covered in this work.

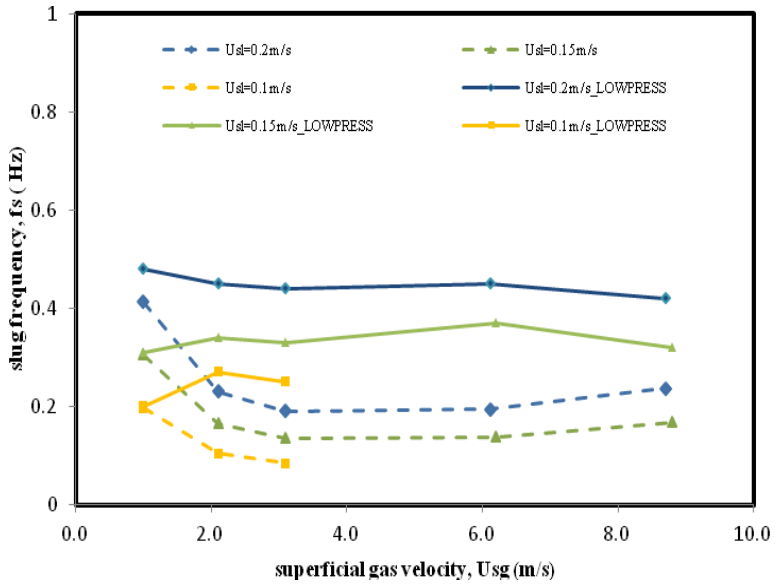

Figure 7.80: Comparison of the LOWPRESS air-oil slug frequency data (solid lines) with the predictions of the Gregory & Scott (1969) correlation (dashed lines).

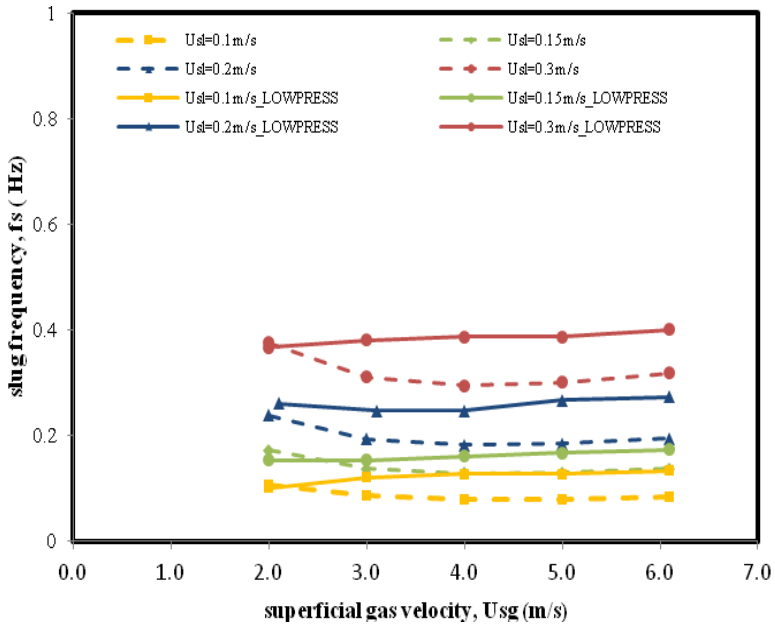

Figure 7.81: Comparison of the LOWPRESS air-water slug frequency data (solid lines) with the predictions of the Gregory & Scott (1969) correlation (dashed lines).

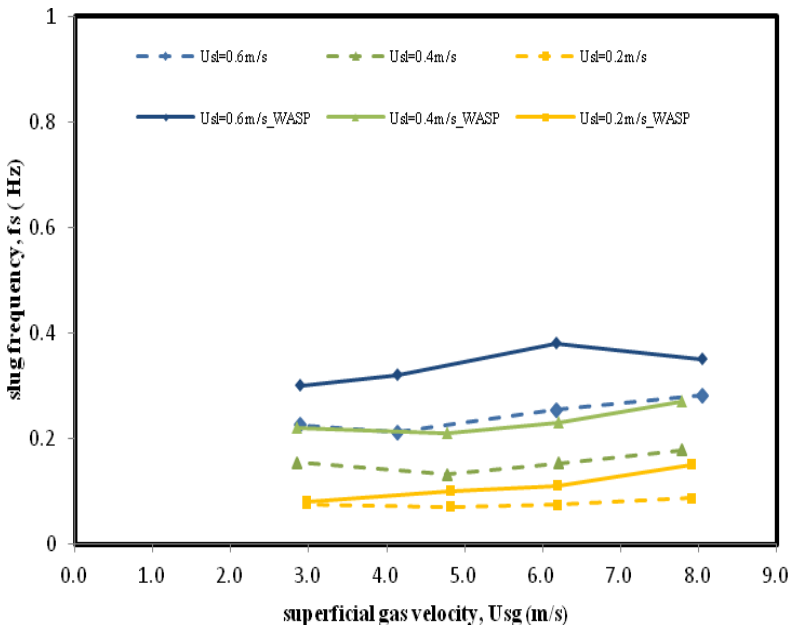

Figure 7.82: Comparison of the WASP air-oil slug frequency data (solid lines) with the prediction of the Gregory & Scott (1969) correlation (dashed lines).

Heywood & Richardson (1979), Nydal (1991), Manolis (1995) and Zabaras (1999) have modified the Gregory & Scott (1969) correlation based on their measured data; the comparisons of their predictions with the present slug frequency data are summarized in Figures 7.84 to 7.95. It can be seen that the Heywood & Richardson (1979) correlation predicts the LOWPRESS air-oil and air-water slug frequency generally better than other correlations. However, similarly to Gregory & Scott (1969) prediction, the shape of the air-oil slug frequency trend is not properly captured, as the correlation over-predicts at lower gas superficial velocities and then begins to under-predict as this velocity increases. The prediction has a better agreement with air-water flow though the deviation is slightly bigger for the smallest gas velocity. Manolis (1995) and Zabaras (1999) correlations also predict a similar trends of slug frequency for LOWPRESS air-oil and air-water data, but with larger discrepancies. The Nydal (1991) correlation of slug frequency only correlates with liquid velocity and pipe diameter. Hence, it predicts constant slug frequency for a given gas velocity and the values are much higher than the measurements. In regards to the comparison with WASP data, the predictions of Heywood & Richardson (1979), Manolis (1995) and Zabaras (1999) have captured the basic experimental trend and among them Heywood & Richardson (1979) prediction is closest to the measurement. The Manolis (1995) and Zabaras (1999)

correlations consistently under-predict the frequency and Nydal (1991) predictions generally over-predict the frequency for the velocity range covered.

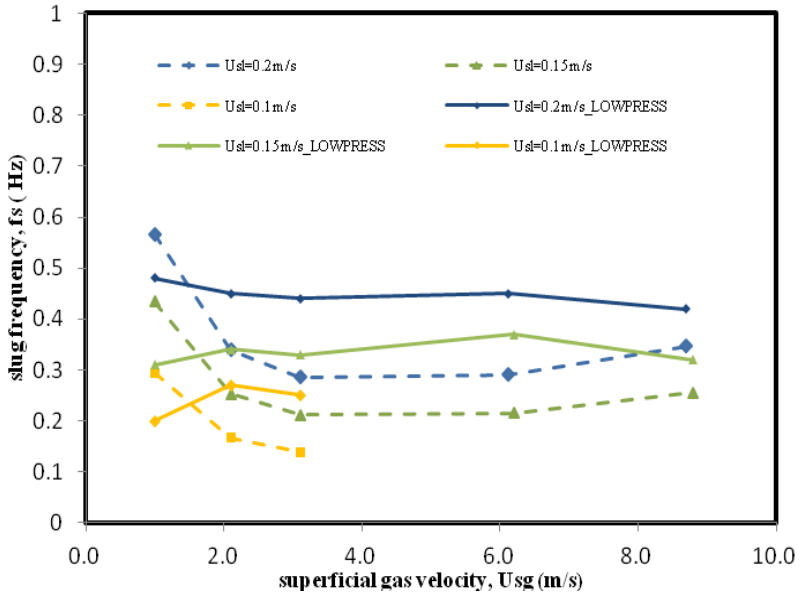

Figure 7.83: Comparison of the LOWPRESS air-oil slug frequency data (solid lines) with the prediction of the Heywood & Richardson (1979) correlation (dashed lines).

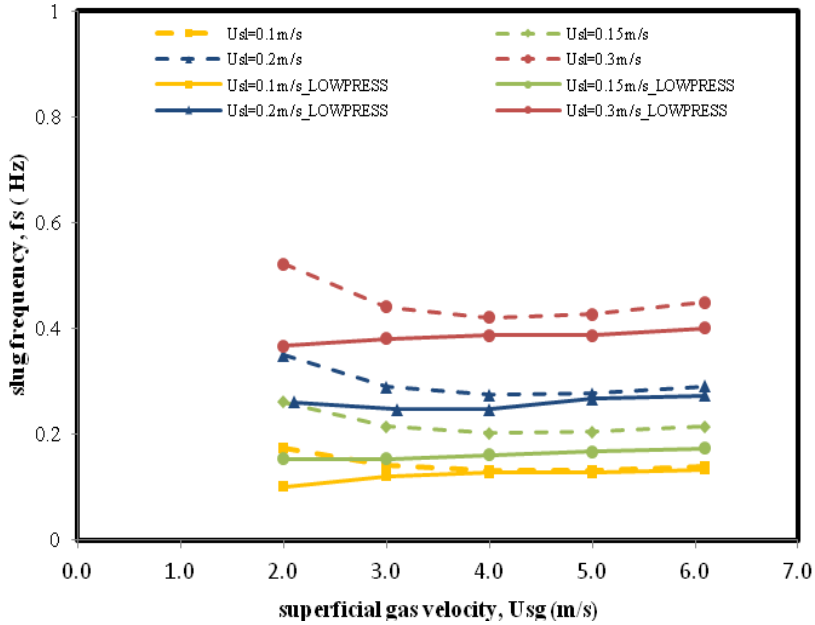

Figure 7.84: Comparison of the LOWPRESS air-oil slug frequency data (solid lines) with the prediction of the Heywood & Richardson (1979) correlation (dashed lines).

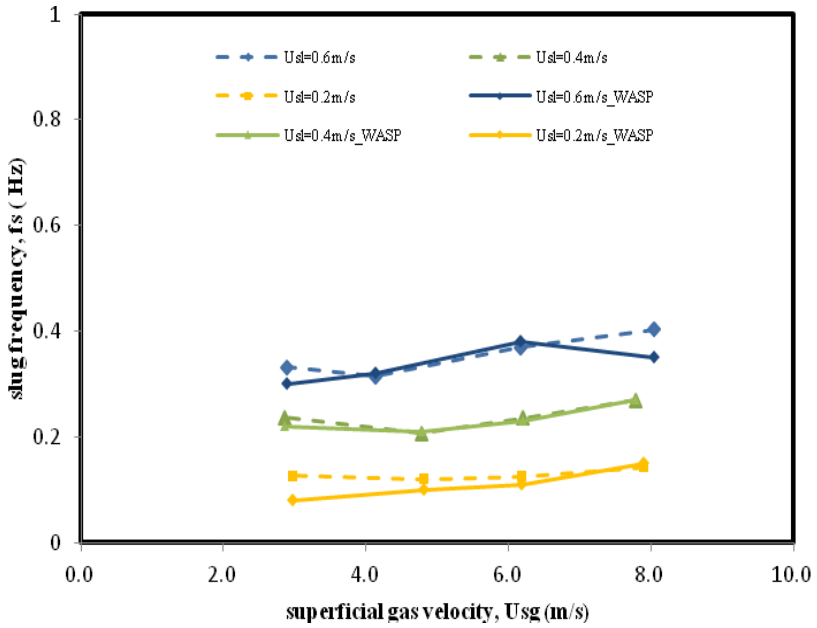

Figure 7.85: Comparison of the WASP air-water slug frequency data (solid lines) with the prediction of the Heywood & Richardson (1979) correlation (dashed lines).

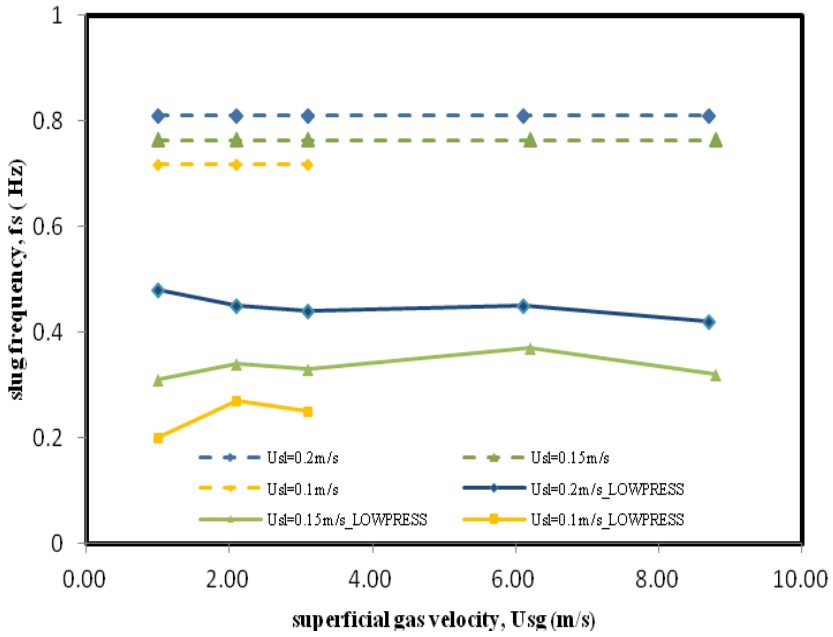

Figure 7.86: Comparison of the LOWPRESS air-oil slug frequency data (solid lines) with the prediction of the Nydal (1991) correlation (dashed lines).

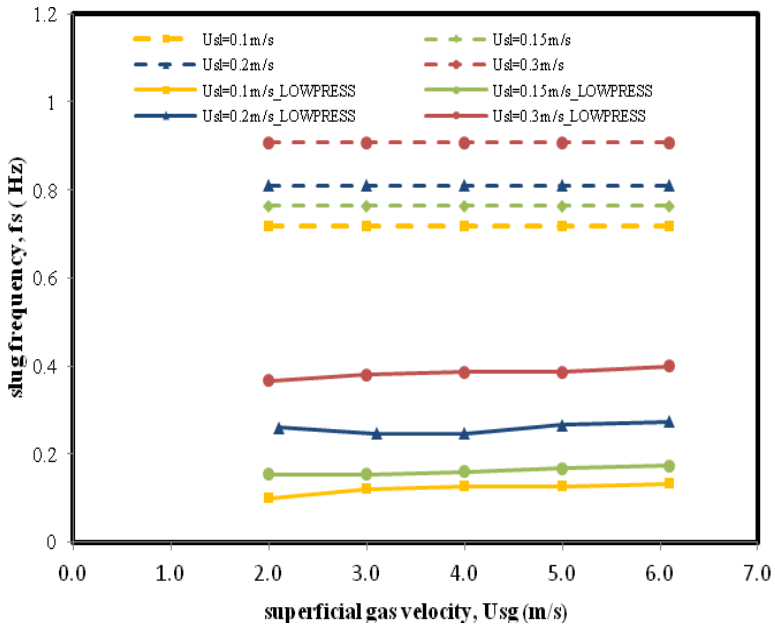

Figure 7.87: Comparison of the LOWPRESS air-oil slug frequency data (solid lines) with the prediction of the Nydal (1991) correlation (dashed lines).

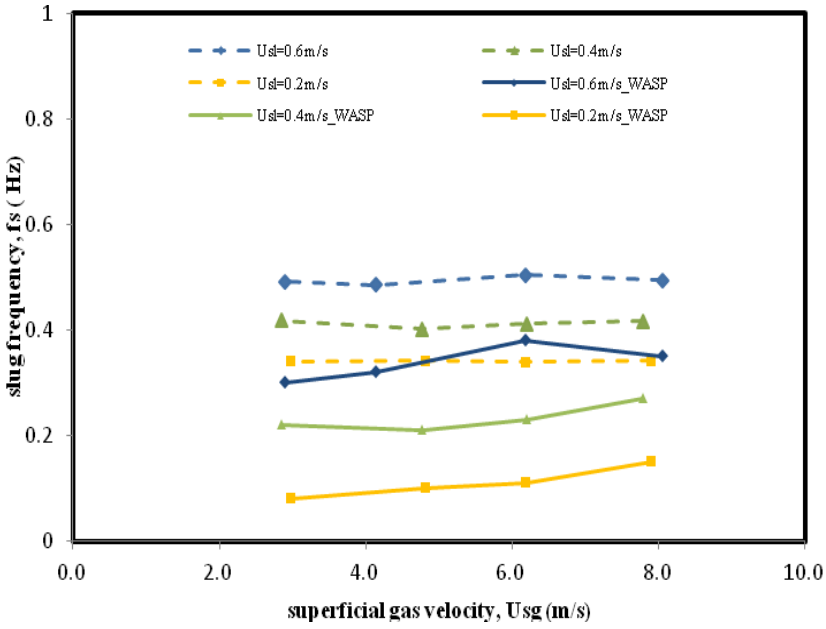

Figure 7.88: Comparison of WASP air-water slug frequency data (solid lines) with the prediction of the Nydal (1991) correlation (dashed lines).

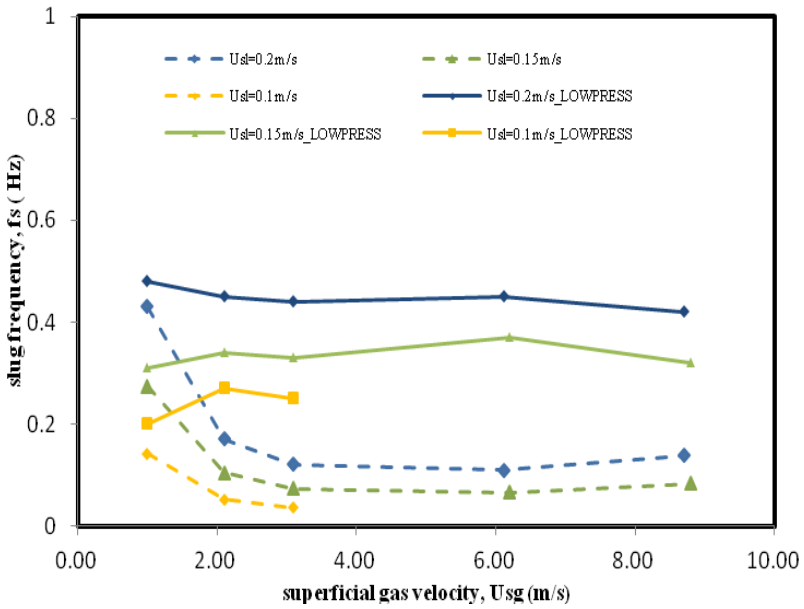

Figure 7.89: Comparison of the LOWPRESS air-oil slug frequency data (solid lines) with the prediction of the Manolis (1995) correlation (dashed lines).

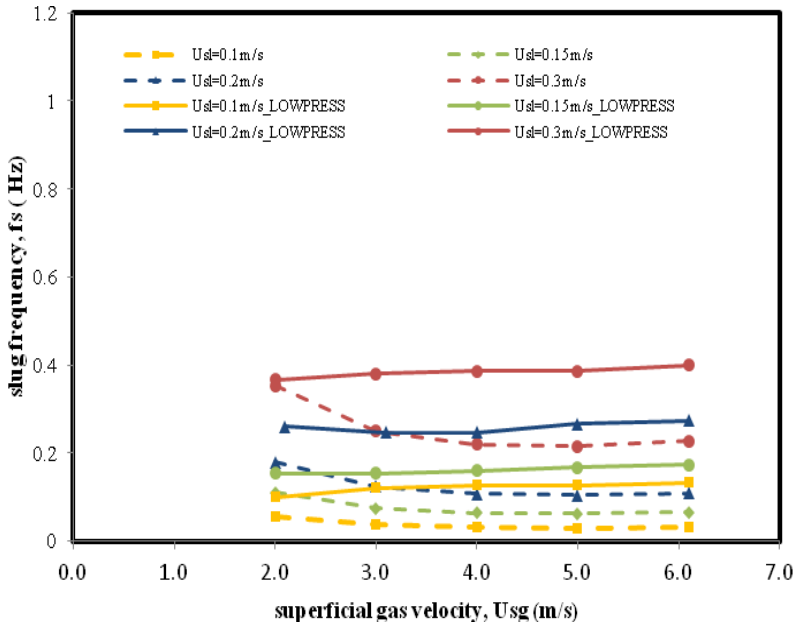

Figure 7.90: Comparison of the LOWPRESS air-water slug frequency data (solid lines) with the prediction of the Manolis (1995) correlation (dashed lines).

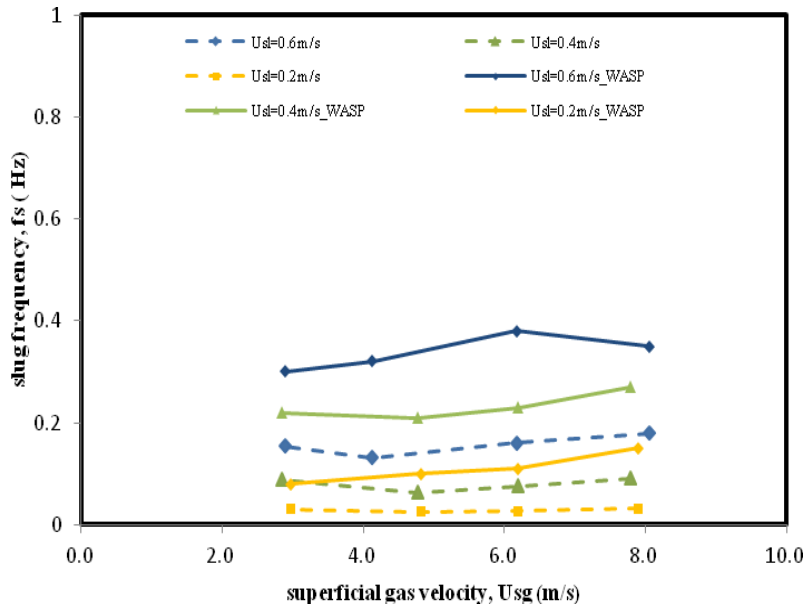

Figure 7.91: Comparison of the WASP air-water slug frequency data (solid lines) with the prediction of the Manolis (1995) correlation (dashed lines).

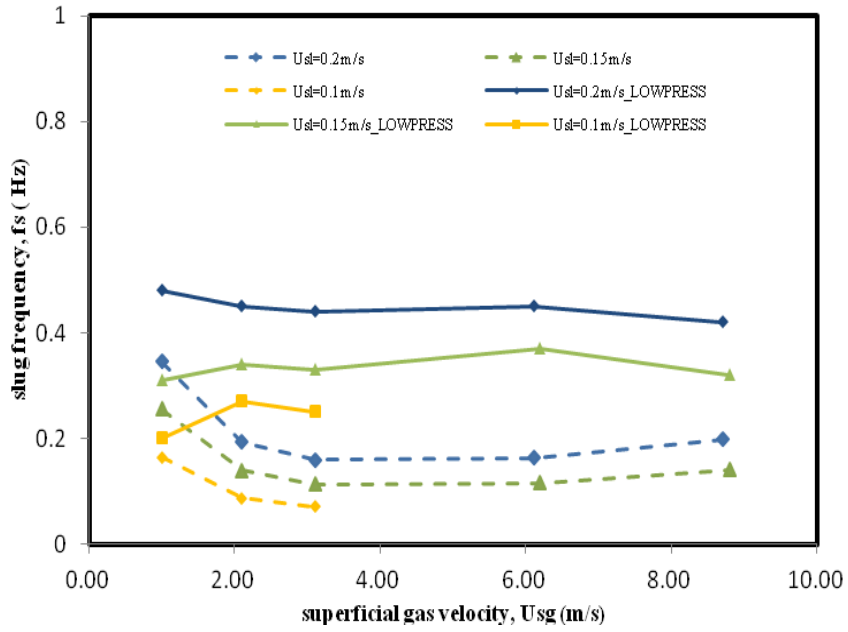

Figure 7.92: Comparison of the LOWPRESS air-oil slug frequency data (solid lines) with the prediction of the Zabaras (1999) correlation (dashed lines).

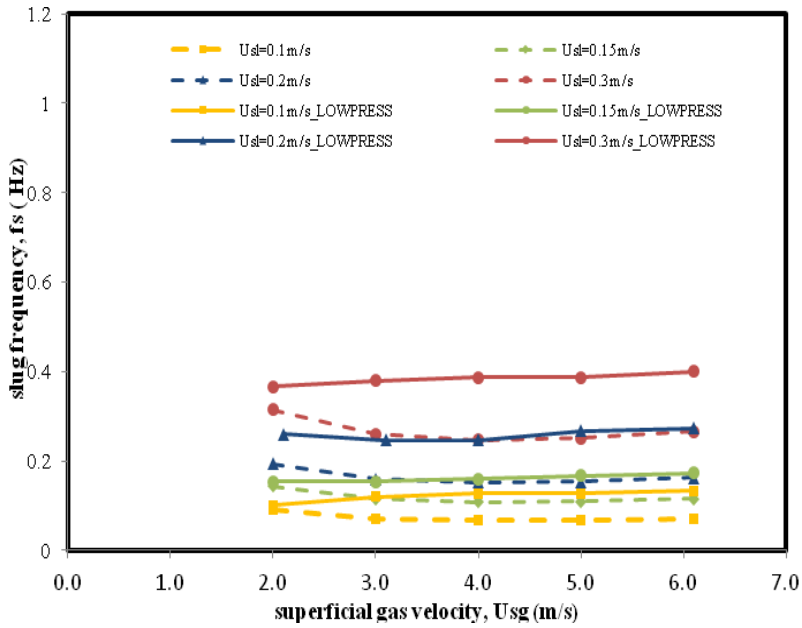

Figure 7.93: Comparison of the LOWPRESS air-water slug frequency data (solid lines) with the prediction of the Zabaras (1999) correlation (dashed lines).

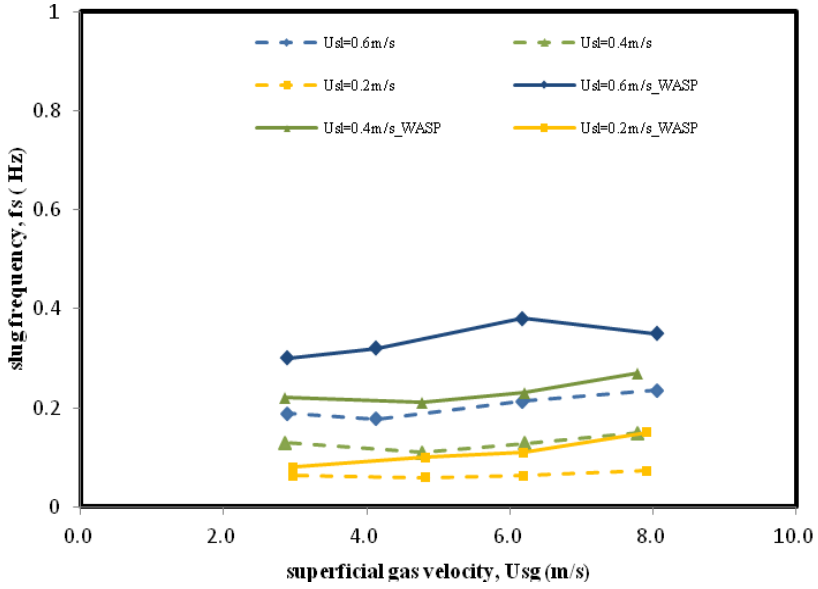

Figure 7.94: Comparison of the WASP air-water slug frequency data (solid lines) with the prediction of the Zabaras (1999) correlation (dashed lines).

Figure 7.96 and Figure 7.97 show the comparisons of the predictions of Tronconi (1990) correlation with LOWPRESS air-oil and air-water slug frequency data respectively. Although

a semi theoretical model has been used to provide the frequency prediction, slug frequency is consistently greatly over-predicted air-oil slug frequency over the whole range of velocity. On the other hand, the correlation has captured the trend exhibited by the air-water slug frequency and the discrepancy is much smaller. Comparisons between the correlation and the WASP air-water data are shown in Figure 7.98; as can be seen, reasonable agreement with the correlation is obtained for the higher liquid superficial velocities but there are larger discrepancies for the lowest liquid superficial velocity.

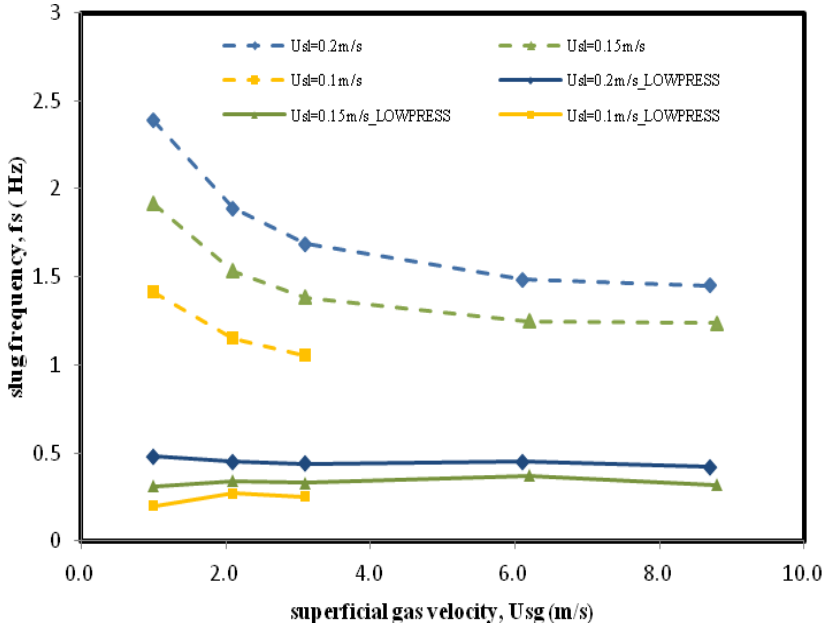

Figure 7.95: Comparison of the LOWPRESS air-oil slug frequency data (solid lines) with the prediction of the Tronconi (1990) correlation (dashed lines).

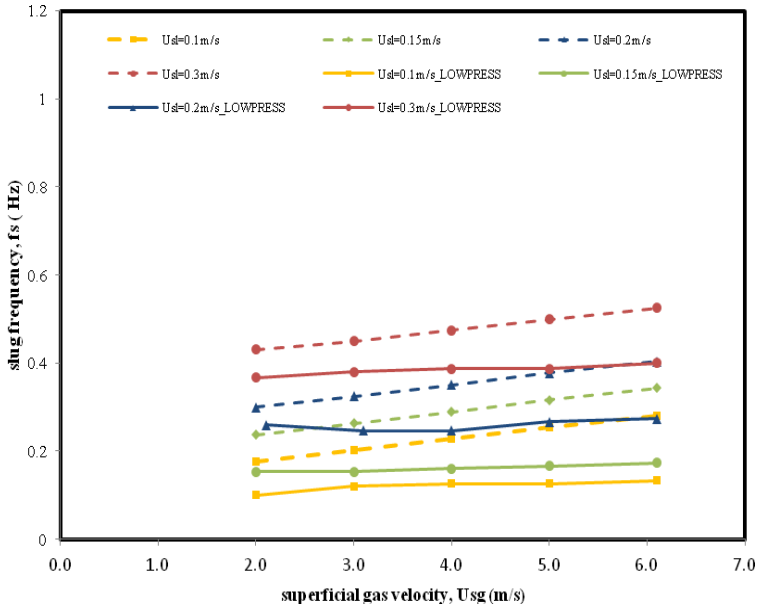

Figure 7.96: Comparison of the LOWPRESS air-water slug frequency data (solid lines) with the prediction of the Tronconi (1990) correlation (dashed lines).

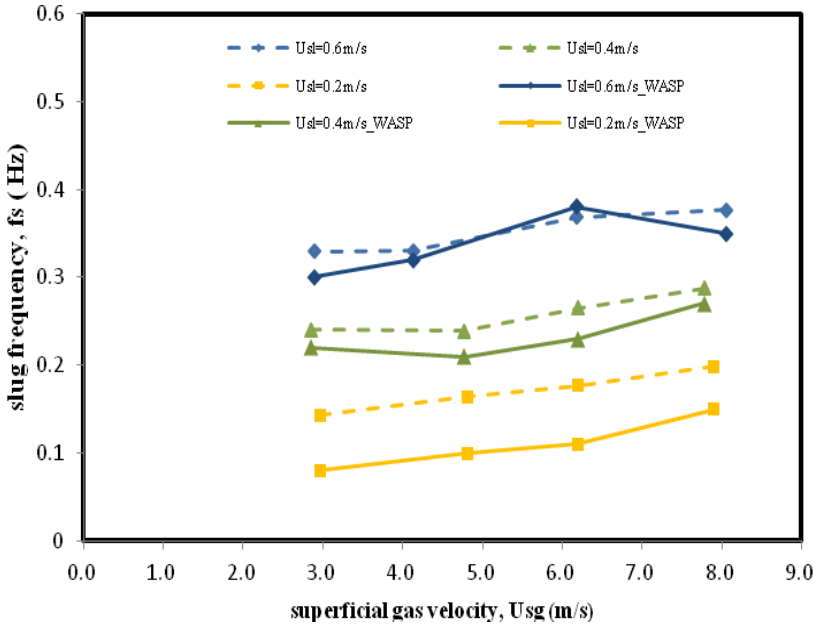

Figure 7.97: Comparison of the WASP air-water slug frequency data (solid lines) with the prediction of the Tronconi (1990) correlation (dashed lines).

The Hill & Wood 1 (1990) correlation is a modification of the Tronconi (1990) correlations (see Chapter 2) and also accounts for the liquid equilibrium height and hence implicitly the momentum balance. Figures 7.99 and 7.100 show comparisons of the predictions of Hill & Wood_1 (1990) correlation with the LOWPRESS air-oil and air-water slug frequency data, respectively. The predictions greatly over-predict the LOWPRESS air-oil slug frequencies over the whole range of velocity. The large discrepancy might due to the fact that Hill & Wood_1 (1990) correlation was developed for low frequency, low equilibrium stratified liquid holdup cases which cannot be applied to LOWPRESS air-oil data. However, a much better agreement is obtained for LOWPRESS air-water slug flow, the correlation predicts about the right values for slug frequencies with lower gas velocity, and then starts to under-predict the slug frequency with increasing gas velocity. Similar predictions are found in comparison with WASP air-water data as can be seen in Figure 101.

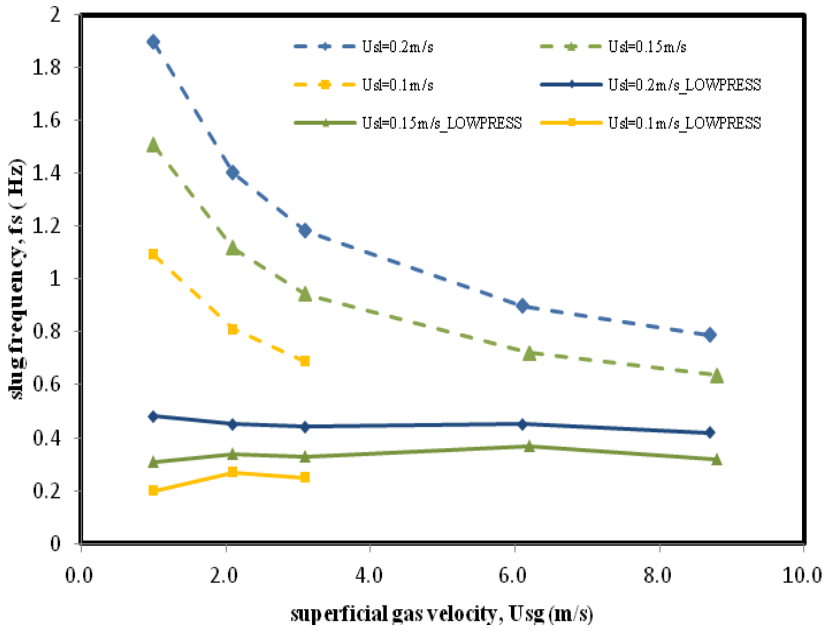

Figure 7.98: Comparison of the LOWPRESS air-oil slug frequency data (solid lines) with the prediction of the Hill & Wood_1 (1990) correlation (dashed lines).

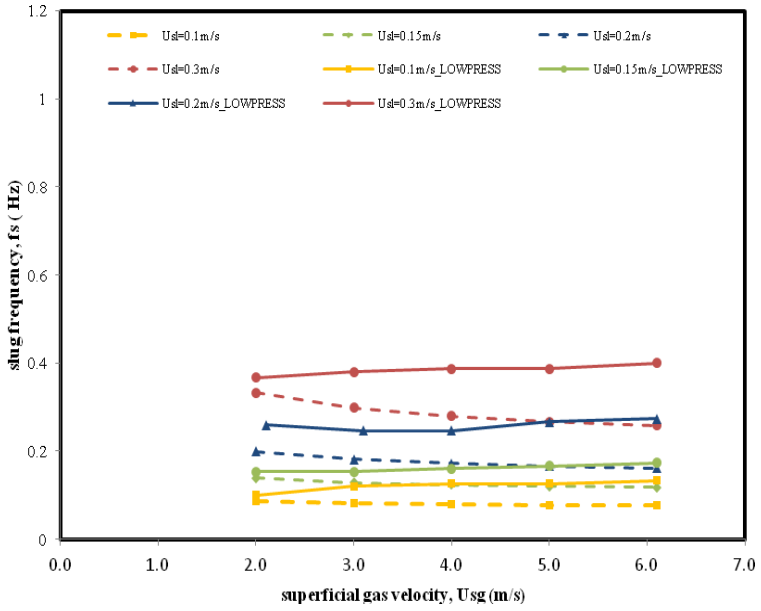

Figure 7.99: Comparison of the LOWPRESS air-water slug frequency data (solid lines) with the prediction of the Hill & Wood_1 (1990) correlation (dashed lines).

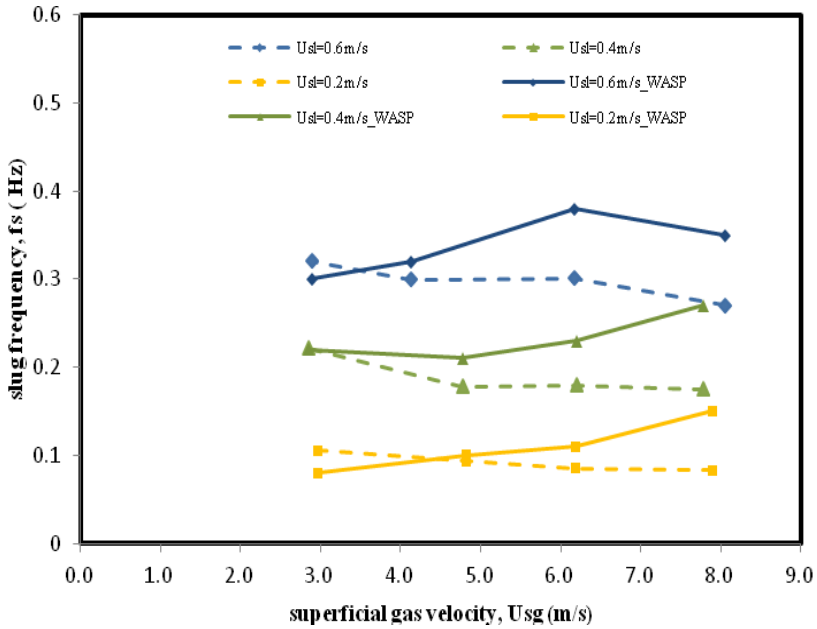

Figure 7.100: Comparison of the WASP air-water slug frequency data (solid lines) with the prediction of the Hill & Wood_1 (1990) correlation (dashed lines).

Figure 102 and Figure 103 show comparisons of the predictions of Hill & Wood_2 (1990) correlation with the LOWPRESS air-oil and air-water slug frequency data respectively. The correlation over-predicts the air-oil slug frequency over the whole range of superficial gas velocities whereas it predicts about the right values for the LOWPRESS air-water slug frequencies. Figure 104 shows comparisons of the predictions of the Hill & Wood_2 (1990) correlation with the WASP air-water slug frequency data. Good agreement is found for the lowest gas velocity, and then the prediction shows a consistent decrease in slug frequency with increasing gas velocity which is not in agreement with the experimental trend.

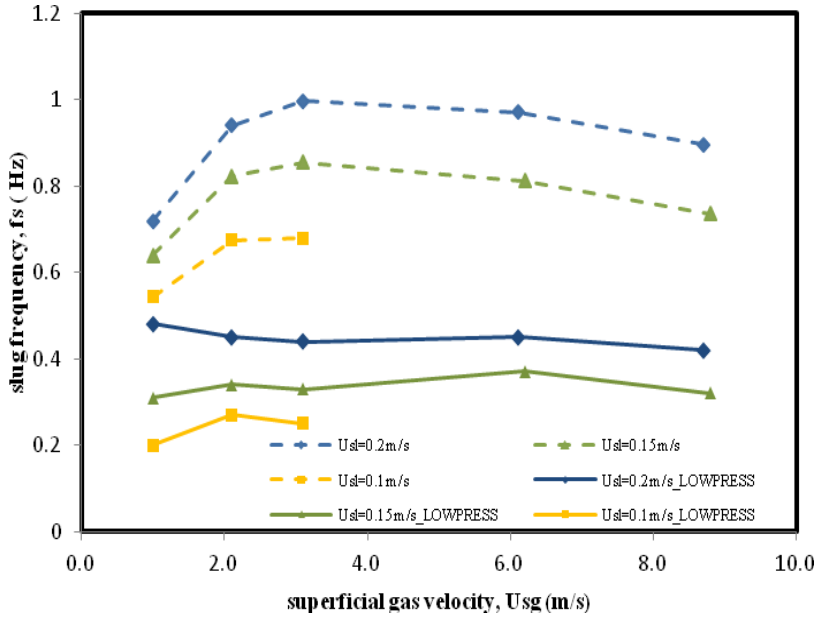

Figure 7.101: Comparison of the LOWPRESS air-oil slug frequency data (solid lines) with the prediction of the Hill & Wood_2 (1990) correlation (dashed lines).

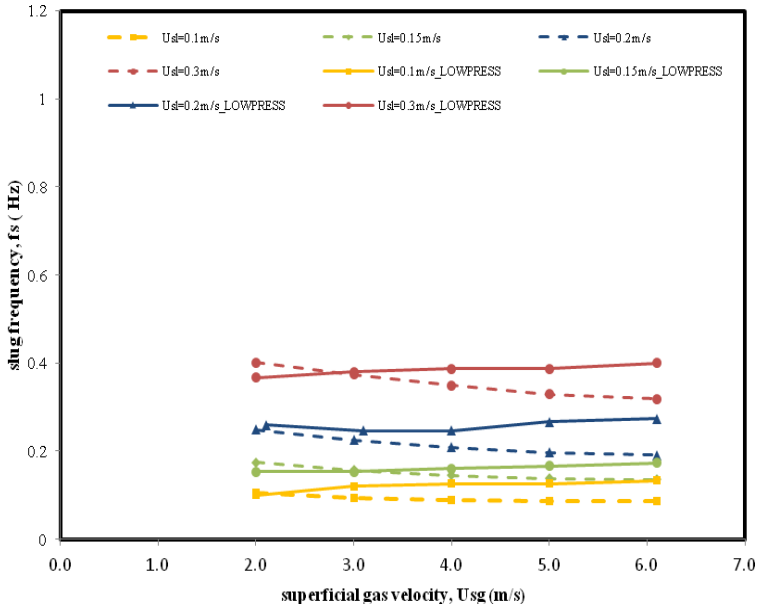

Figure 7.102: Comparison of the LOWPRESS air-oil slug frequency data (solid lines) with the prediction of the Hill & Wood_2 (1990) correlation (dashed lines).

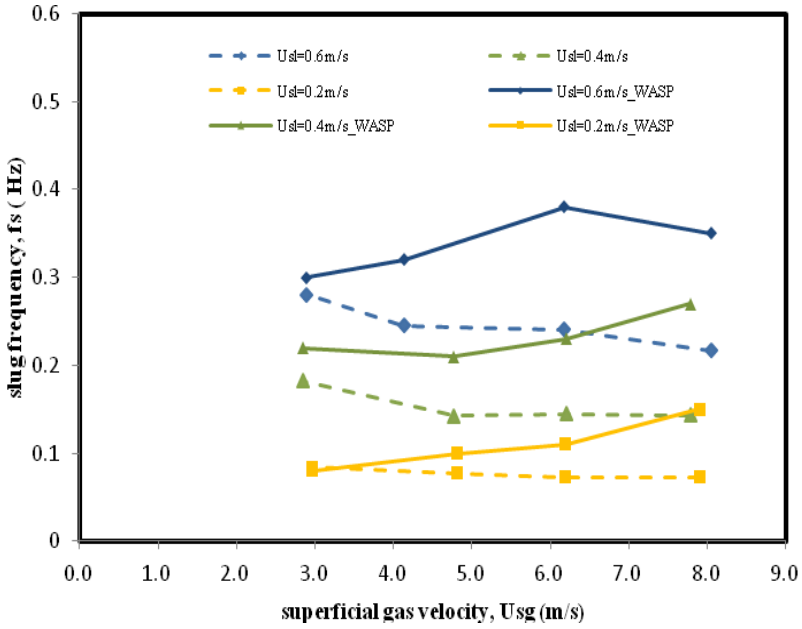

Figure 7.103: Comparison of the WASP air-water slug frequency data (solid lines) with the prediction of the Hill & Wood_2 (1990) correlation (dashed lines).

Al-Safran (2008) relates slug frequency to the slip and actual liquid velocities which can be calculated from the equilibrium stratified liquid height using Taitel & Dukler (1976) stratified-flow model. Figure 7.104 and Figure 7.105 show comparisons of the predictions of Al-Safran (2008) correlation with the LOWPRESS air-oil and air-water slug frequency data. The correlation predict both air-water and air-oil slug frequencies reasonable well for the lowest velocity, the discrepancy is larger with increasing gas velocity. Figure 7.106 show the predictions of the Al-Safran (2008) correlation with the WASP air-water slug flows. Experimental trends are properly captured for each set of liquid velocity, though slug frequency is consistently under-predicted over the whole range of velocity.

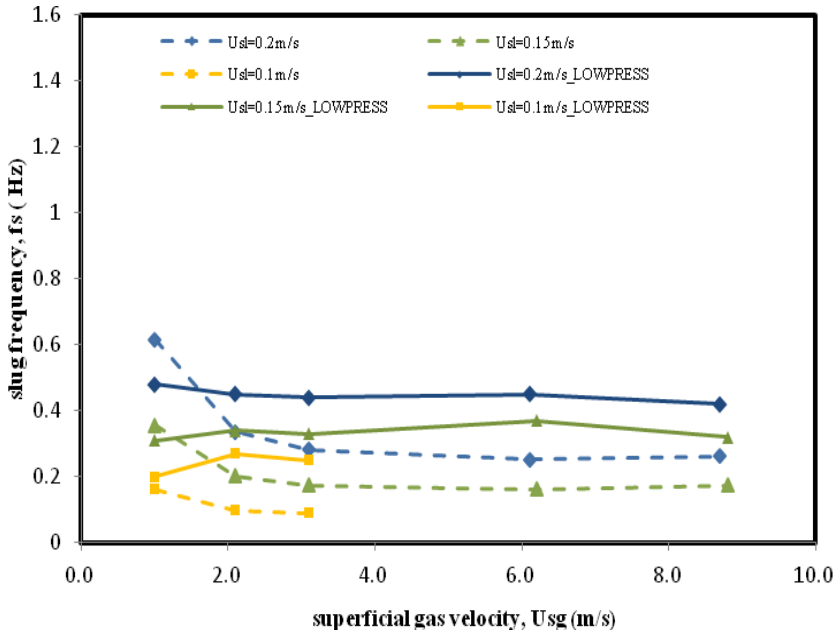

Figure 7.104: Comparison of the LOWPRESS air-oil slug frequency data (solid lines) with the prediction of the Al-Safran (2008) correlation (dashed lines).

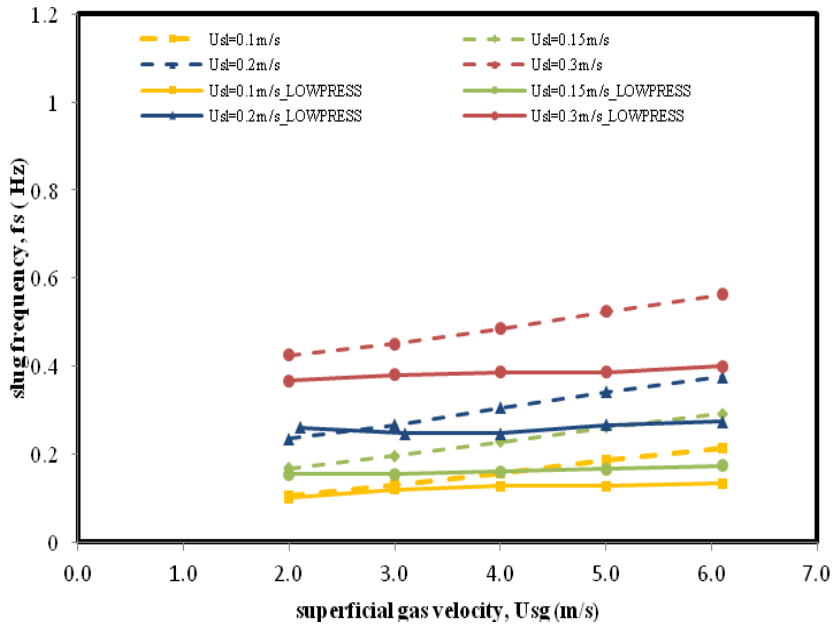

Figure 7.105: Comparison of the LOWPRESS air-water slug frequency data (solid lines) with the prediction of the Al-Safran (2008) correlation (dashed lines).

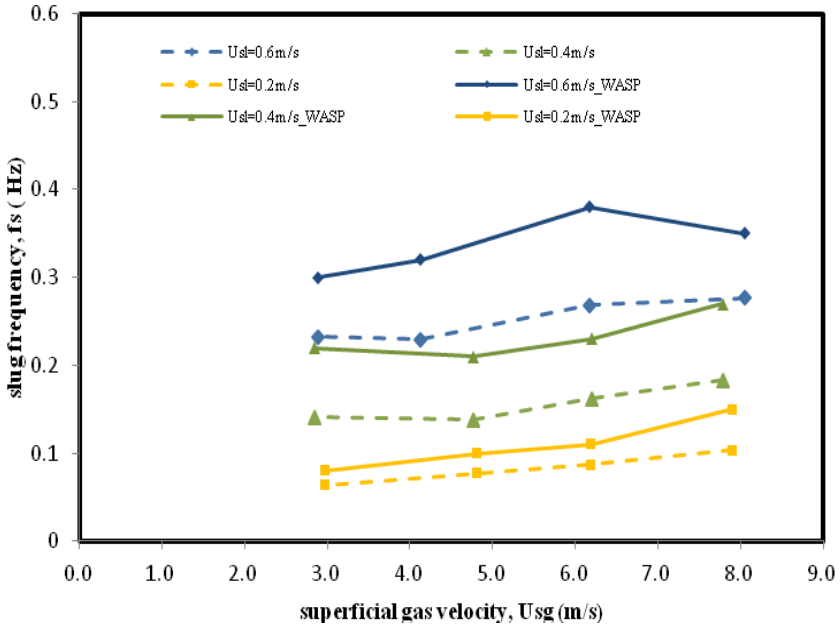

Figure 7.106: Comparison of the LOWPRESS air-oil slug frequency data (solid lines) with the prediction of the Al-Safran (2008) correlation (dashed lines).

Gokcal (2008) derived a correlation on the basis of experiments with high-viscosity fluids. Figure 7.107 and Figure 7.108 show comparisons of the predictions of Gokcal (2008)

correlation with the LOWPRESS air-oil and air-water slug frequency data. The correlation predicts constant values irrespective to the change in gas velocity. It shows a reasonably good agreement with air-oil slug frequency data whereas it greatly underestimates the air-water slug frequency data. Figure7.110 shows a comparison of the predictions of Gokcal (2008) correlation with WASP air-water slug frequency data. As in the case of the LOWPRESS air-water data (Figure 7.109), the predictions from the correlation greatly underestimate the slug frequency data. This reveals the fact that Gokcal (2008) model is not valid for low viscosity fluids such as water.

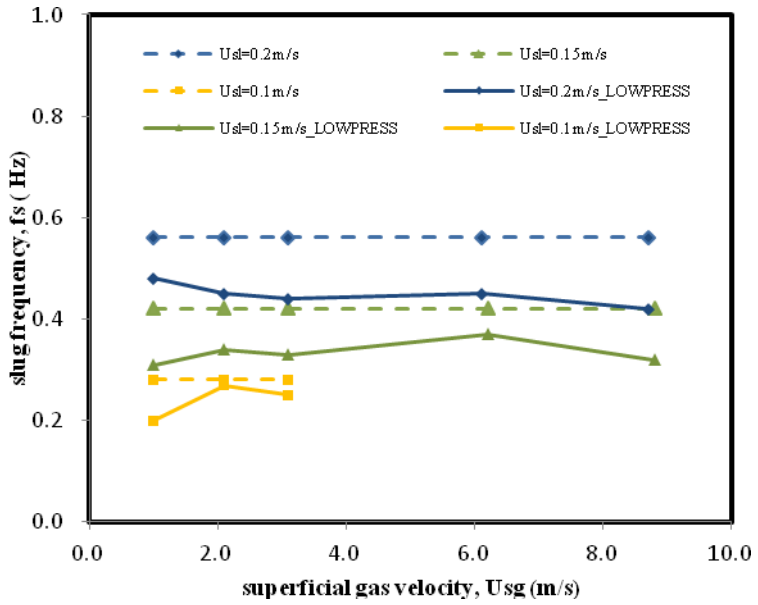

Figure 7.107: Comparison of the LOWPRESS air-oil slug frequency data (solid lines) with the prediction of the Gokcal (2008) correlation (dashed lines).

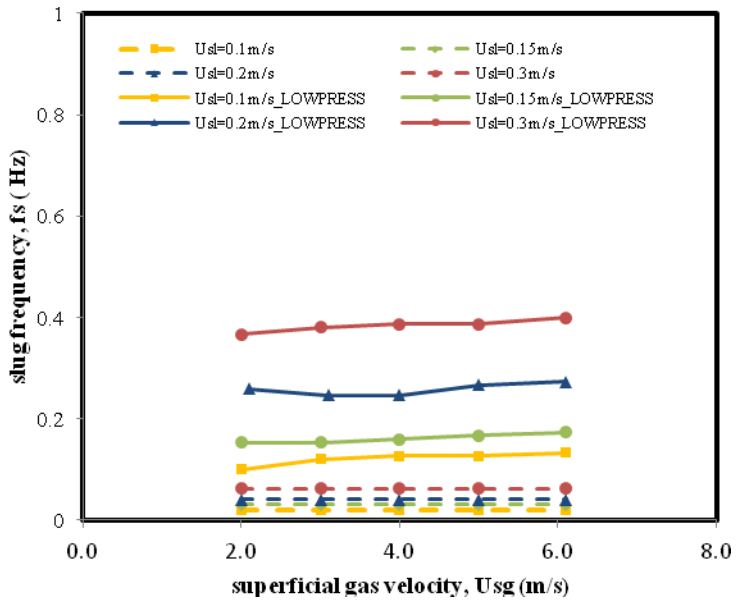

Figure 7.108: Comparison of the LOWPRESS air-water slug frequency data (solid lines) with the prediction of the Gokcal (2008) correlation (dashed lines).

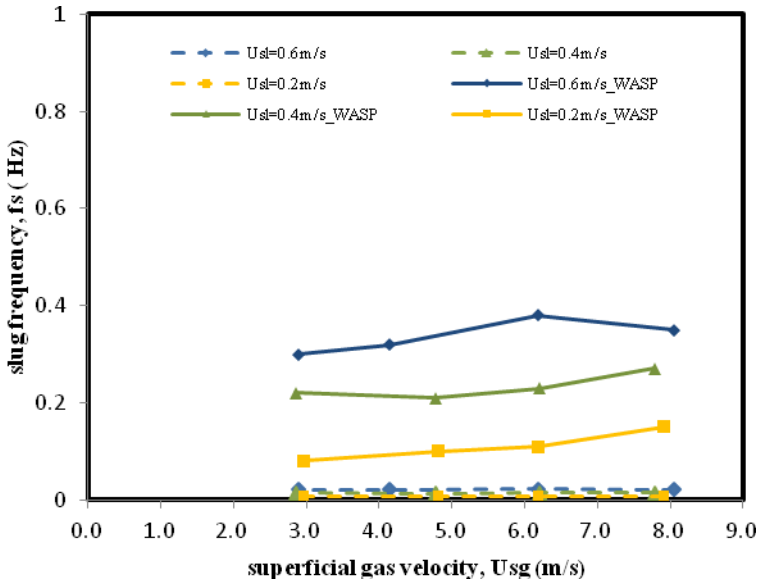

Figure 7.109: Comparison of the WASP air-water slug frequency data (solid lines) with the prediction of the Gokcal (2008) correlation (dashed lines).

Schulkes (2011) reviewed a wide range of published experimental data and a number of Statoil in-house data sets, and then derived a slug frequency correlation which aimed to be dimensionally valid for all available data. Figure 7.110 and Figure 7.111 show comparison of predictions of Schulk (2011) correlation with LOWPRESS air-oil and air-water slug

frequency data. It can be seen that the basic trends of both air-oil and air-water experimental data are reasonably well captured. The correlation over-estimate the air-oil slug frequency for the cases the lowest gas velocity, with the discrepancy getting smaller with increased gas velocity. Figure 7.112 shows comparison of the predictions of Schulkes (2011) correlation with the WASP air-water slug frequency data. The predictions show a good agreement for the cases with the lowest gas velocity, however the correlation slightly under-predicts the slug frequency with increased gas velocity.

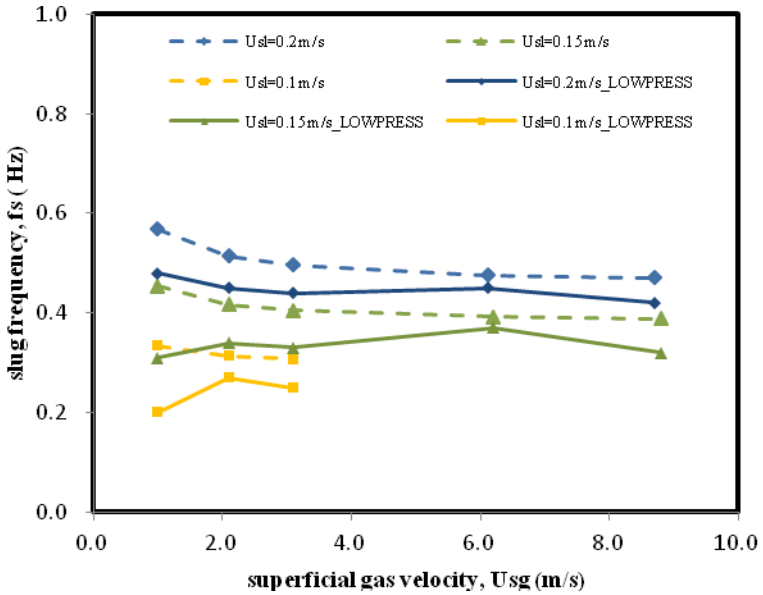

Figure 7.110: Comparison of the LOWPRESS air-oil slug frequency data (solid lines) with the prediction of the Schulkes (2011) correlation (dashed lines).

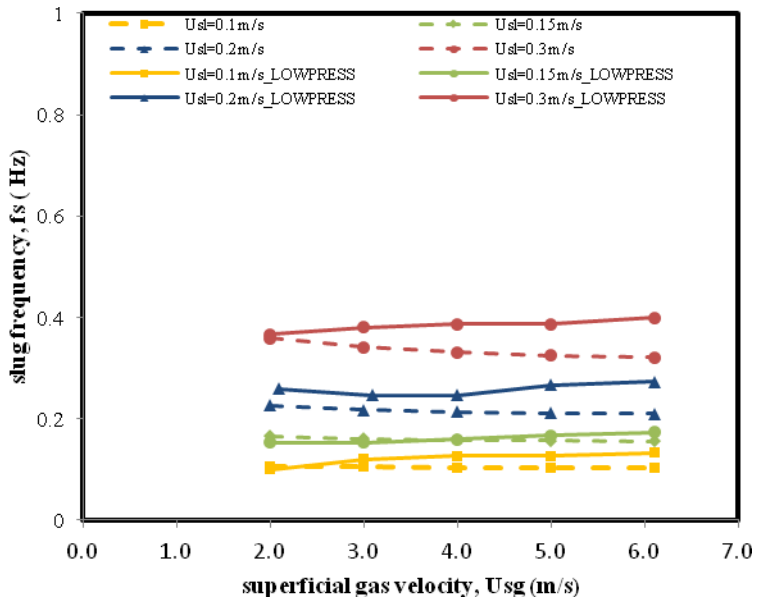

Figure 7.111: Comparison of the LOWPRESS air-water slug frequency data (solid lines) with the prediction of the Schulkes (2011) correlation (dashed lines).

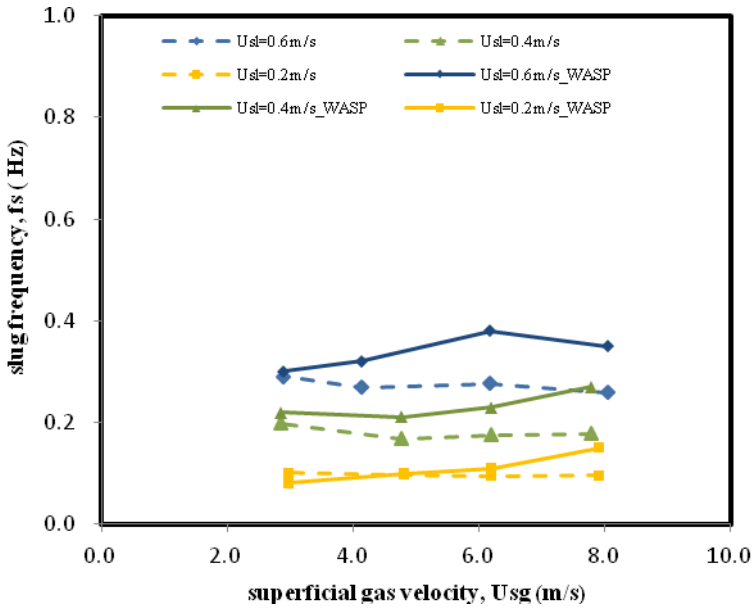

Figure 7.112: Comparison of the WASP air-water slug frequency data (solid lines) with the prediction of the Schulkes (2011) correlation (dashed lines).

The statistical results for performance of the various correlations tested against the LOWPRESS and WASP experimental data are summarised in Table 7.5, including the mean error, the standard deviation and the RMS error. From the table, it can be clearly seen that there is a large difference between the predictions of the correlations themselves. Statistically, Heywood & Richardson (1979) correlation displays the lowest mean error for LOWPRESS air-oil experiments, however as illustrated in Figure 7.83, the shape of the air-oil slug frequency trend is not properly captured by this correlation. The second lowest mean error is displayed by Schulkes (2011) correlation, and it has better captured the observed frequency trend. For LOWPRESS air-water experiments, Schulkes (2011) correlation displays the lowest mean error. For WASP air-water data, Heywood & Richardson (1979) correlation displays the lowest mean error. Overall, for LOWPRESS air-oil and air-water data, the correlation of Schulkes (2011) performed best. For the WASP air-water data, the correlation of Heywood & Richardson (1979) performed best though its performance was not greatly superior to that of the Schulkes (2011) correlation. Therefore, the correlation of Schulkes (2011) is recommended.

Table 7.5: Statistical results for the prediction of LOWPRESS air-oil, air-water and WASP air-water ssytem slug frequency by the various slug frequency predictive methods.

LOWPRESS Air-Oil	Gregory & Scott (1969)	Heywood & Richardson (1979)	Nydal (1991)	Manolis (1995)	Zabaras (1999)	Tronconi (1990)	Hill & Wood_1 (1990)	Hill & Wood_2 (1990)	Al -Safran (2008)	Gokcal (2009)	Schulkes (2011)
Mean. Err. (%)	-43.70	-16.06	128.76	-61.37	-52.93	252.02	128.75	206.89	-33.21	24.76	22.65
Std. Dev. (%)	22.91	31.07	52.95	26.48	19.15	53.51	32.40	111.31	27.76	10.95	16.66
RMS. Err. (%)	48.93	33.90	138.44	66.43	56.04	257.21	132.46	232.89	42.59	26.90	27.73

LOWPRESS Air-water	Gregory & Scott (1969)	Heywood & Richardson (1979)	Nydal (1991)	Manolis (1995)	Zabaras (1999)	Tronconi (1990)	Hill & Wood_1 (1990)	Hill & Wood_2 (1990)	Al -Safran (2008)	Gokcal (2009)	Schulkes (2011)
Mean. Err. (%)	-19.67	22.25	305.5	-51.85	-33.00	25.13	-11.70	-27.21	-27.66	-82.87	-10.27
Std. Dev. (%)	14.04	20.39	141.91	18.47	11.65	28.46	20.98	16.98	6.71	17.4	9.65
RMS. Err. (%)	23.98	29.84	337.80	54.88	34.90	35.41	22.18	30.31	27.18	82.89	14.26

WASP Air-water	Gregory & Scott (1969)	Heywood & Richardson (1979)	Nydal (1991)	Manolis (1995)	Zabaras (1999)	Tronconi (1990)	Hill & Wood_1 (1990)	Hill & Wood_2 (1990)	Al -Safran (2008)	Gokcal (2009)	Schulkes (2011)
Mean. Err. (%)	-26.40	9.41	120.64	-64.28	-41.32	58.40	-27.86	-13.46	28.60	-93.06	-14.75
Std. Dev. (%)	10.80	18.76	95.07	10.86	8.96	30.77	10.19	14.29	19.93	14.3	17.82
RMS. Err. (%)	27.13	19.35	144.48	62.34	40.40	63.88	29.58	19.37	34.57	89.11	21.54

7.11 TRIOMPH code predictions and comparison with experiments

As have been seen from Section 7.10, a wide range of predictions can be obtained for fully-developed slug frequency using the available correlations. Furthermore, the present study has shown that the inlet geometry has an important influence in the slug formation region. Over a number of years, Issa and co-workers (Woodburn, 1998; Kempf, 2003; Bonizzi, 2003, Montini, 2011) at imperial College have developed a transient one-dimensional two-fluid model method (slug capturing) to predict the evolution of slug flow. This model is embodied in the TRIOMPH computer code and the present author is grateful to Dr. Issa for making available this code and giving invaluable advice on its application. The objective of the work described in this Section was to evaluate the performance of the TRIOMPH code in predicting the behaviour in the entrance region for various inlet boundary conditions (Section 7.12.1) and also in predicting measured fully developed slug frequency (Section 7.12.2). The experiments on fully developed slug frequency carried out by Dr. C. P. Hale on the WASP facility (and reported and analysed for the first time in this thesis) were chosen for comparison with TRIOMPH predictions.

7.11.1 The effect of inlet liquid hold-up on TRIOMPH predictions

In TRIOMPH predictions it is necessary to specify the boundary liquid level at the inlet of the pipe. One approach is to specify inlet conditions which correspond to a state of equilibrium (in stratified flow) between a liquid layer flowing at the bottom of the pipe and the gas flowing in the upper part of the pipe. This equilibrium liquid hold-up is derived from the ensemble-average two-fluid momentum equations described in chapter 4. Referring to steady-state condition, by neglecting all derivatives with respect to space, time and the hydrostatic terms of the gas and liquid momentum equations, the equations become:

$$-\alpha_G \frac{\partial p}{\partial x} - \rho_G \alpha_G g \sin\beta - \frac{\tau_{wG} S_G}{A} - \frac{\tau_i S_i}{A} = 0 \qquad [7.6]$$

$$-\alpha_L \frac{\partial p}{\partial x} - \rho_L \alpha_L g \sin\beta - \frac{\tau_{wL} S_L}{A} + \frac{\tau_i S_i}{A} = 0 \qquad [7.7]$$

By eliminating the pressure gradient, the equilibrium liquid holdup can be obtained from the following relation:

$$(\rho_L - \rho_G) g \sin\beta + \frac{\tau_{wL} S_L}{\alpha_{Leq} A} - \frac{\tau_{wG} S_G}{(1-\alpha_{Leq}) A} - \frac{\tau_i S_i}{A} \left(\frac{1}{\alpha_{Leq}} + \frac{1}{(1-\alpha_{Leq})}\right) = 0 \qquad [7.8]$$

Obviously, the value of equilibrium liquid holdup α_{Leq} is a function of the closure relations used to evaluate the gas-wall and liquid-wall and interfacial shear stress. In TRIOMPH code, the standard set of correlations for the evaluation of the shear stresses are:

- Taitel & Dukler (1976) for the gas-wall friction factor (see Eqn. 4.7),
- Taitel & Dukler (1976) for the interfacial shear stress (see Eqn. 4.10).
- Spedding & Hand (1997) for the liquid-wall friction factor (see Eqn. 4.12 & 4.13).

However, in the WASP experiments analysed here, the liquid holdup at the inlet is fixed by the position of the stratification plate, the “low-plate” and “high-plate” inlet configuration corresponding to inlet liquid hold-ups of 0.2 and 0.8 respectively. Therefore, three slug flow simulation runs were performed in order to investigate the effect of inlet liquid hold-up on the slug flow prediction. Table 7.6 summarises the inlet boundary conditions of the three cases; the superficial gas and liquid velocities were identical for the three cases. For each case, a computational grid was set up which had the same length as the WASP test-section (i.e. 36m). The length was subdivided into 1250 cells. For each calculation it was confirmed (by mesh refinement) that the numerical results were independent of the chosen grid size.

Table 7.6: Flow rates and inlet liquid hold-ups applied in three TRIOMPH simulation runs.

	Usg (m/s)	Usl (m/s)	α_L^{inlet} (-)
Run1	8.0	0.6	0.56 (equilibrium)
Run2	8.0	0.6	0.2 (low-plate)
Run3	8.0	0.6	0.8 (high-plate)

In the simulation of run 1, the initial condition of the flow has already attained an equilibrium state; the perturbation grows very quickly at the interfacee. Figure 7.113 shows the time evolution of disturbances in the stratified flow, leading to continuous slugging in the pipe. At the beginning of the simulation when t=0s, the interface is flat and smooth. At t= 1s, small interface instability is generated close to the inlet as shown in the red line. At t=2s, an initial large slug has formed, the liquid level ahead of this slug front remain the same as the initial value, but behind this slug the liquid level drops. At the same time, a second slug has formed upstream closer to the inlet. At t=3s, the initial slug is traveling towards the pipe exit and is growing in size; ultimately, this initial slug leaves the pipe and a steady slug flow is approached. Corresponding to the same run, Figure 7.116 illustrates the time traces of the liquid hold-up at different locations during the first 40 seconds of simulation. The flow remains stratified at the first monitoring location with small instabilities appearing at the interface. Successive slugging is captured at 5.7m.

The results obtained in run 2 (with the plate in the lower position) are illustrated in Figure 7.114. Near the pipe inlet, the liquid level grows downstream until the equilibrium level is approached. In this case (as distinct to the case with an initial equilibrium level illustrated in Figure 7.114) the growth of a large slug from the initial excess liquid is not occurring. The results obtained from run 3 (with the plate in the upper position giving an initial holdup of 0.8)

reveal an interesting feature. As will be seen from Figure 7.115, large waves develop immediately after simulation begins. Subsequently an initial slug is formed close to the inlet at t=0.2s. While the initial slug travels towards the exit, it grows rapidly in length (as in the case of Run 1). Behind this slug, successive slugs are developing upstream. After this large initial slug exits the pipe, the subsequent slugs return as can be seen in Figure 7.118.

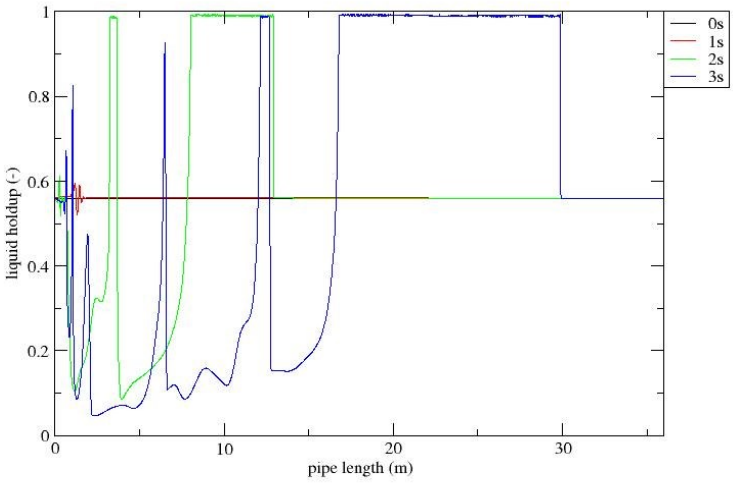

Figure 7.113: TRIOMPH prediction of time evolution of growing disturbance in the gas liquid interface, leading to the slugging in the pipe. Inlet liquid hold-up =0.56.

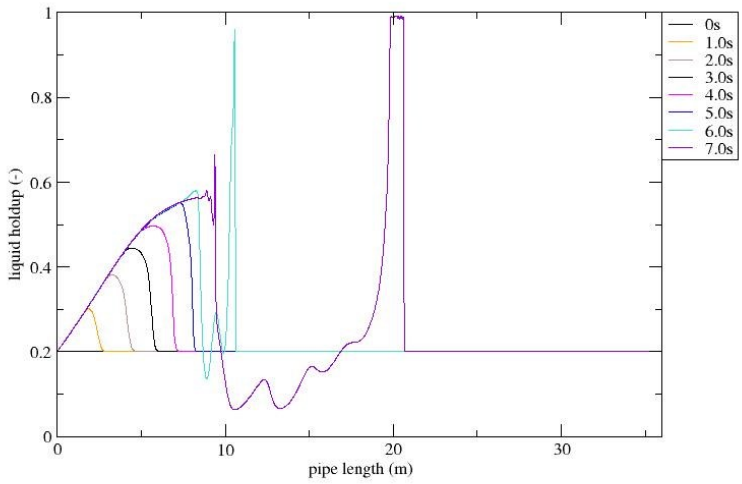

Figure 7.114: TRIOMPH prediction of time evolution of growing disturbance in the gas liquid interface, leading to the slugging in the pipe. Inlet liquid hold-up =0.2.

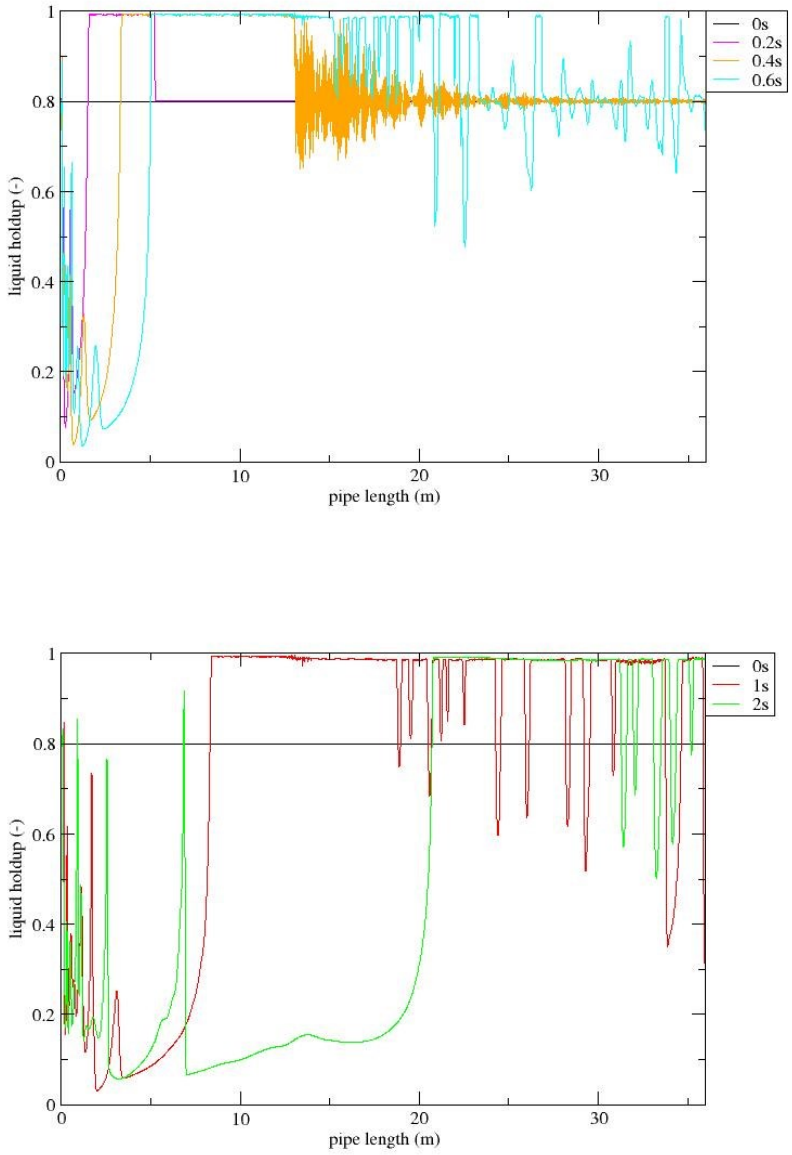

Figure 7.115: TRIOMPH prediction of time evolution of growing disturbance in the gas liquid interface, leading to the slugging in the pipe. Inlet liquid hold-up =0.8 (0 to 0.6s, upper graph. 0-2s, lower graph).

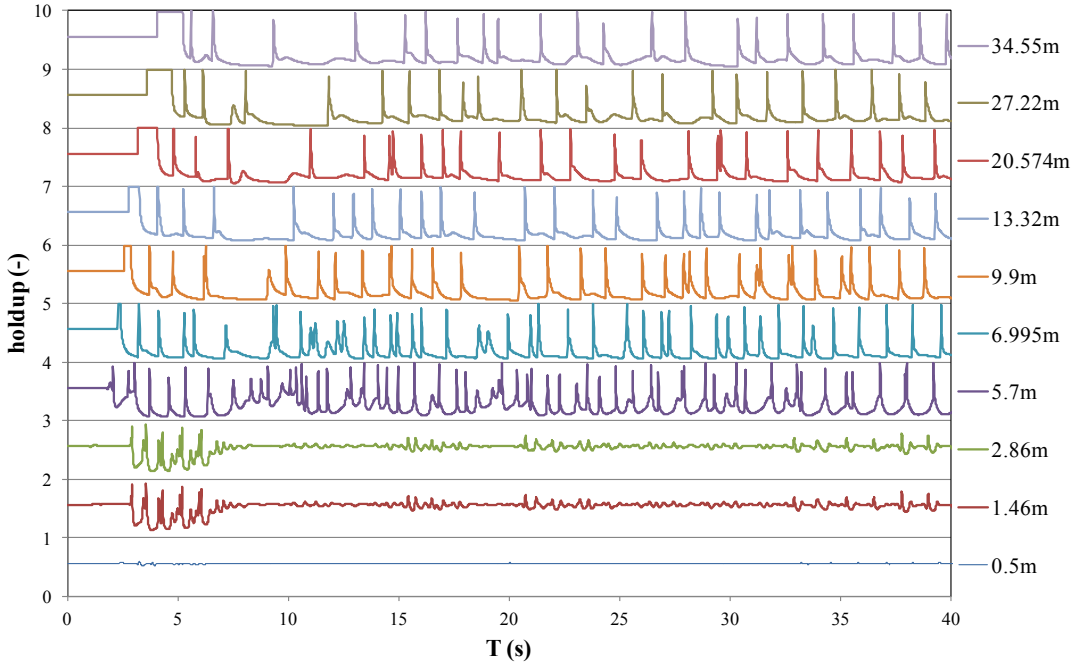

Figure 7.116: TRIOMPH prediction of flow evolution at different locations. Inlet liquid hold-up =0.56, Usl=0.6m/s and Usg=8.0m/s.

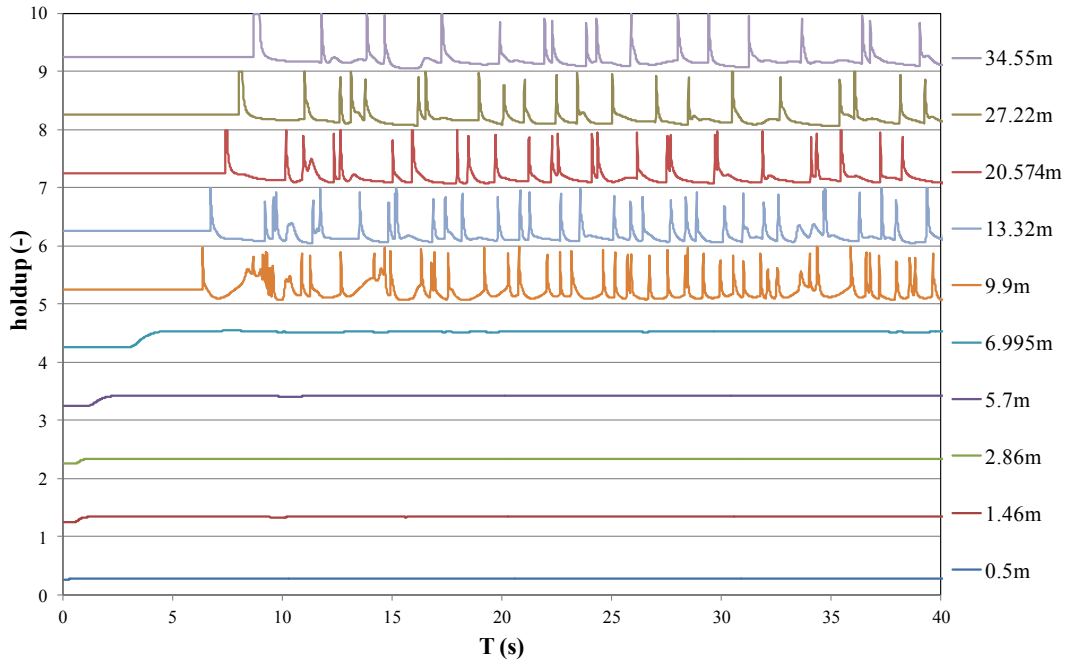

Figure 7.117: TRIOMPH prediction of flow evolution at different locations. Inlet liquid hold-up =0.2, Usl=0.6m/s and Usg=8.0m/s.

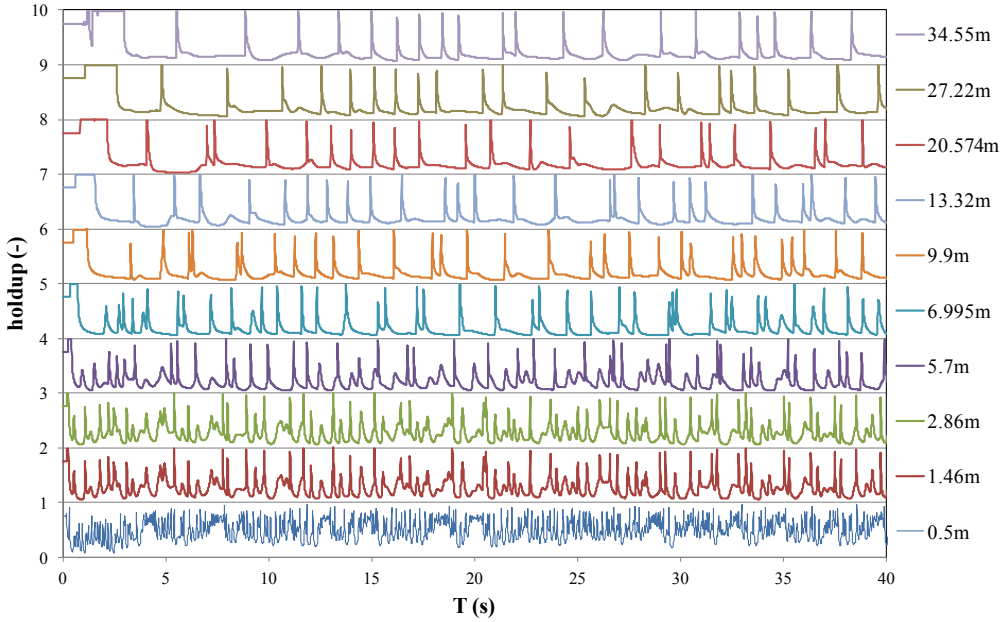

Figure 7.118: TRIOMPH prediction of flow evolution at different locations. Inlet liquid hold-up=0.8, Usl=0.6m/s and Usg=8.0m/s.

Figure 7.119 shows the predictions of slug frequency at different locations along the test section. The trends predicted for the 3 runs point to contrasting outcomes. In Run 1 (with an initial liquid holdup of 0.56, corresponding to an equilibrium stratified flow), slugs are in initiated at 5.7 m from the inlet, after which the frequency rises to 0.576 s^{-1}. The frequency then declines after the peak, increases slightly and finally attains a constant value of 0.265 s^{-1}. In Run2 (with an initial liquid holdup of 0.2), the peak of frequencies has vanished which contrasts with Run1, the flow starts slugging at 9.9 m from the inlet; then the number of slugs grows gradually to reach a plateau in frequency where f = 0.260 s^{-1}. In Run 3, the inlet liquid hold-up has beyond the equilibrium hold-up, small interface perturbation can quickly lead to slugs. Slug frequency increases between 0.5 m and 5.7 m, unlikely as the sharp peak in Run 1, the increase in frequency is rather gradual. Finally slug frequency reaches a plateau with the value of 0.235 s^{-1}.

This study has demonstrated that the choice of the inlet liquid hold-up in TRIOMPH simulation has strong influence on the prediction of the slug initiation position and frequency along the developing region. However, slug frequency approached to an asymptotic value in all three runs which reveals fully developed slug regime was attained in the simulation. The

choice of the inlet hold-up is essential for the analysis of the transient state that precedes fully-developed regime; however, it is not so crucial when the average flow characteristics are considered.

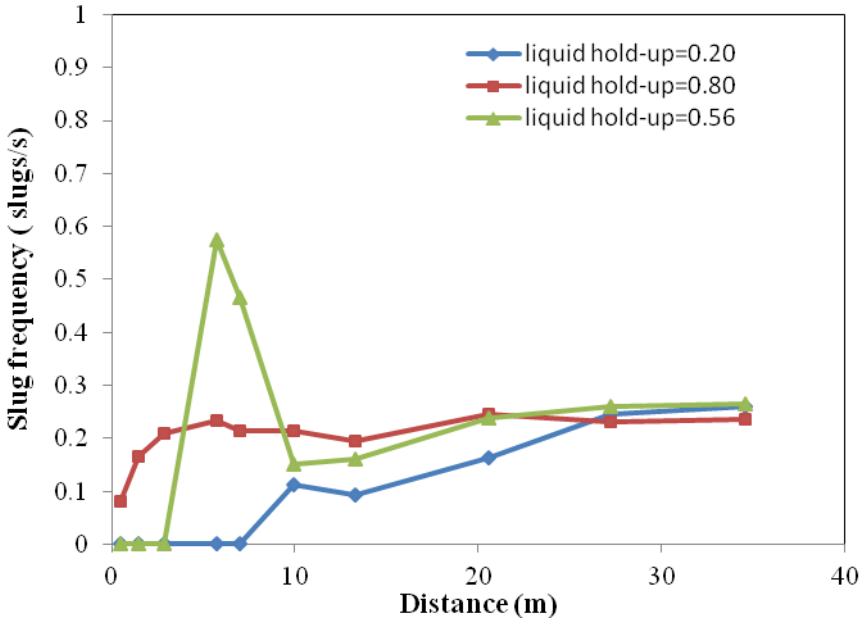

Figure 7.119: TRIOMPH predictions of slug frequency along the WASP test-section, with different inlet liquid hold-ups, Usl=0.2m/s and Usg=8.0m/s.

7.11.2 Prediction of fully developed slug frequency

Comparisons of developed slug frequency were made between the TRIOMPH predictions and values measured at the end of the WASP (37 m, long 78 mm diameter) test section. The experiments were carried out with air-water flows with an outlet pressure close to atmospheric. As was explained above, the data were obtained by Dr. C. P. Hale but are presented and analysed for the first time in this thesis. As discussed in section 7.9.1, the value of the hold-up specified at the inlet is not such crucial for the prediction of slug frequency at fully developed region; an equilibrium liquid hold-up was specified at inlet for each simulation run in this section. Figure 7.120 gives the comparison of the predicted slug frequency with WASP measurement data. For the data sets with liquid velocity of 0.4m/s and 0.6m/s, the numerical simulations demonstrates a reasonably good agreement with measurements, the maximum mean error is 29%.

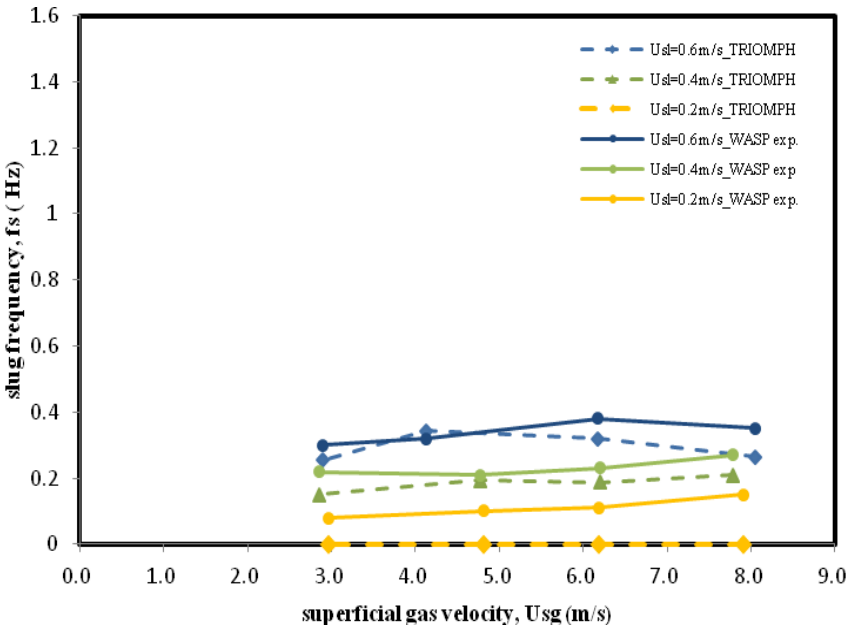

Figure 7.120: Comparison of the WASP air-water slug frequency data (solid lines) with the prediction of the TRIOMPH code (dashed lines).

However, for the data set with liquid velocity of 0.2m/s, the code fails to predict a transition from stratified flow to slug flow, the gas liquid interface remaining flat during the 300s of the simulation run. Mesh refinement studies were performed since, if the grid is not sufficient fine, damping may occur of the interface instability and the interfacial waves may not grow into slugs. However, the interface remained flat even with a refined mesh. A further set of TRIOMPH calculations were carried out with increased inlet liquid hold-up. As expected, the flow became more perturbed at the inlet, the instabilities grew larger and formed slugs downstream. However, the predicted slugging did not persist and the interface became flat at a sufficient distance from the inlet (see Figure 7.121). The slugs initiated in this case were a manifestation of the excess liquid level at the inlet.

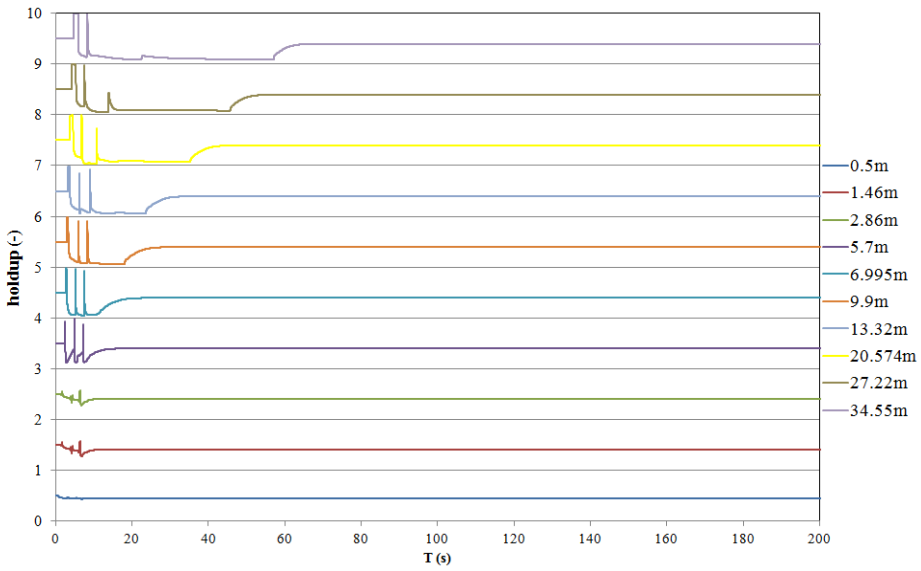

Figure 7.121: TRIOMPH prediction of flow evolution at different locations. Inlet liquid hold-up =0.5, Usl=0.2m/s and Usg=8.0m/s.

In the TRIOMPH code prediction, the main mechanisms responsible for the transition from stratified to slug flow are the growth of natural hydrodynamic instabilities. The following features were established relating the code prediction to the Kelvin-Helmholtz instability and the onset of slug flow (Issa & Woodburn, 1998):

(1) Below the viscous Kelvin-Helmholtz instability limit, the flow was stable over the full range of nodalisation (typically from 10 to 50 nodes per metre).

(2) Above the viscous Kelvin-Helmholtz limit, and below the inviscid Kelvin-Helmholtz limit, the flow was calculated as being unstable provided enough nodes were used in the calculation. As the number of nodes was increased, the wave growth rate became independent of the number of nodes, indicating numerical convergence of the calculations.

(3) Above the inviscid Kelvin-Helmholtz limit, flow is unstable. However, there was no numerical convergence with increasing number of nodes, indicating beyond the inviscid Kelvin-Helmholtz limit, the equations are ill-posed and there are no solutions to the basic equations.

Figure 7.123 is based on a linear stability analysis using an adaptation of the methodology of Barnea &Taitel (1994). Lines were calculated for the Inviscid and Viscous Kelvin-Helmholtz stability boundaries and shown on the plot. The linear stability analysis of the two-fluid model equations and the criteria used to plot the graph is given by Hale (2000).

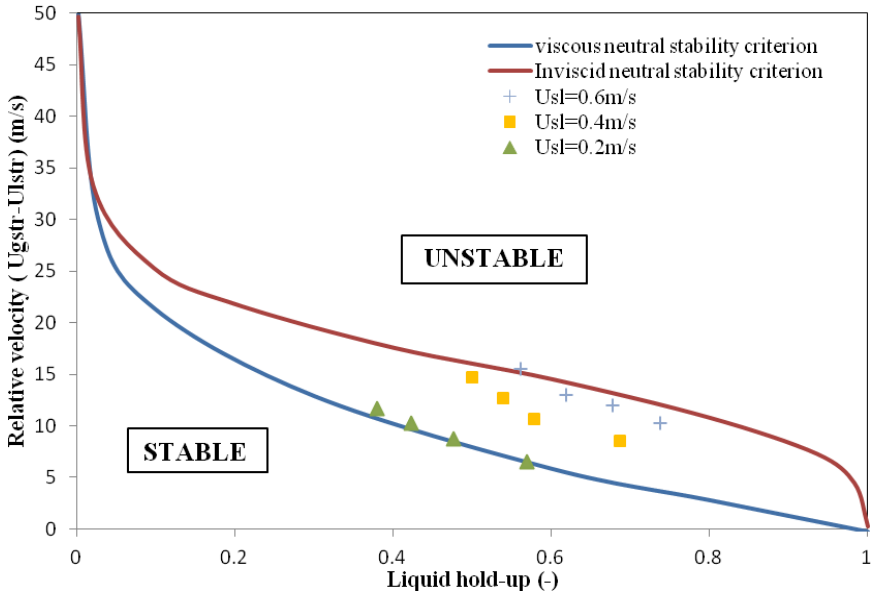

Figure 7.122: Comparison of the Viscous and Inviscid neutral stability criterion.

The initial conditions for the simulation runs are located between the viscous neutral stability and inviscid neutral stability lines, indicating all of the calculations were well-posed. For a liquid superficial velocity of 0.2m/s, and for the range of gas velocities covered, the conditions are located closely to the viscous neutral stability criterion, and this may explain why the simulations only predict stratified flow although the slug flow pattern was observed in experiments.

Although the one-dimensional code has demonstrated its ability to capture slug initiation and development from stratified flow, the discrepancy discussed above reveals that the code cannot always reproduce the experimental data due to the complex nature of slug flow. As already discussed in Chapter 4, the TRIOMPH code is based on the two-fluid model which can only capture long waves generated by Kelvin-Helmholtz type instabilities. However, in reality, the surface disturbances include short waves that the code does not account for. For example, experimental observations have shown that the interface between gas and liquid

becomes wavy when the gas velocity is high, with two-dimensional turbulent effects coming into play. These effects enhance the friction between the gas and liquid, which contributes to the formation of the slugs. In the calculations reported here, the interfacial friction factor f_i was assumed to be given by the same relationship as that used for the gas wall friction factor f_{GW} (Taitel and Dukler, 1976) The assumption is valid if the interface is considered to be plane surface that gas is flowing at relative speed $u_r = u_G - u_L$. The value of f_i is then very similar to the value of f_{GW}. However, at high gas velocity, the interfacial shear rises considerably resulting in an increase in the ratio of f_i / f_{GW}. This explains why the Taitel& Dukler correlation is only appropriate for smooth interfaces (Barbeau, 2008). Furthermore, the experimental observations have shown that the inlet geometry may introduce transient disturbance to the flow, which may trigger instabilities which quickly develop into slugs. The detailed inlet geometry cannot be modelled in the 1D simulation; consequently, the inlet disturbance cannot be captured in the simulation, leading to a mismatch with the experiments.

7.12 Conclusions

The following conclusions are drawn from the results presented in this chapter:

- Slug initiation mechanisms are dependent on the liquid level and wave generation process. The higher the liquid flow-rate, the higher the liquid level and the smaller amplitude of the wave needed to bridge the pipe. The higher gas flow-rates decrease the liquid level, but generate more waves.
- The slug flow initiation position is strongly affected by the inlet configuration. A high-plate inlet configuration shifts the initiation position closer to the inlet, whereas a low-plate inlet configuration shifts the slug initiation downstream.
- Plots of slug frequency as a function of distance show slug begin to be formed at some distance from the entrance of the test-section and their frequency increases rapidly due to the rapid initiation processes. Beyond a certain distance, the slug frequency starts to decrease due to the changing pickup rate at the font of slugs when they advance over a liquid film with varying heights. Eventually, further down the test-section, the slug frequency approaches a constant value invariant with length.
- The slug frequency generally increases as the liquid flow-rate increases due to an increase in the liquid level. The influence of increasing gas flow-rate on slug frequency is

more complex. In the initiation region, increase of the gas velocity increases the slug initiation frequency for the medium gas flow-rate because of more waves is generated. However, with a further increase the gas velocity, the thinning effect on the liquid film outweighs the increase in number of waves, hence the slug frequency decreases. At large distances from the inlet, the slug frequency does not show a strong dependence on the gas velocity.

- The inlet geometry significantly influences slug initiation, the high-plate inlet configuration yield the highest slug initiation frequency. However, the effect of inlet geometry on the liquid level reduces further downstream; hence the effect of inlet geometry on the slug development reduces along the pipe length. Beyond a certain distance, slug frequency approaches a constant value invariant with inlet geometry.
- Mean liquid holdup estimated at the locations near the test-section exit show the values increase with increasing liquid flow-rate and decreasing gas flow-rate as expected. In this fully developed region, the values are not significantly affected by inlet geometry.
- Extensive comparisons were made with empirical slug frequency correlations. For LOWPRESS air-oil and air-water data, the correlation of Schulkes (2011) performed best overall. For the WASP air-water data, the correlation of Heywood & Richardson (1979) performed best though its performance was not greatly superior to that of the Schulkes (2011) correlation. Overall, therefore, the correlation of Schulkes (2011) is recommended.
- In TRIOMPH simulations, the value of inlet liquid hold-up has been shown to have a strong influence on the prediction of slug initiation position and frequency in the developing region. However, if the pipe length is sufficiently great, then the influence of inlet hold-up is not large. These predictions were in qualitative agreement with the experimental observations.
- Slug frequency data obtained for air-water flows from the WASP facility were compared with predictions using the TRIOMPH code. The results show that the code is generally able to predict the data in the region between the viscous and inviscid Kelvin-Helmholtz stability boundaries. However, there were cases (near the viscous Kelvin-Helmholtz boundary) where the code failed to predict the slug flow observed in the experiments. It seems likely that this is because the (one-dimensional) code is only capture long waves generated by Kelvin-Helmholtz type of instabilities, whereas in reality the interfacial disturbances include shorter waves. Furthermore, the 1D nature of the code limits its ability to reproduce the 3-D nature of the slug initiation process.

Chapter 8

Conclusions and recommendations for the future work

8.1 Summary

The overall aim of the present project was to carry out analytical and computational studies to model the processes of slug initiation, growth and collapse in horizontal pipes. This chapter summarizes the conclusions arising from the work; recommendations for further work are also highlighted below.

8.2 Conclusions

In Chapter 2, a review of the various flow patterns which exist in two-phase horizontal flow was presented. A literature review was then carried on slug flow modelling, highlighting the evolution of slug flow which can be divided into three main topics: slug initiation, developing slug flow and steady-state slug flow. Whilst various slug flow models were proposed by earlier researchers, there is relative dearth information on the onset of the slugs and their subsequent development mainly due to the highly complex nature of the slug flow mechanisms.

In Chapter 3, Computational Fluid Dynamics (CFD) results concerning a benchmark for two-phase slug flow conducted in the WASP facility are presented. Six CFD codes were used to

simulate slug flow that implemented a VOF model (STAR-CD, FLUENT), a two-fluid approach (TRIOMPH, CFX, LedaFlow), and interface-tracking methods (TransAT). Apart from CFX which was conducted by present author, the rest of the simulations were performed or checked by code developers. Different assumptions and approximations have been applied in each case, which made the direct comparison among the codes difficult. 1D code TRIOMPH average the flow field over the cross sectional area of the pipe and model the radial variations by closure relations; quansi-3D LedaFlow slice averaged the flow field over the traversal distance z; 3D STAR-CD and FLUENT model the pipe with half cross-section by assuming symmetry over the xy central plane; TransAT modelled the actual geometry of the WASP inlet, whereas the rest of the codes have simplified the inlet as a plane section. Most of the codes were able to predict the transition from stratified flow to slug flow, apart from CFX where the flow was remain stratified and no slug was captured using the current model settings. Quantitively, comparison was made against the experimental measurement in terms of slug frequency. The prediction of TRIOMPH has captured the observed trend of slug frequency along the test-section, including a peak in the slug initiation site and an asymptotic value in the developed region. The rest of the codes including FLUENT, STAR-CD, LedaFlow and TransAT were failed to predict the experimental trends. The predictive capabilities of the various models underlying the CFD codes hence require further investigations.

In Chapter 3, the TRIOMPH code has shown a good capability of predicting slug flow, however the ability of the code is limited in a restrained region where the two-fluid equations employed in the code has to be well-posed. Therefore, in Chapter 4, the well-/ill-posed nature of the two-fluid equations was reviewed. For a well-posed system, a unique solution exists and the computed flow characteristics such as the average slug frequency are agreed with experimental values. Whereas for an ill-posed system, a unique solution no longer exists and the computed slug frequency diverges as the mesh is refined; this is because random unphysical disturbances occur in the stratified flow region due to the assumption of steady inlet boundary conditions. To remedy the ill-posedness of the equations which mainly occurs in the stratified region, the output of the TRIOMPH calculation was stored and recycled at the domain inlet, running a subsequent simulation with unsteady inlet boundary condition, and then a converged solution was obtained for an originally ill-posed case. An alternative method is to generate trains of slugs using slug tracking code, and feed the computed flow

information at the TRIOMPH inlet, similarly a unique solution was obtained regardless of the difference at the inlet. The coupling of the slug tracking code with TRIOMPH code provides a possible solution to overcome the limitation of ill-posedness of the system.

The three-dimensional simulation of WASP test-section was found time consuming and computational expensive. In Chapter 5, a systematic CFD study of slug flow was performed on a much smaller channel with rectangular cross-section, the code used was STAR-CCM+. The experimental data was provided by Forschungszentrum Rossendorf (FZD) from Germany. To track the gas liquid interface, a Volume-Of-Fraction (VOF) model was applied; a mesh sensitivity and parametric study were conducted to determine the settings that optimise accuracy and stability. The flow characteristics such as liquid holdup, average liquid level, and slug velocity were investigated and compared to the experimental measurements. Although the onset of interfacial instability, wave growth, and slug generation processes were qualitatively captured, quantitative comparisons against experimental data was complicated by the deviation in the slug initiation site. As detailed in Chapter 5, it is recommended that the experiment design is influenced by the modelling work at a sufficiently early stage so as to ensure that the data collected are optimal (in terms of spatial and temporal frequency) for this comparative study.

In Chapters 6 and 7, experimental data of air-oil and air-water slug flow performed on the LOWPRESS rig are presented, and a campaign of WASP air-water slug flow experimental data are analysed and presented. The slug initiation mechanisms were intensively studied by viewing the high speed images recorded for the LOWPRESS air-oil two phase flow. The visual observations indicate that the slug initiation mechanisms are dependent on the liquid level and wave generation process. With relative low liquid and gas velocities, the flow is initially stratified and the interface is smooth; the instabilities on the gas-liquid interface gradually grow into larger amplitude waves and finally bridge the pipe, forming slugs. Increasing liquid flowrate leads to an increase in the average film thickness, facilitating pipe-bridging. The rise of liquid level can also cause a higher relative velocity between gas and liquid leading to a wavier interface and more frequent slug formation. The phenomenon of wave develops on the rebuilding film was observed; it may either dissipates or develops into slug. If a wave grows in amplitude more quickly than the decrease in height of the interface, a bridging event will occur, whereas if the decrease in the liquid height is greater than the

gain in amplitude of the waves, the waves may increase in size but no bridging events will occur, this is in line with the work of Davies (1992). Increasing the gas velocity, the liquid level tends to be lower but waves grow more rapidly at the interface. The slug precursors tend to be shorter and formed more frequently with higher gas velocity. As highlighted by Lin and Hanratty (1986), the higher gas velocities will cause higher aeration in slugs, and it is agreed with present observations. The gas entrainment caused by the higher gas velocity interferes with the mechanism of liquid pick-up at the slug front, leading to the development of complex flow structures within the slug. Therefore at high gas velocity, it becomes more difficult to differentiate between slugs and large roll waves which may touch the top of the pipe without forming a liquid bridge. One characteristic of a slug precursor is that the liquid film drops sharply at its tail. In contrast, a large wave normally shows a much gradual decrease of liquid height in its tail profile. Another indicator of slug-formation is by looking at the velocity, slug propagates at a velocity at least equal to the mixture velocity, whereas wave tends to move slower.

The slug evolution including the slug initiation and propagation processes were investigated by looking at the slug frequency distribution at various locations. Slug frequency as a function of distance from the inlet was plotted for both LOWPRESS air-oil and air-water flow systems. Close to the entrance, the slug frequency increases due to the rapid slug initiation, while beyond a certain distance, it tends to decrease due to the slugs merge or collapse. The pickup rate at the font of slug depends on the height of liquid level immediately downstream of that slug. Ultimately, when the pickup and shedding rates of liquid and gas are equal, slugs are fully developed and will persist towards the pipe exit. Therefore, further down the test-section, the slug frequency approaches to a constant, fully-developed value.

The effect of inlet geometry was particularly investigated by changing the inlet configuration in which fluids are introduced into the test-section. One type of the inlet contains a stratification plate, and by varying the level of the plate, the entry liquid level can be altered. Observation indicates the initiation process of the slugs are strongly influenced by the initial liquid level, the higher liquid level would ease the pipe bridging and results in more frequent slug formation. Another type of the inlet does not contain stratification plate, fluids are mixed in a larger pipe section at the inlet and then gradually enter the test-section through a reducer. The reducer unexpectedly introduced disturbance to the flow and leads to a more pronounced

slug initiation rate than another type of inlet. However, in both cases, beyond a certain distance, the influence of inlet on the flow becomes negligible. For the same combination of phase velocities, an asymptotic value of slug frequency was obtained in the downstream close to the exit, regardless of the difference in the inlet configurations.

An extensive comparison with empirical slug frequency correlations was also performed. Some correlations exhibited considerable variance with experimental data; large difference between the predictions of the correlations themselves were also identified. Overall, the correlation of Schulkes (2011) is recommended.

8.3 Recommendations for future work

Some suggestions and recommendations for a future development of this research are proposed in what follows.

8.3.1 Experimental studies

The experiments conducted in the present study provide fresh insights into the phenomena of slug initiation and subsequent development, which are very useful for the modelling of this process, in one- and multi-dimensions. The present studies have revealed a number of possible directions for further investigation on these facilities.

The air-oil experiments conducted in LOWPRESS facility with high-speed photography enables three-dimensional optical observation of the actual bridging process, and hence provides a clear insight into the phenomena of slug initiation and development. However, the fixed position of the high-speed camera limits its ability to synchronously track the evolution of the slug from the inlet to the exit of the test-section, and to record the process of gas entrainment and shedding. This can be improved by using a moving camera system, in which a high-speed camera is attached to an actuation and position unit, linked to a rail parallel to the test-section and driven by a motor. When the fluids enter the inlet, the camera will be pushed along the rail at a controlled speed. Particle Image Velocimetry (PIV) can also can be used to generate 2 and 3D velocity maps of fluid flows. Using PIV could give a better understanding of the mechanisms involved in the liquid phase of slug initiation. Alternative

methods, however, would be needed to provide information on the velocity field in the gas phase; this is crucial to aid our understanding and modelling of slug development.

In present study, the observed slug initiation mechanism supports the slug initiation model suggested by Davies (1992) and Hale (2000). However, a broader range of experimental conditions could lead to a better understanding of the conditions under which certain slug initiation mechanisms dominate. The findings can be used to discriminate between candidate models. The superficial velocities in the present work were measured in limited slug flow region in parameter space; in particular, the liquid velocity was rather small and could not be increased further. The liquid flowrate could be increased by using a more powerful pump with a more accurate Rotameter to record higher liquid flow rates. Whilst the influence of inlet geometry on the slug initiation process was intensively studied on the LOWPRESS facility, this investigation can be further extended in WASP facility, with air-water/air-oil two phase and air-water-oil three phase system, with various pressures. A series of gamma densitometers or conductivity probes can capture the slug initiation and development process along the test-section. The inlet geometry of WASP facility could be altered by inserting a conical cone reducer (see Figure 8.1), and its influence can be investigated.

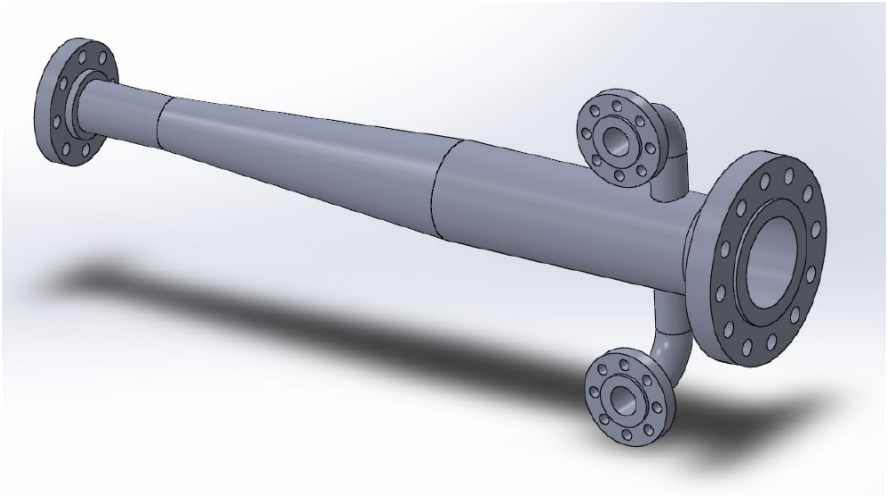

Figure 8.1: The schematic design of the WASP conical shape inlet system.

The onset of gas entrainment into the slug precursor from the time of bridging is an important feature of slug initiation mechanism, and very few studies have been performed to investigate the bubble behaviour in the slug body. It is possible to use an optical probe to achieve the

measurement. A multiple sensor optical probe was designed and fabricated in the present study as shown in Figure 8.2; it is attached to a replacement pipe section and can be inserted into pipe test-section. The sensor tip is in a U shape wielded by two optical fibers, and it is oriented to the direction opposite to the main stream flow. The probe was able to record the bubbles which penetrate through the sensors, hence providing information on bubble size distribution. However, the sensor tip was fragile and broke off in the high-speed flows; an improved design of the optical probe is recommended for future work.

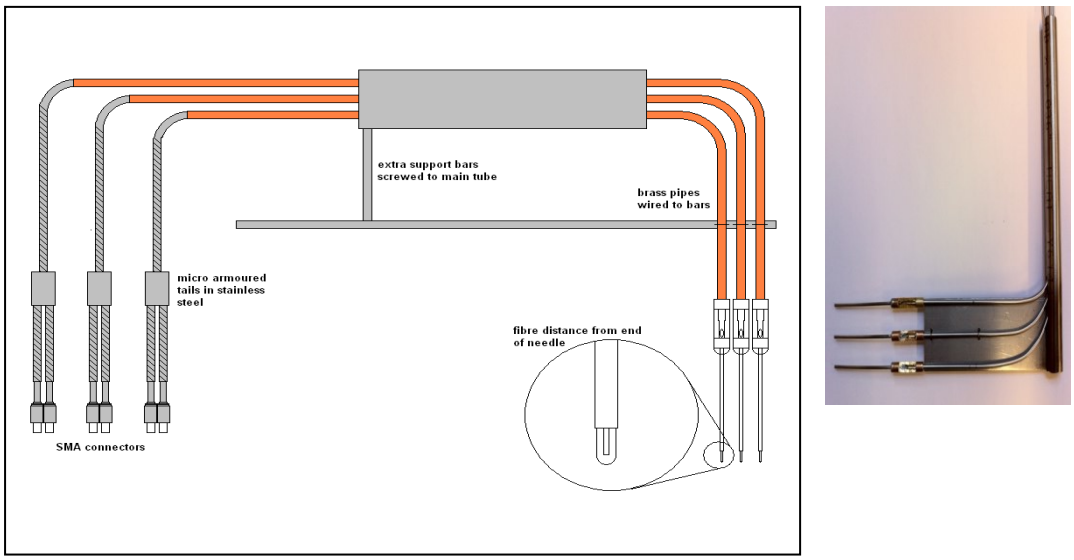

Figure 8.2: Design (left) and actual image (right) of multi-sensors optical probe.

8.3.2 CFD simulation

The CFD work presented in this thesis has demonstrated the ability to qualitatively capture the transition from stratified flow to slug flow. However the deviation between the measurements and numerical predictions motivates continuous study in the CFD modelling of slug evolution. The work can be extended in a number of directions:

1) From the experiments, the slug initiation process was found to be strongly impacted by the inlet condition. This should be accounted for in the CFD simulations. The actual inlet geometry such as feed streams and stratification plate needs to be included in the

modelling domain, in order to reproduce the physics in reality. The influence of the inlet condition on slug flow could be also systematically examined in the numerical study as part of the comparative study.

2) The slug length and velocity were not intensively studied in the CFD simulations, which are important flow characteristics and can serve as reference for the slug identification; investigation of these parameters are recommended for the future study.

3) The gas entrainment was not analyzed in present CFD work, improvements in models and computation grid could lead to proper physical modelling of this process, and should be pursued as an important phenomenon of slug flow.

4) It is recommended that the CFD work should be extended to the three-phase flows to investigate not only the interface instability of the gas-liquid phase but also the liquid-liquid phase.

Bibliography

(2006 December). ANSYS CFX-Solver Theory Guide.

A. Gregory G.,K. Nicholson M.&K. Aziz (1978). "Correlation of the liquid volume fraction in the slug for horizontal gas-liquid slug flow." International Journal of Multiphase Flow **4**(1): 33-39.

Al-Safran E. (2008). Slug frequency in gas/liquid horizontal flow. Proc., 6th North American Conference on Multiphase Technology, Banff, Canada.

Andritsos N.&Hanratty T.J. (1987). "Influence of interfacial waves in stratified gas–liquid flows." Int. J. Multiphase Flow **33**: 444–454.

Andritsos N.,Williams L.&Hanratty T.J. (1989). "Effect of liquid viscosity on the stratified-slug transition in horizontal pipe flow " Int. J.Multiphase Flow **15**: 877–892.

Andritsos N.,Williams L.&Hanratty T.J. (1989). "Effect of liquid viscosity on the stratified-slug transition in horizontal pipe flow." International Journal of Multiphase Flow **15**(6): 877-892.

Ansari M.R.&Shokri V. (2010). "Numerical modeling of slug flow initiation in a horizontal channels using a two-fluid model." International Journal of Heat and Fluid Flow **In Press, Corrected Proof**.

Baker O. (1954). "Designing for Simultaneous Flow of Oil and Gas." Oil and Gas Journal **53**(12): 185-195.

Barbeau S. (2008). Improved models for transient one-dimensional simulations of multiphase slug flows. Mechanical Engineering Imperial College London **PhD**.

Barnea D.&Brauner N. (1985). "Holdup of the liquid slug in two-phase intermittent flow." Int. J.Multiphase Flow **11**(1): 43-49.

Barnea D. (1987). "A unified model for predicting flow-pattern transitions for the whole range of pipe inclinations." International Journal of Multiphase Flow **13**(1): 1-12.

Barnea D.&Taitel Y. (1993). "Kelvin-Helmholtz stability criteria for stratified flow: viscous versus non-viscous (inviscid) approaches." International Journal of Multiphase Flow **19**(4): 639-649.

Baroczy C.J. (1966). "A systematic correlation for two-phase pressure drop." Chem. Eng. Prog.Symp. Ser. **62**(44): 232-249.

Bartosiewicz Y.,Laviéville J.&Seynhaeve J.M. (2008). "A first assessment of the NEPTUNE_CFD code: Instabilities in a stratified flow comparison between the VOF method and a two-field approach." International Journal of Heat and Fluid Flow **29**(2): 460-478.

Beggs H.D.&Brill J.P. (1973). "A Study of Two-Phase Flow in Inclined Pipes." Journal of Petroleum Technology: 607-617.

Bendiksen K.H. (1984). "An experimental investigation of the motion of long bubbles in inclined tubes." Int. J. Multiphase Flow **10**(4): 467-483.

Bendiksen K.H. (1984). "An experimental investigation of the motion of long bubbles in inclined tubes." International Journal of Multiphase Flow **10**(4): 467-483.

Benjamin T.B. (1968). "Gravity currents and related phenomena." J. Fluid Mech. **31, part 2,**: 209-248.

Bonizzi M.&Issa R.I. (2003). "A model for simulating gas bubble entrainment in two-phase horizontal slug flow." International Journal of Multiphase Flow **29**(11): 1685-1717.

Brill J.P.,Schmidt Z.,Coberly W.A.,Herring J.D.&Moore D.W. (1981). "Analysis of Two-Phase Tests in Large-Diameter Flow Lines in Prudhoe Bay Field" SPE Journal: 363-378.

Bruno K.&McCready M.J. (1989). "Processes which control the interfacial wave spectrum in separated gas -liquid flows " Int. J. Multiphase Flow **15**: 531-552.

CD-Adapco (CD-Adapco). Spotlight on parallel performance_STAR CCM+ V7.04, CD-Adapco.

Chisholm D. (1967). "A theoretical basis for the Lockhart-Martinelli correlation for two-phase flow." Int. J. Heat Mass Transfer **10**: 1767-1778.

Davies S.R. (1992). Studies of two-phase intermittent flow in pipelines. Department of Chemical Engineering and Chemical Technology, Imperial College London.

Dhulesia H.,Hustvedt E.&Todal O. (1993). Measurement and analysis of slug characteristics in multiphase pipelines. 6th International Conference on Multiphase Production. Cannes, France.

Dukler A.E.&Hubbard M.G. (1975). "A model for gas-liquid slug flow in horizontal and near horizontal tubes." Ind. Eng. Chem. Fundam. **14**(4): 337-347.

Dukler A.E.,Maron D.M.&Brauner N. (1985). "A physical model for predicting the minimum stable slug length." Chem. Eng. Sci. **40**: 1379-1385.

Espedal M.&Bendiksen K.H. (1989). Onset of instabilities and slugging in horizontal and nearhorizontal gas-liquid flow. European two-phase flow group meeting. Paris**:** 1-30.

Fairhurst C.P. (1988). "Slug-flow behaviour clarified in large-diameter pipeline study." Oil & Gas Journal of Fluids Engineering **86**: 49-57.

Fan Z.,Lusseyran F.&Hanratty T.J. (1993). "Initiation of slugs in horizontal gas–liquid flows." AIChE J. **39**: 1741–1753.

Frank T. (2003). Numerical simulations of multiphase flows using CFX-5. German CFX Users Conference. Garmisch-Partenkirchen, Germany.

Gardner G.C. (1979). "Onset of Slugging in Horizontal Ducts." International Journal of Multiphase Flow **5**(1): 201.

Gokcal B.,Al-Sarkhi A.S.,Sarica C.&Al-Safran E.M. (2009). "Prediction of slug frequency for high viscosity oils in horizontal pipes." SPE 124057: 136-144.

Gregory G.A.&Scott D.S. (1969). "Correlation of liquid slug velocity and frequency in horizontal co-current gas-liquid slug flow." AIChE Journal **15**(6).

Gregory G.A.,Nicholson M.K.&Aziz K. (1978). "Correlation of the Liquid Volume Fraction in the Slug for Horizontal Gas-Liquid Slug Flow." International Journal of Multiphase Flow **4**: 33-39.

Greskovich E.J.&Shrier A.L. (1971). "Pressure drop and holdup in horizontal slug flow." AIChE Journal **17**(5): 1214-1219.

Hale C.P. (2000). slug formation, growth and collapse. Department of Chemical Engineering and Chemical Technology, Imperial College London.

Harlow F.H.&Amsden A.A. (1975). "Numerical calculation of multiphase fluid flow." J. Comput. Phys. **17**(1): 19-52.

Hewitt G.F. (1982). Gas-liquid two-phase flow. Handbook of Multiphase Systems. Hetsroni G., Hemisphere Publishing Corp.

Heywood N.I.&Richardson J.F. (1979). "Slug flow of air-water mixtures in a horizontal pipe: determination of liquid holdup by g-ray absorption." Chem. Eng. Sci. **34**: 17-30.

Hill T.J.&Wood D.G. (1990). A new approach to the prediction of slug frequency. SPE 20629, 65th Annual Technical Conference and Exhibition of the Society of Petroleum Engineers. NewOrleans, LA**:** 141-149.

Hill T.J.&Wood D.G. (1994). Slug flow: Occurrence, Consequences and prediction. SPE 27960. University of Tulsa centennial petroleum engineering symposium, Tulsa, OK, USA, August 29-31**:** 53-62.

Ishii M. (1975). Thermo-fluid dynamic theory of two-phase flow. NASA STI/Recon Technical Report A.

Ishii M. (1982). Wave Phenomena and Two-Phase Flow Instabilities. Handbook of Multiphase Systems, Hemisphere Publishing Corp.

Ishii M.&Hibiki T. (2006). "Thermo-fluid Dynamics of Two-Phase Flow " New York: Springer.

Issa R.I.&Abrishami Y. (1986). Computer modelling of slugging flow. Petroleum Eng. Dept., Imperial College London.

Issa R.I.&Woodburn P.J. (1998). " Numerical prediction of instabilities and slug formation in horizontal two-phase flows. ." In 3rd International Conference on Multiphase Flow ICMF: 98.

Issa R.I.&Kempf M.H.W. (2003). "Simulation of slug flow in horizontal and nearly horizontal pipes with the two-fluid model." International Journal of Multiphase Flow **29**(1): 69-95.

Issa R.I.&Montini M. (2009). Slug Prediction Exercise: 1D Model. TMF, Imperial College Londo.

Jepson W.P.&Taylor R.E. (1988). Slug flow and its transitions in large diameter horizontal pipes, Internal report AERE R 12992. Thermal Hydraulics Division, Harwell Laboratory,Oxfordshire**:** 1-26.

Khor S.H. (1998). Three phase liquid-liquid-gas stratified flow in pipelines. Department of Chemical Engineering and Chemical Technology, Imperial College London.

King M.J. (1998). Experimental and modelling studies of transient slug flow. Department of Chemical Engineering and Chemical Technology, Imperial College London.

Kordyban E. (1985). "Some details of developing slugs in horizontal 2-phase flow." AIChE J. **31**: 802–806.

Kordyban E.S.&Ranov T. (1970). "Mechanism of Slug Formation in Horizontal Two-Phase Flow." Journal of Basic Engineering **T.A.S.M.E**((December)): 857-864.

Kordyban E.S. (1977). "The Transition to Slug Flow in the Presence of Large Waves." International Journal of Multiphase Flow **3**: 603.

Kowalski J.E. (1987). "Wall and interfacial shear stress in stratified flow in a horizontal pipe." AIChE Journal **33**(2): 274-281.

Labois M.,Narayanan C.&Lakehal D. (2010). A New CFD approach for urban flow and pollution dispersion simulation. The Fifth International Symposium on Computational Wind Engineering (CWE2010). Chapel Hill, North Carolina, USA.

Lakehal D. (2010). "LEIS for the Prediction of Turbulent Multifluid Flows for Thermal Hydraulics Applications." Nucl. Eng. Des. **240**: 2096–2106, 2010.

Lakehal D.,Labois M.&Narayanan C. (2011). Advances in the simulation of multiphase flows in pipelines. 8th International Conference on CFD in Oil & Gas, Metallurgical and Process Industries SINTEF/NTNU. Trondheim NORWAY.

Laux H.,Meese E.,Johansen S.T.,Ladam Y.,Bansal K.M.,Danielson T.J.,Goldszal A.&Monsen J.I. (2007). Simulation of multiphase flows composed of large scale interfaces and dispersed fields. Proc. Int. Conf. Multiphase Flows. Leipzig**:** S5.

Lebanon N.H. (2008). "ANSYS-Fluent Inc, Fluent 12.0 User Manual."

Leebeeck A.D.&Nydal O.J. (2009). "Simulation of large amplitude waves in a slug tracking scheme compared to roll wave experiments at high pressure." International Journal of Multiphase Flow **36**(1): 40-50.

Lin P.Y.&Hanratty T.J. (1986). "Prediction of the initiation of slugs with linear stability theory." International Journal of Multiphase Flow **12**(1): 79-98.

Liné A.,Masbernat L.,Miré A.&Soualmia A. (1991). Analysis of the Local Structure of Co-Current Stratified Two-Phase Flow. European Two-Phase Flow Group Meeting. Rome.

Lockhart R.W.&Martinelli R.C. (1949). "Proposed correlation of data for isothermal two-phase, two component flow in pipes." Chem. Engng. Prog. **45**(1): 39-48.

Lunde O.&Asheim H. (1989). An experimental study of slug stability in horizontal flow. the 4th International Multiphase Flow Conference, Nice, France, C.P. Fairhust (Ed.).

Mandhane J.M.,Gregory G.A.&Aziz K. (1974). "A flow pattern map for gas--liquid flow in horizontal pipes." International Journal of Multiphase Flow **1**(4): 537-553.

Manfield P.D. (2000). Experimental, computational and analytical studies of slug flow. Department of Chemical Engineering and Chemical Technology, Imperial College London.

Manolis I.G. (1995). High pressure gas -liquid slug flow. Department of Chemical Engineering and Chemical Technology, Imperial College London.

Matthew K. (1998). Experimental and modelling studies of Transient slug flow. Chemical Engineering and Technology Imperial College London

McAdams W.H.,Woods W.K.&Heroman L.C. (1942). "Vaporisation inside Horizontal Tubes. II - Benzene-oil mixtures 64, Pages: 93-100." Transaction of American Society of Mechanical Engineers (A.S.M.E.) **64**: 93-100.

McAdams W.H.,Woods W.K. &Heroman L.C. (1942). "Vaporisation inside horizontal tubes, 2:Benzene-Oil mixtures." Trans .A.S.M.E., 1942 **66**: 193-200.

Menter F.R. (1994). "Two-equation eddy-viscosity turbulencemodels for engineering applications." AIAA Journal **32**(8): 1598-1605.

Michell J.H. (1893). "The Highest Waves in Water." Phil. Mag. **5**(36): 430.

Minato A.,Ikeda T.&Naitoh M. (1986). "Mechanistic Model of Slugging Onset in Horizontal Circular Tube." Journal of Nuclear Science and Technology **23**: 761-768.

Mishima K.&Ishii M. (1980). "Theoretical Prediction of Onset of Horizontal Slug Flow." Journal of Fluids Engineering **102**(441-444).

Mo S.,Ashrafian A.,Barbier J.C.&Johansen S.T. (2012). QUASI-3D MODELLING OF TWO-PHASE SLUG FLOW IN PIPES. Ninth International Conference on CFD in the Minerals and Process Industries. CSIRO, Melbourne, Australia.

Mo S.,Ashrafian A.,Barbier S.J.&Johansen S. T. (2012). Quasi-3D modelling of two-phase slug flow in pipes. Ninth International Conference on CFD in the Minerals and Process Industries. CSIRO, Melbourne, Australia.

Mohammed K.A. (2012). Slug front gas entrainment in gas-liquid two-phase flow in horizontal and near horizontal pipes. Department of Chemical Engineering and Chemical Technology, Imperial College London

Montini M. (2011). Closure relations of the one-dimensional two-fluid model for the simulation of slug flows. Department of Mechanical Engineering, Imperial College London **PhD**.

Netto J.R. Fagundes,Fabre J.,Grenier P.&Peresson L. (1998). An experimental study of an isolated long bubble in an horizontal liquid flow. the 3rd International Conference on Multiphase Flow, Lyon, France.

Nicklin D.J.,Wilkes J.O.&Davidson J.F. (1962). "Two phase flow in vertical tubes." Trans. Inst.Chem. Eng. Sci. **40**: 61-68.

Nydal O.J.&Andreussi P. (1991). "Gas Entrainment in a Long Liquid Slug Advancing in a Near Horizontal Pipe." International Journal of Multiphase Flow(17): 179-189.

Nydal O.J.&Banerjee S. (1994). " Dynamic slug tracking simulations for gas-liquid flow in pipelines." Chem. Eng. Commun. **141**(1): 13-39.

Ooi S.Y. (2002). Prediction of Slug Body Void Fraction. Final Year Link Project Report, Department of Chemical Engineering and Chemical Technology, Imperial College London.

Paglianti A.,Andreussi P.&Nydal O.J. (1993). The effect of fluid properties and geometry on void distribution in slug flow. 6th International Conference on Multiphase Production. Cannes, France**:** 193-203.

Pan J. (2010). Gas entrainment in two-phase gas-liquid slug flow. Department of Chemical Engineering and Chemical Technology, Imperial College London.

Pan J. (2010). Gas entrainment in two-phase gas-liquid slug flow. Department of Chemical Engineering and Chemical Technology, Imperial College London.

Pan L. (1996). High pressure three-phase (gas/liquid/liquid) flow. Department of Chemical Engineering and Chemical Technology, Imperial College London.

Patankar S.V. (1980). Numerical Heat Transfer and Fluid Flow. McGraw-Hill, New York.

Premoli A.,Francesco D.&Prina A. (1970). An Empirical Correlation for Evaluating Two-Phase Mixture Density under Adiabatic Conditions European Two-Phase Flow Group Meeting.

Renault F. (2007). A Lagrangian slug capturing scheme for gas-liquid flows in pipes. Department of Energy and Process Engineering, Norwegian University of Science and Technology.

Rippiner J.M. (1998). Transient slug flow modelling in horizontal and near horizontal pipelines. . Mech. Eng. Dept. , Imperial College London. **Master's thesis**.

Ruder Z.,Hanratty P.J.&Hanratty T.J. (1989). "Necessary conditions for the existence of stable slugs." Int. J. Multiphase Flow **15**(2): 209-226.

Salvo F.D. (2009). Prediction of transition from Stratified to Slug Flow and Vice-versa. TMF. Imperial College London

Schulkes R. (2011). BHR Group 2011 Multiphase 15.

Scott D.S. (1964). Properties of Cocurrent Gas-Liquid Flow. Advances in Chemical Engineering. Thomas B. Drew John W. Hoopes, Jr.&Theodore Vermeulen, Academic Press. **Volume 4:** 199-277.

Spedding P.L.&Hand N.P. (1997). "Prediction in stratified gas-liquid co-current flow in horizontal pipelines. ." Int. J. Heat Mass Transfer **40**(8): 1923-1935.

Srichai S. (1994). High pressure separated two-phase flow. Department of Chemical Engineering and Chemical Technology, Imperial College London.

Taitel Y.&Dukler A.E. (1976). "A model for slug frequency during gas-liquid flow in horizontal and near horizontal pipes." International Journal of Multiphase Flow **3**(6): 585-596.

Taitel Y.&Barnea D. (1990). "Two-phase slug flow." Advances in Heat Transfer **20**(1990): 83-132.

Taitel Y.&Barnea D. (1998). "Effect of gas compressibility on a slug tracking model." Chemical Engineering Science **53**(11): 2089-2097.

Thompson C.,Verdin P.,Kalogerakos S.&Jia N. (2010). Prediction Options for Slug Flows: Overview of Modelling Work. TMF4/P161(09), Imperial College London.

Tomasello A.&Lo S. (2009). STAR-CD Results of Slug Flow Analysis. TMF4/P163(09), Imperial College London

Tronconi E. (1990). "Prediction of slug frequency in horizontal two-phase slug flow." AIChE Journal **36**(5): 701-709.

Tu J.,Guan H.Y.&Liu C. (2008). Computational fluid dynamics: A practical approach. Oxford, UK, Butterworth-Heinemann.

Ujang P.M. (2003). Studies of Slug Initiation and Development In Two Phase Gas-Liquid Pipeline Flow. Department of Chemical Engineering and Chemical Technology, Imperial College London.

Ujang P.M.,Lawrence C.J.&Hewitt G.F. (2004). A Simple Incompressible and Conservative Slug Tracking Model, Report 2 of TMF3 Sub-project II. Department of Chemical Engineering and Chemical Technology, Imperial College London.

Ujang P.M.,Lawrence C.J.,Hale C.P.&Hewitt G.F. (2006). "Slug initiation and evolution in two-phase horizontal flow." International Journal of Multiphase Flow **32**(5): 527-552.

Vallée C.,Höhne T.,Prasser H.M.&Sühnel T. (2005). Experimental modelling and CFD simulation of air/water flow in a horizontal channel. International topical meeting NURETH-11. Avignon, France.

Vallée C.,Lucas D.,Beyer M.,Pietruske H.,Schütz P.&Carl H. (2010). "Experimental CFD grade data for stratified two-phase flows." Nuclear Engineering and Design **240**(9): 2347-2356.

Wallis G.B.&Dobson J.E. (1973). "The Onset of Slugging in Horizontal Stratified Air-Water Flow." International Journal of Multiphase Flow **1**: 173-193.

Weisman J.,Duncan D.,Gibson J.&Crawford T. (1979). "Effects of fluid properties and pipe diameter on two-phase flow patterns in horizontal lines." Int. J. Multiphase Flow **5**(6): 437-462.

Wong W.L. (2003). Flow development and mixing in three-phase slug flows. Department of Chemical Engineering and Chemical Technology, Imperial College London.

Woods B.D.&Hanratty T.J. (1996). "Relation of slug stability to shedding rate." International Journal of Multiphase Flow **22**(5): 809-828.

Woods B.D.,Fan Z.&Hanratty T.J. (2006). "Frequency and development of slugs in horizontal pipe at large liquid flows." Int. J. Multiphase Flow **32**(8): 902-925.

Xu J.,Wu Y.,Shi Z.,Lao L.&Li D. (2007). "Studies of two-phase co-current air/non-Newtonian shear-thinning fluid flows in inclined smooth pipes. ." Int. J. of Multiphase Flow **33**: 948-969.

Y. Taitel&E. Dukler A. (1977). "A model for slug frequency during gas-liquid flow in horizontal and near horizontal pipes." International Journal of Multiphase Flow **3**(6): 585-596.

Yih C.S. (1967). "Instability due to viscosity stratificaton " J. Fluid Mech. **27**(2): 337-352.

Zabaras G. (2000). "Prediction of Slug Frequency for Gas/Liquid Flows." SPE Journal **5**(3): 252-258.

Zhang H.Q.,Wang Q.,Sarica C.&Brill J.P. (2003a). "Unified model for Unified model for gas-liquid pipe flow via slug dynamics-part 1: modeldevelopment." ASME J. Energy Res. Tech.(125): 266.

Zheng G. (1991). Two-phase slug flow in hilly terrain pipelines. . USA, University of Tulsa. **PhD**.

Zheng G.,Brill J.P.&Taitel Y. (1994). "Slug flow behavior in a hilly terrain pipeline." International Journal of Multiphase Flow **20**(1): 63-79.

Zuber N.&Findlay J.A. (1965). "Average volumetric concentration in two-phase flow systems." J.Heat Transfer 1998 **87**: 453-468.

Zwart P.J. (2005). Modelling of Free surface flows and cavitation, VKI Lecture Series. Industrial Two-Phase Flow CFD. Bruessels, Belgium**:** 1-25.

APPENDIX A

A user defined function term was used in the STAR CCM+ package to implement damping function in the CFD prediction as described in Chapter 5, it took the form of a source term applied to the ω equation of the k- ω model, and is mesh-dependent:

$$A \cdot \Delta y \cdot \beta \cdot \rho_i \left(B \cdot \frac{6 \cdot \mu_i}{\beta \cdot \rho_i \cdot \Delta n^2} \right)^2$$

where A is the interface area density, Δn is the typical grid cell size across the interface, ρ_i and μ_i are the density and viscosity of the phase i.

The steps of applying the user defined function to STAR CCM+ are as following:

1. Define a field function term1

   600*$DynamicViscosity/(0.075*$Density*0.003*0.003)

   where 0.003 is the mesh size used in this case.

2. Define a second field function (called, for example, turbSource) with the following definition:

   $VolumeFractionwater*$VolumeFractionair*1800.*0.075*$Density*$term1*$term1

   The expression is mesh size dependent, therefore the constants in these expression requires tuning.

   Once the field functions are ready, expand

Regions > Fluid > Physics Conditions > Turbulence Source Option

and choose Specified.

Then go to

Regions > Fluid > Physics Values > Specific Dissipation Rate Source

and choose Field Function.

For the Field function, select the “turbSource” as previously defined.

APPENDIX B

```
% this program is to perform cross correlation of two holdup signals for conductance probes.

% export slug speed

%% setting your parameters here
data=importfile('run5.txt');
smoothparameter=200; % parameter to smooth the holdup data
tshift=3; % second, for cross-correlation
samplefreq=500; % sampling frequency
SlugLengthMinInSec=0.05; % minimum time interval of a slug in second
SlugDistanceMinInSec=2; %minimum time interval between slugs in second
thresholdSpeed=2;
ProbeDistance=1;

%% data
t=data(:,1);
holdup=data(:,2);
holdup2=data(:,3);
SlugLengthMin=SlugLengthMinInSec*samplefreq;
SlugDistanceMin=SlugDistanceMinInSec*samplefreq;
%% smoothing
holdup1=smooth(holdup,smoothparameter);
holdup2=smooth(holdup2,smoothparameter);
plot(t,holdup1,t,holdup2)
pause(1)
```

```
%% segementation
threshold=mean(holdup1)*1.5;
f_squre=(holdup1>threshold);
if(f_squre(1)==1)
   f_squre(1)=0;
end
if(f_squre(end)==1)
   f_squre(end)=0;
end

temp=diff(f_squre);
left=find(temp==1);
right=find(temp==-1);
if(length(left)~=length(right))
   fprintf('error')
   return
end

SegmentLength=right-left;
while (sum(SegmentLength<SlugLengthMin))
   SegmentLength=right-left;

   % check the last one
   if(SegmentLength(end))<SlugLengthMin
      left(end)=[];
      right(end-1)=[];
   end

   %check the ones in the middle
   for i=length(right)-1:-1:2
      if(SegmentLength(i)<SlugLengthMin)
         distleft=(left(i)-right(i-1));
         distright=((left(i+1)-right(i)));
```

```
        if(distleft<SlugDistanceMin)
           % very close to the left
          left(i)=[];
          right(i-1)=[];
        end
         if (distright<SlugDistanceMin)
            %very close to the right
          left(i+1)=[];
          right(i)=[];
         end
      end
   end

   % check the first one
   if(SegmentLength(1))<SlugLengthMin
      left(2)=[];
      right(1)=[];
   end
end

%% check segment distance
NumSegmentDist=length(right);
for i=NumSegmentDist:-1:2
   if(left(i)-right(i-1)<SlugDistanceMin)
       left(i)=[];
       right(i-1)=[];
   end
end

plot(t,holdup,t,holdup*0+threshold,t(left),holdup1(left),'.',t(right),holdup1(right),'.');
title('Segmentation')
pause(1)
```

```
%% Cross-correlation
SegmentLength=right-left;
for i=1:length(right)
    left1=left(i);
    right1=right(i);
   profile1=holdup1(left1:right1);
   rightshift=right1+tshift*samplefreq;
   if(rightshift>length(holdup2))
      rightshift=length(holdup2);
   end
   CCsection=holdup2(left1:rightshift);
   c=CrossCorrelation(CCsection,profile1);
[minVal, minInd]=min(c);
CCposition(i)=left1+minInd-1;
subplot(2,1,1);plot(t,holdup1,t(left1:right1),profile1,'r')
title('Probe 1')
xlabel('Time (s)')
ylabel('Liquid holdup (-)')
subplot(2,1,2);plot(t,holdup2,t(CCposition(i):CCposition(i)+right1-
left1),holdup2(CCposition(i):CCposition(i)+right1-left1),'r')
title('Probe 2')
xlabel('Time (s)')
ylabel('Liquid holdup (-)')
pause(0.1)
saveas(gcf, ['Cross-Correlation' num2str(i) '.png'])
end

%% Check whether it is a slug or a wave
plotcolor=['rgbcmy'];
timeDiff=(CCposition'-left)/samplefreq;
Speed=ProbeDistance./timeDiff;
subplot(1,1,1)
plot(t,holdup1,'k');hold on
```

```
CCpositionSlug=CCposition';
leftSlug=left;
rightSlug=right;
for i=length(right):-1:1
   if(Speed(i)>thresholdSpeed)
      plot(t(left(i):right(i)),holdup1(left(i):right(i)),plotcolor(mod(i,6)+1));
   else
      leftSlug(i)=[];
      rightSlug(i)=[];
      CCpositionSlug(i)=[];
   end
end
maxholdup=max(holdup1);
for i=1:length(leftSlug)
      text(t(leftSlug(i)),maxholdup,num2str(i))
end
xlabel('Time (s)')
ylabel('Liquid holdup (-)')
title('Slugs')
saveas(gcf, ['Slugs' num2str(i) '.png'])
%% post-processing
SlugTimeDiff=(CCpositionSlug-leftSlug)/samplefreq;
SlugSpeed=ProbeDistance./SlugTimeDiff;
save SlugSpeed.txt SlugSpeed -ascii
slugTimeInterval=diff((leftSlug+rightSlug)/2)/samplefreq;
slugFreq=1/mean(slugTimeInterval);
fprintf(['Number of slug:' num2str(length(leftSlug)) '\n'])
fprintf(['The slug frequency is:' num2str(slugFreq) '\n'])
```